SISSA
Scuola
Internazionale
Superiore di
Studi Avanzati

Graphene oxide nanoflakes enable targeting dysfunctional synaptic plasticity in the amygdala

CANDIDATE
Elisa Pati

SUPERVISORS
Laura Ballerini
Giada Cellot

Academic Year 2021-22

CONTENTS

SUMMARY

In the last decade, graphene-based nanomaterials (GBNs) have been proposed as innovative therapeutic tools in the field of precision medicine for neuroscience applications (Kostarelos K. et al., 2017; Bramini M. et al., 2018; Cellot G. et al., 2022). In detail, graphene oxide (GO) nanoflakes with small lateral dimension (s-GO) were found to target specifically and transiently glutamatergic synapses of the hippocampus *in vivo*, by reducing the release of neurotransmitter from the presynaptic terminal (Rauti et al., 2019). Recently, it has been suggested that this precise targeting of excitatory synapses could be applied to rescue the aberrant glutamatergic transmission characterizing several brain diseases, from dementia to anxiety disorders. Among these, post-traumatic stress disorder (PTSD) is related to a hyper-function of the lateral amygdala (LA), a nucleus involved in the storage of aversive memory induced by stressful events, resulting in long-term potentiation (LTP) of glutamatergic synapses (Parsons M.P. et al., 2014).

In this framework, in my thesis I have addressed the following issues:

(i) To investigate if s-GO could be used to hamper the aberrantly increased glutamatergic transmission observed in pathological conditions, such as in the PTSD;

(ii) to identify the subcellular target of s-GO in order to dissect the mechanism of interaction between the nanomaterial and potentiated synapses;

(iii) to explore the potential of s-GO as nanocarrier in drug delivery systems, by using neuropeptide Y (NPY) as carried biologically active molecule.

With the aim to elucidate how s-GO interferes at synaptic level with the pathological LTP underlying PTSD, I developed an *in vitro* model of amygdala potentiated glutamatergic synapses. In rat dissociated amygdala cultures, I induced chemical LTP (cLTP) through the brief application of glutamate (50 μM) that was monitored through patch clamp recordings as a 30-minute-long lasting increase in the amplitude of spontaneous excitatory postsynaptic currents (sEPSC, Franceschi B.A. et al., 2021). When s-GO (20 μg/mL) was applied during cLTP induction, the synaptic potentiation was not expressed. In addition, by combining the recording of miniature postsynaptic currents (mPSC) with confocal analysis of pre- (VGlut1) and post-synaptic (PSD95) markers, both informative for modifications in synaptic structure, I detected that in amygdala cultures cLTP induced a synaptic potentiation characterized by pre- as well as postsynaptic sites of expression. The application of the nanomaterials during cLTP induction reverted all these plastic changes of excitatory synapses observed in potentiated cultures.

Next experiments were aimed to identify the subcellular target of s-GO. Once excluded that the nanomaterial could affect the activity of postsynaptic glutamatergic receptors or could remove the exogenously applied glutamate, I focused on the dynamics of presynaptic vesicle release as key mechanism on which s-GO could act to reduce the glutamatergic signalling. Firstly, I performed real-time imaging of recycling vesicles labelled with the fluorescent styryl dye FM1–43 dye (Betz W.J. et al., 1992; Ryan T.A. 1999). Results indicated that s-GO rescued the cLTP dependent increased mobility of synaptic vesicles from presynaptic sites. Secondly, to directly assess nanomaterial-induced changes in the probability of presynaptic release at glutamatergic synapses, I performed dual electrophysiological recordings from pairs of monosynaptically connected excitatory amygdala neurons. By using a pair pulse stimulation protocol (Gasparini S. et al., 2000; Murthy V.N. et al., 1997; Zucker R.S. 1989; Debanne D. et al., 1996), I monitored changes in the amplitude of the consecutive evoked excitatory postsynaptic currents (eEPSC), indicative for modifications in the probability of glutamate release from presynaptic terminals. While cLTP induced the appearance of a strong short-term depression of consecutive eEPSC (due to an increment in the probability of glutamate release), the application of s-GO during cLTP prevented such effect. This result strongly

indicated that the rescue of cLTP expression detected upon application of the nanomaterial was due to a s-GO mediated decrease in the probability of glutamate release from presynaptic site.

In order to translate the ability of s-GO in interrupting amygdala plasticity from an *in vitro* setting to an *in vivo* condition, colleagues in Prof. Ballerini's group performed experiments by using a rat behavioural model of PTSD. In this paradigm, the exposure of rats to a predator odour (a collar previously worn by a cat) induced an increase in the excitability of LA glutamatergic synapses (Rosenkranz J.A. et al., 2010), causing the long-lasting anxiety related behavioural responses, typical feature of the disorder (Dielenberg R.A. et al., 2001). Contextual fear memory and the anxiety-related response were studied through the avoidance box (Muñoz-Abellán C. et al., 2009) and the elevated plus maze (EPM, Coimbra N.C. et al., 2017), respectively. Results showed that a single injection of s-GO delivered in the LA during the consolidation of predator odour-elicited plastic changes was sufficient to prevent long-term aversive memory and long-lasting anxiety-related responses. Furthermore, the inhibition of anxiety-related behaviours was longer respect to the persistence of s-GO in the LA, thus corroborating the hypothesis that the nanomaterial hampered the building up of the pathological plasticity rather than merely interfering with the synaptic communication between neurons. By using post-mortem LA slices, it was also demonstrated that the behavioural effects of animals exposed to the predator odour and injected with s-GO arose from a lack of LTP in amygdala synapses, as dendritic spines of amygdala neurons were decreased respect to those of untreated stressed rats. All together, these experiments suggest that the nanomaterial, when administered in the *in vivo* PTSD model, could ameliorate anxiety-related behaviours by targeting excitatory synapses. We speculated that the s-GO mediated reduction in the probability of glutamate release from presynaptic terminals is the core event in preventing the formation of pathological plasticity and related anxiety-behaviours in the PTSD rat.

Finally, I focused on the potential hold by s-GO as nanocarrier in drug delivery systems for the treatment of PTSD. In particular, as bioactive carried molecule, we used NPY, a modulator of neuronal transmission (Colmers W.F. et al., 1988; Klapstein G.J. et al., 1993; Bacci A. et al., 2002) which has been demonstrated to be involved in several physiological CNS functions, including modulation of fear and anxiety (Zhang Y. et al., 2021). Nevertheless, the fast kinetic of NPY degradation limits its use in therapeutic application (Wagner L. et al., 2015), thus the complexation to nanomaterials might be advantageous to improve its pharmacokinetic properties.

In such a context, I provided some preliminary results to explore the biological effects of s-GO:NPY complexes, composed of peptides absorbed onto the surfaces of the nanomaterials. By using acute and sub-acute applications of the complexes while recording spontaneous neuronal activity on dissociated hippocampal cultures (our standard in testing new nanomaterials, Rauti R. et al., 2016; Rauti R. et al., 2019; Secomandi N. et al., 2020; Di Mauro G. et al., 2021), we found that both s-GO and NPY when complexed together were still bioactive on neurons, as they produced modulatory effects on synaptic activity. In addition, when I investigated their impact on the *in vitro* model of amygdala cultures undergone to cLTP, I detected a similar effect of s-GO:NPY or free NPY in hampering the expression of synaptic potentiation. Preliminary experiments carried out by my colleagues on the PTSD rat model confirmed that NPY retained *in vivo* its biological activity when complexed to the nanomaterials. However, differently from not complexed s-GO effect, the rescue of the contextual fear memory, but not of the anxiety-related responses, observed in animals treated with s-GO:NPY or NPY suggested that the drug delivery system could be driven to specific neuronal circuits by NPY.

In conclusion, this work of thesis characterized in a pathological condition the efficacy of s-GO, free or in complexation with bioactive compounds, as modulator of synaptic activity and correlated behaviours, thus identifying a novel nano-tool that might be used for the treatment of anxiety-related disorders and, more in general, for other neuropatholgies characterized by exceeding glutamatergic transmission.

INTRODUCTION

1. NANOTECHNOLOGY AND NANOMATERIALS

Nanotechnology, the 21st century technology which deal with matter at the nanometer scale (1-100 nm), can exploit nanoscience theory to important and useful applications. The origin of nanoscience concepts, although not explicit, can be ascribed to the Greek and Democritus ancient time (5th century B.C.), when scientists debated if matter was continuous and infinitively divisible or composed by indivisible particles which are nowadays known as atoms of 0.1 nm.

Curiously, the most famous and oldest type of dichroic glass is represented by Lycurgus cup, dating back to the 4th century AD, due to the presence of nanoparticles (NP) of 50-100 nm in diameter. However, the origin of nanotechnology as an identified branch of science and engineering goes back to 1959, when the Nobel Prize laureate and physicist Richard Feynman, presented a lecture titled "There's Plenty of Room at the Bottom" during the American Physical Society at the California Institute of Technology (Feynman R.P., 1960). Feynman is considered the father of modern nanotechnology which was defined 15 years later by Norio Taniguchi as "the processing of separation, consolidation, and deformation of materials by one atom or one molecule" (Taniguchi N. et al., 1974).

Nowadays, after more than 50 years, the interest in, and understanding of nanotechnology and related applications has constantly increased and its definition has changed to "science, engineering and technology conducted at the nanoscale (1 to 100 nm), where unique phenomena enable novel applications in a wide range of fields, from chemistry, physics and biology, to medicine, engineering and electronics." (National Nanotechnology Initiative, NNI, ww.nano.gov).

The first book of nanotechnology was published by K. E. Drexler in 1986 entitles "Engines of Creation: the Coming Era of Nanotechnology" (Drexler E.K., 1986). The book describes as individual atoms can independently self-assembly and be manipulated, thus generating complex nanostructures and machines. From this book, the term "nanomedicine" emerged (Drexler E.K. et al., 1991).

There are principally two distinct ways through which NP can be synthetised: the top-down and the bottom-up technologies (**Fig. 1.1)**. The first approach started from bulk materials that can be manipulated by precise techniques such as lithography to get nano-sized particles. Conversely, the bottom-up strategy permits to build up complex nanostructures form the bases, such as self-assembly of molecules or atoms which organize themselves by chemical-physical interactions (Bayda S. et al., 2019). Modern nanotechnology researchers use different instruments with nanometer scale resolution as the atom force microscopy (AFM) and the scanning probe microscope (SPM) (Binnig G. et al., 1986). Thanks to these tools, novel carbon chemistries, inorganic NP and materials have been characterised, such as fullerene or buckybulls (very stable spheres of carbons). Particularly in the fullerene family, carbon and graphite nanotubes have been introduced in 1991 by Iijima (Iijima S. et al., 1991). Among other properties, they possess strength and flexibility which make them useful components of nanomedicine devices. In fact, thanks to their nanoscale dimension, these nanomaterials show advantageous physical and electro-chemical properties. For example, carbon dots (CD) can be considered a rising star for drug delivery or bioimaging due to their excellent biocompatibility, good optical and electronic attributes, and low toxicity (Esteves da Silva J.C.G. et al., 2011).

Bio-nanotechnology is considered one of the most promising areas of nanoscience application, targeting molecular imaging, drug delivery and diagnosis. In this regard, DNA nanotechnology and nano-oncology represent two recent concepts. DNA nanotechnology is considered an interdisciplinary research area which uses biopolymers like DNA for diagnostic and sensing approaches. The "scaffold-DNA origami" was developed in 2006 by P.W. Rothemund through "one-pot" reaction of self-assembly DNA nanostructures (Rothemund P.W., 2006).

Regards to nano-oncology, nanomaterials are extremely effective for the delivery of drugs, therapeutic, cytotoxic agents, and antibodies, exerting anticancer activity or modulating biological processes without the systemic toxicity related to the traditional chemotherapeutic drugs. An extensive review (Song W. et al., 2019) reports the application of nanotechnology to microbiome modulation for cancer therapies/prevention. It is demonstrated that tumour-associated bacteria, which are found in metastases, cause inhibition and resistance against widely used chemotherapies. Conversely, nanotechnologies can either block bacteria-secreted toxins carcinogens and immunosuppressive agents or interact with microscopic metabolites in order to release chemotherapeutics in the tumour environment.

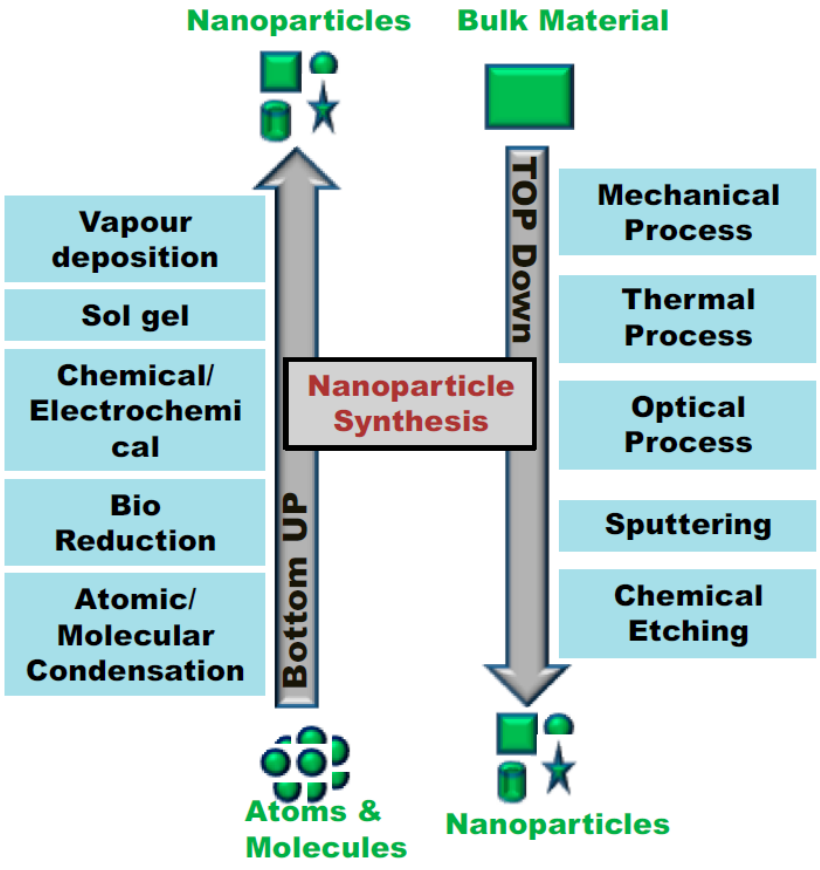

Figure 1.1 The concept of bottom-up and top-down technology: different methods for nanoparticles synthesis (Bayda S. et al., 2019)

An increasing body of research emerged in the last two decades hinting at the potential contributions that nanotechnologies could make to basic and clinical neuroscience. In fact, the

application of nanotechnology in neuroscience research enables targeting the nervous system at a fundamental molecular level.

The mammalian brain is composed by around 100 billion of neuronal cells (neurons) and other 100 billion of non-neuronal cells (glia). The complexity of the human nervous system resides in the local and long-range connectivity of these cells. Traditionally, electrical activity of single neurons has been measured by glass or metal microelectrodes, while, more recently, voltage probes, optical and magnetic methods allow the recording from groups of neurons through optochemistry, optogenetics or magnetic stimuli, scaling up the complexity of the observed neuronal ensemble. Nevertheless, all these tools still lack in the systematic manipulation and control of entire neural circuits with single-cell precision. In this framework, the field of neurotechnology achieves enormous importance since nanotools can investigate the "big data" of neuronal dynamics with unprecedented resolution and across several biological length scales, from ten of nanometres for synapses to ten of centimetres for axonal projections. For instance, injectable mesh nanoelectronics have allowed for the first time long-term *in vivo* recordings from single ganglion cells of the retina in awake animals (Acaròn Ledesma H. et al., 2019).

Recently, the miniaturization of the Complementary-Metal Oxide Semiconductor (CMOS) technology has given birth to novel designs that permit the recording from orders of magnitude more neurons than before, like flexible and wireless nanoelectrode array for surface recordings, with over 65,000 electrodes (Garcia-Etxarri A. et al., 2021). For deeper recordings, silicon-based probes have been designed for optical-stimulation and imaging since they have emission and detection pixels (Segev E. et al., OSA, 2016). Similarly, nanopillars on a surface are used for intracellular recordings and for chemical sensing (Robinson J. T. et al., 2012). All these nanotools, opposite to the traditional bulky implantable metal electrodes, interface the nervous system at novel spatiotemporal scale and with higher biocompatibility with negligible glia activation and scare formation (Zhou T. et al., 2017; Kotov N. A. et al., 2009). For instance, quartz nanoelectrodes generate long-lasting intracellular recordings *in vivo* without mechanical neuronal damage thanks to their few nanometres tip (Jayant K. et al., 2019). Thus, these devices can be used for patient therapies leading to a personalized electronic medicine.

Another interesting and promising nanotool which can be exploited in a wide range of biomedical applications is represented by plasmonic or metal NP. They can be synthesized through both top-down and bottom-up strategies and with different shapes and resonant frequencies according to the use. Their plasmonic effect makes NP as optical nano-antennas with signal enhancements of up to eight orders of magnitude in light driven processes like fluorescence, Raman scattering, infrared-absorption spectroscopy, or thermal effects (Garcia-Etxarri A. et al., 2021). NP can be excited by light locally generating high temperatures that, in turns, can be exploited to activate neurons, as well as to trigger action potentials through the manipulation of membrane capacitance or thermosensitive channels (Cohen M.R., Moiseenkova-Bell V.Y., 2014). They can be functionalized to selectively target and activate cells with visible or two-photon light (**Fig. 1.2 a,b**).

Even smaller than NP, quantum dots (QD) are semiconductor particles with several advantages compared to classical fluorescence probe, in both optical and stability terms. QD were accidentally discovered during the purification of single wall carbon nanotubes (CNT) by Xu X. and collaborators in 2004 (Xu X. et al., 2004). Importantly, QD photoluminescence is modulated by electric field, in fact, due to the quantum-confined Stark effect (Bar-Elli O. et al., 2018), it shifts in the emission spectra. These changes in fluorescence intensity are used in neuroscience to optically measure the neuronal electrical activity. Moreover, QD can be functionalized as NP, allowing the

measurements of membrane potentials. Interestingly, in 2017, Nag O.K. et al. developed a nanobioconjugate with QD and fullerene which was attached to the membrane by peptide linkers: they exploited the electron transfer between QD (donors) and fullerene (acceptors) to visualize membrane potential *in vivo* and measure action potentials *in vitro* (Nag O. K. et al., 2017). Together with QD, nanodiamonds, nanoscale-level size diamonds with high electrical and magnetic sensitivity quantum cavities, have been used for the measurement of magnetic fields produced by the firing of single neurons with a resolution of one microsecond (Barry J. F. et al., 2016).

It is worth to mention another type of NP which exhibit photon upconversion (low energy photons converted into high energy emitted ones) and thus called upconverted NP (UCNP). Due to their sensibility to environmental conditions, they could tract pressure changes in animals or neural circuits. Moreover, UCNP have been used to monitor membrane potential's fluctuations through their luminescence, behaving as donors in membrane-bound charges molecule acceptors (Garcia-Etxarri A. et al., 2021, **Fig. 1.2 c**).

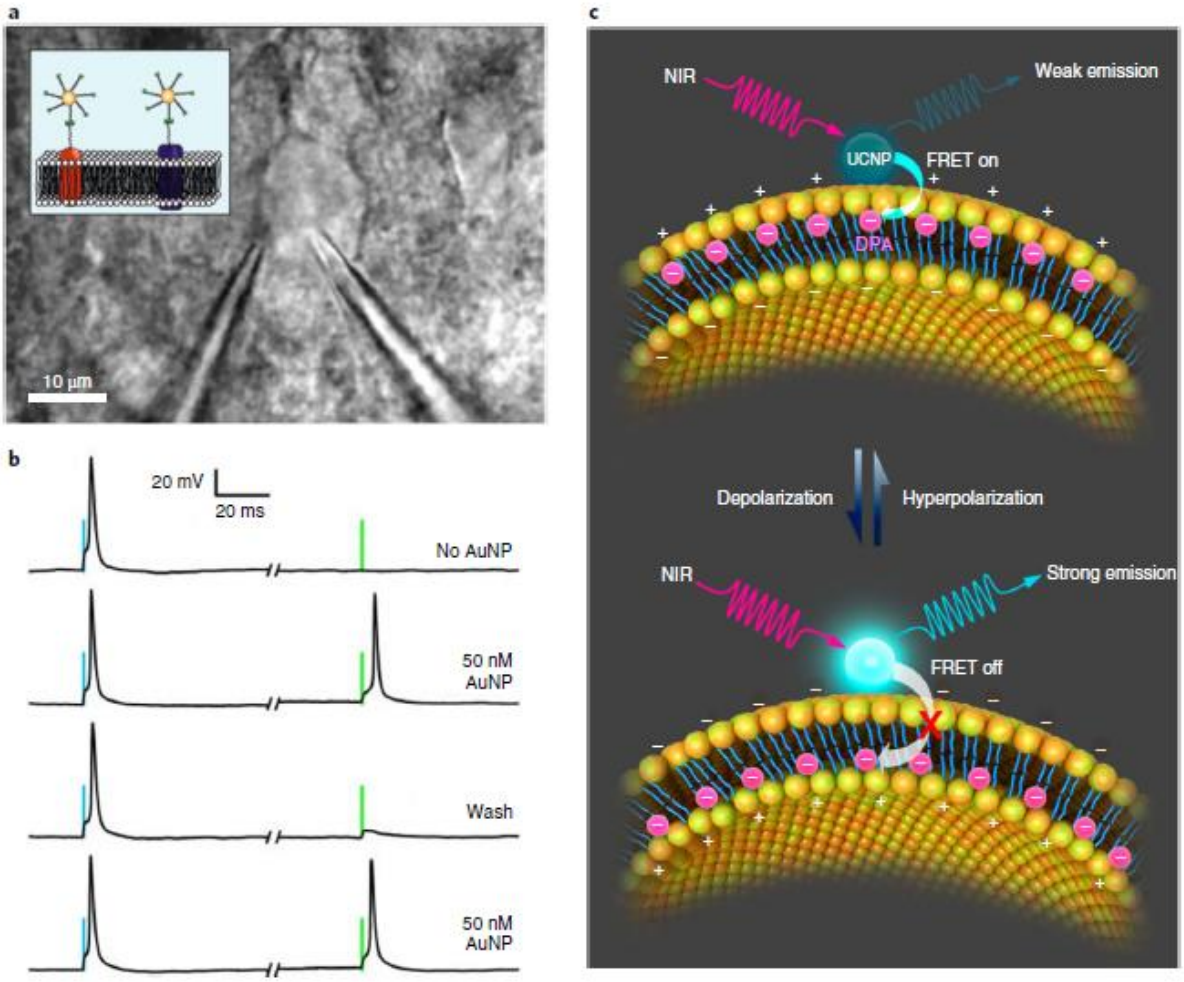

Figure 1.2 Nanoparticle-based recording and manipulation of neuronal activity. **A**. Patch clamped neuron covered with nanoparticles. Inset: nanoparticles attached to the cell membrane through streptavidin–biotin binding. **B**. Optically evoked neuronal activity through plasmonically enhanced photothermal stimulation. Blue lines indicate current injections and green lines indicate laser pulses. **C**. UCNPs and a charged molecule in the membrane (DPA) act as donor and acceptor pair in a FRET process. (Garcia-Etxarri A. et al., 2021)

All these nanotools together with molecular-biology approaches (hybrid nano-genetic tools) are giving birth to a new scientific field, the NanoNeuro, that is the application of nanoscale technologies to neuroscience (Garcia-Etxarri A. et al., 2021). Recently, nanowire topography has been demonstrated to be effective in the study of neural communication, synapse formation and neurite growth (Gautam V. et al., 2017). The same application, replicating the *in vivo* neuronal organization, could led to advances in three-dimensional (3D) neuron cultures and brain organoids field.

NanoNeuro tools development promises good opportunity for modern neuroscience research allowing experimental measurements and investigations which were inaccessible to the traditional techniques and, importantly, at different length scales. According to that, nanostructures with physical characteristics on the same order as subcellular organelles (i.e., fluorescence nanodiamonds, photoluminescence QD, engulfed Au nanorods) can pass the plasma membrane of cultured neurons without any or low cytotoxic effects and allow real-time imaging of axonal transport (Haziza S. et al., 2017) or the intracellular modulation of calcium level (Fang Y. et al., 2018). Even fine and small structures like dendrite spines which play important roles in synaptic plasticity and other neural processes, have been targeted with nano-field-effect transistor (FET) (nanoFETs), nanowire modulators and QD-coated nanopipettes (Jayant K. et al., 2017) to depict the relationship between the somato-dendritic excitatory postsynaptic potentials on spine neck resistance.

Considering the range of biological length scale, the blood brain barrier (BBB), a dense tight junctions made by endothelial cells and blood vessels, represents a limit for the freely passage of molecules from blood to nervous systems. However, thanks to nanovectors, polymers and magnetic NP, receptor-mediated endocytosis through the BBB can be enhanced for drug delivery. Another approach consists of the reversible permeabilization of the BBB through magnetothermal NP, mesh nanoelectrical scaffolds or optoelectronic devices (Chen Y., Liu L., 2012).

Beyond the BBB, synthetic extracellular matrix-like devices have been recently developed, creating 3D neural cultures, and investigating neurons development, growth, and activity. For instance, folded microporous nanoelectronics mesh devises have recorded local fields potentials and pharmaceutical responses from 3D cultures of neurons (**Fig 1.3**) through the generation of interpenetrating recording networks with neurites (Acaròn Ledesma H. et al., 2019; Tian B. et al., 2012). Furthermore, thanks to the great flexibility of these devices, they can be packaged into small injection vehicles for subcortical brain delivery. Once released, they intimately contact the surrounding neurons thus recording their activity in freely moving animals at a single-cell resolution level (Tian B. et al., 2012). *In vivo* neural stimulation can be achieved through Si nanomembrane stimulator, as well as with graphene sensors which can be used together with optogenetics or fluorescence imaging replacing metals or semiconductors (**Fig 1.3**).

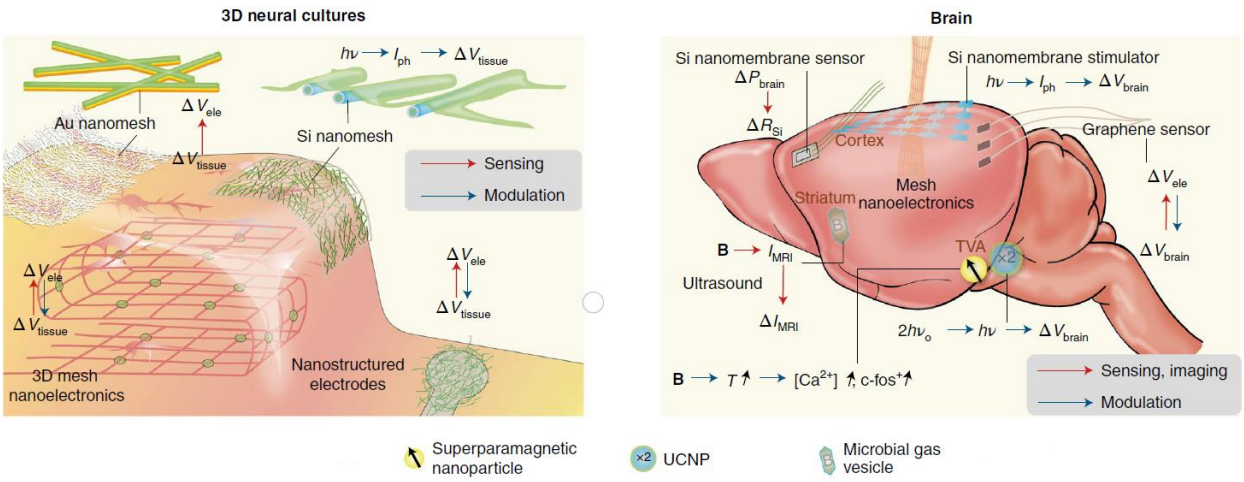

Figure 1.3. Interfacing 3D neural cultures and the brain (Acaròn Ledesma H. et al., 2019).

2. CARBON-BASED NANOMATERIALS: FOCUS ON GRAPHENE

"Carbon is the sixth element in the periodic table, the fourth most abundant element in the universe and the basic building block for all life." (Littlejohn S.D. et al., 2014). The abundancy of carbon is due to its unique electronic structure that permits the formation of several types of bonds. In fact, carbon with its six electrons (two in the innermost tightly bound shell and four in the outer valance shell), can undergo three types of hybridization: sp, sp^2 and sp^3. The ability to hybridize permits the creation of the basic and stable forms of carbon nanomaterials: the zero-dimension (0D) nano-size balls, the one-dimension (1D) long thin tubes, the two-dimension (2D) single layers and the 3D crystals. Even if these nanostructures are mainly composed by one element carbon, the diverse structures exhibit amazing features. These structures comprise CNT, fullerene, diamond, CD, graphite, graphene and graphene oxide (GO) (**Fig 2.1**), whose physical and chemical properties are well summarized in the review of Liu S. et al (Liu S. et al., 2017). Due to carbon extraordinary properties, more and more nanomaterials continue to be fabricated or discovered. Buckminister-fullerene (or buckyballs) were discovered in 1985: they are 60 carbon atom-spherical particles (C60) which resemble a football ball because of their truncated icosahedral structure. C60 and its derivates (i.e., C20, C32, C60 etc) were discovered in 1985 and immediately raised a lot of interest for their multiple potential applications in medicine, chemistry and electronics. The discovery of CNT in 1991 derives from C60 fullerene.

The geometries of CNT which are mostly used in biology can be divided into two types according to the carbon layers: single wall nanotubes (SWNT) of just one layer thick, or multi-wall nanotubes (MWNT) with concentric layers. Typically, they have a diameter of 1nm but can reach up to cm of length. The electronic properties of CNT (semiconductive or metallic) derive from their chirality.

Both 3D diamond and 3D graphite have been known to humans for thousands of years. Particularly, diamond was used in the Ancient India for jewellery and are characterized by exceptional hardness and thermal conductivity thanks to the sp^3 hybridization. The sp^2 hybridized graphite is made by layers of graphene which are loosely bound through Van der Waals interaction from the pz electron in the π orbital and which makes graphite very anisotropic (Littlejohn S.D. et al., 2014).

2D Graphene monolayers were recently isolated in 2004 by A. Geim and K. Novoselov on a SiO_2 substrate and through a simple mechanical technique of cleavage with scotch tape (Novoselov K.S. 2004). The importance of this discovery, which was acknowledged by the Nobel Prize for Physics in 2010, shed light on several thermal, electrical, and mechanical properties of the sp^2 hybridized graphene. In fact, graphene obtained a lot of attention in biomedical applications because of its unique structure: a single layer, one atom thick, two-dimensional array of carbon hexagons. The very large surface area on both sides and one atomic thickness makes it very useful in innovative therapeutics, such as drug delivery multifunctional platforms or nano-carriers.

Graphene is an outstanding conductor of heat as well as the world's thinnest and strongest material (Han X. et al., 2016). From its discovery, graphene started to be the pillar of science and engineering and this "graphene explosion of interest" led to the creation of a European initiative funded by the flagship scheme: the Graphene Flagship (https://graphene-flagship.eu/).

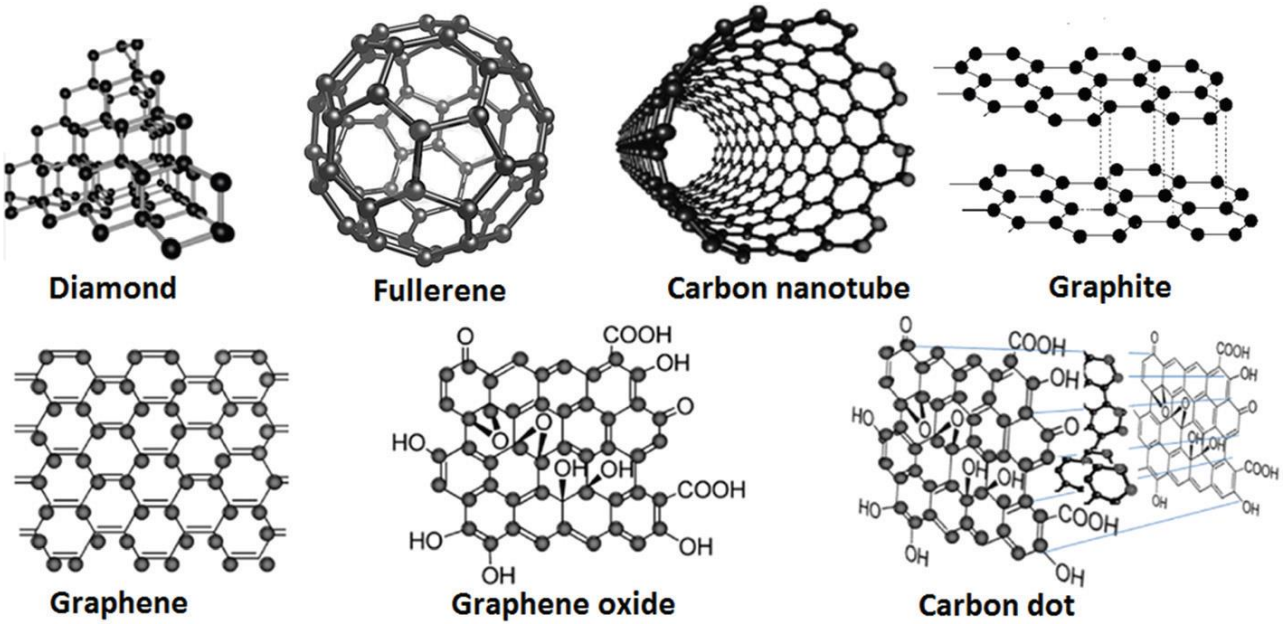

Figure 2.1 Different carbon-based nanomaterial structures (Yan Q.L. et al., 2016).

"Graphene is a wonder material with many superlatives to its name. It is the thinnest material in the universe and the strongest ever measured." (Geim A.K., 2009).

Graphene, a 2D sheet of sp^2-hybridized carbon atoms formed in honeycomb lattice, led to an enormous interest among scientists from 2004, when the few-layers graphene (FLG) flakes were firstly isolated from graphite (Novoselov K.S., 2004). Graphene is the basic building block for graphitic materials of other dimensions: it can be wrapped up into 0D fullerenes, rolled into 1D nanotubes and stacked into 3D graphite (Geim A. and Novoselov K., 2007).

There are two principal routes to make graphene. The oldest one, through which graphene was first isolated, is the previously mentioned "scotch tape" technique. It consists of micromechanically splitting layered graphite into atomic planes. The second route is less time consuming and more precise via chemical vapor deposition (CVD) from a non-graphite source. (Whitener K.E. and Sheehan P.E., 2014). Methods for producing graphene include direct exfoliation

in organic liquids, electrochemical exfoliation, solvothermal methods, graphitization, redox methods, mechanical stripping, graphene thermal/chemical/photothermal (PTT) reduction in GO, organic synthesis, epitaxial growth by CVD on copper or epitaxial growth on silicon carbide (Kostarelos K. and Novoselov K.S., 2014).

Graphene has several and important properties which make it useful in various fields, from physics to medicine. Among the graphene features, the most exciting are its electronic ones which are unique and diverse compared to other known condensed matter systems. Firstly, graphene has an electronic spectrum which is described by a Dirac like equation instead of the Schrodinger one. It consists of electron waves that completely lose their effective mass propagating through the honeycomb lattice. (Castro Neto A.H. et al., 2009). Moreover, these electron waves are accessible to various scanning probe since graphene is only one atom thick, therefore they can cover long distance without scattering. This last property makes quantum effect in graphene very robust even at room temperature (RT). Graphene boasts incredible chemical, mechanical and thermal properties too. About graphene chemistry, its surface, which is similar to the graphite's one, can adsorb and desorb different atoms and molecules, and reagents can attach to both sides of graphene allowing stable chemical bonds (Elias D.C. et al., 2009). Moreover, graphene has a high thermal and electrical conductivity, high carrier mobility (Novoselov K.S., et al, 2005), large specific surface area (Stoller M.D. Et al., 2008), high transparency (Nair R.R. et al., 2008), as well as high mechanical flexibility. It is impermeable to gases and could be elastically stretched by as much as 20 % as no other crystals (Lee C. et al., 2008).

Monolayer graphene and its derivates form a family of nanomaterials which is named graphene-based nanomaterials (GBNs). The members of this family particularly differ for properties which are most relevant for their biological effects, such as lateral dimension, surface area, composition, and purity, as well as density or quality of individual graphene sheets.

Particularly, surface is relevant for the nanomaterial biological interaction (Nel A.E. et al., 2009): monolayer graphene has the theoretical maximum surface area (m^2/g) of an $2p^2$-hybridized carbon sheet since each atom is exposed to the surrounding environment in both sides. The surface area of GBNs and, therefore, their absorptive capacity for biological molecules, decrease as their layers increases in number (Sanchez V.C. et al., 2012). Conversely, their stiffness increases with the third power of layer number and material thickness whose characterization is typically performed through AFM. Monolayer GBNs are extremely thin and can be deformed by weak forces during the cellular interaction (i.e., water surface tension), opposite to multilayer rigid GBNs. In addition, the chemistry of the GBNs surface is very important, since hydrophobic materials have a limit in biological interactions, hydrogen bonding or metal ion complexing unless stabilized with surfactants.

The lateral dimension of GBNs, (their size) covers orders of magnitude, from 10 nm (some protein size) to ≥ 20 μm (larger than most cells). Lateral dimension of particles influences several biological phenomena (i.e., cell uptake, BBB transport, renal clearance...), but also deformability (larger compound are more deformable than smaller ones with the same number of layers). The lateral dimension of GBNs dictates their route in the cellular environment, since smaller particles can be phagocyted or endocytosed while larger ones can spread cells around or even be harmful.

Among the most relevant graphene derivates, few-layered graphene (FLG) represents the precursor or the by-product for the fabrication of monolayer graphene (Novoselov K.S., 2004). FLG samples, which contains from 2 up to 10 layers of graphene, originate from the powders obtained

through thermal-exfoliation and can subsequentially be processed into graphene or graphene oxide (GO).

The latter consists of single-atom thick carbon sheets with carboxylate groups on the periphery. It is the product of the chemical modification of graphene which is highly oxidized. In fact, the monolayer GO derived from a strong oxidation of crystalline graphite followed by sonication, usually in aqueous suspensions (Park S. et al., 2009).

Monolayer GO has a surface area which is similar to the monolayer graphene one, but it is modulated by atomic-scale roughness because of the random presence of oxygen. The basal surface can be covered with diverse functional groups, like hydroxyl (-OH), carbonyl (=CO), epoxide (-O-) or phenol groups, while the periphery contains carboxylate groups which are responsible for the colloidal stability and the pH dependent negative surface charge. GO stability is very important in biological experiments since GO is reported to aligned perfectly in GO papers creating interlayer spaces that are not accessible for biological interactions/aggregations (Zhang L.L. et al., 2010). Moreover, the negative charge on edges associated to the carboxylate groups makes these regions hydrophilic, even if its surface is partially hydrophobic, with a water contact angle of 40-50 degrees (Hasan S.A. et al., 2010; Cote L.J. et al., 2009). Conversely, the unmodified hydrophobic graphenic domains are able to adsorb dyes or drugs via μ-μ interactions. This amphiphilic molecule can, therefore, act as a surfactant or stabilizer of hydrophobic molecules in solution. The wide range of functional groups that can be attached to its surface through old and new chemical methods are well suited for thermal/electrical conductance, control optical transparency as well as novel attractive application areas in green technologies like the use of nuclear wastes or energy storage (Dideikin AT. And Vul' A.Y., 2019).

Since GO is a graphene derivate with lower electrical conductivity, in 2007 it was reduced for the first time through high temperature (24h at 100 °C) with hydrazine (N_2H_2) (Stankovich S. et a., 2007) generating reduced-GO (rGO). Later, other chemical agents have been used to reduce GO, like ascorbic acid or sodium borohydride or thiophene which confers to rGO high electrical features (Si Y. and Samulski E.T., 2008).

According to the surface chemistry, rGO is intermediate in hydrophilicity and basal reactivity among GBNs because, when the oxygen is removed, basal vacancy defects or holes appear in the carbon lattice due to the CO/CO_2 liberation. (Bagri A. et al., 2010).

Important to mention is nano-GO (nGO) which is the GO with small lateral dimension, in particular 5 to 50 nm instead of 50 to 500 nm of GO. Thanks to its small size which increases the nanomaterial dispersion stability, cell entry, intrinsic optical properties, and the functionalization ability, nGO are selected for various biomedical application (Gonçalves G. et al., 2014).

2.1 GBNs: APPLICATION IN BIOMEDICINE AND NEUROSCIENCE

The different methods of graphene production can produce a layer of graphene with unique parameters in terms of chemistry and physic (i.e., thickness, lateral extent, functionalization of surface...) which make it suitable for precise biomedical applications (**Fig. 2.1 A**). Particularly, graphene mechanical properties place it among the strongest materials with Young's modules ranges between 20-40 GPa, while tensile strength is between 15-520 MPa for graphene cast into films (Reina G. et al., 2017) These features together with the high flexibility make graphene able to accommodate on the surrounding biological environment without fatigue, thus permitting the

development of flexible biomedical electronic implants as integral and structural element. Moreover, different graphene types can interact with different living cells, tissue, or cell compartments (**Fig. 2.1 B**). The electronic properties of graphene (e.g., 2×10^4 cm^2 V^{-1} s^{-1} carrier mobility and 10^{13} cm^2 carrier density for mechanically exfoliated graphene) are also important for medical purpose (Reina G. et al., 2017). In fact, it can act as conducting component, support, or electrode in bioelectronic devices, as well as in optoelectronic stimulation thanks to its broadband absorption and high transparency in the visible range (2.3 % absorption for single-layered graphene, Kang P. et al., 2016).

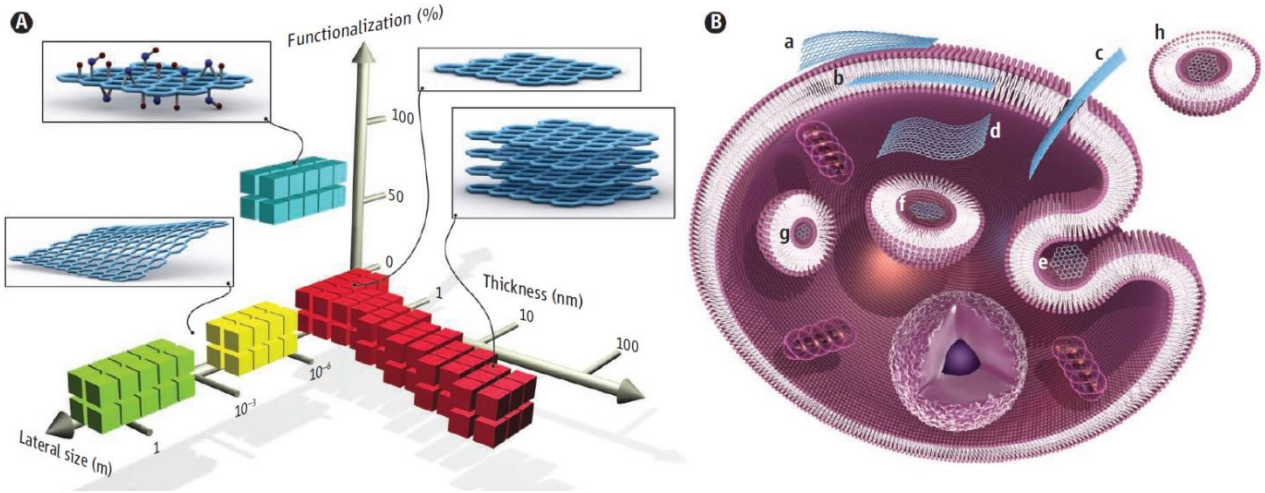

Figure 2.1 Graphene materials and their biological interactions. a) A parameter space for the most widely used graphene materials can be described by the dimensions and surface functionalization of the material, the latter defined as the percentage of the carbon atoms in sp3 hybridization. Green squares represent epitaxially grown graphene; yellow, mechanically exfoliated graphene; red, chemically exfoliated graphene; blue, graphene oxide. (B) Possible interactions between graphene-related materials with cells. (a) Adhesion onto the outer surface of the cell membrane. (b) Incorporation In between the monolayers of the plasma membrane lipid bilayer. (c) Translocation of membrane. (d) Cytoplasmic internalization. I Clathrin-mediated endocytosis. (f) Endosomal or phagosomal internalization. (g) Lysosomal or other perinuclear compartment localization. (h) Exosomal localization. The biological outcomes from such interactions can be considered to be either adverse or beneficial, depending on the context of the particular biomedical application. Different graphene-related materials will have different preferential mechanisms of interaction with cells and tissues that largely await discovery. (Kostas Kostarelos and Kostya S. Novoselov, 2014)

Therefore, graphene and functionalized graphene are applied to disease diagnostic (Tabrizi M.A. et al., 2019), bio sensing and imaging, antibacterial and antiviral materials (Akhavan O. et al., ACS Nano 2012; Akhavan O. et al.,2010), as well as cancer (Sun X. et al., 2018), photothermic therapy (Akhavan O. et al., 2012b), drug delivery (Wang K. et al., 2021; Gui W. et al., 2018), DNA sequencing (Nelson T. et al., 2010), stem cell field, tissue engineering and regenerative medicine (Jiang H. et al., 2018; Liu C. and Luo X., 2021). Thanks to the graphene structure which have delocalized π electrons, several aromatic molecules can be attached to graphene sheets via π-π interactions and/or electrostatic interactions improving drug delivery. Moreover, the rich oxygen-containing functional groups of GO could be directly functionalized by biological ligands to enhance drug delivery or targeted imaging, either by covalent or non-covalent methods (Georgakilas V. et al., 2016). In drug delivery nanosystems, a controlled chemical modification permits a fine control over the amount of drug released in specific tissues. Their surface can therefore be modified with

monoclonal antibody, lectins, oligonucleotides, short peptides and so on. Even aptamers A10, albumin, hyaluronic acid (HA), biotin, chitosan, polyethyleneimine (PEI) or folic acid are used, while complete hydrophilicity and "invisibility" against phagocytes are obtained by the modification of the surface through polyethylene glycol (PEG) or PEGylation (Nelson T. et al., 2010; Jiang H. et al., 2018). In addition, PEGylated graphene sheets show reduced toxicity and increased stability under physiological conditions (Jiang H. et al., 2018). For the best possible benefits, a graphene-based drug delivery system would have good biocompatibility and water solubility, as well as high blood circulation time. For this reason, GO and rGO are often preferred since they show good water dispersibility together with a very rich surface chemistry. Very recently, F. Yaghoubi and collaborators developed a GO-based, pH-sensitive drug delivery system by combining Doxorubicin (DOX), a well-known anticancer drug, with natural medicine curcumin (CUR) to dimmish DOX side effect and enhance its efficacy (Yaghoubi F. et al., 2022). The drug in the nano-formulation acquires particular physical and chemical properties and, because of the improved membrane permeability, its bioavailability is modified.

Functionalization of GBNs have been extensively used for the development of anticancer drug delivery system. Cancer is one of the major causes of death worldwide and its therapy is still a health challenge. Indeed, chemotherapy is limited by several factors (i.e., systemic toxicity, multidrug resistance bioavailability and immunogenicity) that could be overcome with drug delivery systems. In 2008, Liu Z. et al., demonstrated that PEG-decorated GO as a nanocarrier to deliver anticancer drugs can improve biocompatibility therapeutic efficacy, bioavailability, circulation time in the blood stream, cellular uptake, and stability (Liu Z. et al., 2008). In 2019, 6-armedPEG functionalized GO-nanocarrier has been developed for the anticancer oridonin and methotrexate (MTX) delivery, (Chai D. et al., 2019). This complex showed higher cellular uptake and anticancer efficacy against CAL27 tumour cells compared to free drugs. In 2018, a chitosan-graphene drug delivery system was developed as well (Zhao X. et al., 2018). It consists of a core-shell structure with GO NP as core and chitosan as surface charge-reversible shell which was linked to graphene via self-assembly. Through π-π stacking, DOX bound to the core GO. In this formula, chitosan shell blocked the premature DOX secretion on the medium, which was instead allowed and accelerated once the coated chitosan was separated by lower pH in cancerous tissues. This type of pH-sensitive drug delivery system to control the release of drugs at cancer sites is considered a smart platform where the therapeutic agent can be activated by endogenous or exogenous stimuli. In this regard, graphene-based platforms conjugated to pH-sensitive ligands are good candidates since they respond to changes in intracellular signals/tumour microenvironments and have been widely explored (Tu Z. et al., 2018).

Starting from drug delivery, the use of GBNs has been extended to a flexible plethora of therapeutic modalities, as gene therapy, immunotherapy, PTT and photodynamic (PDT) therapy (**Fig. 2.2**). Gene delivery is a process through which foreign DNA is transferred into target cells to express an exogenous gene to treat various disease included osteoporosis, cancer, and myocardial infraction (Liu Z. et al., 2008). The use of graphene and its derivates in gene delivery and immunotherapy has recently gained attention thanks to their superior transfection efficiency and their ability to interfere with different cellular signalling and differentiation (Liu Z. et al., 2008; Chai D. et al., 2019).

The large sp^2 hybridized carbon area of GBNs allow their interaction with other molecules along with drugs, like the nucleic acids DNA and RNA. Thus, graphene has been proposed as an efficient 2D non-viral gene transfer system because its unique properties (protection of nucleic acid from enzymatic degradation, fats cellular uptake and versatile chemical functionalization among

others). nGO sheets are reported to be used for gene delivery functionalized with or covalently bounded to cationic polymers or ligands thus improving their biostability and biocompatibility. A nanoparticle-based RNAi delivery platform has been developed to protect siRNA from the activity of nuclease and deliver it to target cells effectively (Zhao X. et al., 2018). In 2018, GO functionalized with PEI was developed and loaded with miR-7b plasmid to deliver it into bone marrow macrophages: it exhibited outstanding transfection efficiency and low toxicity (Tu Z. et al., 2018). Moreover, the hybrid branched PEI-GO system with high photoluminescence properties and transfection efficacy allows simultaneously bioimaging and gene delivery.

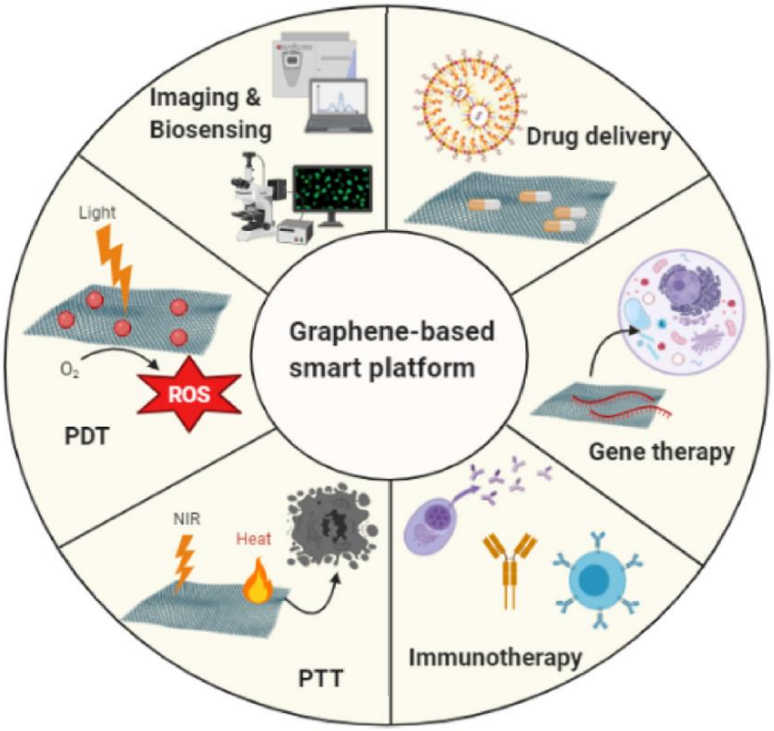

Figure 2.2 Schematic of applications of GBNs in diagnosis and therapy (Fo C.Y. and Fu R.Z., 2021)

GBNs high surface-to-volume ratio, small bandgap, excellent conductivity, and tuneable optical properties make them good candidates for electrochemical sensing, as well as for fluorescence and plasmonic sensors. Biosensors based on GBNs can detect DNA, proteins, drugs, cancer cells, glucose etc. According to glucose, its detection is one of the most important biosensing application because of the wide diffusion of diabetes. Graphene-based glucose sensors are extensively studied and generally consist of immobilized glucose oxidase and a graphene surface to detect low glucose concentration. For instance, Zhang et al. covalently connected the amino group of glucose oxidase to GO through 1-ethyl-3-(3-dimethylaminopropyl) carbodiimide and N-hydroxysulfosuccinimide. (Jiang B. et al., 2018). The oxidized glucose levels were evaluated through changes in the refractive index of the local microenvironment which were in turns converted into measurable information with a sensitivity of ~ 0.25 nm/mM. Owing to the low cost and high sensitivity, GBNs have also been used in the selectivity of biomarker detection, for the prediction, diagnosis, or detection of various diseases. A representative study was that of Nezhad et al. (Khetani S. et al., 2018) where a PEI-coated graphene electrode covalently bound to glial fibrillary acid protein

(GFAP) antibody was developed for electrochemical biosensing of GFAP with a dynamic linear response of 1-100 ng/mL.

The graphene zero bandgap makes it suitable in FET-based biosensors, important for the detection of DNA and other charged molecules, and, recently, for viruses' analysis too. (Dong X. et al., 2010). For instance, the SARS CoV-2- spike antibody was functionalized on the fabricated GFET for the detection of SARS-CoV-2 (Seo G. et al., 2020).

In addition to biosensing, GBNs are explored for the development of new probes and agents in bioimaging techniques, which are used in a broad range of biomedical applications such as the investigation of tissues at the cellular level or for diagnosis. Examples of bioimaging techniques include magnetic resonance imaging (MRI), X-ray computed tomography (X-ray CT), ultrasound, radio-wave technology, and others. In addition, optical and electron microscopy (laser scanning confocal microscopy and liquid cell electron microscopy, respectively) are used to highly magnify living tissues. GBNs can be exploited in this field either by loading fluorescence probes onto their surface or by their inherent optical features as Raman signals and quenching (Jampilek J. and Kralova K., 2021). Conversely to graphene, which has not photoluminescence due to its zero bandgap, GO emits a broad range of fluorescence from ultraviolet (UV) to near infra-red (NIR) and, therefore, it has been largely used in cancer cell imaging (Sun X. et al., 2018). In general, diverse GBNs are considered good candidates in the detection of biomolecules thanks to their high electron transport rate, elevated tensile strength, T resistance, as well as their large surface area which can be easily modified for several imaging tools, like PET or MRI (Llenas M. et al., 2019).

In addition, GBNs find applications in medical diagnostic thanks to their small size and unique physio-chemical features. They can be used in both sensing/enzymatic experiments and in primary prevention to follow and measure diverse disorders, from metabolic to neurodegenerative disorders. In terms of preclinical diseases, examples in the use of GBN for diagnosis include rGO-functionalized $BiFeO_3$ for signal amplification in the detection of prostate-specific antigen (PSA) (Zhou Q. et al., 2018), graphene-based sensors for the detection of dopamine, DA (Yao J. et al., 2019), and aptamer-modified graphene bioFETs for the detection of human immunoglobulin E (Ohno Y. et al., 2011).

The high absorption ability in the near NIR region of GBNs and their ability to generate heat efficiently is exploited in the PTT and PDT therapy. Until recently, the widely used PTT agent was represented by CNT, but Markovic et al., for the first time, showed as NIR-excited graphene NP have higher PTT sensitivity and antitumor effect on glioma cells compared to CNTs under the same irradiation state (Markovic Z.M. et al., 2011).

In cancer field, PTD therapy is a very low invasive approach which, generating ROS by irradiation of hydrophobic photosensitizers with visible or NIR light, exerts a targeted cytotoxic effect. However, this technique has some limitations due to the poor hydrophilicity of some photosensitisers as well as for the low anatomical access of target tissues. These issues are overcome with the use of GBNs. For instance, Zhou L. et al., developed a GO-based model for PDT where the hypocrellin A (HA) drug was immobilized on GO surface through π-πstacking interactions and hydrogen bonding (Zhou L. et al., 2011). In this system HA was efficiently internalized by tumour cells whose NIR irradiation led to their dead. Furthermore, a mesoporous silica grown on rGO nanosheets-PEG-conjugated iron-oxide nanocarrier for sonodynamic therapy and ultrasound hyperthermia has been recently proposed (Han S. et al., 2019). By using ultrasound instead of a laser, deeper tissues can be easily reached.

In recent years, the excellent properties of GBNs have started to be exploited in the field of tissue engineering (TE) and regenerative medicine (RM), emerging interdisciplinary fields with increasing developments involving the materials science/engineering and organ/cell transplantation fields (Menaa F. et al., 2015). TE produces biological functional tissues by using scaffold materials for extracellular matrix stimulation, thus providing the correct microenvironment for cell differentiation, proliferation, adhesion etc. Fully functional, and biomimetic alternative tissues have been developed starting from both natural and synthetic biopolymers like polycaprolactone (PCL), polyacrylamide, polyvinyl alcohol (PVA), etc. All these polymers together with other materials such as natural proteins (i.e., collagen, keratin, fibronectin), elastomer scaffolds and polysaccharides act as cell promoters in replacing the damaged tissues. Recently, in order to improve the electrical conductivity of these materials and their long-term life, nanomaterials like polypyrrole, silver, gold, CNT and others are also incorporated in substitute bone, cardiac, cartilage, skin, adipose, neural and musculoskeletal tissues (Llenas M. et al., 2019).

According to the TE of the nervous tissue, neural stem cells (NSCs) have been extensively used as a promising therapy for various CNS damages as Huntington disease, Alzheimer's disease (AD), Parkinson's disease (PD), traumatic brain injury, spinal cord injury etc. However, to completely recover a specific impaired neuronal tissue, NSCs must differentiate into an uniaxially arranged neuronal lineage with a precise set of proteins, wiring projections and ability to secrete certain neurotrophic factors. This ability is still an effort to reach in nervous TE. Thanks to its superior performance graphene-based scaffolds have been exploited in this field. A nice example is given by the recent development of a novel composite scaffold system with aligned electrospun silk nanofibers and conductive reduced graphene papers (AS-Rgop, Qing H. et al., 2018). This structure was used to directionally enhance the growth and differentiation of SH-SY5Y cells: the cell cultivation and the correct neurite development and branches was supported by the well-arranged directional matrix of nanofibers, while the biocompatibility and electrical conductivity of the system was assured by the rGO papers. In another study, GO has been used to obtain the oligodendrocytes differentiation starting from NSCs (Shah S. et al., 2014). 2D and 3D graphene-based scaffolds have demonstrated to be perfect substrates for culturing neurons which exhibit improved adhesion, good viability and enhanced neurite outgrowth and sprouting (Sahni D. et al., 2013; Li N. et al., 2011; Bendali A. et al., 2013). For instance, adult hippocampal NSCs grown on 3D graphene-based scaffolds seem to preferentially differentiate into neurons and astrocytes (Li N. et al., 2013).

The integration of diagnostic and therapeutic approaches, the so-called theranostic field, has acquired recent advances through the application of GBNs. Recently in this field, scientists developed a targeted delivery system with nGO conjugated to Poly-lactil-*co*-glycolic acid (PLGA) and loaded with the radiosensitizing agent 5-iodio-2-deoxyuridine (IudR) (Kargar S. et al., 2018). They integrated PTT with this radiosensitizer delivery to synergistically treat glioblastoma multiforme (GBM) and for the first time studied the combined effect of NIR and X-ray. According to the potential of GBNs in the improvement of therapeutic approaches, an excellent example is supplied by the glioblastoma therapy since GBM is one of the most malignant and lethal types of CNS tumour (Rock K. et al., 2012). Unfortunately, it is also the hardest to cure due to several issues including drug resistance, impaired drug delivery across the BBB, very delicate surgery procedures with the risk to damage healthy brain areas. The unique properties of graphene and its derivates make them very suitable for an engineered and multimodal therapeutic platform, such as co-delivery of multiple anti-cancer drugs with higher drug loading capacity and accumulation at the disease site beyond the BBB, thus enhancing the chemotherapy efficacy and decreasing the side effects. A promising strategy for chemotherapeutics delivery to malignant cells is to functionalize their surfaces

with ligands whose receptors are overexpressed only on glioma cells and BBB vascular-endothelial cells, like lactoferrin (Lf), a glycoprotein of the transferrin (Tf)-family. Recently, M. M. Song et al. developed a dual magnetic and molecular targeting delivery system loaded with the anticancer drug DOX (Song M.M. et al., 2017). They loaded Lf-conjugated GO with superparamagnetic FE_3O_4 NP obtaining greater efficacy and stronger cytotoxicity.

An easier BBB crossing can be achieved by the extremely small, planar and finite graphene nanoribbons (GNR) or the zero-dimensional graphene-QD, both representing novel and formidable candidates for chemotherapy. Perini G. et al. (Perini G. et al.,2020) showed as graphene-QD functionalized to DOX and delivered to *in vitro* glioma cells can increase the permeability of the cell membrane through van der Walls interactions, thus indirectly increasing the efficacy of the anticancer drug (Perini G. et al., 2020).Along with biomedical applications, studies on GBNs are also motivated by environmental health and safety (EHS) which have the same scientific goal: unravel the graphene-biological interface.

In the past ten years, the potential toxicity of GBNs has been deeply explored in the EU-founded Graphene Flagship and elsewhere, both *in vivo* and *in vitro*. It is fundamental to evaluate the safety profile of multiple graphene forms correlating their biological effects and impact on health to their physiochemical unique properties (lateral dimension, thickness, C/O ratio, functionalization, charge, surface, shape etc.). The latter are responsible for the fate of the GBNs in the body of an exposed organism, together with their acquired properties once they contact the surrounding environment. In fact, the intrinsic properties of the new material can influence their biodistribution, accumulation in some organs, degradation, and clearance, but the biological milieu with its proteins and biomolecules can alter these properties and, thus, the biological behaviour of the material towards different compartments (Ou L. et al., 2016; Scaini D. and Ballerini L., 2018). The portal of entry of the nanomaterial in animal models (airway exposure, oral administration, intravenous injection, intraperitoneal injection, and subcutaneous injection) is an important determinant of the material fate and degree of toxicity. The potential adverse outcome of the nanomaterial exposure is generally first performed at the cellular level since, once inside the cell, the material could undertake diverse routes like going to the nucleus or cytoplasm and may show certain cytotoxicity (**Fig. 2.3**). Anyway, the *in vivo* toxic effect of GBNs in animal models have also been investigated (Krishna K.V. et al., 2013; Kostarelos K. et al., 2017). Unfortunately, the results in the current literature are often contradictory and this is mainly due to the huge diversity of GBNs and their functionalization states. For example, in GBM cells, scientists reported that GO flakes did not cause cytotoxicity, conversely to graphene and rGO which caused sever genotoxicity to U87 cells. This discrepancy was attributed to rGO and graphene sharp, hydrophobicity and roughened edges through which can penetrate the lipid membrane directly affecting the nuclear DNA (Foo C.Y. and Fu R.Z., 2021). In other studies, the presence of oxygen-containing functional groups and electron clouds were evaluated in terms of anti-cancer effects of GBNs. Briefly, their lower amount in rGO compared to GO resulted in an increased number of delocalized electrons and, thus, the direct rGO interaction with cellular structures which are sensible to electrochemical potential, as cell membrane or mitochondria, Foo C.Y. and Fu R.Z., 2021).

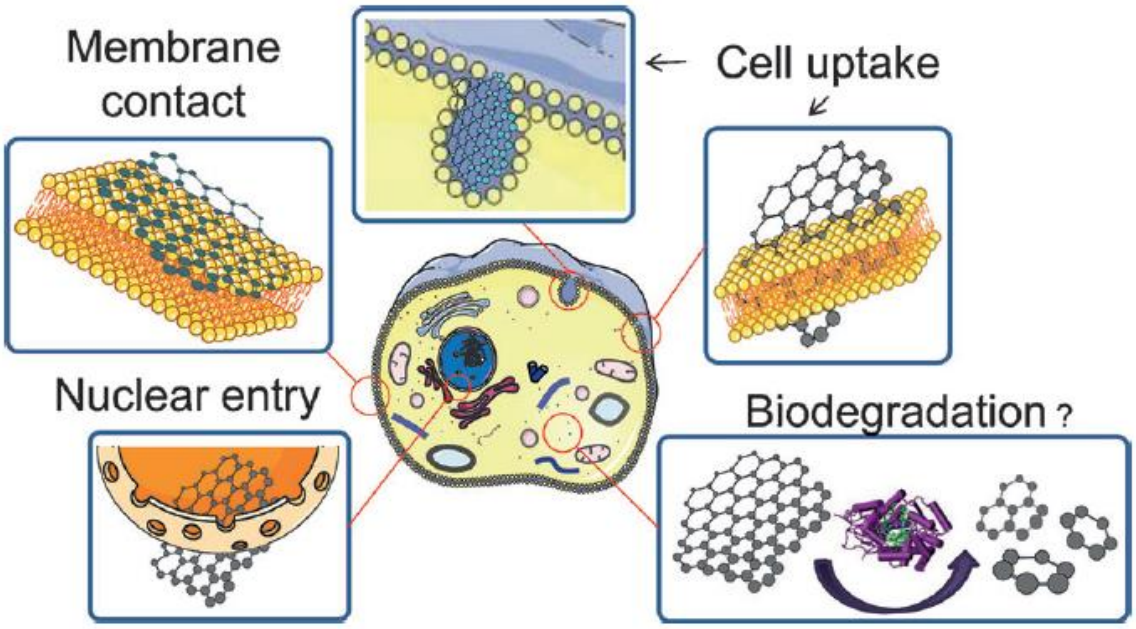

Figure 2.3 Possible interactions of GBNs at the plasma membrane level, during cell uptake at the nuclear membrane, and in the cytoplasm where degradation may occur. (Krishna K.V. et al., 2013).

As elsewhere mentioned, functionalization of graphene could improve its bioavailability, circulation lifetime and anti-cancer properties. It has been evaluated that PEGylation increases graphene stability and reduces toxicity under physiological conditions (Jampilek J. et al., 2021). Serval techniques are used to track GBNs in the body, such as TEM, Raman spectroscopy, isotopic labelling, and rare-earth element labelling. For instance, Liang S. et al. used the La/Ce dual elemental labelling method to follow the bioaccumulation, route, and clearance of PVP-GO *in vivo* (Liang S. et al., 2020). They showed as this system accumulates in the lungs, liver, and spleen and then it is cleared through the kidney. Similar results were reported for injected PEGylated-I-labelled graphene sheets (Yao Y. et al., 2020). GBNs degradation is another important topic in biomedicine and nanotechnological approaches which is also influenced by the physiochemical properties of the materials and their functionalization. In this regard, a Graphene Flagship study demonstrated that when GO is functionalized with natural HRP ligands (coumarin and catechol) is degraded at a larger extent (Kurapati R. et al., 2018). Zhang C. et al. studied the effect of graphene, GO and rGO on HRP stability showing that only rGO was able to preserve it presumably by scavenging superoxide radicals and avoiding the enzyme oxidation (Zhang C. et al., 2015).

Furthermore, in several studies PEGylation was demonstrated to reduce the cytotoxic effect of GO on macrophages, even if it has also been suggested that small, PEGylated GO flakes (200 nm lateral size) caused a strong cytokine response (Fadeel B. et al., 2018). In the screening of new materials is also crucial determine its interaction with the immune system and macrophages to understand if it can be eliminated or if its persistence can cause issues at certain levels. One of the first studies on that compared the effect of different sizes GO on murine and human macrophages (Russier J. et al., 2013). The smaller GO (130-270 nm) were internalized in a large amount and affected more the cell viability compared to the larger one (1320 nm), but all GO sheets arranged parallel to the cell membrane. Opposite results were achieved by another study that showed no

differences in cell viability comparing 350 and 200 nm-large GO, which were both internalized in an energy-dependent manner (Yue H. et al., 2012). A protocol for sterile production of GO with different lateral dimensions according to Hummers' method has been established by the Graphene Flagship and the cytotoxicity assessment was performed (Mukherjee S. P. et al., 2016). The study concluded that both small and large GO did not cause any toxicity once internalized by human macrophages. It is important to note that some GBNs have shown antibacterial activity and are currently being investigated for their usefulness as antibacterial systems (Zhang C. et al., 2015).

In conclusion, more studies are needed to elucidate the biocompatibility and biodegradation of diverse GBNs, both *in vitro* and *in vivo*, with the final objective to make them safer-by-design.

In neuroscience, GO finds relevant implications. Wang K. et al. (Wang K. et al., 2021) have recently demonstrated as a nano formulation of GO loaded with Dauricine (Dau), greatly reduced oxidative stress in both *in vitro* and *in vivo* AD models through increasing superoxide dismutase level and decreasing reactive oxygen species and malondialdehyde level. It also alleviated the cognitive memory deficits and brain glial cell activation in AD mice models. They demonstrated, therefore, that the combined anti-oxidative stress and anti-inflammatory effect of Dau together with the inhibition of misfolded aggregated amyloid-β proteins (Aβ) by GO have the potential to be an effective agent for a rapid AD treatment. A density functional theory study was recently performed for future AD drug development and chelation therapy (Liu C. and Luo X., 2021). In details, scientists tested the potential of diverse molecular and GO chelators, since the elevated levels of metals (copper, zinc, iron and aluminium) accumulate in senile Aβ plaques hampering cognitive functions and brain homeostasis. They calculated the binding energy of each molecule-metal complex showing as 8-hydroxyquinoline-2-carboxaldehyde 2-furoyl hydrazone (HQFUH) has copper, zinc, iron and aluminium ability, while GO complex with a 12.5 % oxygen concentration holds direct ability to chelate aluminium. Furthermore, graphene QD have been reported for their application in inhibiting Aβ peptides aggregation (Liu Y. et al., 2015). Importantly, they show important advantages compared to other drugs for AD treatment thanks to their low cytotoxicity, high biocompatibility and small size which permits the BBB crossing. According to this, Kajal Tak and colleagues synthesized graphene QD from the flowers of *Clitoria Ternatea* with the help of one-pot microwave-assisted green synthesis for the treatment of AD (Kajal T. et al., 2020) . Fundamental in neuroscience is the increment in spatio-temporal resolution to reveal the important working mechanisms of the brain. The high spatial resolution is essential to determine single unit activity to catch local information progression at the microscale, while, at the macroscale, it is important to resolve neural dynamics in large brain areas. The temporal resolution in the brain ranges from milliseconds and seconds regarding the spiking activity and synaptic transmission, to hours, months and years regarding memory and learning processes. Although the activity of different brain areas can be studied indirectly through non-invasive approaches like imaging tools (PET or MRI), the electrical basis of the brain activity makes electrophysiology essential for both fundamental and clinical applications (Guimerà-Brunet A. et al., 2021). Therefore, state-of-the-art neuroscience technologies represented by neuroelectronic interfaces with the nervous system, as multichannel neural probes or recording site architectures (i.e., intracortical implants), represent a decisive achievement. For instance, retinal or cochlear implants can improve the lives of patients with damaged receptors transforming sound and light stimuli into electrical signals (Rubinstein J.T., 2004; Sekirnjak C. et al., 2008). In efforts to cure several neurological disorders like PD (Benabid A.L. et al., 1987), epilepsy (Nuttin B. et al., 2003) or obsessive-compulsive disorder (Loddenkemper T. et al., 2001) has been used the so-called deep brain stimulation (DBS) or closed-loop interfaces between brain activity and motor outputs for spinal cord injuries (Capogrosso M. et al., 2016). This linkage

of the brain to computers through intracortical, scalp or subdural electrodes is referred to "brain-computer interface" (BCI), while "neurobionics" is the science of directly integrating electronics with the nervous system to repair or substitute impaired functions (Rosenfeld J.V. et al., 2017). Importantly, these neural interfaces must be compatible with the soft, easily damaged, elastic and curvilinear surface of the brain. In fact, flat or rigid materials of the conventional neural interfaces can damage living tissues limiting their *in vivo* applications. Moreover, chronic recordings need a high signal-to-noise ratio which has to be stable for years. To increment lifetime, the development of novel devices is based on valid testing protocols and a knowledge of the critical parameters controlling electrophysiological performance (Harris A.R. et al., 2019). Recent development in brain-compatible neural interfaces are based on the use of soft-nanomaterials which are more appropriate for complex neural circuit analysis and modulation, like polyimide (PI, polyethylene terephthalate (PET), and polydimethylsiloxane (PDMS) (Jeong Y.C. et al., 2020). Advances in nanoscience technology have a big impact on BCI. CNT and other nanomaterials have been used in novel electrode designs with anti-inflammatory coatings or mechanically flexibility to minimise micromotion (Schouenborg J., 2011). In order to improve neural signal recording and stimulation, conducting polymers as polymer poly (3,4-ethylenedioxythiophene) or PEDOT have been widely investigated as coating materials for implantable metal electrodes because of their mixed high electronic-ionic conduction, electrochemical stability and high biocompatibility (Bodart C. et al., 2019).

Noticeable neural interfaces include also light-emitting diode (LED) or μLED modules as light sources for optogenetic (Jeong Y.C. et al., 2020), as well as devices for drug release (Jeong Y.C et al., 2020, **Fig 2.4**). Some of them include the flexible, paper-like brain surface wrapping electrode array which read information from a wide-range of cortical surfaces, insertable wrapping electrodes beneath the skull (iWEBS) and the flexible vertical μLED (f-VLED) system insertable beneath the skull (iLEBS), which write information on the brain (**Fig. 2.4**, Jeong Y.C. et al., 2020). In addition, self-powered flexible energy harvesters and closed loop (MIDAS) and feedback control systems (Park S.G. et al., 2018) make neural interfaces more useful in behaviour or in the control of specific symptoms (**Fig. 2.4**).

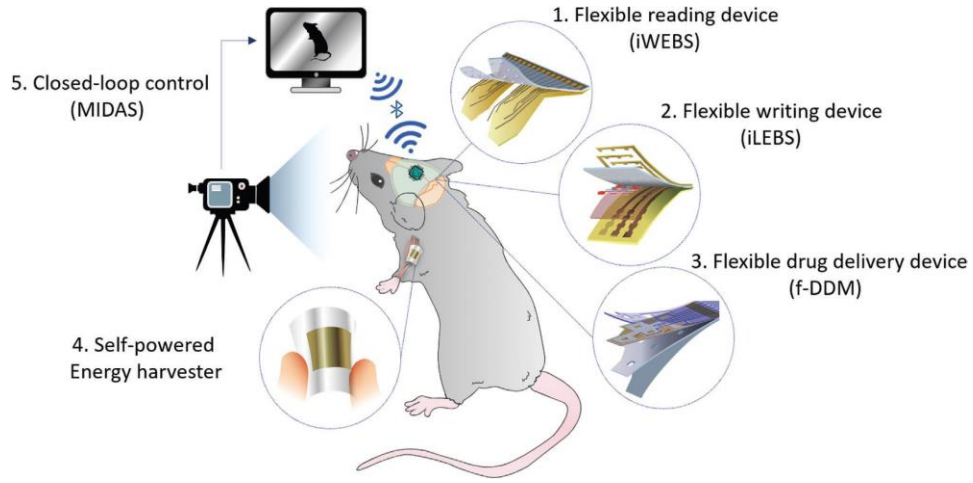

Figure 2.4 Bio-compatible materials for use in interface for the modulation of neural circuits and behaviour (Jeong Y.C. et al., 2020).

3. GBNs IN NEUROBIOLOGY: A FOCUS ON GRAPHENE OXIDE AND SMALL GRAPHENE OXIDE

GO surface allows a range of chemical techniques for attachment of functional groups for electrical/thermal conductance and optical transparency. GO surface modification results in important enhancement of its physicochemical properties allowing applications in various fields of biomedicine, including tissue engineering, drug delivery, anticancer therapy and bioimaging (Cao W. J. et al., 2020; Jagiello J. et al., 2020; Jampilek J. et al., 2021), as well as in green technology areas like energy storage and nuclear waste (Dideikin AT and Vul' AY, 2019).

The production of GO by the known methods of Hoffman, Staudenmaier and Brodie, are based on the application of potassium chloride and nitric/sulphur acid as strong oxidizing agents. The most popular method by Hommers-Offeman uses a mix of concentrated H_2SO_4, $NaNO_3$, and $KmnO_4$ generating a yellow-coloured aqueous suspension of GO particles (Park S. and Ruoff R.S. 2009). Modern methods of GO preparation are instead based on exfoliation and oxidation of graphite (Rothemund P.W, 2006).

GO sheets are highly hydrophilic thanks to the negative surface charged offered by the oxygen-containing functional groups such as -OH, -COOH, and epoxide groups which contribute to its optical and electronic properties too. GO generates stable aqueous dispersions in diverse polar solutions, while graphene tends to aggregate. Conversely, GO is stable in diverse organic solvents owing to hydrogen bonding between hydroxyl and epoxy groups on their surface and solvent interface (Dideikin AT and Vul' AY, 2019).

GO has both aromatic (sp^2) and aliphatic (sp^3) domains due to the introduction of oxygen atoms, which further increases alternative types of interactions with the surface. The -COOH group permits esterification, covalent acylation and amidation for functionalization on both sides, but strong cross-linking of GO sheets are also possible through the nucleophilic opening of the epoxide ring. In addition, non-covalent functionalization of GO surface through cation–π or van der Waals interactions allow its attachment to nucleic acid or proteins for bio sensing and other cargo molecules (Georgakilas V. et al., 2016).

Biocompatibility, processing, and toxicity of GO and derivates in the mammalian tissues have been largely discussed and it has been proven their cytocompatibility both *in vivo* and *in vitro*. Conversely to graphene, which can result in inflammation, cytotoxicity, and genotoxicity due to the less steric hindrance, GO and derivates are easily internalized by cells and show peculiar antibacterial properties for TE and RM. During the last decade, several studies reported the use of GO in drug delivery and cancer therapy. In fact, the covalent and non-covalent modifications of GO are responsible for UV, pH, T, visible light, electric fields etc. rendering GO with "smart-tumour responsive properties" (Sharma S. et al., 2020). GO nanocomposites are largely used also for the PDT and PTT applications for cancer treatments. In fact, the delocalization of its long-chain aromatic pi-electron clouds allows the absorption in the NIR-region which, in turns, produce heat and subsequent cell death (Sharma S. et al., 2020).

As previously mentioned, 3D scaffolds based on GO or rGO have widely been used in regenerative medicine too, since they were shown to boost proliferation and differentiation of stem cells, even if more studies are needed to overcome some issues related to long term toxicity, immune response, biotransformation and biodistribution. For example, GO-based hydrogels allow the differentiation of embryonic NPCs towards both glia and neurons facilitating neurite arborization and synaptic connections (Rauti R. et al., 2016).

GO is characterized by different lateral dimensionality. In general, large GO (lGO) has > 1000 nm lateral dimension, while small GO (s-GO) has< 500 nm lateral dimension.

GO with diverse lateral dimensions has been tested *in vitro* to study its interference with neural subcellular compartments. Importantly, these dimensions influence the nanomaterial effect and outcome on neuronal substrates in a radical way. Results showed lGO toxicity in reducing the viability of hippocampal neurons, while s-GO interfered with their synapses but did not affect cell viability (Rauti R. et al., 2016; Rauti R. et al., 2019). These studies showed that s-GO effects on synaptic activity were specifically and transiently targeting glutamatergic excitatory transmission, which was downregulated, while the inhibitory one was not affected (Rauti R. et al., 2016; Rauti R. et al., 2019). This specificity was reported *in vitro* and *in vivo* (Rauti R. et al., 2016; Rauti R. et al., 2019; Cellot G. et al., 2020) The same result was obtained in another recent study which tested s-GO on amygdala neurons in both *in vitro and in vivo* conditions (Franceschi B. A. et al., 2021).

The mechanism of s-GO modulation of synaptic activity is not known, even if the dynamic of presynaptic vesicle recycling seems to be involved, and this has been confirmed in both hippocampal, (Rauti R. et al., 2016; Rauti R. et al., 2019; Secomandi N. et al., 2020) and amygdala cultures (Pati et al., *in preparation*). Rauti R. et al. (Rauti R. et al., 2019) exposed hippocampal cultured neurons to a growth medium containing nanosheets of graphene or s-GO at a low concentration (1 to 1o ug/mL, Fonnum F. 1984; Hirai K. et al., 1999; Palazzo E. et al., 2014) and for 1 week. They used both patch clamp and fluorescence imaging to study the effect of these materials on both the synaptic signalling and the astrocyte-neuron communication.

Bramini M. et al., (Bramini M. et al., 2016) tested monolayer GO flakes with larger dimensions (100-1500 nm) which were found free in the cytoplasm, in contact with the neuronal membranes, and internalized through the endosomal pathway. The larger dimension of the used nanomaterial could justify their data regarding the small enhancement of inhibitory postsynaptic activity simultaneously at the inhibition of excitatory transmission, as well as the altered lipid and protein content of primary cortical neurons. In fact, this was accompanied by induction of macroautophagy and a modified Ca^{2+} homeostasis which affected both excitatory and inhibitory neurons. An independent research group (Kang Y. et al., 2020) has recently confirmed the same results of Bramini et al (Bramini M. et al., 2016) regarding the impact of lGO on Ca^{2+} homeostasis and cytoskeleton following the nanomaterial-synapses interference. Researchers chronically exposed neurons to rGO which was internalized by them and oxidized via ROS to GO which, in turns, acted as a neurotransmission modulator. In fact, it depressed neurotransmission by disturbing the actin cytoskeleton and, therefore, blocking the synaptic vesicles docking and fusion of excitatory synapses.

Three dimensional organotypic spinal cord cultures have also been used for the investigation of central nervous system (CNS) tissue reactivity and glial responses upon long-term exposure to s-GO nanosheets of diverse doses (Musto M. et al., 2019). With this aim, scientists explored the effect of chronic s-GO accumulation on innate immunity focusing on resident microglia, in both organotypic slices and isolated neuroglia culture. Through patch clamp recordings of ventral interneurons and confocal imaging they demonstrated as the accumulation of the nanomaterial led to a rection of the microglia population which, in turns, may trim down synaptic activity, even if no active pro-inflammatory responses or neuronal cell death were detected.

However, these differences compared to the effect of s-GO on hippocampal neurons (Rauti R. et al., 2016; Rauti R. et al., 2019) could depend also on the modified astrocyte physiology and

subsequent astrocyte-neuron communication induced by the nanomaterial which were observed *in vitro* (Chiacchiaretta M. et al., 2018). These authors investigated the long-term exposure of primary rat cultures to GO flakes (100-1500 nm size) observing important functional alterations in astrocytes after GO internalization (i.e., upregulation of Na^+-dependent glutamate uptake, significant for the control of extracellular homeostasis). They also investigated the effect of pre-treated astrocytes on cocultured primary neurons showing an increment in both density and excitability of inhibitory synapses. Therefore, in the CNS, not only the synaptic activity but also other modes of interneuron communication systems can potentially be altered by GO, as the astrocyte-neuron interaction. Musto M. Et al. (Musto M. et al., 2019) further confirmed this theory exploring the ability of astrocytes to release synaptic-like microvesicles (MVs), which contribute to intercellular communication in pure glial cultures after 6-8 days-exposure to s-GO and in the absence of cell toxicity. The same authors extensively demonstrated through different experimental models that the target of s-GO flakes is the vesicles release at the glutamatergic synapses which is modulated by the nanomaterial without interfering with complex biochemical pathways (Rauti R. et al., 2019). In cultured hippocampal neurons, scientists performed a fine electrophysiological study through the study of miniature postsynaptic currents (mPSC) and pair pulse stimulation, thus directly investigating the interference of s-GO with the machinery of vesicle release at the presynaptic terminal (Raastad M. et al., 1992; Zucker R.S. 1989; Manabe T. et al., 1993; Debanne D. et al., 11996) By local delivery of s-GO at the recorded neurons, they showed as the nanomaterial sheets ultimately deplete evoked release at the glutamatergic synapses. Furthermore, the authors confirmed the same specific s-GO effect on more mature glutamatergic synapses of acute hippocampal slices, scaling up the complexity of the tissue to the third dimension.

Besides *in vitro* experiments to test the effect of s-GO to interact with the smallest components of the brain, like synapses and vesicles, and their potential use to manipulate neuronal function, also *in vivo* exploration of this nanomaterial has been extensively conducted (Rauti R. et al., 2019; Cellot G. et al., 2020; Di Mauro G. et al., 2021). Stereotactic injections of s-GO into the dentate gyrus of the hippocampus of juvenile rats led to a significant and selective reduction of excitatory synaptic activity compared to saline injection with minimal tissue reaction or reduction in the number of synapses, as demonstrated by 48h-after surgery *ex vivo* patch clamp recordings from brain slices (Rauti R. et al., 2019). Importantly, this dampened glutamatergic signalling in the CNS was transient and reversible since it recovered 72h after the treatment, supporting a direct and mechanical interaction at the presynaptic plasma membrane. This result is in accordance with further investigations where even the downstream outcome in modulation of behaviour relying on the activation of s-GO-exposed synapses was studied (Cellot G. et al., 2020; Franceschi B.A. et al., 2021). In the first work, early-stage zebrafish larvae were used as an *in vivo* model to test s-GO effect on the nervous system physiology (Cellot G. et al., 2020). In details, once s-GO was microinjected in the spinal cord of embryonic zebra fish larvae, the excitatory synaptic transmission of the local neurons was reduced without any effect on spinal cell survival. Notably, the locomotor behaviour of fish which depends on the spinal network activity, that is the swimming activity, was also modified, paving the way for use of s-GO as a modulator of CNS function and related behaviours. Moreover, further *in vivo* patch clamp recordings of the synaptic input to motor neurons during fictive locomotion (electrical activity which correlates with bouts of locomotor behaviour in paralysed fish) confirmed the downregulation of glutamate release from the presynaptic terminals as mode of s-GO action. Interesting, Di Mauro G. et al., (Di Mauro G. et al., 2021) noticed as different specific GO chemical properties (diverse oxygen/carbon ratios obtained by GO thermal reduction) differentially influence the sensory-motor neurophysiology of early-stage zebrafish larvae and, therefore, their

locomotor behaviour. In particular, GO nanoflakes downregulated their swimming performance, while rGO boosted it, probably because they interfere with different signalling pathways.

The test of s-GO efficacy *in vivo* is the ultimate potential of any s-GO in the development of innovative nanomaterial-based therapeutic tools and medical devices which targets specifically the glutamatergic synapses which are pathologically dysregulated or exceeded in several diseases (i.e., anxiety-related disorders, obsessive-compulsive disorders, seizures, epilepsy, tumour, Tourette syndrome, autism, and others, Brocke K. S. et al., 2020; Naaijen J. et al., 2017; Macaster F. P. 2010; Barker-Haliski M. and White S. H., 2015). A relevant study has explored the translational potential of s-GO to target selectively the glutamatergic synapses in a post-traumatic stress disorder (PTSD) rat animal model, which is characterized by a hyper-excitability (or long-term potentiation, LTP) of glutamatergic neurons in the lateral amygdala (LA) (Franceschi B.A. et al., 2021). Scientists demonstrated that a single stereotactic injection of s-GO precisely to the LA nucleus and during the consolidation of the pathological plastic changes, was able to hamper LA glutamatergic transmission and to prevent the PTSD-related behavioural response. They combined behavioural tests with tissue histology, *ex vivo* electrophysiology and confocal analysis demonstrating as s-GO was able to prevent the LTP of amygdala excitatory synapses *in vitro*, thus impairing long-term aversive memory retrieval and long-lasting anxiety related responses *in vivo*. According to the *in vivo* administration of GBNs, it is worth to mention that a lower tissue reactivity was observed in s-GO injected animals compared to saline treated ones (Portioli C. et al., 2020) suggests a neuroprotective effect exerted by the nanomaterial against the tissue damage usually observed upon surgery. The hyperexcitability of the amygdala glutamatergic neurons is strictly correlated to anxiety-related pathologies and this topic will be deeply explored in the following chapters.

Of course, the GBNs translation in therapy requires more steps besides the *in vivo* validation of the nanomaterial, as the optimization of its best dose and administration way. Regarding the administration route, intracranial brain injection is not the only way to enter the CNS and cross the BBB. In fact, several studies proved alternative and successful methods to cross the BBB, like rat tail vein injection (Sweeney M. D. et al., 2019; Mendoça M. C. p. et al., 2015,156) or nasal/oral administration (Newman L. et al., 2020). The lateral dimension of the nanomaterial seems to be important in the outcome of uptake and transportation through the BBB, with larger size nanosheets showing higher permeability than small size ones (Su S. et al., 2020).

The ability of s-GO to influence and modulate the synaptic activity of neurons makes it the most promising and interesting among the GBNs components for innovative pharmacological applications in the field of nanotechnology and precision medicine to treat several CNS disorders. Moreover, the further functionalization of s-GO could be exploited for drug delivery systems, allowing to target specific sites in the brain and release the therapeutic agent in a controlled way. In this regard, recent applications, and state-of-the art-studies of engineered GBNs for the treatment of brain pathologies have extensively been reviewed by Cellot G. et al., with a particular focus on untreatable, paediatric disorders (Cellot G. et al., 2022).

4. THE AMYGDALA

"We do not run because are afraid, but we are afraid because we run" (James W., 1890). These are the words of William James who, exactly as C.G.Lange, suggested that emotions accompany our physiological responses to the same stimuli, the external ones. Therefore, by the

simple examination of the physiological responses to the environment, it is possible to study emotions. Around the same historical period, Charles Darwin gave a strong biological contribution to emotions in "Expression of Emotions in Men and Animals" indicating that through the examination of animal behaviour it is possible to study human emotions (Darwin C., 1872).

"Responses that occur when we defend against danger, interact with sexual partners, fight with an enemy, or have a tasty bite to eat promote the survival of individuals and their species. Emotional responses are thus inherently interesting and important. So, what happened? Why did research on the brain mechanisms of emotion come to a halt after mid-century?" J. Ledoux (Ledoux J., 2020).

Critically to the James-Lange theory, Cannon and Bard developed the first neurophysiological theory of emotions in 1920 indicating the hypothalamus and its projections to the cortex and brain stem the original locus of emotions (Cannon W.B., 1927). Later, Papez and McLean added the forebrain circuits to the emotional circuitry, the so called "visceral brain" or limbic system and included also the amygdala (Mclean P.D., 1949), an almond-shape structure deep within the temporal lobe (**Fig 4.1**).

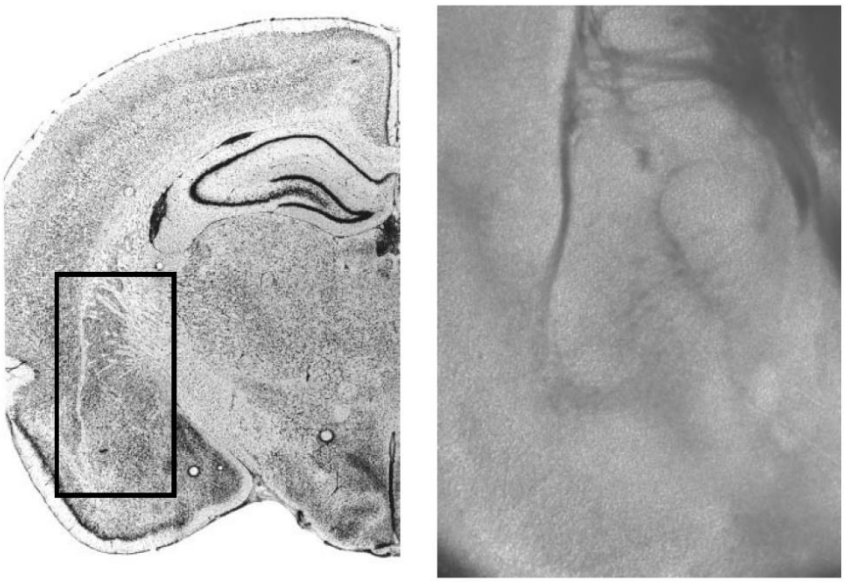

Figure 4.1 An example of the amygdaloid region as it appears in acutely prepared coronal sections. Left: a Nissl-stained hemisection of a rat brain around bregma-3. The areas shown in the outlined region are shown in an acutely prepared coronal brain slice as it appears under brightfield illumination (right). [Adapted from Paxinos G. and Watson C. The Rat Brain in Stereotaxic Coordinates (2nd ed.). Sydney, Australia: Academic, 1986.]

Soon after the discovery of Kluver and Bucy that several emotion abnormalities ("psychic blindness" with access of anger or fear, hyperorality, loss of social interactions, hypersexuality…) occur in monkeys following medial temporal lobe damage (Klüver H. and Bucy P. C. 1973), it was demonstrated by Weiskrantz L. that an amygdala damage could generate them too (Weiskrantz L., 1956). In fact, in 1956, once observed the impairment in acquiring behavioural responses to shock-predictive clues, Weiskrantz L. concluded by saying that "the effect of amygdalectomy is to make

difficult for reinforcing stimuli, whether positive or negative, to become established or be recognized as such" (Weiskrantz L., 1956).

Even if the amygdala is not the only brain area implicated in emotions and emotions are not the only amygdala's functions, no other brain areas has been so consistently implicated in the emotion system from that moment. Moreover, circuitries and functions of the amygdala have been well-conserved across evolution (McDonald AJ., 1998). Although some species variability, non-mammalian beings like fishes, birds or reptiles possess an amygdala-like area too, which is very similar to the mammalian amygdala in terms of functions and circuitry (Jarvis E.D. et al., 2005; Johnston J.B., 1923; Lanuza E. et al., 1998).

Given that the amygdala is involved in several diseases including autism, addiction, anxiety disorders and others, the knowledge of its circuitry is of enormous importance. Much of our understanding about the amygdala role in emotions come from animal studies on Pavlovian fear conditioning and its consequences which are represented by a variety of autonomic and hormonal responses. Fear is a normal and common reaction to threatening situations in daily life, but when it becomes greater than normal or inappropriate, a fear/anxiety disorder starts. A classical fear conditioning task occurs when a neutral stimulus such as a tone or a light (the conditioned stimulus, CS) is paired with an aversive stimulus (a foot-shock). The latter produces a fear response or behavioural state which typically occurs in the presence of danger, such as defensive behaviours (freezing or escape responses), autonomic nervous system responses (changing in heart rate and blood pressure), neuroendocrine responses (release of hormones from the pituitary and adrenal glands) etc. (LeDoux J., 2003). These outcomes are not voluntary or learned, but they are innate, species-related, and automatically expressed in the presence of appropriate threats or stimuli. Importantly, following few numbers of pairings (neutral and aversive stimuli), the neutral stimulus alone becomes sufficient to elicit such behavioural states and this learned behaviour is long lasting and rapidly acquired (**Fig 4.2**). Animals also exhibit fear when return to the chamber where the tone-shock pairing, or shock alone occurred (Maren S. et al., 1997; Phillips R. G. and LeDoux J. E., 1992). This is the so-called contextual fear conditioning and requires both amygdala and the hippocampus.

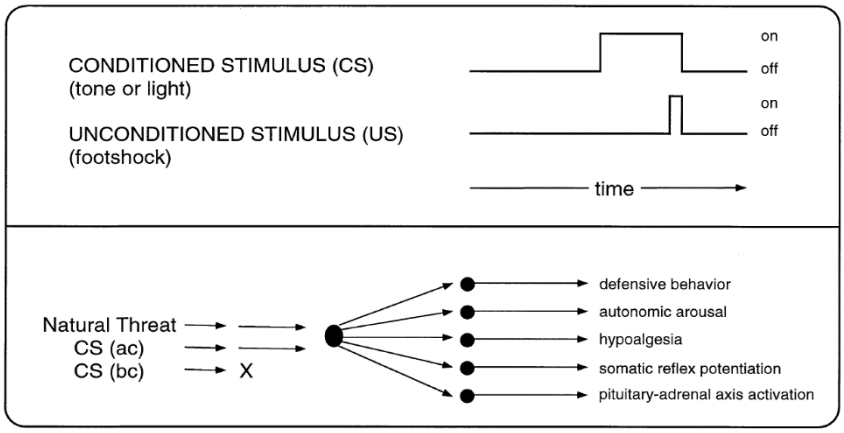

Figure 4.2 Fear conditioning involves the temporal pairing of an innocuous conditioned stimulus (CS), such as a light or tone, with a noxious unconditioned stimulus, typically foot shock (above). After conditioning (ac), but not before (bc), the CS enters fear network and activates defence systems typically activated by a natural threat, such as a predator (below, LeDoux J., 1998).

Because of the simplicity of that learning task and the physiological similarities between human and animal fear, the study of fear conditioning represents an important model to understand the pathophysiology of anxiety disorders in humans as well as learning and memory consolidation processes.

4.1 NEUROANATOMY AND NEUROPHISIOLOGY OF THE AMYGDALA

In the early 19th century, a group of cells was described by Burdach which are nowadays known as the basolateral complex. Conversely to the past anatomical literature which considered the amygdala as a structure with just two subareas (the basolateral and the cortico-medial area), nowadays the amygdala is conceived as a complex brain structure with several nuclei, each with its own subdivisions and unique set of afferent and efferent connections, as well as internuclear and intranuclear connections.

Price et al. (Price J.L. et al., 1987) classified the rat amygdaloid complex into three major groups (**Fig. 4.1.1**): the basolateral (BLA) group or complex (a deep group including the basal, B, or basolateral, BL, nucleus, the lateral nucleus, LA, and accessory basal nucleus, AB, or basomedial nucleus), the cortical-like group (a superficial group including the cortical nuclei and the nucleus of the lateral olfactory tract, NLOT), and the centromedial group (medial, M, and central, CeA, nuclei, as well as the amygdaloid part of the bed nucleus of stria terminalis, BNST).

The LA is subdivided in the smaller celled dorsolateral subdivision, the larger celled ventrolateral subdivision, and the medial subdivision, while the BL is subdivided into the magnocellular subdivision and the intermediate and parvicellular subdivisions. Ventrally to the BL, the AB comprises the magnocellular, the intermediate and the parvicellular subdivision (Pitkänen A., 2000; Pitkänen A. et al., 1997). Together with the NLOT, the superficial and layered cortico-like nuclei comprise also the bed nucleus of the accessory olfactory tract (BAOT), the anterior and posterior cortical nucleus (CoA and CoP, respectively), and the periamygdaloid cortex (PAC). The latter is further subdivided into the medial division, and the sulcal division (Pitkänen A. et al., 2000; Price JL et al., 1987). Finally, the CeA has four divisions: the capsular subdivision (CeC), lateral subdivision (CeL), intermediate subdivision (CeI), and medial subdivision (CeM) (McDonald A.J., 1982; Jolkkonen E. and Pitkänen A., 1998). The M has also four subdivisions: rostral, central (dorsal and ventral), and caudal (Sah P. et al., 2003). In this classification, other amygdaloid nuclei have to be mentioned: the anterior amygdala area (AAA), the amygdalo-hippocampal area (AHA) with its lateral and medial subdivisions, and the intercalated nuclei (I), small, clustered nuclei within the fiber bundles which separate the different amygdaloid nuclei (Sah P. et al., 2003). Recently, it has been argued that the amygdala complex is a functionally and structurally heterogenous group which must be divided into four functional systems: the frontotemporal system comprising the BL, the autonomic system including the centromedial nuclei, the main olfactory and the accessory olfactory systems with the cortico-like group (Swanson L.W. & Petrovich G.D., 1998).

According to afferent and efferent connections of the amygdala, several works demonstrate as they are very similar across species, even if the physiology of the rat amygdala has been the most explored through anterograde and retrograde tracers (McDonald A.J., 1998; Pitkänen A., 2000; Sah P. et al., 2003).

The main amygdala inputs can be grouped into sensory inputs which come from the sensory areas of cortex and thalamus (olfactory, somatosensory, gustatory and visceral, auditory, and visual modalities), polymodal inputs whose sources include hippocampus perirhinal or prefrontal cortex,

and inputs which arise from the hypothalamus and brain stem and are related to autonomic and behaviour systems (**Fig. 4.1.2**).

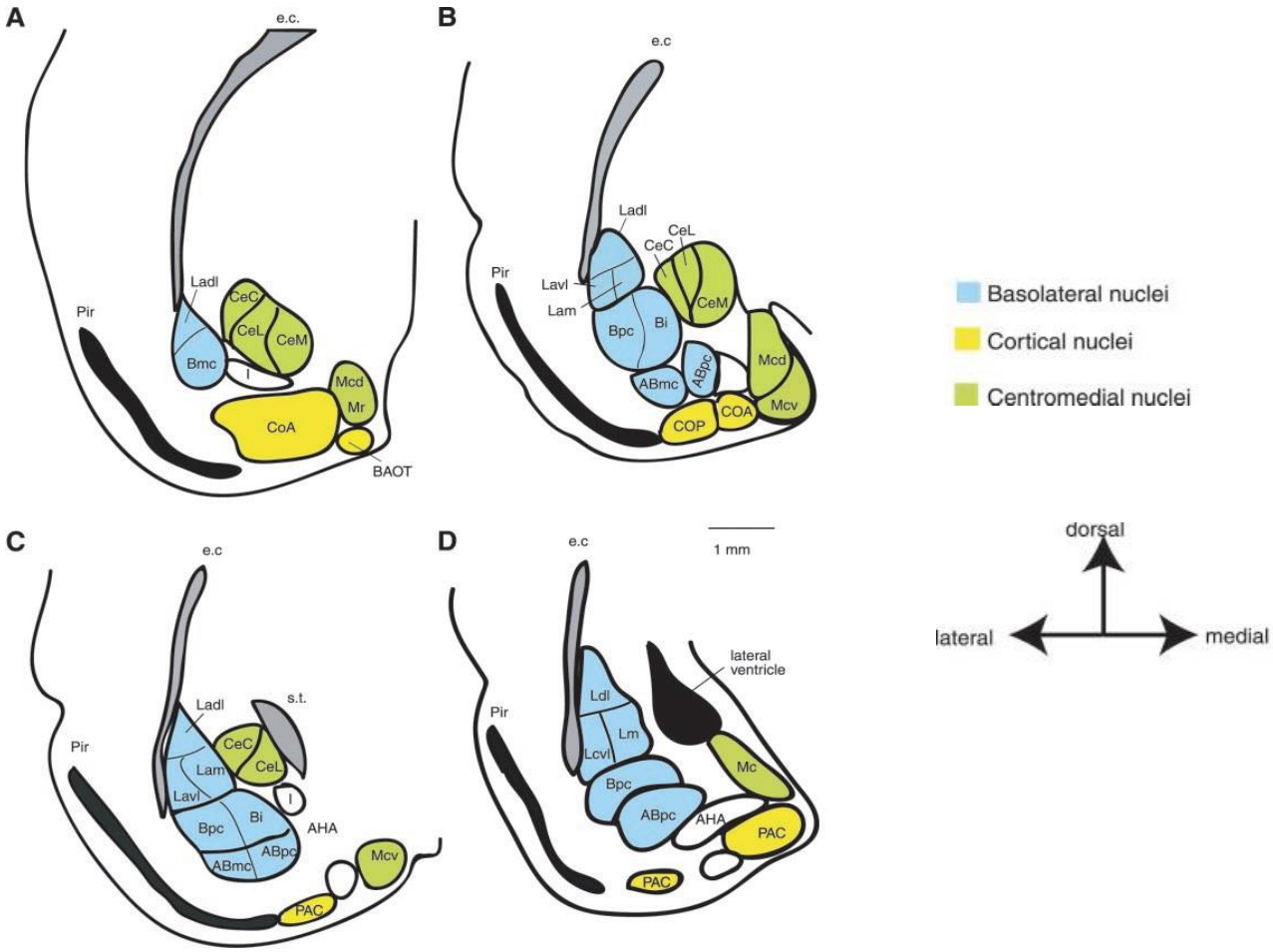

Figure 4.1.1 Nuclei of the rat amygdaloid complex. Coronal sections are drawn from rostral (A) to caudal (D). Abmc, accessory basal magnocellular subdivision; Abpc, accessory basal parvicellular subdivision; Bpc, basal nucleus magnocellular subdivision; e.c., external capsule; Ladl, lateral amygdala medial subdivision; Lam, lateral amygdala medial subdivision; Lavl, lateral amygdala ventrolateral subdivision; Mcd, medial amygdala dorsal subdivision; Mcv, medial amygdala ventral subdivision; Mr, medial amygdala rostral subdivision; Pir, piriform cortex; s.t., stria terminalis. (Sah P. et al., 2003).

The major source of sensory information to the amygdaloid complex arises from the glutamatergic projection of layer V pyramidal neurons of the cerebral cortex, or, more generally, from unimodal association areas of the temporal cortex (Ottersen O.P. et al., 1986; Amaral D.G and Insausti R., 1992). These sensory projections end to the lateral amygdaloid nucleus and have been implicated in a variety of sensory systems together with emotional learning and processes. For example, the auditory processing modality of the LA originate in a thalamic cell population called posterior intralaminar nucleus which receives auditory inputs from the inferior colliculus and is linked to medial geniculate body, MGB (Ledoux J.E. et al., 1990). Since the importance of the LA in emotional and sensory functions, a lesion of it produces disruptive outcomes disconnecting the entire amygdala from the environmental inputs. The effect of this disconnection is evident in several behavioural tasks and emotional responses, like the classical fear conditioning (LeDoux J.E.,

Cicchetti P. et al., 1990). In the past, several studies in non-human primate showed as subtotal lesions of the LA lead to the loss of fear and the Kluver-Bucy syndrome because of interrupted sensory information to the central nucleus of the amygdala (Zola-Morgan S. et al., 1991).

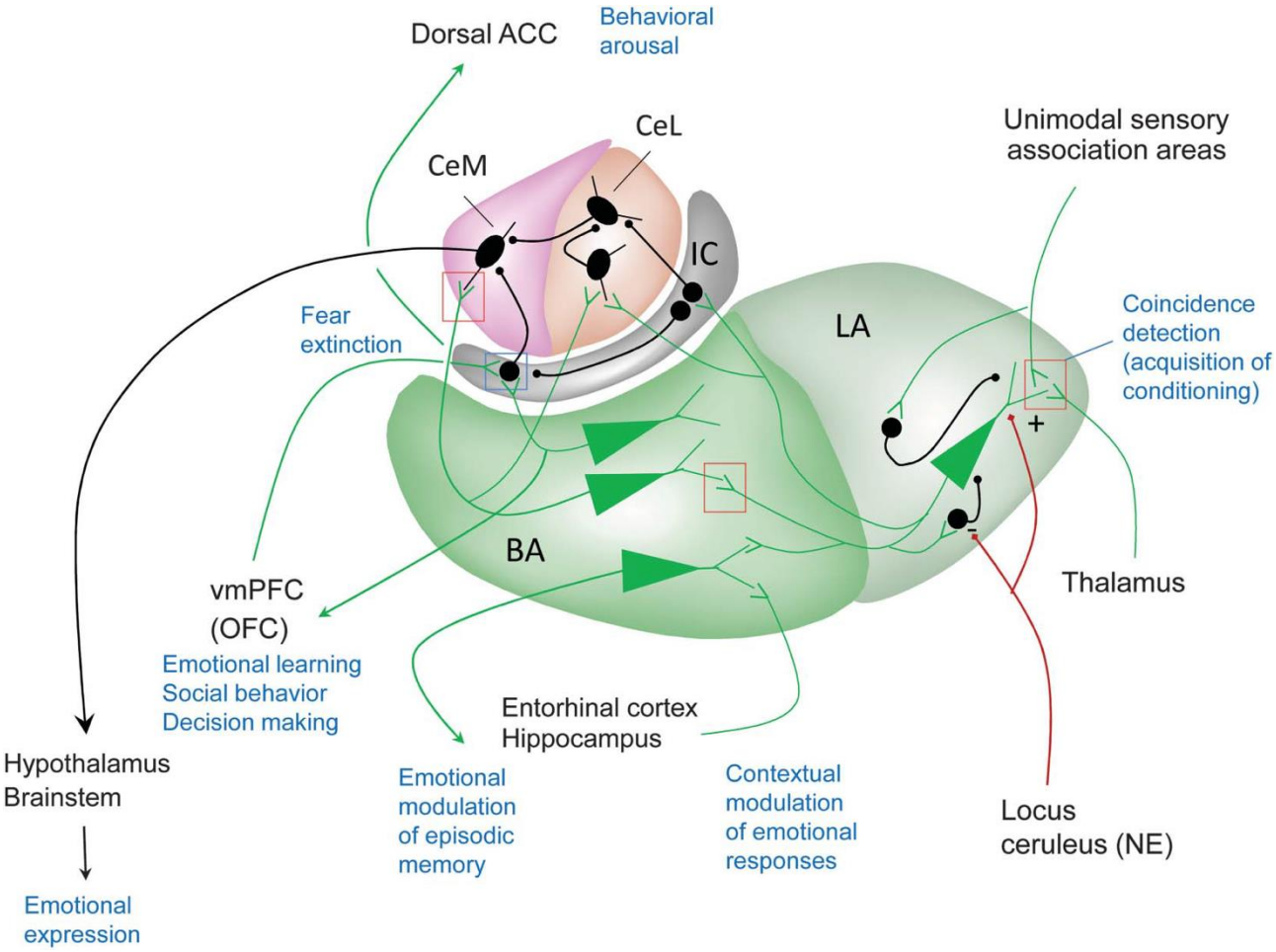

Figure 4.1.2 Inputs from cortical sensory areas and thalamus terminate primarily in the LA; Pyramidal neurons of the lateral nucleus (LA) receive convergent excitatory synaptic inputs conveying conditioned and unconditioned stimuli and are the site of synaptic plasticity responsible for acquisition of conditioning. Monoamine neurotransmitters released in emotional situations, such as norepinephrine (NE) released from projections of the locus ceruleus, positively modulate plasticity of excitatory synapses in LA neurons both directly and via inhibitory effects on feedforward GABAergic interneurons. The LA projects to the BA; the BA is interconnected with the ventromedial prefrontal cortex (vmPFC) including the orbitofrontal cortex (OFC) and ventral anterior cingulate cortex (ACC) as well as the dorsal ACC hippocampal formation, and striatum and projects to the CeM, which provides the main output of the amygdala to the hypothalamus and brainstem, including the parabrachial nucleus. Control on the CeM involves multiple disinhibitory networks mediated by different subsets of GABAergic neurons in the IC and CeL. A subset of BA neurons project to the dorsal anterior cingulate cortex (dACC), which is also engaged in fear conditioning and is involved in behavioral arousal. Fear extinction involves an interactive network that includes the amygdala, the ventromedial prefrontal cortex (vmPFC) including the orbitofrontal cortex (OFC), and the anterior hippocampus. The vmPFC participates in fear extinction via an excitatory input from the OFC to GABAergic neurons of the IC, which gate the BA inputs to the CeM. (Benarroch E. E., 2016)

Besides fear conditioning, the lateral nucleus of the amygdala has also been implicated in conditioned place preference learning in rodents, an appetitive emotional reaction proven by suppling reinforcing stimuli (i.e., foods) in a certain place. In this case, the amygdala lesions interrupt the flow of sensory information from the *nucleus accumbens* whose lateral/basolateral areas are associated to reward by connecting with DA containing terminals (Ldoux J.E., 1992). Together with acoustic inputs to the amygdala, also visual ones originate from thalamic and high-order visual areas (Sah P. et al., 2003), while gustatory and visceral information arise from their primary areas of the anterior and posterior insular cortices as well as subcortical structures. They all reach the dorsal subdivision of the LA, central nucleus, and posterior basal nucleus. Conversely, primary somatosensory areas send few projections directly to the amygdaloid complex, which, instead, receives somatosensory afferents via the dysgranular parietal insular cortex of the parietal lobe.

Information regarding behaviour and reward circuits in rats converge to the prefrontal cortex whose afferents reach the basal nucleus of the amygdala. The latter is the main target of hippocampal inputs too, while the central, lateral, and medial nuclei receive inputs from the hypothalamus. Finally, brain stem inputs (midbrain, pons, and medulla) have the central nucleus as the major target. The central nucleus of the amygdala plays important roles in the expression of behavioural and autonomic responses, as it regulates the cholinergic arousal system of the neocortex. In fact, the cholinergic neurons of the nucleus basalis which project to the neocortical level permit emotional information evolution by the amygdala to affect memory, attention, perceptual and other cognitive pathways occurring at the neocortex.

Regarding efferent projections from the amygdala, the basolateral complex (AB, B, LA) sends information from glutamatergic pyramidal-like neurons to hippocampus, perirhinal cortex and *nucleus accumbens* (Parè D. et al., 1995). The reciprocal interactions between amygdala and hippocampus have strong implications for the emotional regulation of episodic memory: inputs from the amygdala to the hippocampus, supplying an event-related emotional importance, support episodic memory consolidation; inputs from hippocampus to the amygdala furnish contextual information regarding such event. The central nucleus is important in the activation of autonomic and hormonal systems which are responsible of behavioural and visceral responses to fear (freezing, potentiated startle, change in blood pressure and heart rate, stress hormones' release…). Therefore, the central nucleus projects to hypothalamus, BNST, midbrain, pons and medulla. All these projections trigger endocrine and autonomic responses to stress like activation of the adrenocortical axis or sympathoexcitaion. In turns, the BNST and CeA have strong projections to ascending cholinergic and monoaminergic neuron groups (noradrenergic locus coeruleus, dopaminergic substantia nigra and ventral tegmental area, cholinergic nucleus basalis, serotonergic raphe..) which innervate regions of the temporal lobe and forebrain memory systems.

Importantly, the cellular composition of BLA and CeA is different, with the one of BLA which resembles the cerebral cortex (mostly pyramidal-like spiny glutamatergic projection neurons) and the one of CeA which is similar to the striatum or globus pallidus (with highly branched spiny γ-aminobutyric acid (GABAergic interneurons). In the BLA, the sparsely spiny local GABAergic neurons are mostly parvalbumin (PV)-containing neurons and somatostatin (SOM) neurons which contact the soma/proximal dendrites and distal dendrites of glutamatergic neurons, respectively. Electrophysiological recordings from animal models revealed as the majority of BLA neurons are regular spiking neurons exhibiting spike frequency adaptation because of the differential expression of Ca^{2+}-dependent and voltage-gated K^+ channels (Tully K. et al., 2007). In emotionally arousing conditions, stress hormones, as norepinephrine (NE) and glucocorticoids, by reducing this spike

frequency adaptation, can enhance the excitability of the BLA neurons (Duvarci S. et al., 2007). Conversely, in the CeA, the large number of GABAergic neurons seem to innervate local inhibitory cells in brain stem nuclei (Pitkänen A. et al., 1994). Between the CeA and BLA, it has been found another interconnected group of GABAergic neurons which is known as intercalated cell mass (IC) and which provides an important source of inhibition (Marowsky A. et al., 2005; Ehrlich J. et al., 2009).

Together with afferent and efferent connections, anatomical track tracing studies combined with electron microscopy analysis of synapses and branches reveal that extensive intranuclear and internuclear connections in the amygdala further process locally all the information arriving in the amygdala before their correct behavioural outcome. It has been proposed that the basolateral nuclei represent the primary area for the entering information, while the centromedial nuclei act as an output station after a predominantly lateral to medial progression of the information (Pitika Nen A., 2000). In a simple depiction of amygdala intrinsic connectivity, multiple axon collaterals from the LA form *en passant* excitatory synapses with interneurons and projection neurons of the BA, thus integrating the cortical sensory information. In turns, the BA projects to the CeM which supplies the main amygdala output towards the brain stem and hypothalamus (**Fig 4.1.2**). Anyway, the physiology under the local connections of the amygdaloid complex is still elusive: reconstructed neurons seem to have a very complex structure and distribution with cell bodies and large dendritic trees often localized in different subdivisions. For instance, BA neurons influence CeM neurons not only via direct glutamatergic excitation, but also through disynaptic GABAergic inhibition sending axons to the CeL and IC-located interneurons, which in turns send inhibitory projections to the CeM (Benarroch E. E., 2016). Moreover, intercalated inhibitory circuitries add further complexity to the regulation of activity within the LA, BA, IC, CeL and CeM (**Fig. 4.1.2**)

The amygdaloid complex is involved In a variety of memory- and learning-related tasks. Electrical stimulation of the amygdala elicits fear and anxiety responses (Kaada B.R.., 1951; Gloor P., 1990), while its lesion blocks some types of unconditioned fear (i.e., freezing, heart rate, analgesia, Blanchard D.C., Blanchard R.J., 1972; Bellgowan P.S. et al., 1996), as well as the acquisition of both active avoidance- (escape from fear) and passive avoidance-conditioned responses (Sah P. et al., 2003). Together with fear and aversive stimuli, a direct role of the amygdala has also been seen in conditioning with appetitive stimuli (food, sex, drug), or in the acquisition and consolidation of memories that evoke an emotional response (Neugebauer V. et al., 2000; Sutherland R.J. et al., 1990). Electrophysiological studies, lesion approaches in animal models, neuroimaging (particularly MRI) experiments and neuronal recordings in patients after surgery for temporal lobe epilepsy (TLE), have largely contributed to the comprehension of the human amygdala's function and circuitry behind it. Studies on human amygdala confirm its fundamental role to link representations of the concept of fear to visual representations of a facial expression (Benarroch E.E., 2016). Recordings taken from patients with implanted electrodes demonstrated that the amygdala encodes the subjective judgment of emotional faces, predominantly responding to eye contact but without the involvement of an intact primary visual cortex (Wang S. et al., 2014; Burra N. et al., 2013). Moreover, bilateral human amygdala lesion impairs the recognition to fear in facial expression even if the recognition of facial identity is maintained (Adolphs R. et al., 1994).

4.2 NEUROPATHOLOGY OF THE AMYGDALA

Physiological dysfunctions of the amygdaloid complex are responsible for a variety of syndromes with different manifestations. The previously mentioned KBS (Klüver H. and Bucy P.,

1973) is characterized by changes in eating and sexual behaviours, inappropriate object recognition (visual agnosia), excessive oral exploration of objects, loss of fear or anger (placidity) and other specific hallmarks. In humans, these symptoms have been observed after many lesions affecting the amygdala including TLE (Nakada T. et al., 1984) or limbic encephalitis (Conlon P. et al., 1988), and in neurodegenerative disorders including AD (Kile S.J. et al., 2009). Patients with mesial TLE (MTLE) or with hippocampal sclerosis (HS) show epileptogenic clinical features which involve the amygdala, like sensation of fear, temporal lobe seizures, olfactory hallucinations, recall of memories with a strong emotional component, anxiety, or depression (Benarroch E.E., 2016). Moreover, an increment of the amygdala volume has been detected in 14 % of patients affected by HS or MTLE (Coan A.C. et al., 2013). The balance between the activity of both the amygdala and ventromedial prefrontal cortex (vmPFC) results altered in most cases of psychiatric disorders including anxiety disorders, social anxiety disorders and PTSD. In fact, an enhanced activity of the amygdala has been detected in anxious individuals exposed to both threat-related and no-threat related stimuli, while a reduced activity of the amygdala because of an increased top-down regulation of it mediated by the vmPFC, has been recorded in situations of reduced anxiety (Somerville L.H. et al., 2004; Hare T.A. et al., 2008). Particularly, PTSD is a disorder in which a person who has directly experienced a traumatic event develops a characteristic set of symptoms. Recent revisions in the DSM-5 (American Psychiatry Association, 2013) categorize symptoms into four clusters: intrusion/re-experiencing symptoms, avoidance symptoms, negative cognitions and mood, and symptoms of hyper-arousal" (Kirkpatrick H.A. et al., 2014). In other words, PTSD is a *failure of recovery* which is in partly due to an impaired fear learning. The latter sees the involvement of the hippocampus, amygdala and vmPFC (Bonne O. et al., 2001; Craske M.G. et al., 2008), and, in particular, an alteration in the inhibitory control mediated by the vmPFC towards the amygdala (Kirkpatrick H.A. et al., 2014). Some studies reported that amygdala activation is positively correlated with PTSD symptom severity (Shin L.M. et al., 2010).

Anxiety disorders are the most prevalent psychiatric disorders in the world (Kessler R.C. et al., 2012). Specific/isolated phobias are the most prevalent anxiety disorder, followed by panic disorders (PDA), social anxiety disorders/social phobia (SAD) and generalized anxiety disorders (GAD) (Kessler R.C. et al., 1994). The amygdala together with medial prefrontal cortex are considered the main regions involved in these diseases (Shin L.M. et al., 2010). In PDA, patients experience recurrent, unexpected panic attacks (discrete episodes of intensive fear, sympathetic nervous system arousal and discomfort occurring in the absence of true danger) along with a persistent worry about the implications of the attack or an important change in behaviour related to the attack (American Psychiatric Association, 2013). Relative to one of the neurocircuitry involved in PDA, the "fear network" including amygdala, hippocampus, thalamus, and brain stem is hypersensitive. In addition, the frontal cortex does not inhibit the amygdala trough top-down inhibition, resulting in magnified amygdala activity and exaggerated activation of the entire fear network (Gorman J.M. et al., 2000). SAD is characterized by a persistent and marked fear of social or performance situations involving scrutiny by people (American Psychiatric Association, 2013). The fear of embarrassment can result in avoiding the social situations, as well as impairment in occupational and social functioning. GAD is characterized by excessive diffuse anxiety, which is difficult to control, with patients experiencing irritability, fatigue, sleep and concentration difficulties and restlessness (American Psychiatric Association, 2013).

Moreover, dementia with Lewy Body (LB) pathology, PD or α-synucleinopathy (i.e., AD with amygdala LB) see an involvement of the amygdala, particularly of the BLA and cortical nuclear complex, which may contribute to anosmia or visual hallucinations (Yoshimura N. et al., 2005). In

fact, at the early stages of AD, the amygdala represents one of the most vulnerable areas of the brain, since its atrophy may play a role in cognitive/behavioural alterations and memory decline (Poulin S.P. et al., 2011). A lack of dopaminergic modulation of the amygdala has been found in PD patients, together with a reduced response to facial expressions of fear (Yoshimura N. et al., 2005; Tessitore A. et al., 2002).

4.2.1 Abnormal hyperexcitability of glutamatergic neurons: a common base of neurodisorders

Effective information managing in the brain demands a precisely regulated balanced between excitatory and inhibitory activity (E/I balance, Shew W.L. et al., 2011; Yizhar O. et al., 2011). A slightly and persistent perturbation of this delicate balance could lead or contribute to main defects which, in turns, may manifest as brain diseases named "synaptopathies". In general, neurodegenerative or neurodevelopmental diseases can be linked to an altered excitatory (**Fig 4.2.1.1**) or inhibitory (**Fig.4.2.1.2**) synapse physiology. In the pathophysiology of several of these disorders, including affective, psychiatric, and degenerative disorders, an increasing importance has been attributed to the glutamatergic excitatory activity. In fact, glutamate neurotransmitter has a peculiar role in the CNS and its abnormal, toxic accumulation results to an hyperfunction of the glutamatergic system. Glutamate acts upon two main neurotransmitter ligand-gated ionotropic receptors, NMDA and AMPA receptors which are crucial in synaptic plasticity and transmission (Strack S. et al., 1998).

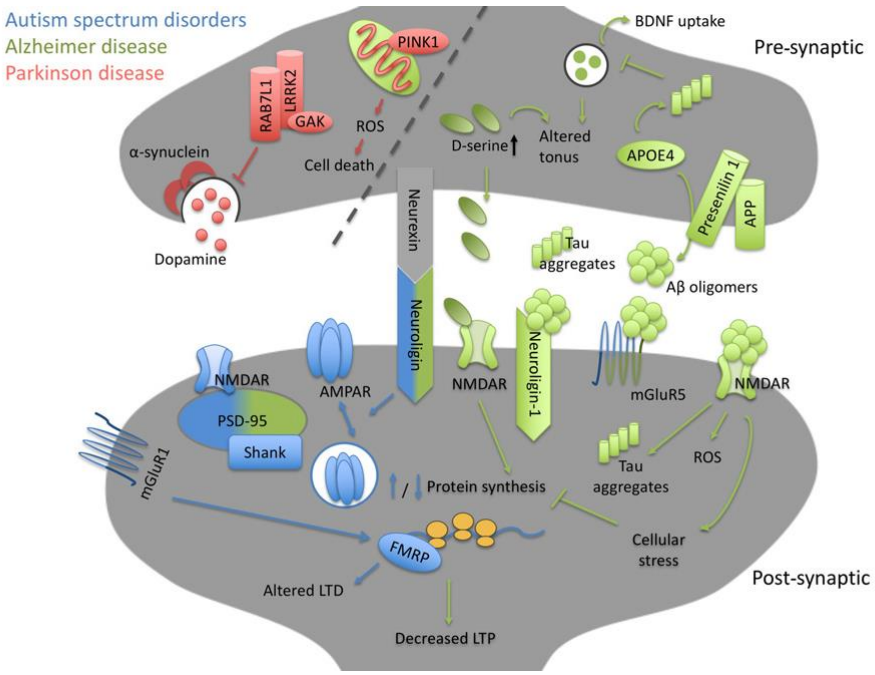

Figure 4.2.1.1 Schematic overview of excitatory synapse-linked disease mechanisms. Functional overview of the excitatory synapse with main proteins and pathways affected in ASD, AD, and PD. Proteins and pathways are colour-coded for each disorder. Dashed line divides the pre-synaptic part into dopaminergic and glutamatergic terminals. In AD, the post-synaptic action of Ab oligomers and tau aggregates result in deregulation of NMDA receptors, cellular stress, and decreased protein synthesis. Ab oligomers further act

through interaction with neuroligin-1 and mGluR5 to impair neuronal homeostasis. Pre-synaptic disturbances, including impaired BDNF transport and excessive D-serine production, have also been associated with AD. Such abnormal molecular cascades ultimately result in defective LTP and memory. In PD, defective autophagy and a-synuclein-mediated mislocalization of SNARE complexes associate with decreased DA release and mitochondrial function. This leads to increases in oxidative stress, likely driving impaired dopaminergic tonus and neuronal death that are characteristic of PD. (Lepeta K. et al., 2016).

AMPA receptors consist of 4 subunits (gLuR1-4) and depolarize the postsynaptic membrane through Na^+ influx, while NMDA receptors, through their Ca^{2+} influx, their voltage-dependent opening mechanism, and their coupling to intracellular signalling molecules, are crucial in signal transduction and synaptic response modulation (Strack S. et al., 1998).

Several novel genetic mutations which affect synapse formation and functions have been related to autism spectrum disorders (ASD) and epilepsy (Huguet G. et al., 2013). Despite the fact that these variants are very diverse affecting all phases of neuronal excitability (i.e., anchoring synaptic machinery, neurotransmitter release, control of neural network or subcellular signalling processes, Huguet G. et al., 2013), they seem to share a common pathway (Shew WL et al., 2011). In fact, a core process underlying ASD pathogenesis has been proposed and rely upon the imbalance between the excitatory and inhibitory circuitry in neocortical areas (Huguet G. et al., 2013). In ASD etiology, genetic variants in the subunits of NMDA receptors (GluN2A and GluN2B subunits) affecting synaptic plasticity seem to be implicated (Won H. et al., 2012). Mice lacking exon 7 of the post-synaptic protein scaffold shank (*Shank2 -/-* mice) showed up-regulation of NMDA receptors in synaptosomes, increased NMDA-dependent LTP and enhanced NMDA/AMPA ratio (Etherton M.R. et al., 2011). Also in AD, one of the most prevalent neurodegenerative disorders (60% of all dementia cases, Gray E.G. et al., 1987), NMDA seems to play a critical role. Most of the common therapies furnish symptomatic relief by decreasing the NMDA receptor function at excitatory synapses or increasing the cholinergic signalling, even if they do not treat the underlying cause of disease (Pickrell A.M. et al., 2015).

This E/I imbalance is recognized as a cause for epilepsy and seizures too: an hyperexcitability has been linked to sodium or calcium channelopathy which altered the membrane depolarization or to greater glutamate release/enhanced number of glutamatergic synapses. Another key factor in the pathogenicity of epilepsy is represented by neuromodulators as neuropeptides and small molecule co-agonists whose role is the regulation of homeostatic plasticity and network dynamics. Among them, brain-derived neurotrophic factor (BDNF) seems to facilitate epileptogenesis trough TrkB, while neuropeptide Y (NPY) was shown to repress hyperexcitation in human epileptic tissues (Lepeta K. et al., 2016).

Synapse alterations pave the way also for the PD progression trough dysfunctions in mitochondria physiology, autophagy, and protein trafficking (Pickrell AM et al., 2015; Hunn BH et al., 2015. In particular, α-syn is one oligomerization-prone chaperone which causes delocalization of SNARE protein complexes linked to reduce DA release (**Fig.4.2.1.1**, Rockenstein E. et al., 2014). A risk factor for OD and stroke is represented by traumatic brain injury (TBI), a temporal or permanent impairment of brain function due to an external mechanical force to the head (Jamjoom A.A.B. et al., 2021). Even if synaptopathy in TBI is a very complex and multifaceted process, several studies demonstrate as oxidative stress, glutamate excitotoxicity and inflammation play crucial roles in its pathophysiology (Jamjoom A.A.B. et al., 2021). For instance, elevated glutamate levels in TBI have been linked to abnormal intracellular Ca^{2+} levels and subsequent neuronal death (Nilsson P. et al., 1996). This increment in the intracellular Ca^{2+} leads to the expression of GluR2-lacking AMPA

receptors which are more permeable to Ca^{2+} and, thus, exacerbate excitotoxic neuronal death within one hour after injury (Contractor A. et al., 2015).

Increasing evidence suggests that network hyperexcitability and neuronal hyperactivity including altered excitatory synaptic connections and function, altered ion channels' conductance/expression, and reduced inhibitory circuitry leading to an E/I imbalance, could be relevant point of convergence in the pathophysiology of Fragile-X-syndrome, FXS (Contractor A. et al., 2015). FXS is a leading inherited cause of autism and ID due to the expansion and hyper-methylation of CGG-repeats around the FMR1 gene and subsequent silencing and loss of its protein product Fragile X mental retardation protein, FMRP, (Liu X. et al., 2022). This protein is a well-conserved neuronal RNA-binding protein which regulates (probably as translational repressor) a lot of neuronal mRNAs (approximately 4-8% of all mRNAs in the brain) covering a wide-range of effects on neuron functions. In fact, the targets of these mRNA include ion channels, pre- and postsynaptic proteomes, transcription factors and chromatine-modyfing proteins. The disruption of these targets perturbs a lot of signalling pathways which are essential for the maintenance of neural network stability and physiological synaptic function (Bhakar A.L. et al., 2012) leading to the generation of the circuitry hyperexcitability of FXS. The most observed synaptic plasticity phenotype in FMR1 KO models is excessive mGluR1/5-dependent long-term depression (LTD) at excitatory synapses (mediated by post-synaptic AMPA receptors' internalization, Liu X. et al., 2022), probably because FMRP acts as a negative feedback regulator limiting mGluR-mediated protein synthesis (Bear M.F. et al., 2004), even if it is unclear how this exaggerated mGluR-LTD plays a part in network hyperexcitability in FXS. A possible hypothesis is a subsequent stimulation of protein synthesis in dendrites which facilitates the LTP priming (Raymond C.R. et al., 2000) or extended epileptiform discharges (Bianchi R. et al., 2009).

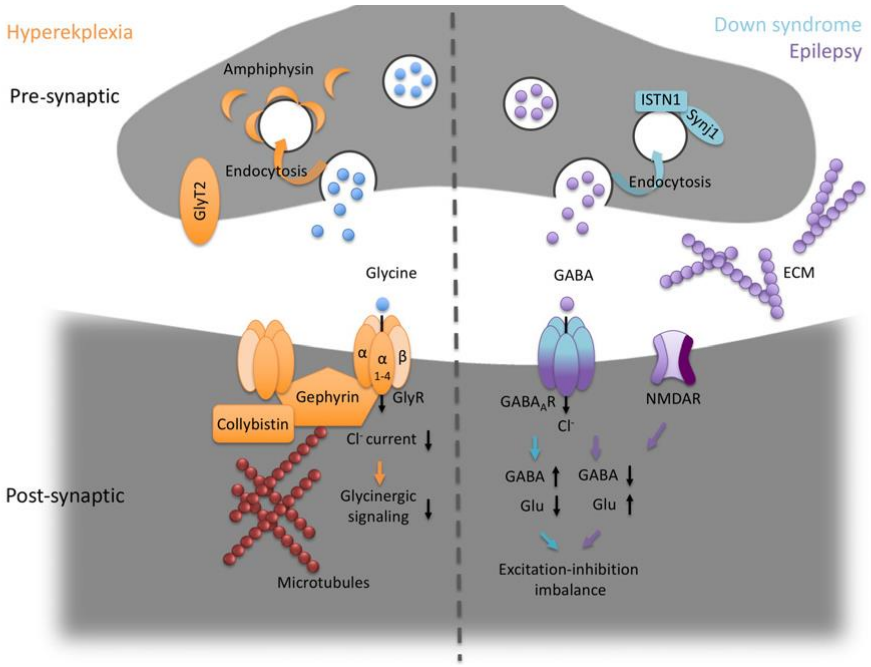

Figure 4.2.1.2 Schematic overview of inhibitory synapse-linked disease mechanisms. Functional overview on the inhibitory synapse with main proteins and pathways affected in hyperekplexia, DS, and epilepsy. Proteins and pathways are colour-coded for each disorder. Dashed line divides the scheme into glycinergic and GABAergic synapse. The major cause of hyperekplexia is defective glycinergic signaling resulting from

mutations in genes involving subunits of GlyRs, glycine transporter, or GlyR-interacting proteins. E/I imbalance underlies deficient synapse function in epilepsy and DS. In epilepsy, abnormal excitatory tonus results from decreased GABA release and concurrent enhanced glutamatergic neurotransmission. In DS, an over-inhibition of synapses by increased GABAergic circuitry and endocytic dysfunction is considered the main synaptic hallmark of the disease. (Lepeta K. et al., 2016)

Dysfunction in corticolimbic glutamatergic neurotransmission may contribute to or account for the schizophrenia symptoms and manifestation (Uno Y, Coyle JT, 2019; Coyle JY, 1996). Schizophrenia is a chronic and severe psychiatric disorder with a profound impact on society and individual's life. It is characterized by both positive (i.e., hallucinations, disorganized thinking, delusions) and negative symptoms (i.e., diminished emotional expressions, alogia, asociality), as well as cognitive defects (in attention, working memory, and executive function (Uno Y. and Coyle J.T., 2019). The anaesthetics ketamine and phencyclidine (PCP), have been seen to induce schizophrenic-like symptoms, including also negative and cognitive symptoms in healthy humans (Javitt D.C. and Zukin S.R., 1991). Since the binding sites for ketamine and PCP are non-competitive antagonists of the NMDA subtype of glutamate receptor, it was proposed that schizophrenia results from hypofunction of NMDA receptors (Javitt D.C. and Zukin S.R., 1991). In fact, the endogenous NMDA receptor antagonist N-acetyl-aspartyl glutamate seems to have enhanced activity in the frontal cortex and hippocampal formation in patients of schizophrenia, as well as clinical studies with drugs that enhance NMDA receptor function have shown a reduction in negative symptoms and cognitive defects in patients with chronic schizophrenia (Coyle J.T., 1996).

4.2.1.1 Anxiety-related pathologies

Dysfunctional amygdala neuroplasticity due to physiological changes in principle glutamatergic output neurons often causes alterations of intrinsic amygdala neurocircuits. The hyperexcitability of the amygdala leads to anxiety which is present in both animal models and human patients affected by neurodegenerative (i.e., AD; Klein R.C. et al., 2014), neurodevelopmental (autism, fragile x syndrome, attention-deficit hyperactivity disorder/ADHD, Martin B.S. et al., 2014; Hadley D. et al., 2014) and neuropsychiatric disorders (PTSD, addiction, Duval E.R. et al., 2020 Truitt W.A. et al., 2007). Particularly, the pathologically enhanced excitability in BLA neurons, which bi-directionally communicates with prefrontal cortex, hippocampus, *nucleus accumbens* and other brain regions regulating motivation, stress responses and cognition, is linked to behavioural diseases characterized by excessive emotional responses to fear and anxiety-inducing stimuli, as well as altered motivation, cognition, and autonomic activities (Prager E.M. et al., 2016). In fact, the orchestrated somatic and behavioural responses to stressful stimuli in the BLA involve the activity of the principal, pyramidal glutamatergic output neurons and the local GABAergic interneurons which co-ordinately participate in the local circuits like feed-forward and feedback inhibition. Preclinical studies show that mouse strains differ in anxiety-related responses to chronic stress in a manner parallel by diverse stress-induced changes in glutamatergic signalling in the BLA. Moreover, Thomas Kash's lab demonstrated that alterations in gene expression of the GluN1 NMDA and GluK1 kainate receptors in the amygdala are linked to stress-induced alterations in anxiety-like behaviours in the C57BL/6J mouse strain (Masneuf S et al., 2014). The same group further elucidated changes in BLA glutamate neurotransmission due to stress through *in vivo* behavioural pharmacological and *ex vivo* physiological approaches. They suggest the presence of a stress induced BLA glutamatergic neuronal network hyperexcitability and a compensatory increase in GABAergic neurotransmission, with GluK1 agonism enhancing GABAergic inhibition and preventing behavioural sequelae of stress

(Masneuf S. et al., 2014). In fact, together with the important role of excitatory synaptic transmission in stress-induced synaptic plasticity in the amygdala, several lines of evidence also point to a central role for GABAergic inhibitory transmission in gating these effects (Davis M. et al., 1994). In fact, the GABAergic intraneuronal network regulates the excitability of amygdala principal neurons and thus determining behavioural outcomes to anxiety/fear-involved external stimuli. Therefore, stimuli that induce acute stress or tissue damage could pathologically alter this inhibitory network causing hyperexcitability of principal glutamatergic neurons which results in behavioural disorders like generalized anxiety and PTSD.

The excitability of principal neurons can also be altered by synaptic signalling governed by dysfunctional neurotrophines or receptors, as BDNF, important for memory consolidation of fear and conditioning and extinction (Chhatwal J.P. et al., 2006). In regards, it has been shown as a single-nucleotide polymorphism in its gene (Val66Met), which causes dysfunctional BDNF signalling in humans (Egan M.F. et al., 2003), was sufficient to alter glutamatergic projections from BLA to CeM in mice (Galvin C. et al., 2015). Norepinephrine (NE) is another modulator of the intrinsic excitability of BLA neurons, through the activation of their β-adrenergic receptors. *In vivo* iontophoresis of NE in behaving rodents that undergo Pavlovian fear condition attenuated both spontaneous and evoked firing of action potentials in single BLA neurons recorded *in vivo* (Buffalari D.M. and Grace A.A., 2007). Even if this inhibitory effect was mediated by α2-adrenoreceptors, NE had also a smaller, excitatory effect through the activation of β-adrenergic receptors. The latter mediate both the facilitative effect of NE on memory consolidation and the excitatory effects in BLA. In fact, these receptors modulate the intraneuronal trafficking of calcium-activated potassium channels (SK) which, in turn, control the afterhyperpolarization (AHP) of the neuronal membrane (Faber E.S. et al., 2008). Thus, NE and chronic exposure to stress intensively activate β-adrenergic receptors which reduce SK channels activity: the followed decrement of AHP augments neuronal firing in both dorsal striatum and BLA (Hopf F.W. et al., 2010). The latter effect is particularly interesting because SK channels seem to be located in the immediate proximity of NMDA receptors in the dendritic spines of BLA neurons, which explains how they can regulate synaptic plasticity so efficiently (Hopf F.W. et al., 2010).

These findings indicate that NE could have an overall inhibitory effect on spontaneous spiking in most BLA neurons but an excitatory effect on a smaller subset of neurons to amplify the signal-to-noise ratio in those neurons that are involved in memory modulation (Roozendaal B. et al., 2009). Together with NE, the other monoamine neurotransmitters serotonin (5-HT) and DA have long been associated with fear and anxiety, therefore drugs that alter monoaminergic functions are often effective in a wide range of anxiety disorders (Forster G. L: et al., 2012). Increased 5-HT release or activity of serotoninergic neurons in the amygdala have been observed in response to restraint or footshock, or in association with expression of conditioned fear behaviour (Mo B. et al., 2008; Zanoveli J.M. et al., 2009; Yokoyama M et al., 2005). *In vivo* recordings and immunocytochemical analysis have shown that the ability of 5-HT to inhibit glutamatergic activity in the LA is dependent on the presence of corticosterone (Stutzmann G.E. et al., 1998). However, other electrophysiological studies in LA slices have showed as *in vitro* delivery of high stress level of corticosterone results in a reduction of GABAergic inhibitory transmission along with an enhanced intrinsic excitability of principal excitatory neurons (Duvarci S. and Prè D., 2007). Together these studies lead to hypothesis that the direction of corticosterone effects on amygdala function depends on its concentration and that stress-induced amygdala activation and inhibition may be tightly coupled.

A strong body of evidence involves the corticotropin-releasing factor (CRF) as an important mediator of fear and anxiety (Butler P.D. et al., 1990; Basso A.M. et al., 199; Kikusui T. et al., 2000; Bledsoe A.C. et al., 2011), as well as in anxiety disorders (Risbrough V.B. et al., 2006), being a modulator of amygdala monoaminergic activity in response to anxiogenic stimuli. Like anxiogenic and fearful stimuli, central infusion of CRF or CRF receptor agonists increases 5-HT, NE and DA levels in the amygdala, and stress-induced increases in monoamine levels in the amygdala are prevented by CRF receptor antagonists (Forster G. L. et al., 2012).

4.2.1.2 Lateral amygdala as a neuronal substrate for fear conditioning

Thanks to studies over the last 50 years, it is well recognized that the amygdaloid complex plays a central role in a variety of learning- and memory-related tasks, but its key role in Pavlovian fear conditioning and fear-motivated operant conditioning is the most studied since it has obvious implications for understanding anxiety disorders.

Excitatory amino acid receptors in the amygdala play a crucial role in synaptic transmission and plasticity of sensory projections and the consequent emotional processing. Synaptic plasticity determines the induction of memories through experience (LeDoux J.E., 1992) and LTP is the most studied form of plasticity. It consists of the strength of the efficacy of synaptic transmission because of high frequency stimulation of an afferent pathway (tetanizing). As in several hippocampal regions, also in the amygdala LTP is mediated by excitatory amino acids (glutamate) receptors which are highly concentrated in the lateral and basolateral nuclei. Therefore, the stimulation of the thalamus-amygdala projections or the external capsule (cortico-amygdala projections) induces the LTP in the LA (Chapman P.F. et al., 1990), while the blockade of NMDA receptors influences the fear memory acquisition (Miserendino M.J. et al., 1990).

Studies in rodents both *in vivo* and *in vitro* reveal as the LA is the critical site of synaptic plasticity for the acquisition and maintenance of Pavlovian fear response and the BLA is thought to be critical for remote fear memories (Pape H.C. and Pare D., 2010). Rosenkrantz and Grace, by using intracellular recordings *in vivo*, showed as pairing an odour (CS) with a foot-shock (US) enhanced the amplitude of the response to the paired odour, while the response to an unpaired odour is unaffected (Rosenkranz J.A. and Grace A.A., 2002). This result indicates that LA plasticity is of an associative nature and not due to processes like sensitization. A scheme of the pathways to the amygdala for the most studied auditory modality is provided in **figure 4.2.1.1.**

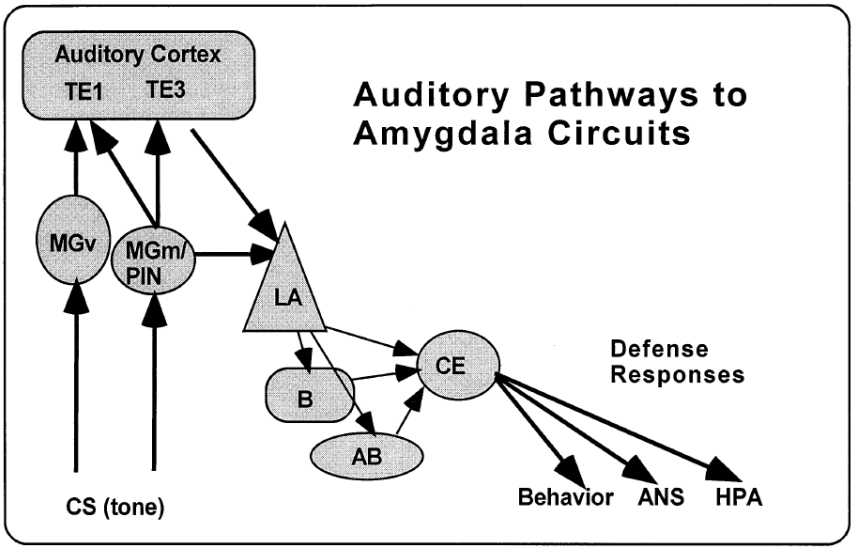

Figure 4.2.1.1. The basic neural pathways underlying fear conditioning involve transmission of sensory stimuli about a CS to the amygdala from the thalamus and cortex and the control of emotional responses by outputs of the amygdala. The illustration shows auditory signals from the thalamic nuclei (MGm/PIN) and auditory cortex (TE3) reaching the LA. LA then projects to the CE directly and by way of intra-

amygdala pathways involving the B and accessory basal AB nuclei. CE, in turn, controls the expression of defense responses, including behavioral, autonomic nervous system (ANS), and hormonal (HPA, hypothalamic–pituitary–adrenal axis) responses. (LeDoux J.E., 1998).

Mechanistically, the LTP in the amygdala (that is the acquisition and storage of fear-related memories) results from coincident activation of one weak input (the CS) and a strong one (the US) to a single cell. For the principle of associativity of LTP (Bliss T.V. and Collingridge G.L, 1993), initially only the strong input is able to activate the postsynaptic neuron (with a strong depolarization or repetitive action potential firing), but the pairing stimulation potentiates the weak input which undergoes LTP and becomes able in driving the postsynaptic neuron too. *In vivo* studies (Rogan M.T. et al., 1997) and acute amygdala slice preparations (McKernan M.G. et al., 1997) show as in the LA the CS-US pairings enhance measures of excitatory synaptic plasticity probably because of potentiation of sensory inputs onto LA neurons. This experience-dependent synaptic strengthening permits the activation of LA neurons by the presentation of the CS only. In regards, an optogenetic study expressed the excitatory channelrhodopsin2 (ChR2) in LA principal neurons which were simultaneously and reversibly photoactivated when paired with an auditory cue, allowing for their use as a substitute for the foot-shock US in conditioning freezing (Johansen J.P. et al., 2010). Again, another study briefly photoactivated ChR2-expressing LA axonal terminals from the MGm and auditory cortex substituting for a tone CS when paired to a foot-shock leading to synaptic potentiation and conditioned freezing (Nabavi S. et al., 2014).

Importantly, alternative mechanisms to classical LTP may occur in the LA during fear conditioning, as demonstrated by a study where the plasticity of CS occurred despite the lack of relevant postsynaptic depolarization during the paired stimulation (Rosenkranz J.A. and Grace A.A., 2002).

Ehrlich I. et al. (Ehrlich I. et al., 2009) demonstrated as both principal glutamatergic neurons and GABAergic interneurons of the LA receive cortical and thalamus excitatory inputs, and probably they converge onto the same postsynaptic dendrites of the principal glutamatergic LA neurons.

Several studies demonstrated input specificity of LA plasticity by revealing that LTP occur only at those inputs which underwent paired stimulation (Pape H.C. and Pare D., 2010). Even tetanic microstimulation of the MGB (rather than a sensory CS) paired with a US resulted in conditioned fear behaviour and LTP-like increment of evoked field potentials in LA, confirming this associative form of LTP (Kwon J.T. et al., 2009). It has been showed both *in vivo* and *in vitro* (Sah P. et al., 2003) that a rise in postsynaptic calcium is required for the induction of LTP at either cortical or thalamic inputs to BLA neurons. Some earlier controversial studies *in vitro* (Huang Y.Y. and Kandel E.R., 1998; Chapman P.F. et al., 1990) questioned if the NMDA receptors' activation was required for this LTP induction. The activation of L-type voltage-gated calcium channels (VGCCs) for LTP induction was also observed by paring action potentials with thalamic excitatory postsynaptic potentials (Weisskopf M.G. et al., 1999). Anyway, behavioural studies where NMDA receptor antagonist AP5 blocked the acquisition of fear conditioning challenge the notion that NMDA-mediated plasticity is the process supporting the acquisition and storage of fear-related memories within the amygdala (Lee H.J. et al.,2001; Fendt M., 2001). Nowadays, the consensus is that postsynaptic LTP induced by weak stimulation protocols is dependent on NMDA receptors, while stronger induction protocols (i.e. pre and postsynaptic pairing) may also require the VGCC activation (Pape H.C. and Pare D., 2010).

According to the expression of LTP, at thalamo-LA synapses it is expressed postsynaptically being linked to postsynaptic AMPA receptor trafficking (Rumpel S. et al., 2005), while the LTP at

cortico-LA synapses is mostly expressed presynaptically with a cAMP/pKA-dependent increase in the probability of release (Huang Y.Y. and Kandel E.R., 1998; Tsvetkov E. et al., 2002). This agrees to the fact that LTP induction at thalamic and cortical inputs involves NMDA receptors, which are predominantly located at postsynaptic and presynaptic sites, respectively (Pape HC and Pare D., 2010). Moreover, the LTP gating at both synapses is modulated by several neuromodulators which, by acting on the local inhibitory neurons, control the activity of LA principal glutamatergic neurons in the emotional inputs (Bissière S. et al., 2003)

While the LA is the major site of termination from both thalamic and cortical inputs, the central nucleus is the interface with motor system for the control of conditioned outcomes (LeDoux J.E., 1992). In other words, while the LA is implicated in the acquisition and consolidation of conditioned fear responses, the CE is involved in their expression, via its projections to the brain stem and hypothalamus.

In the first demonstration of optogenetic projection-specific manipulation in a freely moving animal, the increased/decreased of transmission between LA and central nucleus was shown to cause the reduction/augmentation of anxiety-related behaviour, complementing the fMRI studies (Janak P.H. and Tye K.M., 2015).

Finally, it is worth to mention the maintenance, the reconsolidation and the extinction of fear memory. The maintenance sees the involvement of the actin cytoskeleton which rearranges and structurally modifies synapses. The reconsolidation of fear memory occurs when a memory-associated environmental clue reactivates previously acquired fear memories and alters them (Nader K. et al., 2000). During this labile state, memories are altered through protein-synthesis inhibitors (Nader K. et al., 2000) or with non-invasive presentation of non-fearful presentation in mice, rats, and humans (Janak P.H. and Tye K.M., 2015). The process known as fear extinction consists in the gradual abolition of the fear response through a repeated exposure of the initial neutral stimulus without the following aversive stimulus. This is due to the formation of a new inhibitory memory via an active learning process which is time- and context-dependent. In fact, the fear reactions can re-occur if a new neutral stimulus is presented in a new context (Benarroch E.E., 2015).

5. DYSFUNCTIONAL PLASTICITY: LTP IN HEALTH AND PATHOLOGY

During the first half of the twentieth century, Santiago Ramòn y Cajal proposed that synapses are the sites at which memories are stored and where one neuron can influence the excitability of one other. Soon after, Jerzy Konorsky introduced the term “synaptic plasticity” (Bliss Tim V.P. et al., 2018), which refers to the ability of synapses to change their tonus/structure at either pre- or postsynaptic compartment following persistent electrical activity. This feature of synapses permits learning and memory processes to occur. At the same time, Donald Hebb introduced the “neurophysiological postulate” asserting that the effect of the simultaneous pre- and postsynaptic activity is the strengthening of the synaptic connection between pre- and postsynaptic neuron (Bliss Tim V.P. et al., 2018). From that moment it has been tried to demonstrate the long-lasting synaptic plasticity in mono-synaptic neural pathways of the CNS by giving tetanic (high frequency) stimuli to the presynaptic cell and obtaining a transient increment of synaptic efficacy named as post-tetanic potentiation (Bliss Tim V.P. et al., 2018). Another approach consisted in delivery trains of stimuli at 10 Hz to the axons projecting to the hippocampus getting “frequency potentiation”, that is a rapid increment of neurons firing action potentials during the train (Gloor P. et al., 1964). Unfortunately,

these protocols ensured an efficacy in strengthening that was too short-lived (few minutes) to be linked to a putative learning and memory mechanism. Only in 1966, Terje Lomo succeeded in demonstrating a long lasting (some hours) increment of synaptic evoked responses in the dentate gyrus of the hippocampus after repeated high-frequency stimulations (Lømo, T., 1966).

5.1 MOLECULAR AND PHYSIOLOGICAL MECHANISMS OF LTP

"…I saw that the field spike and excitatory postsynaptic potential (EPSP) potentiation that occurred during tetanization, persisted afterwards. I presented this observation in August 1966 at the XII Scandinavian Congress of Physiology in Turku (Åbo), Finland. Figure 1 (**Fig. 5.1.1**) shows one of the figures that I presented at that meeting. There is marked frequency potentiation during each train of stimuli at 12 Hz (a), persistent potentiation after each train and increasing potentiation until apparent saturation after successive trains (b, c) (see figure legend). In the abstract from that meeting, I described the result as "an example of a plastic change in a neuronal chain, expressing itself as a long-lasting increase of synaptic efficiency. The effect, which may last for hours, is dependent upon repeated use of the system". In my notes from that time I wrote: "If it is correct that the hippocampus is involved in memory function, this is a region where one should expect long lasting changes in synaptic efficiency to occur", and further: "The phenomenon may represent a kind of banung of individual synapses and may have relevance to theories of learning" (Bahnung, misspelled in my notes, means facilitation or opening, and is a German term now used to describe LTP). Probably to the surprise of many today, I did not immediately follow up on this result." Terje Lømo, *Discovering Long-Term Potentiation (LTP)–- Recollections and Reflections on what came after* (Lømo T., 2018).

Learning is considered the mechanism through which new information is acquired, while memory is the mechanism by which that knowledge is retained (Lynch M.A., 2004). Information storage in neural circuits relies on Hebbian forms of synaptic plasticity, attributable to LTP or LTD. Once LTD is inducted, the potentiated synapses are submitted to a positive feedback loop of synaptic strengthening and circuit hyperexcitability (Turrigiano G.G. and Nelson S.B., 2000; Turrigiano G.G., 2008). Conversely, LTD weaken the synapses in an activity-dependent manner and if it persists would lead to their silencing (Collingridge G.L. et al., 2010). Several areas in the brain play a role in consolidation of different forms of learning and memory, but the hippocampus' role has been recognized as vital in the formation of declarative memory, that is the synthesis of episodic and semantic memories. According to this, it is nice to mention the observations od Scoville and Milner (Scoville W. and Milner B., 1957) who, in 1957, diagnosed anterograde amnesia in the H.M. epileptic patient after the bilateral removal of hippocampus.

Bliss and Lomo originally described LTP as the manifestation of two physiological conditions (Lømo T., 2018). The first is the increment in synaptic strength which is measured as an increase of the initial slope/magnitude of the EPSP, followed by enhanced postsynaptic receptor number/efficacy and/or enhanced presynaptic neurotransmitter release. The second component of LTP described by Bliss and Lomo is referred to as EPSP-slope (E-S) potentiation, that is the increased probability of the postsynaptic cell to fire an action potential at a constant strength of synaptic input (Lømo T., 2018). The most extensive studied form of LTP occurs in the hippocampus

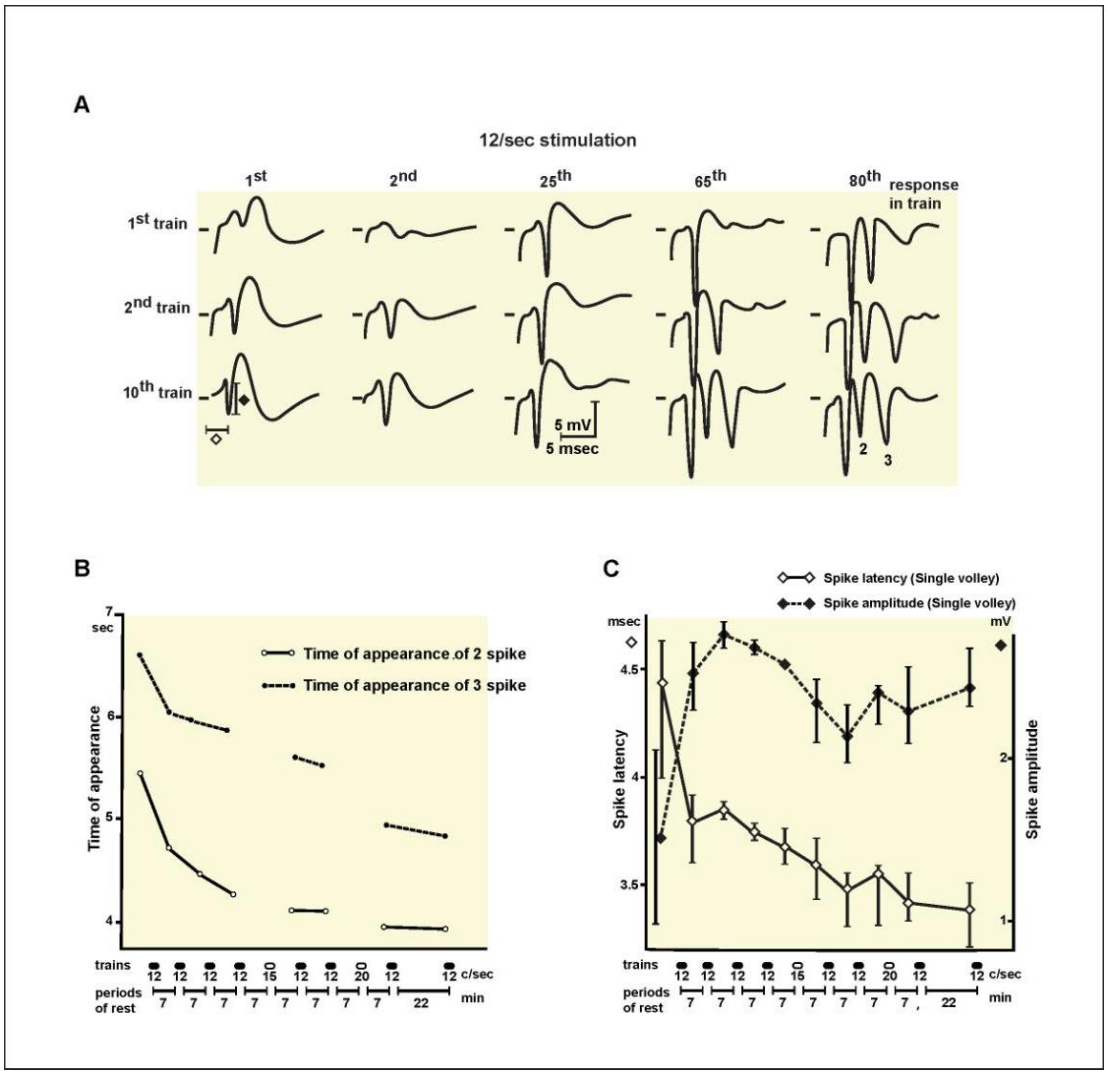

Figure 5.1.1 From Lømo T., 2018

at excitatory synapses between the Schaffer collaterals and CA1 pyramidal neurons (**Fig.5.1.2 a. b.,** Malenka R.C. et al., 1989; Madison D.V. et al., 1991)

In the LTP literature, three defined terms are widely used to describe the molecular mechanisms of LTP: the *induction* mechanism refers to transitory events which trigger the LTP formation; the *maintenance* mechanism refers to the persisting biochemical signal that occurs in the neuron; this persisting biochemical signal plays atop an effector (i.e., glutamate receptor) resulting in the *expression* mechanism of LTP (Sweatt J.D., 1999).

Other key important terms are used to define the different phases of LTP which, in turns, time the three different described mechanisms. These phases are sequentially induced overtime through repeated trains of high frequency stimulation at the CA1 area of the hippocampus defining the LTP. The first phase is defined *initial-LTP* (Roberson E.D. et al., 1996) or short-term plasticity and consists of a persistent-form of NMDA receptor-dependent plasticity which lasts for 30-45 minutes and does not need any kinase activity to be induced/expressed. It anticipates the so following *early-LTP* (*E-LTP*) and *late-LTP* (*L-LTP*) phases. After ~30 minutes, the persistent activation of protein kinases is essential for the following *early-LTP* (*E-LTP)* phase which lasts 2-3 hours. Finally,

changes in gene expression are needed for the induction of the last *late-LTP* phase (*L-LTP*) which lasts many hours.

Finally, more defined terms describe the basic properties of LTP **(Fig. 5.1.2 c.)**: *input specificity* (when LTP is induced at one set of synapses on a postsynaptic cell, neighbouring synapses, which are not affected by the stimulation, do not show LTP), *cooperativity* (a significant number of presynaptic fibres must be simultaneously activated to evoke LTP) and *associativity* (low-intensity stimulation of two pathways or higher intensity stimulation of weak inputs, converging on the same cell, is sufficient for the induction of LTP, Bliss T.V. and Collingridge G.L., 1993).

Studies in hippocampus show as the LTP induction needs a rise in postsynaptic Ca^{2+} since the injection of calcium chelators in the postsynaptic cells block hippocampal LTP induction. In the classical LTP model, the peculiar step is characterized by the depolarization of the postsynaptic neurons which permits the removal of the Mg^{2+} blockade from NMDA receptors and their activation. The channels of these receptors allow Ca^{2+} to enter and rise in the postsynaptic neurons to trigger signal transduction cascades which, in turn, start the molecular changes of LTP (Bliss T.V. and Collingridge G.L., 1993). The depolarization needed to activate NMDA receptors is due to AMPA receptors during titanically induced LTP or to backpropagating action potentials (Magee JC and Johnston D, 1997). Anyway, NMDA receptor-independent forms of LTP have also been described, both postsynaptic forms where calcium arrives from VGCCs (Wyllie D.J. et al., 1994) or calcium-permeable AMPA receptors (Mahanty N.K. and Sah P., 1998), as well as presynaptic forms (Nicoll R.A. and Malenka R.C., 1995).

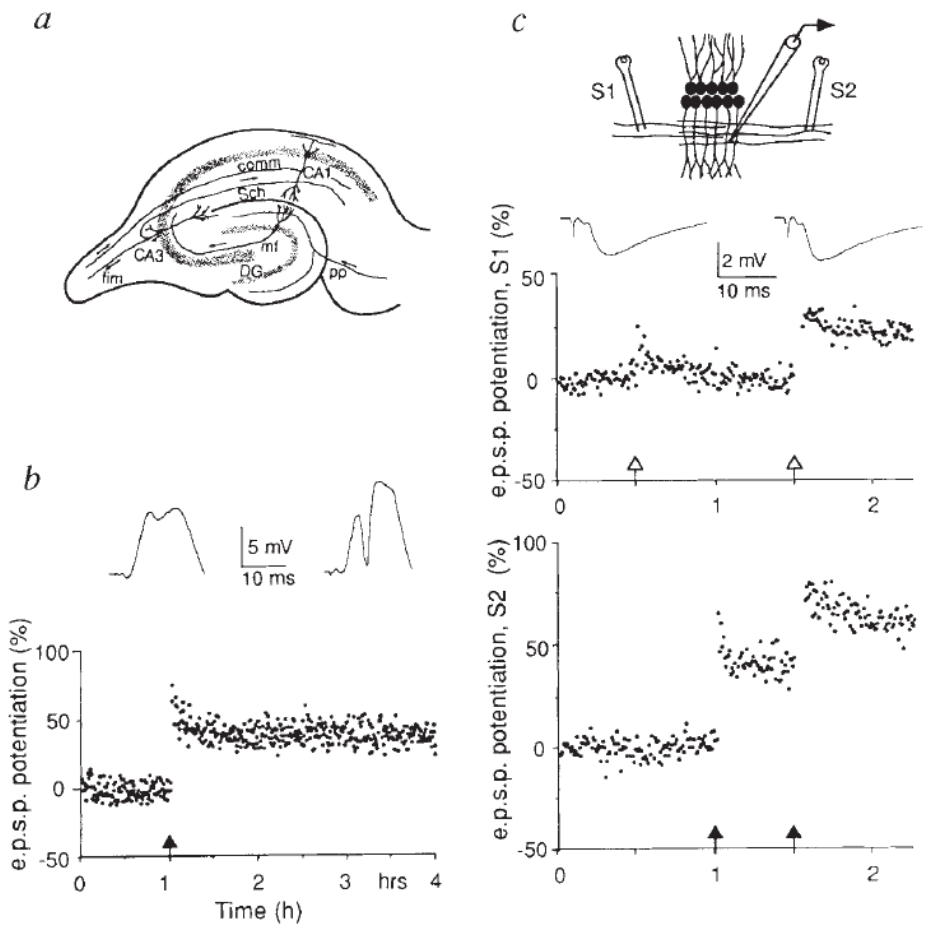

Figure 5.1.2 Basic properties of LTP (cooperativity, input-specificity and associativity). a) simplified diagram of a transverse section through the rat hippocampus showing the principal neuronal fields (granule cells of the dentate gyrus (DG) and the pyramidal cells of CA3 and CA1 areas, and the main excitatory afferents projections (the prefrontal path (pp) from enthorinal cortex to granule cells, the mossy fiber projections (mf) from granule cells to CA3 cells, and the Scaffer collateral (Sch)-commissural (comm) system which connects ipsilateral and

controlateral CA3 cells to Ca1 cells). b) An example of LTP in the perforated pathway recorded *in vivo*. The graph plots the slope of the rising phase of the evoked response (population e.p.s.p.) recorded from the cell body region in response to constant test stimuli, for 1 h before and 3 h following the tetanus (250 Hz, 250 ms) delivered at the time indicated by the arrow. Representation traces before and after LTP are illustarted at the top of the plot: note the increase in slope of the population e.p.s.p and the increase in size of the superimposed population spike (downward deflaction). c) Demonstartion of the propeties of coopeartivity, input-specificity and associativity. The top diagram show the experimental arrangement in area CA1 of the hippocampal slice. Two indiepndent set of afferent fibers converging on a common population of cells are activated by stimulating electrodes (S1 and S2) placed either side of the extracellular recording electrode. The stimulus intensities are adjusted so that S1 acttivates fewer fibers than S2. The slope of the popualtioon e.p.s.p. in repsonse to stimuli delivered alternatively to S1 and S2 at 15 s intervals are plotted as a function of time. Arrowds denote episodes of tetanic stimulation to S1 (the stron pathway, solid arrows). The tetanus to S1 produced a rapid decaying phase of PTP, lasting 2-3 min, with a small tail of STP but not stable increase of synaptic transmission; the intensity of the tetanus was below the cooperativity treshold for LTP. The srtronger tetanus to S2 (first filled arrows) produced PTP and LTP, but there was no tranfer of the effect to the first input (test shocks to S1 were out of phase with the high-frequency bursts to S2), demonstarting the input-specificity of LTP. The coincident activation of a weak, subtreshold input with a strong input induced associative LTP in the weak input. The traces above the graph illustrate field e.p.s.p. evoked by test shocks in S1 and recorded in the synaptic layer, before and after the induction of associative LTP. (Bliss T.V. and Collingridge G.L., 1993).

A signalling transduction cascade for LTP has been presented graphically by Sweatt JD (Sweatt J.D., 1999; Fig. **5.1.3**) and consists of three wide temporal steps:

1. the transient activation of second messenger-dependent protein kinases leads to temporary effects for both E-LTP and L-LTP induction. Particularly for L-LTP induction, the transcription factor CREB has been demonstrated to be a prominent effector (Sweatt J.D., 1999);

2. the persistent activation of second messenger-independent protein kinases as PKC and CAMKII leads to long term effects which maintain the increased excitability and synaptic strength in E-LTP. Regarding the CaMKII activation, it is thought to represent a critical step. The active CAMKII permits the phosphorylation of existing, and insertion of additional AMPA receptors at the synaptic membrane facilitating postsynaptic response (**Fig.5.1.4**) (Nicoll R.A. and Malenka R.C., 1995). More than 30 isoforms of CaMKII represent one of the most prevalent proteins in neurons (1-2% of the total). Even if it is expressed both pre- and postsynaptically, in the postsynaptic density it is higher expressed since it controls the calcium oscillations. In fact, CaMKII seems to be a mediator of peculiar importance in linking transient calcium signals to synaptic plasticity (Lynch M.A., 2004), as demonstrated by two independent groups in 1989 which reported as CaMKII inhibitors blocked LTP in CA1 (Malinow R. et al., 1989; Malenka R.C. et al., 1989). It has been proposed that this protein, once active, contributes to the morphological changes that distinguish the more persistent phases of LTP. Indeed, CaMKII binds to several postsynaptic density proteins like α-actinin and PSD95 as well as densin-180, the synaptic adhesion molecule.

The active form of CaMKII phosphorylates also cytoskeletal proteins which are pivotal in the cytoskeletal regulation like microtuble-asscociated protein 2 (MAP2) and neurofilament L. Moreover, some of the CaMKII substrates include presynaptic proteins like synapsin, synaptogamin and synaptophysin which play important role in the neurotransmitter release which, in turn, is enhanced in LTP (Lynch M.A., 1998).

A great deal of evidence suggests that increased AMPA receptor expression on the postsynaptic membrane is likely to be another primary requisite for the LTP expression. Studies on LTP-linked changes in CA1 neuronal sensitivity to ionophoretically applied glutamate receptor ligands represent the first findings about the modulation of postsynaptic AMPA receptor expression after LTP induction, and in particular an increased number of receptors (Davies S.N., 1989). The so called "silent synapse theory" of LTP started with the discovery of functionally silent synapses because of lack of AMPA receptors, although the presence of NMDA receptors (Liao D. et al., 1995; Isaac J.T. et al., 1995). However, stimulus-induced LTP in the hippocampus resulted in the recruitment of AMPA-receptor-mediated responses because of the postsynaptic insertion of these receptors after LTP induction (Liao D et al., 1995; Isaac J.T. et al., 1995). These and other works contributed to the theory that AMPA receptor expression is a dynamic cellular process being controlled by a cycle of exo- and endocytosis. In cultured cells it has been showed that this process is modulated also by LTP-mediated NMDA receptor activation, which leads to the recruitment of more AMPA receptors and to increased AMPA-mediated miniature EPSPs (Liao D. et al., 2001). Moreover, it seems that silent synapses exhibit a developmental profile: the number of synapses expressing NMDA but not AMPA receptors in the developing hippocampus (Liao D. et al., 1999), cerebellar granular cells (Losi G. et al., 2002) and thalamocortical synapses (Feldman D. et al., 1999) decreases with age. LTP may therefore lead to the conversion of these synapses from silent to non-silent and this is fundamental in the modulation of experience-dependent changes in these circuities.

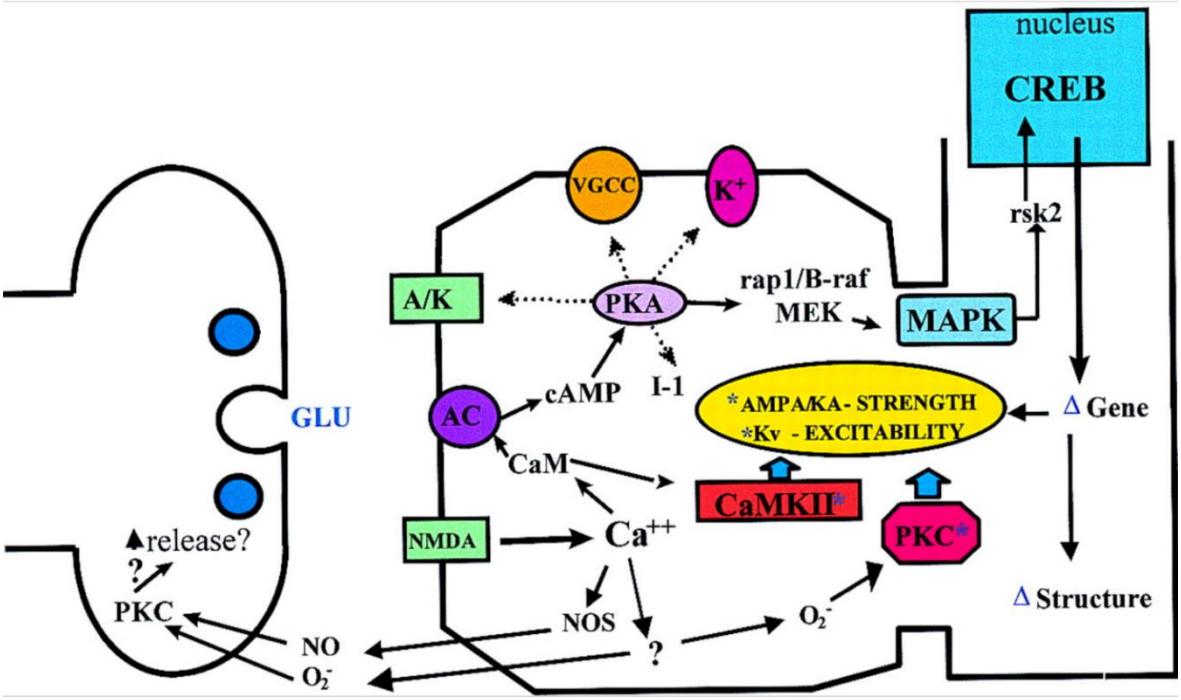

Figure 5.1.3 Core signal transduction pathways operating in LTP. This schematic diagram shows several of the signal transduction pathways documented as operating in LTP in hippocampal area CA1. (A/K) AMPA/KA receptors; (CaM) calmodulin; (NMDA) NMDA receptor; (NOS) NO synthase; (O2−) superoxide anion; (AC) adenylyl cyclase; (PKC) oxidized, autophosphorylated (persistently activated) PKC or the autonomously active proteolytic form of PKC (z isoform); (CaMKII*) CaMKII, either transiently or persistently activated; (I1) protein phosphatase inhibitor 1; (VGCC) voltage-gated calcium channels; (K+) voltage-dependent K channels; (rsk2) ribosomal S6 kinase 2. (Sweatt J.D., 1999).

3. the alteration of gene expression/protein synthesis leads to the long-lasting effects of L-LTP. The ultimate effectors of the different pathways for this alteration have not been completely identified yet, but AMPA receptors, potassium channels and cell surface structural models are the major candidates (Sweatt J.D., 1999). Several studies indicated that LTP relays on a cascade of cellular signalling events which are activated by an increment of intracellular cAMP concentration; among these events there is the PKA activation, which, in turns, leads to activation of transcription factors such as CREB and translation (Lynch M.A., 2004). For instance, in pre-frontal path granule cells synapses L-LTP was inhibited by the PKA inhibitor R*p*-cAMPs and mimicked by the adenylate cyclase activator forskolin (Lynch M.A., 2004) proposing that the primary effect of PKA was to promote protein synthesis. Another downstream consequence of increased cAMP concentration is the activation of the mitogen-activated protein kinase (MAPK/ERK) which can exerts various outcomes because of its myriad substrates (Lynch M.A., 2004). ERK relevance in LTP expression came out once it was demonstrated that its inhibition resulted in LTP suppression (English J.D. and Sweatt J.D., 1997). In particular, it seems that ERK is important during both the E- and L-LTP exerting its effects by phosphorylating potassium channels and synapsin I. Specifically, a decrease in voltage-dependent activation of Kv4.2 would lead to increased excitability and, thus, LTP (Sweatt J.D., 2001); ERK-mediated phosphorylation of synapsin I reduces synapsin-actin building, a process that induces vesicle movement to the active zone augmenting the probability of release (Greengard P. et al., 1993).

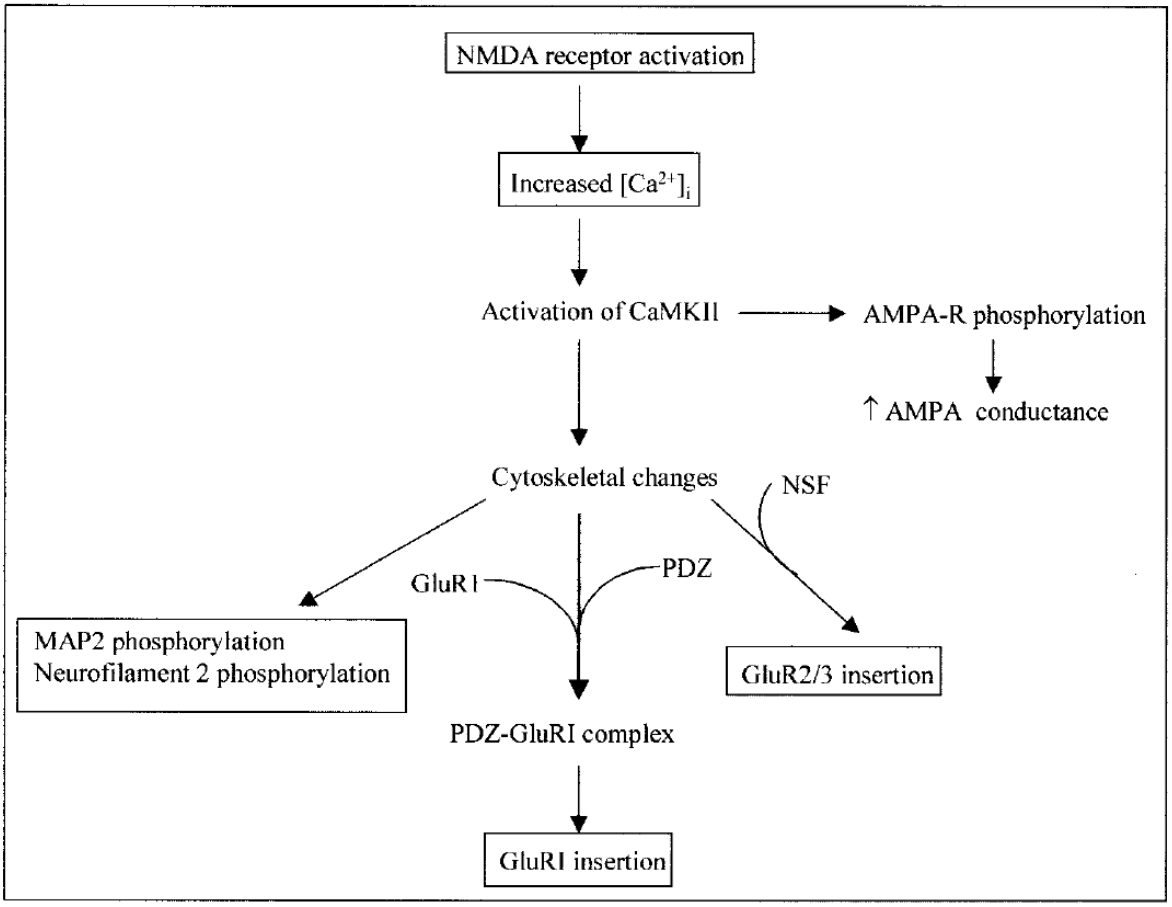

Figure 5.1.4 Among the consequence of the increase in intracellular Ca^{2+} concentration ($[Ca^{2+}]_i$) which accompanies N-methyl-D-aspartate receptor (NMDA-R) activation is increased CaMKII activity which exerts multiple actions. One significant effect is increased AMPA conductance as a result of AMPA receptor

(AMPA-R) phosphorylation and increased recycling of AMPA-R, which is due to CaMKII-induced changes in cytoskeletal proteins. NSF, N-ethylmaleimide- sensitive factor (Lynch M.A., 2004).

LTP can last from diverse hours to even weeks, depending to the experimental approach. Besides molecular changes affecting the protein synthesis and gene transcription, LTP is maintained in time thanks to morphological changes as the enlargement of dendritic spines or occurrence of new ones (Malenka R.C. and Bear M.F., 2004).

Although the locus of LTP expression, if pre- or postsynaptic, has been largely debated and is still source of controversy, there is convincing evidence that postsynaptic changes in AMPA receptors play an important role for LTP expression. In new-born rats it has been showed that postsynaptic modifications relay mostly to the increase of AMPA receptors' responsiveness (by CAMKII-mediated phosphorylation of GluR1 subunit, Barria et al., 1997) or AMPA receptors' number (by their selective and rapid CAMKII-mediated up-regulation and trafficking, Lu W. et al., 2001). Conversely, in mature animals a rapid surface expression of NMDA receptors has been detected under LTP (Grosshans D.R. et al., 2002). Relative to LTP-induced presynaptic modifications, enhanced neurotransmitter release from synaptic vesicles has been detected (Zakharenko S.S. et al., 2001; Tyler W.J. and Pozzo-Miller L.D., 2001).

5.2 EXPERIMENTAL APPROACHES TO INDUCE LTP

The scientific discovery of LTP of synaptic transmission (Bliss T.V. and Lomo T., 1973) and its counterpart LTD (Lynch G.S. et al., 1977) gave rise to a cascade of neurobiological studies which, finally, resulted in the widely accepted hypothesis that synaptic plasticity is necessary and sufficient for memory formation (Letzkus J.J. et al., 2007). In fact, during the first decade after the LTP discovery was announced, there were some scepticisms that it could serve as a memory mechanism, because of the needed conditions to induce it. Experimentally, hundreds of electrophysiological studies over the years developed several paradigms of LTP to model synaptic plasticity. Only in the Erik Kandel's lab, 77 papers were published on mechanisms of learning in *Aplysia* (Larson J. and Munkácsy E., 2015).

Nowadays, LTP is considered a widely accepted process that link synaptic plasticity with both physiological processes (memory) and pathological conditions (i.e., neurological disorders which affect synapses). Parallels between hippocampal LTP and behaviourally defined memory have been critically studied founding similarities, as rapid induction, strengthening by repetition, long-lasting processes, dependence on NMDA receptor activation and correlations of LTP decay with the time course associated with normal forgetting (Otto, T. et al., 1991). More recently, scientists provided a direct demonstration that hippocampal LTP is induced by learning (Whitlock J.R. et al., 2006) and that the process required to maintain LTP sustains spatial memory (Pastalkova E. et al., 2006).

5.2.1 Electrically-induced LTP protocols

All these studies tried also to identify electrical stimulation protocols to induce and mimic the physiology under the formation of new memories. In these electrically induced LTP protocols, the strength of synaptic efficacy is controlled by the frequency of synaptic activation. Brief and high

frequency bursts (~100 Hz) result in LTP or long-lasting increase in the strength of synaptic transmission, while prolonged low frequency stimulations (~1 Hz) result in LTD or a persistent reduction of synaptic transmission (Bliss T.V. and Collingridge G.L., 1993; Malenka R.C. and Bear MF, 2004).

Whitlock JR et al. (Whitlock J.R. et al, 2006) observed that high-frequency stimulation (HFS)-induced LTP in rats produced the same changes in hippocampal glutamate receptors as did one-trial inhibitory avoidance learning, directly demonstrating learning-induced LTP in CA1. High frequency potentiation/tetanus consists in a train (s) of 50-100 stimuli (**Fig 5.2.1.1a**, square pulses) at 100 Hz (Bliss T.V. and Collingridge G.L., 1993) and are effective for inducing both NMDA receptor -dependent and independent forms of LTP.

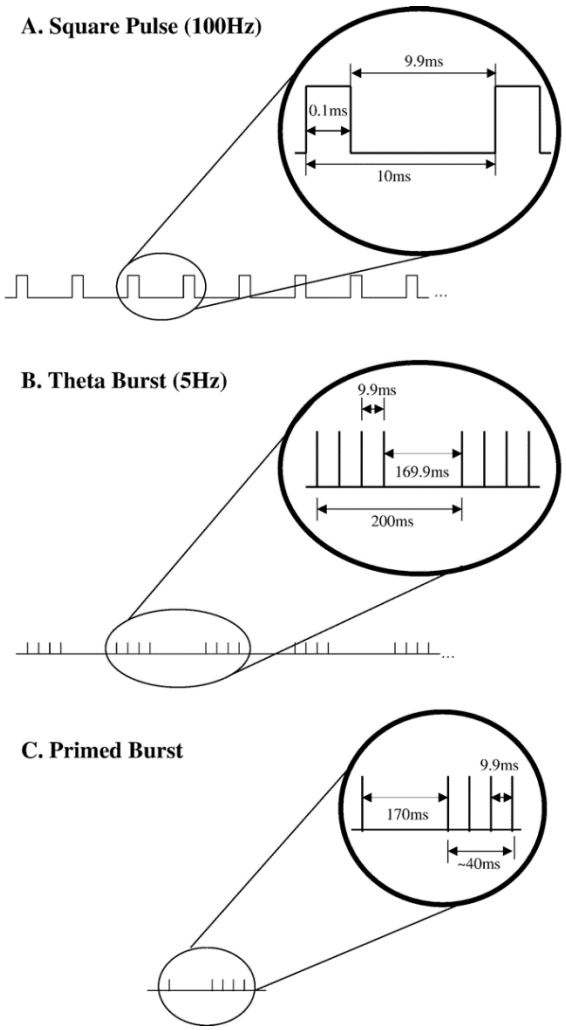

Figure 5.2.1.1 Pulse sequence dimensions. (A) Representation of a 100 Hz square pulse, commonly used for LTP induction. The pulse width=0.1 ms; interpulse interval=9.9 ms and the pulse length is 10 ms. (B) Representation of a theta burst stimulation pattern commonly used for LTP induction. This stimulation protocol illustrates four 100 Hz pulses applied in rapid succession, 5 times/s. The pulse width=0.1 ms (not shown); interpulse interval=9.9 ms; interburst interval =169.9 ms; burst length=200 ms. (C) Representation of a primed burst protocol that is used to induce LTP. The pulse width=0.1 ms (not shown); interpulse interval=9.9 ms; interval between primed burst +4=~40 ms; primed burst interval=170 ms. (Albensi B.C. et al., 2006)

However, the "strong stimulation" (Vertes R.P., 2005) of three 100 Hz trains (100 pulses for 1 s repeated 3 times with an interval ranging from 0.5 to 10 s for a total of 300 pulses) is effective at producing the 3 h-long lasting L-LTP which involves protein synthesis (Albensi B.C. et al., 2006). Conversely, the "weak stimulation" of a single 100 Hz train (100 pulses over 1s, Vertes R.P., 2005) leads to the 1-3h long-lasting E-LTP which is protein synthesis-independent.

Since naturally occurring firing of hippocampal neurons in living animals probably do not fire at 100 Hz for one full second but typically fire for only 30-40 ms bursts of 3 to 4 spikes (Albensi B.C. et al., 2006), standard HFS patterns appear questionable. For this reasons, other electrical protocols for inducing LTP (Rose G.M. and Dunwiddie T.V., 1986; Pavlides C. et al., 1988) were developed and appeared physiologically closer to what occur in the hippocampus during episodes of learning and memory in living animals (**Table 1**, Albensi B.C. et al., 2006).

Representative electrical stimulation protocols for inducing synaptic plasticity

Protocol type/ expected response	Pulse frequency (Hz)	Total no. of pulses/pulse duration (μs)	No. of bursts/burst duration	Trains[a] (i.e., a sequence of bursts)	Intervals	Reference(s)
LFS/LTD	1	900/100	1/15 min	1	~999.9 ms IPI	(Albensi and Mattson, 2000)
LFS/LTD	3	900/100	1/5 min	1	~333 ms IPI	(Mockett et al., 2002)
LFS/LTD	3	1800/100	1/10 min	1	~333 ms IPI	(Mockett et al., 2002)
LFS/no change	10	900/200	1/90 s	1	~99.8 ms IPI	(Adams and Dudek, 2005)
HFS/LTP	50	50/200	1/1 s	1	~19.8 ms IPI	(Adams and Dudek, 2005)
HFS/LTP	100	100/200	1/1 s	1	9800 μs IPI	(Hernandez et al., 2005)
HFS/LTP	100	300/200	3/1 s	1	9800 μs IPI 10 s IBI	(Hernandez et al., 2005)
Theta/LTP	100	4/100	1/40 ms	1	9900 μs IPI	(Morgan and Teyler, 2001)
Theta/LTP	100 (repeated at ~5 Hz)	40/100	5/40 ms	2	9900 μs IPI 200 ms IBI 10 s ITI	(Morgan and Teyler, 2001)
Theta/LTP (*in vivo*)	400	5/150	3/12.5 ms	1	2–3 s IBI	(Hyman et al., 2003)
Primed Burst/LTP	100	5 (1+4)/100	2 (PB+4)/~40 ms	1	170 ms PBI	(Rose and Dunwiddie, 1986; Diamond et al., 1988)

Abbreviations: Hz=hertz; HFS=high frequency stimulation; IBI=interburst interval; IPI=interpulse interval; ITI=intertrain interval; LFS=low frequency stimulation; LTD=long-term depression; LTP=long-term potentiation; min=minutes; ms=milliseconds; No.=number; NR=not reported; PB=primed burst; PBI=prime burst interval (time between first pulse and the onset of 4 pulses of 100 Hz); s=seconds; μs=microseconds.

[a] It should be noted that some investigators use the terms burst and train interchangeably, but we have defined a train to be a sequence of bursts.

Table 1. Adapted from Albensi B.C. et al., 2006.

Theta burst stimulation (TBS) protocols (**Fig. 5.2.1.1.b**) started to be tested once it was observed that rat hippocampal EEG waveform was dominated by a 5 to 12 Hz (theta, ɵ) frequency during learning-related exploratory behaviours (Grastyan E. et al., 1959). Pavlides C et al (Pavlides C. et al., 1988) shown that the LTP in the dentate gyrus of anesthetized rats were much more efficient when the stimulation trains were delivered during the positive phase (peak) of theta, while the same type of burst given during a trough of the theta oscillation induced LTD (Huerta P.T. and Lisman J.E., 1995). In TBS, the lack of feed-forward inhibition allows temporal summation of EPSPs which activates NMDA receptors. This disinhibitory process referred to as "priming" involves presynaptic GABA autoreceptors that inhibit GABA release. Moreover, Nguyen et al (Nguyen P.V. et al., 1994) showed that theta burst protocols in CA1 mouse hippocampal slices induced an LTP of >180 min duration, demonstrating that these protocols were also effective in inducing long-lasting LTP. -In summary, the TBS discovery (Larson J. and Munkácsy E., 2015) to effectively induce LTP was significant for three mayor reasons: first, it showed that spontaneously occurring patterns of neuronal firing (complex-spikes) could induce LTP if well timed; second, the optimal repetition rate

corresponded to the hippocampal theta rhythm frequency; third, patterned stimulation paradigms allowed the uncovering of several events that contribute to LTP induction.

Rose GM and Dunwiddie T.V. (Rose G.M. and Dunwiddie T.V., 1986) in 1986 was among the firsts to report that another protocol, the primed bursts (PB), was effective in inducing LTP as HFS enhancing the population spike (PS) amplitude (i.e., PB-PS 243 % baseline, HFS-PS 331 % baseline). PB stimulation protocol typically consists in five pulses at 100 Hz where the first pulse precedes the last 4 ones by 170 ms (**Table1**, Albensi B.C. et al., 2006). In the same period, Larson and Lynch (Larson J. and Lynch G., 1986) conducted a study in CA1 hippocampal slices where they hypothesize that a burst of synaptic activity may result in a diffuse priming effect which alters the postsynaptic response to the high frequency activity (Albensi B.C. et al., 2006).

Besides the previously described frequency-dependent protocols to induce LTP, other relevant protocols are paring-dependent, where the synaptic strength is controlled by the coincidence of presynaptic activation and postsynaptic depolarization. A lot of studies have addressed the importance of the temporal order of pre- and postsynaptic spiking in long term modification of a variety of glutamatergic synapses, defining the "critical window" for spike timing (Dan Y. and Poo M.M., 2006). The duration of coincident activation can cover a range of time going from several hundred msec to just one pre- and postsynaptic action potential. This latter case consists in a specific form of timing-dependent LTP (tLTP) termed spike-timing dependent plasticity (STDP). As illustrated in **Figure 5.2.1.2**, LTP is induced when presynaptic spiking precedes postsynaptic spiking ("pre-post", positive timing) within a window of several tens of msec, while LTD is induced through spiking of the reverse order ("post-pre", negative timing). In other words, STDP is a form of bidirectional plasticity in which the temporal order of pre- and postsynaptic action potentials on a precise timescale of msec triggers changes in synaptic scale (Dan Y. and Poo M..M, 2006).

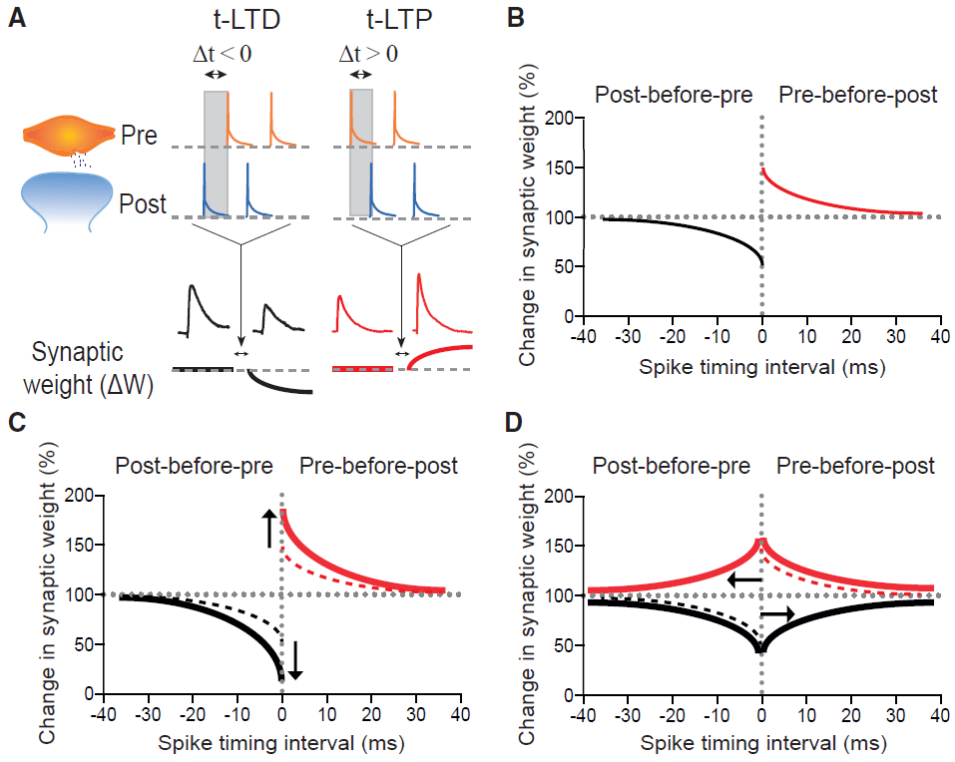

Figure 5.2.1.2. Induction and Expression of Spike-Timing-Dependent Plasticity (STDP) (A) After a stable baseline period, STDP is typically induced by repeated pairings of single presynapticand postsynaptic spikes.

In its classic form, STDP depends on the order and milli second-precision timing of spikes: multiple pre before-post spike pairings induce timing-dependent long-term potentiation (t-LTP), whereas post-before-pre pairings induce timing-dependent long-term depression (t-LTD). The magnitude of change, as an indicator of synaptic plasticity,is defined as a percentage change in synaptic weight from baseline. (B) The classic Hebbian STDP window: induction protocols with positive (pre-before-post) spike timing intervals induce synaptic potentiation; protocols with negative (post-before-pre) spike timing intervals induce synaptic depression. (C and D) The relative spike timing is not the sole determinant governing timing-dependent plasticity. Instead, STDP is malleable. Both the magnitude (C) and the temporal requirements for STDP (D) can be modulated (Brzosko Z. et al., 2019).

In Hebbian STDP, LTP occurs when presynaptic spikes precede postsynaptic spikes by ~0 to 20 ms (positive Δt), whereas LTD occurs when post leads pre by ~0 to 20-100 ms (negative Δt) (Feldman D.E., 2012). Anyway, STDP do not depend only on spike timing, but also on firing rate, synaptic cooperativity (the need for multiple coactive inputs to generate sufficient depolarization or spiking to drive LTP) and postsynaptic voltage (Markram H. et al., 1997). Hebbian-STDP at glutamatergic synapses is ruled by the same signalling pathways that rule most correlation-dependent, classical LTP and LTD: NMDA receptor-dependent LTP and NMDA receptor-dependent LTD, where paired presynaptic vesicle release and postsynaptic depolarization trigger calcium influx through postsynaptic NMDA receptors and VGCCs.

Briefly, induction of t-LTP involves several mechanisms: (1) removal of the Mg2+ block from the NMDA receptors, (2) inactivation of A-type currents and activation of Na+ channels to improve signal propagation and (3) AMPA receptors depolarization to boost NMDA receptor calcium signal (Inglebert Y. and Debanne D., 2021). However, the NMDA receptors are the major player since their blockade prevent the induction of LTP.

STDP has been demonstrated *in vivo* and *ex vivo* at both excitatory (Inglebert Y. and Debanne D., 2021; Markram H. et al., 1997; Bi G.Q. and Poo M.M., 1998) and inhibitory synapses (Ormond J and Woodin M.A., 2009; Takkala P. and Woodin M..A, 2013), as well as in different brain areas in a range of species, from locust and xenopus through rodents to non-human primate and humans (Brzosko Z. et al., 2019). Therefore, STDP is nowadays considered a biological plausible model for synaptic modifications occurring *in vivo*, since its physiological relevance has been assessed (Caporale N. and Dan Y., 2008).

Classically, STD is local in nature, involving only the pre- and postsynaptic neurons (and maybe supporting glial cells), detecting the timing of arrival of presynaptic action potentials at the bouton and back-propagating spikes (bAP) at the dendrite (**Fig. 5.2.1.3**).

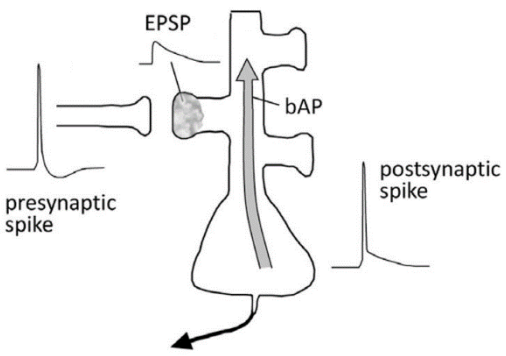

Figure 5.2.1.3 Induction of STDP by pairing presynaptic spikes and associated EPSPs with postsynaptic spikes. (modified from Bi G.Q. and Poo, 1998)

5.2.2 Iontophoresis or chemically-induced LTP

Electrically induced protocols for the induction of LTP have furnished an enormous contribution for the understanding of synaptic plasticity and related memory and learning processes, both *in vitro* and *in vivo*. However, conventional electrophysiological LTP induction protocols through standard electrode stimulation involve just a small set of synapses which are intensively but transiently activated. Moreover, these highly localized protocols make it very hard to analyse molecular and cellular changes associated with LTP since most imaging and biochemical studies require a large fraction of potentiated synapses. Therefore, chemical protocols for inducing LTP (cLTP) also have been developed and have gained in popularity (Anikszteijn L. and Ben-Ari Y., 1995; Otmakhov N. et al., 2004). cLTP consists in the strengthening of synaptic transmission using compounds such as neurotransmitter, neuromodulators, drugs, chemical agents, and others which are chronically or acutely administered to the culture. In this way, the very easy and manageable bath application of these compounds can activate the entire neuronal network maximizing the likelihood of detection of molecular and morphological changes in neurons involved (Molnár E., 2011).

Over the last twenty years, several protocols of cLTP have been developed for electrophysiological studies as the investigation of the NMDA receptor dependent LTP. Originally these protocols were used in brain slices (Otmakhov N. et al., 2004; Turner R.W. et al., 1982; Kopec C.D. et al., 2007; Hosokawa T. et al., 1995) and further adapted to induce LTP in homogenous neuronal cultures (MacDonald J.F. et al., 2001; Salter M.W., 2001). In fact, dissociated neuronal cultures have the obvious advantage to make individual living cells and their synapses more accessible compared to the brain *in vivo* where synapses are densely packed together. Dissociated cells grow as a monolayer where all the membrane proteins, as the surface-expressed neurotransmitter receptors, are easily accessible for immunocytochemical/biochemical assays. In addition, once cultured, the dissociated cells are postmitotic (already committed to their differentiation) meaning that they maintain all their properties in the dish (i.e. expression of ion channels, organization of the cytoskeleton components, characterization of specific synapses).. The characterization of these plasticity models based on neuronal cultures demonstrates that they share the same key features of the NMDA-dependent LTP of neurons in slices. In fact, also in neuronal cultures c-LTP needs NMDA receptor activation and a rise in postsynaptic intracellular Ca2+ levels (Molnár E., 2011). All protocols of c-LTP aim to produce a synchronized, temporary, and powerful Ca2+ influx through NMDA receptors in response to synaptically released- or exogenously applied-glutamate.

A common form of cLTP is the glutamate-induced LTP. This protocol was applied in both hippocampal (Malgaroli A. and Tsien R.W., 1992) and amygdala neuronal culture (Franceschi B. A. et al., 2021) by brief (30 s) challenge with exogenous L-glutamate (50 uM). Another approach to induce cLTP in hippocampal neuronal culture is the synaptically release of L-glutamate elicited by 30 s challenge with hypertonic (400 mosM) Mg^{2+}-free solution supplemented with 100 mM sucrose (Malgaroli A. and Tsien R.W., 1992). Glutamate application produces a long-lasting LTP of the amplitude of spontaneous postsynaptic currents (sPSC) and evoked excitatory postsynaptic currents (eEPSC) as well as of the frequency of miniature excitatory postsynaptic currents (mEPSC, Malgaroli A and Tsien RW, 1992). In hippocampal slices, a LTP induction protocol using glutamate iontophoresis was developed without afferent stimulation too (Cormier R.J. et al., 1993). The authors demonstrated that iontophoresis LTP was Ca^{2+} dependent, it was blocked by ME-801, and occluded tetanus induced LTP (Cormier R.J. et al., 1993). Importantly, iontophoresis LTP was induced when excitatory postsynaptic potentials were completely blocked by adenosine plus tetrodotoxin (TTX),

suggesting constraints on the involvement of presynaptic mechanisms and putative retrograde messengers in LTP induction and expression (Cormier R.J. et al., 1993).

Another cLTP induction protocol named aminophosphonovaleric acid (APV) pre-conditioning of neuronal culture (APV-pre cLTP) was applied by (Liao D. et al., 1999) who cultured hippocampal neurons in the presence of APV, NMDA receptor antagonist. They obtained an upregulation of these receptors as well as an enhanced proportion of "silent synapses" that expressed NMDA receptors only. Exposure of these APV preconditioned (APVpc) neurons to an APV and Mg^{2+} free medium for 3 min favours activation of the NMDA receptors and increases correlated activity of neurons in the culture. This process requires an increment of intracellular calcium level, and it is associated with either the formation of novel dendritic spines and the pruning of older ones (Molnár E., 2011; Goldin M. et al., 2001).

The pre-conditioning of neurons with APV is required also for the glycine-induced cLTP protocol. Once the APV is removed, the synaptic activation of NMDA receptors is further enhanced by glycine stimulation (100-200 uM for 5-10 min) in Mg^{2+}-free medium often with Ca^{2+} elevated to 3mM to develop Glycine-cLTP (Shahi K. and Baudry M., 1993; Goldin M.. et al., 2001; Lu W et al., 2001). This LTP form is blocked by APV, MK-801 or BAPTA chelator which increases Ca2+ buffering in the postsynaptic cells (Lu W et al., 2001). Moreover glycine-LTP occurs with an increased clustering of AMPA receptors at dendrites and insertion of native or recombinant AMPA receptors (Molnár E., 2011). This facilitated AMPA insertion into excitatory synapses occurs via SNARE-dependent exocytosis during LTP since it is blocked by intracellular tetanus toxin (Lu W. et al., 2001). Through this approach Ivenshitz M. et al (Ivenshitz M. and Segal M., 2006) observed an enhanced network activity and synchronization resulting in a long-lasting strengthening of excitatory connections and weakening of inhibitory ones up to 1h after the conditioning.

This induction protocol has been widely used in both slices (Makino H. and Malinow R., 2009; Otmakhov N. et al., 2004) and neuronal cultures (Oh M.C. et al., 2006). A very sensitive form of cLTP is based on the increment of intracellular cAMP level through a 16-min long application of adenyl cyclase activator forskolin (50 μM) and the phosphodiesterase inhibitor rolipram (0.1 μM) in Mg^{2+} and 2-Cl-adenosine free artificial cerebrospinal fluid (forskolin/rolipram-induced cLTP, Otmakhov N. et al., 2004; Oh M..C et al., 2006). Through the rising of cAMP, the synaptic activation is bypassed and a direct activation of PKA and the following pathways of synaptic plasticity are achieved (Otmakhov N. et al., 2004). In fact, a direct activation of both transcription and transitional pathways underlying the consolidation and maintenance of the L-LTP have been observed (Brandon EP.. et al., 1995; Bolshakov V.Y. et al., 1997). For long-term changes in network activity, brief and transient (3*1 s) depolarization of neurons by high K^+ application (90mM) is commonly used (KCl-depolarization-induced cLTP) in both neuronal cultures (Appleby V.J. et al., 2011; Fitzjohn S.M. et al., 2001; Wu G.Y. et al., 2001; Nash J.E. et al., 2009) and brain slices (Lengyel I. et al., 2004; Migues P.V. et al., 2006). As a result, synaptic NMDA receptors are activated by endogenous release of glutamate with temporal windows that resemble the *in vivo* ones (Fitzjohn S.M. et al., 2001). The rapid depolarization induced by KCl-LTP depends on NMDA receptors and postsynaptic Ca^{2+} levels and it leads to an increment of mEPSC frequency (Fitzjohn S.M. et al., 2001). Finally, it is worth to mention the so-called *calcium-evoked dendritic exocytosis (CEDE)* from the postsynaptic neurons by the activation of CAMKII. This is achieved by 1 min-long application of the Ca^{2+} ionhophore A23187 at 1mM (Maletic-Savatic M. et al., 1998). CEDE is regulated developmentally and within a time course which is parallels to the expression of αCAMKII (Maletic-Savatic M. et al., 1998).

CEDE is likely to be involved in structural and functional modification of spines since organelles that undergo CEDE often are found on the base of spines (Maletic-Savatic M. et al., 1998). At this site, it may contribute to synaptic plasticity involving changes in receptor/channel density, release of active compounds affecting pre- and postsynaptic function, and/or growth of synaptic structures.

6. *IN VITRO* MODELS OF POTENTIATED AMYGDALA GLUTAMATERGIC SYNAPSES TO EXPLORE NANOMATERIAL INTERACTION

The brain is by far the most complex biological organ of the human body, and both its physiology and pathology are still not fully understood. This is mainly due to the limited accessibility and experimental freedom which make the observation and manipulation of *in vivo* brain processes very complex. Due to this lack in understanding and measuring the important pathological processes in brains' patients, a lot of neurological disorders are usually classified and diagnosed by the occurrence of clinical symptoms. For instance, LB are strongly associated to PD but also to Dementia with LB and the diagnosis discrimination is often based on the temporal evolution of symptoms (le Feber J., 2019).

Animal models whose primary criterion is the ability to recapitulate clinical symptoms represent an important tool to obtain new insights of brain disorders. Nevertheless, it is also known that these symptoms may be due to different mechanism respect to the ones leading to the human's disorders. In consequence, promising therapeutic approaches in animal models cannot be totally translated to the clinic (van der Worp H.B. et al., 2010).

An interesting and valid option to overcome these limitations is represented by the *in vitro* conditions (acute or organotypic brain slices or cultured isolated neurons) which offer much more accessibility and less complexity to study synaptic function in brain physiology and disorders and to develop valid treatments. Acute slices can be used for several hours and, recently, also longer (Buskila Y. et al., 2014), allowing the electrophysiological study of single or more neurons in a controlled system which is isolated form the rest of the brain. Organotypic slices resembles a more *in vivo* structure with a long-time experimental window, even if they are technically more challenging (Hutter-Schmid B. et al., 2015). Alternatively, neuronal cell cultures are obtained from embryonic or new-born rats/mice whose neurons are plated on coated coverslips or multi-electrode arrays (MEAs). Neuronal cell culture exists in the field of neurobiology research for more than a century and its refinement has progressed steadily since its inception. In addition, the differentiation of iPSCs into neurons has become a valid tool in disease modelling. After a maturation period of ~ 3 weeks, neurons develop *in vitro* forming branches, neurites, axons and dendrites with stable firing patterns. Newly formed synapses are glutamatergic or GABAergic with the latter exerting a net excitatory effect until 10 days *in vitro* (Ben-Ari Y., 2002). Although dissociated neurons loose the structural connections of *in vivo* conditions which are instead partially maintained in brain slices, these models are enormously applied to explore basic physiological neuronal functions as well as relevant brain disorders like circulation disorders, excitability disorders and memory disorders (le Feber J., 2019). In fact, they are extremely useful thanks to their fastness and simplicity of application and production. Moreover, the literature is extremely well characterized and their data about the study and evaluation of cellular behaviour in highly controlled systems are easily comparable.

Together with the study of disease pathophysiology, other scientific project deal with these models, as the identification of novel biomarkers, the exploration of toxic effect mediated by chemical compounds (McCool B.A. et al., 2003) the evaluation of interaction between neurons and nanomaterials, as well as for high-throughput drug screening. The *in vitro* conditions are faster and cheaper respect to the *in vivo* ones, even if they present some limitations too, as life span, cell composition or brain structure preservation (le Feber J., 2019). Moreover, its high experimental freedom is not always translated to treatment since the less free clinical practice (i.e., drugs may not pass the BBB or may cause systemic issues.

6.1 *IN VITRO* AMYGDALA CULTURES: A NEURAL NETWORK MODEL

The current notions about the roles of amygdala in human beings is due to enormous research and laboratory investigation on the neural pathways and physiological mechanisms of the rodent emotional behaviour (Gallagher M. and Holland P.C., 1994). Several works are based on the electrophysiological activity of various amygdala nuclei during a behavioural task (Rogan MT and LeDoux JE, 1996) or after a selective lesion (Killcross S. et al., 1997), leading to a deeper understanding of amygdala connectivity at molecular, cellular, and functional levels. However, the simplest, cheapest and fastest tool to study the complex circuitry underlying the amygdaloid complex of the human brain or to model pathological dysfunctions of it, is represented by the *in vitro* culturing of rat isolated amygdaloid cells (Kaneda M. and Akaike N., 1989; Lin C.H. et al., 2001; McCool B.A. and Farroni J.S., 2001; Meis S and Pape H.C., 1997). In fact, the amygdaloid bodies has a restricted anatomical access which limits specific experimental studies of synapses *in vivo*. Therefore, a more simplified model of amygdala circuitry, as *in vitro* neuronal cultures, is extremely important. In particular, this model has turn to be essential for the exploration of the interference between synapses and nanomaterial in the nanobiotechnology field, as well as for the screening of new drugs/biomolecules and nanosized material that might have potential therapeutical applications.

In 1996, two isolated group developed to different protocols to acutely isolate and dissociate rat amygdala neurons, both from Sprague-Dawley rats 1 to 3-weeks old and started from transverse slices (400-500 μm-thick) which were cut from tissue block of the brain using a vibroslice (Wang S.J. et al., 1996; Viana F. and Hille B., 1996). Wang SJ et al. (Wang SJ et al., 1996) isolated the amygdala regions under a stereomicroscope and dissected from the brain slices with a scalpel. Neurons were dissociated by trituration through a fire-polished Pasteur-pipette with 1mm-tip diameter and allowed to settle in coated coverslip (Wang S.J. et al., 1996). During the following years, the same approach was used by other groups (McCool B.A. and Farroni J.S., 2001; Lin C.H. et al., 2001) who isolated basolateral amygdala neurons from coronal brain slices of juvenile rats (from post-natal days, P, 10-28). On the other hand, F. Viana and B. Hille (Viana F. and Hille B., 1996) dissected the amygdala from the slices under a binocular microscope (20x) with a home-built micro puncher consisted of a sharpened 18-gauge stainless steel tube (1.2 outer diameter). Tissue pieces containing the amygdala were digested for 20-30 min and triturated by aspiration in a graded series of fire polished Pasteur pipettes (Viana F. and Hille B., 1996). They directly pipette the cell suspension into the recording chmabers (Viana F. and Hille B., 1996).

Other groups (Budde T. et al., 1992; Meis S. et al., 1996, Meis S. and Pape H.C., 1997) developed another protocol to isolate rat amygdala neurons with the use of minimal enzymatic treatment from Long Evans rats of P12-16. The basolateral amygdaloid complex was dissected under stereomicroscopic control from the amygdalostriatal transition area, caudate putamen and central

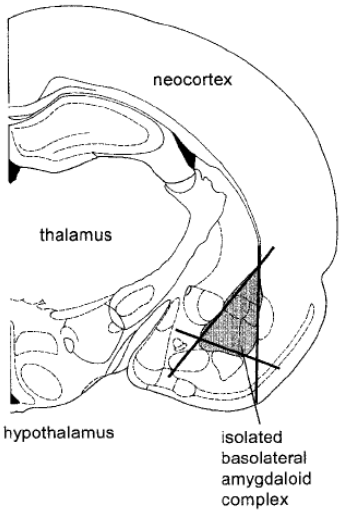

amygdaloid nucleus, external capsule, and piriform cortex by three cuts (**Fig. 6.1.1**). After 22–30 min of incubation in digestion enzyme, tissue was repeatedly rinsed with enzyme-free solution and neurons were mechanically dissociated by trituration of a single slice with fire-polished Pasteur pipettes and transferred into a recording chamber.

Figure 6.1.1 Schematic drawing of rat amygdaloid areas dissected for dissociation of cells (*modified from* PAXINOS, G. AND WATSON, C. The Rat Brain in Stereotaxic Coordinates. San Diego, CA: Academic, 1986).

Recently, Secomandi N. et al (Secomandi N. et al., 2020) developed and validated an easily accessible and simplified *in vitro* model of amygdala neural network through an enzymatic and mechanic dissociation protocol of the amygdala nuclei collected from 8/10 days old Wistar rats. The activity of the *in vitro* amygdala network was investigated through path clamp technique and used as a screening tool to target synapses towards development of future anxiety disorder treatments. The electrophysiological characterization showed that, when the tissue of origin is collected from adolescent animals and cells are allowed to differentiate *in vitro* for 8-12 days, cultures have single cell and synaptic features resembling those of *in vivo* amygdalar neurons of juvenile animals.. (**Fig. 6.1.2**).

Thereafter, the same experimental dissection protocol was applied by the same group (Franceschi B.A. et al., 2021) to mimic the hyperexcitability observed in anxiety disorders. In particular, the authors potentiated the *in vitro* amygdala circuitry through a cLTP protocol and tested the ability of s-GO in interfering with potentiated synapses.

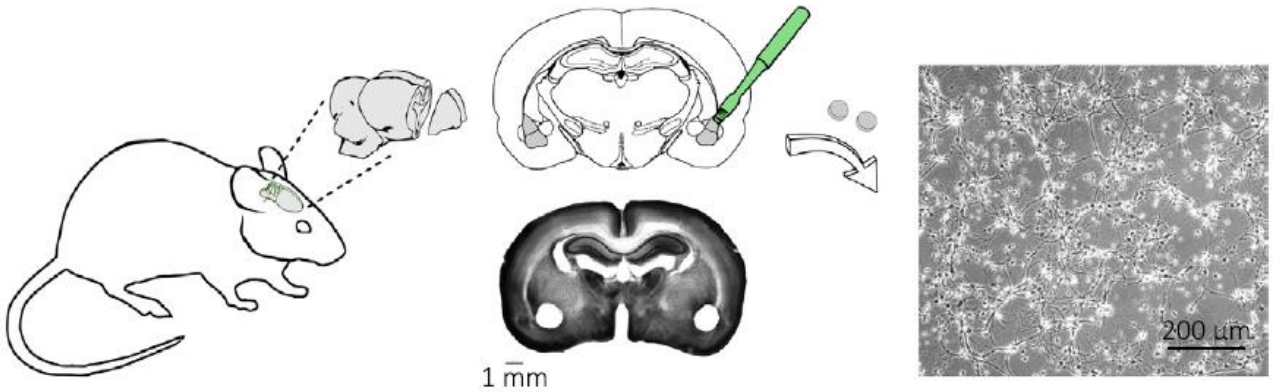

Figure 6.1.2 Schematic representation of dissociated amygdalar culture procedure: brains isolated from juvenile rats are sliced (left); amygdaloid nuclei are precisely isolated by a biopsy punch (in green) and

enzymatically dissociated to get pure cultures (right). The remaining tissue is stained with Nissl procedure (middle) to confirm the sampling of the amygdalae (Secomandi N. et al., 2020).

7. *IN VIVO* MODELS OF ANXIETY DISEASES

Anxiety disorders, like PTSD, are difficult to model in animals since they are complex phenotypes diagnosed by patient interviews and influenced by both genetic and environmental factors. Nevertheless, mammals show biologically preserved neurobiological and behavioural outcomes to valent stimuli which permit the use of rodent models of anxiety disorders. In fact, since anxiety disorders derive from traumatic experiences, rodent models can mimic stress induction and disorder development. These preclinical models have the advantage to manipulate stress type, intensity, frequency, and duration, thus recapitulating the disorder's phenotype which is, in turns, measured through different behavioural tests. Moreover, to inform anxiety model validity and importance to human psychopathology, rodent models incorporate individual, sex, strain, and stock differences, as well as early life stress effects, biomarkers, stringent success criteria for drug development, Research Domain Criteria, technological advantages, and cross-species comparisons (Verbitsky A. et al., 2020).

One of the major limitations in deciphering mental disorders through human investigations is that these diseases are variable and seldom studied throughout disorder development, observing population already exposed to uncontrolled stressors. The diagnosis of PTSD is established when an individual, once experienced a traumatic event, passes a symptom threshold for three clusters: re-experiencing (involuntary re-living the traumatic event in several ways), avoidance (individual efforts to emotionally and physically avoid persons, places..) and hyperarousal (heightened physiological reactivity as exaggerated startle response, hypervigilance..). Conversely, animal models permit to longitudinally monitor PTSD development pre-trauma through post-trauma with controlled stressors. Particularly, rodent represent key models to learn about PTSD induction, facilitating target identification for therapies, and testing drugs for human treatments (Verbitsky A. et al., 2020). Since animal models are simplified representation of PTSD, they are expected to capture PTSD symptomatology (face validity), etiology, (construct validity), treatment/drug response (predictive validity), and to differentiate between those with and without PTSD (discriminant validity) (Willner P., 1986; Belzung C and Lemoine M., 2011). Five criteria for the face validity of translational models were defined by Yehuda R. and Antelman SM. (Yehuda R. and Antelman SM.., 1993): 1. the stressor induces PTSD biological and behavioural outcomes; 2. responses are intensity-dependent; 3. biological alterations persist or progress; 4. biobehavioural alterations are bidirectional; 5. outcomes have inter-individual variability caused by genetic, environment or both.

In both animal and human, a similar network of brain structures regulates fear learning, therefore the leading experimental model to study how organisms learn to predict danger based on experience is classical fear conditioning (LeDoux J.E., 2000). Animal models for anxiety disorders, like PTSD, are exposed to different types of stressors which develop anxiety-like behaviours assessed by standard tests (EPM, open field, social interaction test, acoustic startle test). Paradigms model PTSD through the application of social, physical (inescapable footshock, underwater/forced swim paradigm, immobilization) and psychological stressors (i.e., housing instability, social defeat, or isolation), individually or in combination. Stressors can vary along different dimensions like frequency (single or repeated), duration (acute or chronic), and controllability (controllable or not).

For all stressors, peripheral biologic correlates of PTSD have been evaluated, typically satisfying construct validity. For instance, strong hypothesis about the hyperactivity of the corticotropin-releasing hormone system involved in PTSD have been verified also in rodents (Siegmund A. and Wotjak C.T., 2006). Physical stressors are advantageous for their simplicity in procedure, ease of scaling and clear symptom impact. They include underwater trauma, electric shock, restrain/immobilization stress, and single prolonged stress (Verbitsky A. et al., 2020). Physical and psychological stressors are largely used to differentiate individual variability and include social defeat and predator stress (Verbitsky A. et al., 2020).

In humans and particularly during development, prior exposure to a traumatic event may cause long term hormonal anomalies and enhanced risk of PTSD occurrence (Delahanty D.L. and Nugent N.R., 2006). Pioneering investigations with Harlow's monkey (Young LD. et al., 1973) examined the impact of early life stressor and maternal separation showing as neonatal separation increases anxiety upon exposure to important stress later in life (Diehl L.A. et al., 2012). Moreover, when juvenile rats are exposed to important psychological stressor are more incline to manifest anxiety-like phenotype once re-exposed to the same stressor in adulthood (Cohen H. et al., 2007).

Animal behavioural tests mimic the tests performed in humans and are used to assess stress effects allowing scientists to make inferences on rodent psychology. Many of these tests were validated and developed in rats, but later they had been adapted on mice too. Rats are considered the species of choice in preclinical studies since they have a great performance in operant tasks and because they are large enough in size to test compounds for toxicity and perform other invasive techniques. On the other hand, mice are advantageous for their breeding, group housing and genetic modifications.

In addition, genetic models from both rat or mouse strains have been developed to exhibit abnormal fear extinction or high level of anxiety (Holmes A. and Singewald N., 2013; Neumann I.D. et al., 2011).

In summary, animal models provide an important tool to investigate the pathophysiology of anxiety disorders since they circumvent different problems and limitations associated to human studies: (1) in animal models all aspects of the stressor can be manipulated including intensity, type and timing; (2) through these manipulations, pre-existing factors can be separated from those acquired after stress exposure; (3) more ethically acceptable and invasive techniques can be performed in animal models. However, behavioural, and neurobiological understanding of animal models has still to be refined, focusing on sex differences, early life stress effects, biomarkers, individual variability and behavioural test batteries, stringent success criteria for drug development, technological advantages and so on (Verbitsky A. et al., 2020).

8. NEUROPEPTIDE Y: ALTERNATIVE STRATEGIES FOR THE THERAPY OF ANXIETY DISORDERS

Anxiety disorders are the most prevalent psychiatric disorders and are associated with ahigh burden of illness (Bandelow B. et al., 2017). Whether or not these diseases are becoming more prevalent in recent years is not well documented with anxiety disorders being often underrecognized and undertreated in primary care. In fact, there is evidence for substantial undertreatment of anxiety disorders: in a large European study, only 20.6% of participants with an anxiety disorder sought

professional help. Of those participants who contacted health care services, 23.2% received no treatment at all, 9.6% received only psychological treatment, 30.8% received only drug treatment, and 26.5% were treated both with drugs and psychotherapy (Bandelow B. et al., 2017). It seems that women are 1.5 or 2 times more likely than men to receive a diagnosis of anxiety disorders (Bandelow B. et al., 2015).

Not all anxiety disorders have to be treated with therapies when symptoms are transient or mild, but treatments are indicated when marked distress and several complications occur in the patient (i.e suicide ideation, secondary depression, alcohol abuse). Treatment recommendations are based on guidelines for anxiety disorders (Bandelow B. et al., 2012; Bandelow B. et al., 2015). First line drugs are the selective 5-HT-reuptake inhibitors (SSRIs), and 5-HT-NE reuptake inhibitors (SNRIs). The onset of the anxiolytic effect of these drugs has a latency of 2-6 weeks and after the second week the adverse effects start to be stronger, like jitteriness and increased anxiety. Some SSRIs and SNRIs are inhibitors of cytochrome P450 enzymes and hence may interact with other psychopharmacological drugs for medical illnesses (Cipriani A. et al., 2009); moreover, withdrawal reaction may occur once stopping their treatment (Cipriani A et al., 2009). Other therapy options include pregabalin, tricyclic antidepressants (TCAs), moclobemide, buspirone.

Pregabalin is a calcium modulator acting at the α2δ subunit of voltage-gated calcium channels, it has sedating properties with an earlier onset of efficacy compared with antidepressants. However, there were concerns about the abuse of pregabalin in individuals suffering from substance abuse and withdrawal syndromes after abrupt discontinuation (Bandelow B. et al., 2017).

TCAs are a second-generation antidepressant in the treatment but the frequency of adverse events is higher, while buspirone, a 5-hydroxytryptamine receptor 1A (5-HT1A) agonist, has been shown in some controlled studies to be effective in the treatment of GAD. However, in the United States, 55% to 94% of patients with anxiety disorders are treated with benzodiazepines (Stahl S.M, 2002). The anxiolytic effects of benzodiazepines begin soon without leading to insomnia or jitteriness, but they are not recommended for daily use. In fact, their usage is associated with CNS depression, resulting in fatigue, dizziness, increased reaction time, impaired driving skills, and other adverse effects. Even cognitive functions may be impaired, and dependency may occur after long term administration (Schweizer E. et al., 1990).

Current medication for anxiety disorders is suboptimal in tolerability, leading to an urgent need for improved and novel treatments. Considering the current knowledge about the relevant neurocircuitries and neurobiological mechanisms underlying pathological fear and anxiety, the search for compounds with novel mechanisms of anxiolytic action should be considered an innovative approach. For example, ketamine, riluzole, xenon and the neurosteroid aloradine, but also NMDA, L-DOPA, endocannabinoids and D-cycloserine are promising novel candidates currently in clinical development, some also showing efficacy in fear extinction learning in humans (Sartori S.B. and Singewald N., 2019).

Available data point for novel pharmacological treatments of stress-related disorders, as anxiety and depression, regards the potential of the neuropeptide Y (NPY) system. Anti-stress actions of NPY involved diverse brain areas, with the most extensive data available for amygdala and hippocampus, and some data for areas within the septum, and locus coeruleus (**Fig 8.1**).

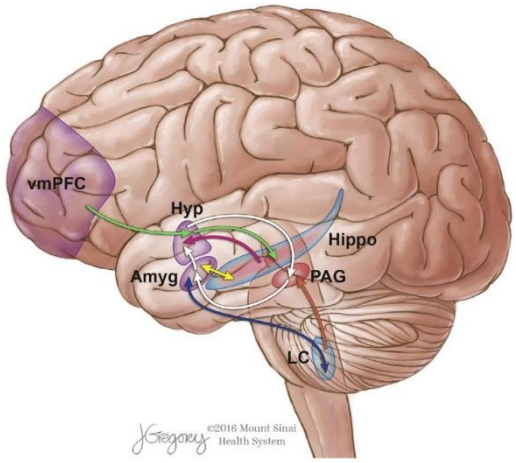

Figure 8.1 Schematic illustration of the NPY system in the brain. Neural pathways utilizing NPY as a neurotransmitter and brain regions expressing NPY Y1 and Y2 receptors are shown. Depicted regions that are both modulated by NPY and important for the regulation of fear and anxiety include the ventromedial PFC (vmPFC), the amgydala (amyg), the hippocampus (hippo), the periaqueductal gray (PAG), and the locus coeruleus (LC). Red = Y1 receptor, blue = Y2 receptor and purple = both Y1 and Y2. (Kautz M. et al., 2017)

NPY is a 36 amino-acids peptide belonging to the pancreatic polypeptide family (including the peptide YY, PYY, and the pancreatic polypeptide, PP) with widespread functions in the CNS and periphery in both behavioural and physiological terms (Sabban E.L. et al., 2016). NPY is highly evolutionary conserved, being one of the most abundant peptides in the mammalian nervous system, and its regulation is mediated by at least 5 diverse G-protein coupled receptors (Y1, Y2, Y4, Y5 and Y6; Michel M..C et al., 1998). Originally, the proposed Y3 receptor was characterized pharmacologically in bovine adrenal chromaffin cells, to be later found in several rat organs, but it has not been confirmed as a cloned entity receptor (Yulyaningsih E. et al., 2011).

NPY was discovered in the 1982 and described as a co-transmitter of sympathetic neurons modulating the actions of norepinephrine in the cardiovascular system (Wu G. et al., 2011), but later many other important functions of NPY have been discovered, particularly within the CNS. Among the physiological functions of NPY, there are the regulation of food intake, energy balance homeostasis, reproduction, sleep, inflammatory processes, tissue growth and remodelling, blood pression and memory. Moreover, NPY plays a key role in the control of anxiety related behaviours modulating fear and responses to stress. In particular, the potential role of NPY in the pathophysiology of anxiety and mood disorders has widely been explored. Preclinical and clinical studies have shown the involvement of NPY in these diseases including PTSD, depression, substance-abuse disorders, epilepsy, and other neurological disorders (Brothers S.P. et al., 2010). In regards and considering the hyperexcitability observed in this kind of neuronal pathologies, NPY has been shown to inhibit glutamate release within the hippocampus (McQuiston A.R. and Colmers W.F., 1996).

NPY expression is widespread among several brain areas. In particular, it has been detected in elevated quantity in cell bodies and fibres within cortical and subcortical regions which are involved in fear and anxiety, detection, and arousal, including amygdala, hippocampus, basal ganglia, cortex, PAG and locus coeruleus (Kask A. et al., 2002). In the brain, the NPY receptors are differentially distributed and, in particular, autoradiography demonstrates that the concentration of human Y1 is elevated in the dentate gyrus, hypothalamus, cortex, thalamus and caudate putamen; conversely, Y2 is found in the cerebral cortex, amygdala, hippocampus, striatum and nucleus accumbens (Hostetler E.D. et al., 2011; Caberlotto L. et al., 2000).

Shared properties between sedative compounds (i.e., benzodiazepines, alcohol, barbiturates) and NPY have been supported by EEG experiments in awake animals (Heilig M., 2004). In fact, intracerebroventricular (ICV) administration of NPY decreases EEG power generally, particularly

acting on amygdala and cortical regions which is a shared pattern with benzodiazepines (Ehlers C.L. et al., 1997). Conversely, low NPY levels in the brain have been observed in a rat model of PTSD (Cohen H. et al., 2012). Even behavioural studies demonstrate that high doses of NPY administration antagonize behavioural outcomes of stress. Particularly, through the EPM, (Pellow S et al., 1985), the social interaction test (File S.E., 1980), the light-dark compartment test (Pich EM et al., 1993) and the Vogel punished drinking conflict test (Heilig M. et al., 1989), it was demonstrated that NPY at lower doses mimics anti-anxiety action of benzodiazepines, suggesting a common core-process under fear and stress-related behaviours. Finally, in the fear-potentiated startle test (based on fear potentiation and not on behavioural inhibition) the anti-anxiety effect of NPY has been demonstrated too (Broqua P. et al., 1995), providing further supporting that the observed NPY outcomes are linked to emotions. In other study, ICV administration of NPY in spontaneously hypertensive rats (SHR) led to anxiolytic outcomes by enhancing the exploratory activity in the light-dark compartment test (Pich E.M. et al., 1993).

Importantly, it seems that the magnitude of behavioural anti-stress actions of NPY surpasses that of other endogenous compounds, as seen also in genetically modified animals (Heilig M., 2004).

Findings coming from a large range of studies suggest that the anxiolytic effect of NPY is primary mediated by the Y1 receptor which requires the full length NPY sequence for recognition and activation (Heilig M., 1995). More recent studies using Y1-receptor knockout mice confirmed that Y1 receptor is necessary for the anxiolytic effects of ICV-administered NPY (Karlsson RM. Et al., 2008). Anti-stress actions of NPY are mimicked by Y1-receptor agonists, and blocked by Y1 antagonists, although Y5 receptors may substitute for Y1 actions in some cases (Heilig M., 2004). However, administration of an Y1 receptor agonist in the amygdala did not ameliorate the expression of conditioned fear, and Y1 antagonist failed to block the NPY anxiolytic outcome when co-infused to NPY (Fendt M. et al., 2009). Probably, there is a multi-level interaction between Y1 and the other receptors in the regulation of fear expression. However, conversely, Y2 receptor antagonists produces anti-stress effects, as the Y1 agonists, as potentiation of Y2 signalling seems to be anxiogenic (Kautz M. et al., 2017). The mechanism of this effect seems to relate to the presynaptic location of Y2 on NPY-ergic neurons where it controls the endogenous NPY release: acting as an autoreceptor, Y2 activation leads to a reduction of NPY release through a negative feedback loop while its blockage leads to a potentiation of presynaptic NPY release (Kautz M. et al., 2017). Therefore, in contrast to Y1, potentiation of Y2 signalling may be anxiogenic. The Y2 is also involved in the NPY-regulated vascular effects, such as angiogenesis and blood pressure modulation, together with the regulation of circadian rhythm, feeding response and bone formation (Wu G. et al., 2011).

All these notions originally came from the observation that the full-length NPY peptide produced an anxiolytic-like effect in the EPM and Vogel test (Heilig M. et al., 1989), whereas the C-terminal (maybe the Y2- selective fragment) did not. Conversely, administration of a selective Y2 agonist was shown to increase the preference of mice for the closed arms of the EPM, consistent with an anxiety-producing effect (Kautz M. et al., 2017). Antisense oligonucleotides targeting Y1 receptor confirmed these data on EPM, inducing behavioural anxiety-like effects opposite to those seen after NPY administration (Wahlestedt C. et al., 1993).

It has been proposed that also Y5 receptor could be involved in emotion together with Y1, as in food intake regulation. Supporting this hypothesis, when NPY3-36 was administered into the amygdala, the Y5 rather than the Y1 receptor accounted for the anxiolytic action (Sajdyk T.J. et al., 2002; 2002a) even if in the EPM or open field test the selective Y5 antagonist CGP71683A failed to

influence anxiety-related behaviour (Kask A. et al., 2001). Anyway, little is known regarding the specific role of Y4, Y5, and Y6 receptors in humans. The Y4 was the third one to be cloned and it was found to be one of the most rapidly evolving G-protein -coupled receptor known (Raposinho P.D. et al., 2001). Evidence suggests that Y4 may play a role in the regulation of energy homeostasis and reproduction (Heilig M. et al., 1989), but recent findings indicate that, together with Y5, it may be involved also in depression-like behaviours (Sørensen G. et al., 2004). Knock-out studies of theY4 receptor in rodents found an anxiolytic effect in the OF, EPM and light–dark box tests, but also an impairment in fear extinction (Kautz M. et al., 2017). The interactions between Y2 and Y4 receptors have been found to increase the anxiolytic effect of the Y4 receptor removal in Y2/Y4 receptor double knockout conditions (Kautz M. et al., 2017). The Y5 receptor has been shown to reduce energy expenditure, inhibit reproductive hormone release, regulate brain excitability, induce feeding behaviour and regulate circadian rhythm (Wu G. et al., 2011). The Y6 receptor is a truncated receptor in many mammals including humans because of a mutation. Anyway, it is transcribed at an abundant level in several tissues in humans, like skeletal muscles, intestine, colon and adrenal gland (Yulyaningsih E. et al., 2011).

The arrival of subtype selective, NPY receptor antagonists, as the first member BIBP3226, has led to a more detailed analysis. BIBP3226 binds Y1 both *in vivo* and *in vitro* producing anxiogenic-like effects, but it has limited solubility and produces non-receptor side effects (Heilig M., 2004). Later, the structurally related Y1 antagonist BIBO3304 arrived showing improved affinity, higher solubility and lacking the non-specific side effects. Intra-amygdaloid administration of BIBO3304 blocked anxiolytic-like effects in the social interaction test (Heilig M., 2004). While ICV-administered NPY has been shown to inhibit acoustic startle and fear-potentiated startle, BIBO3304 led to a deep deficit in extinction retention (Gutman A.R. et al., 2008). On the other hand, consistent with the anxiogenic effect of Y2, administration of the Y2 antagonist BIIE0246 showed an increment in time spent in the open arm of the maze (Heilig M., 2004).

Initially, it was thought that the central amygdala was the target of NPY effect, but following works has re-evaluated the data, reporting is the lateral/basolateral amygdala complex in mediating anti-stress effects of NPY within the amygdala (Sajdyk T.J. et al., 2002; 2002a). Administration of diverse types of selective Y1 antagonists into lateral ventricles or the basolateral nucleus of the amygdala induced anxiogenic outcomes in rats (Wu G. et al., 2011).

Under the light of translational and therapeutic research, NPY is acquiring a lot of attention for the treatment of PTSD and other anxiety-disorders. Nevertheless, according to the therapeutical development with NPY, it is important to note the difficulties associated with the nature of peptides in general, including the short half-life, the obstacle in bypassing the BBB and the acid environment of the gastric mucosa. Moreover, many peptides largely act in the periphery of the CNS too, their introduction could result in unwanted side effects. Particularly the lack of passage across the BBR renders both oral and parental administration routes unavailable in peptide-based treatments of CNS disorders. Anyway, the intranasal administration of NPY seems to be the most promising in reaching the CNS since it avoids the BBB and affects multiple sites within the brain through intracellular neuronal olfactory and extracellular trigeminal-associated pathways (Kautz M. et al., 2017). A scientific group reported that intranasal NPY administration prior to a stressor, attenuated PTSD behaviours after 7 days post-stress, while its administration 7 days following stress, reversed these pathological behaviours (Kautz M. et al., 2017). A human phase I clinical trial of NPY administered intranasally in patients with PTSD is currently underway as an initial translational test of NPY as a therapeutic strategy for PTSD or other anxiety disorders (Clinicaltrials.gov, ID:NCT01533519).

In addition to the intranasal route, the potentiation of the Y1 signalling has become a promising strategy in PTSD treatments. For example, the Y1 receptor [Leu31,Pro34]-agonist NPY was found to inhibit the glutamatergic pyramidal neurons (Molosh A.I. et al., 2013), while anxiogenic effects are provided by the Y1 gene knockout (Olesen M.V. et al., 2012). However, administration of an Y1 receptor agonist in the amygdala was unsuccessful in ameliorating the expression of conditioned fear and, when NPY was co-infused with an Y1 receptor antagonist, the antagonist failed to impede the anxiolytic effect of NPY, suggesting a multi-level interaction between Y1 and the other Y receptors in the regulation of fear expression (Kautz M. et al., 2017).

In conclusion, currently available medications for mood and anxiety disorders have limited efficacy, with a significant percentage of patients showing partial response or treatment resistance (Trivedi M.H. et al., 2006). The consequent need for novel drugs which target other than monoaminergic systems, together with the vast discoveries on the NPY involvement in anxiety and mood disorders, make NPY system a promising goal for the development of personalized and innovative treatment interventions.

Nanomedicine and drug delivery systems offer a valid alternative route for the development of safe, selective, and potent compounds with activity at NPY receptors that achieve adequate brain exposure.

AIMS OF THE STUDY

To date, GBNs, with their outstanding and peculiar properties, have received extensive attention as tools for a wide range of biomedical applications in neuroscience (Kostarelos K. et al., 2017; Bramini M. et al., 2018; Cellot G. et al., 2022). Thanks to their nanoscale dimension, these nanomaterials show advantageous physical and electro-chemical properties, together with strength and flexibility, making them useful components of nanomedicine devices (Bayda, S. et al., 2019). In addition, they show great potential in the fields of drug deliver, diagnosis or bioimaging systems due to their good biocompatibility and low toxicity (Geim A.K. and Novoselov K.S., 2007).

Considering neurons as biological objects with their smallest organization level at the nanometer scale (i.e., dendritic spines and synaptic vesicles), GBNs emerge as promising nanotechnology tools for the manipulation of the mammalian CNS function with potential relapses for physiological studies as well as for the development of novel approaches for the treatment of neuropathology (Feng L. et al., 2014). It is therefore extremely urgent to investigate the interaction between nanomaterials and neuronal function, with a focus on the precise mechanisms of action of the nanomaterial at the subcellular level.

Our group previously reported that s-GO nanoflakes targeted excitatory synapses of hippocampal neurons, by downregulating specifically and transiently their glutamatergic synaptic transmission (Rauti R. et al., 2016; Rauti R. et al., 2019). Owing to this ability, s-GO have been proposed as an alternative nano-based approach for the treatment of neurodiseases characterized by abnormal glutamatergic signalling, including anxiety disorders. Among these, PTSD exhibits alterations in the amygdala neuronal circuitry, that are due to a pathological long-term enhancement in excitatory neurotransmission of the LA (Cortese and Phan, 2005) and that correlates with the emergence of anxiety-related behaviours.

In this framework, the aims of my thesis were the following:

- To investigate if s-GO could be used to hamper the aberrantly increased glutamatergic transmission observed in pathological conditions, such as in the PTSD;
- to identify the subcellular target of s-GO in order to dissect the mechanism of interaction between the nanomaterial and potentiated synapses;
- to explore the potential of s-GO as nanocarrier in drug delivery systems, by using neuropeptide Y as carried biologically active molecule (complexes in which the peptides were adsorbed on nanomaterial surface).

To address these issues, I developed an *in vitro* model of potentiated amygdala cultures, thus recapitulating the LTP of amygdala glutamatergic neurons observed in anxiety disorders. The accessibility of such paradigm to a variety of techniques, including dual patch clamp recordings to monitor eEPSC, live imaging with a styryl FM dye to assess vesicles dynamics at the presynaptic sites and confocal microscopy to image synaptic structures allowed me to investigate the impact of s-GO, alone or complexed to NPY, on synaptic function undergone to LTP.

My *in vitro* experiments were completed and corroborated by treating a rat behavioural model of PTSD with s-GO injections in the LA (work done by other collaborators in Prof. Ballerini's group under the supervision of Dr. Audrey Franceschi Biagioni).

This thesis generated three manuscripts, one already published (Franceschi B.A. et al., 2021) and two at draft stage.

Biomaterials 271 (2021) 120749

Contents lists available at ScienceDirect

Biomaterials

journal homepage: www.elsevier.com/locate/biomaterials

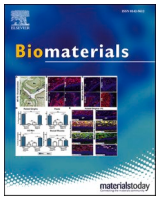

Graphene oxide prevents lateral amygdala dysfunctional synaptic plasticity and reverts long lasting anxiety behavior in rats

Audrey Franceschi Biagioni [a,1], Giada Cellot [a,1], Elisa Pati [a], Neus Lozano [b], Belén Ballesteros [b], Raffaele Casani [a], Norberto Cysne Coimbra [c], Kostas Kostarelos [b,d], Laura Ballerini [a,*]

[a] Neuron Physiology and Technology Lab, International School for Advanced Studies (SISSA), Neuroscience, Via Bonomea 265, 34136, Trieste, Italy
[b] Catalan Institute of Nanoscience and Nanotechnology (ICN2), CSIC and BIST, Campus UAB, Bellaterra, 08193, Barcelona, Spain
[c] Laboratory of Neuroanatomy & Neuropsychobiology, Department of Pharmacology, Ribeirão Preto Medical School of the University of São Paulo (FMRP-USP), Av. Bandeirantes 3900, 14049-900, Ribeirão Preto, SP, Brazil
[d] Nanomedicine Lab, National Graphene Institute and Faculty of Biology, Medicine & Health, The University of Manchester, AV Hill Building, Oxford Rd, Manchester, M13 9PL, United Kingdom

ARTICLE INFO

Keywords:
Graphene-based nanovectors
Biotechnology of brain disorders
Synaptic plasticity
Patch-clamp
Amygdala

ABSTRACT

Engineered small graphene oxide (s-GO) sheets were previously shown to reversibly down-regulate glutamatergic synapses in the hippocampus of juvenile rats, disclosing an unexpected translational potential of these nanomaterials to target selective synapses *in vivo*. Synapses are anatomical specializations acting in the Central Nervous System (CNS) as functional interfaces among neurons. Dynamic changes in synaptic function, named synaptic plasticity, are crucial to learning and memory. More recently, pathological mechanisms involving dysfunctional synaptic plasticity were implicated in several brain diseases, from dementia to anxiety disorders. Hyper-excitability of glutamatergic neurons in the lateral nucleus of the amygdala complex (LA) is substantially involved in the storage of aversive memory induced by stressful events enabling post-traumatic stress disorder (PTSD). Here we translated in PTSD animal model the ability of s-GO, when stereotaxically administered to hamper LA glutamatergic transmission and to prevent the behavioral response featured in long-term aversive memory. We propose that s-GO, by interference with glutamatergic plasticity, impair LA-dependent memory retrieval related to PTSD.

1. Introduction

Emerging evidence in mammals indicates the amygdala complex as the brain structure implicated in the development of anxiety disorder [1–3]. In animal models, core behavior related to anxiety can be induced by responses to fear stimuli [4,5] and previous elegant experiments suggested that the over-activation of distinct populations of basal amygdala neurons, such as glutamatergic ones effectively sustain fear behavior [6–8]. Moreover, dysfunctions in the glutamatergic system have a primary role in several brain diseases [9] and severe mood disorders are increasingly associated to altered synaptic plasticity [10]. In such a context, the glutamatergic system, known to play a major role in tuning neuronal plasticity [11,12], may represent a promising target to treat pathologies involving alterations in excitatory neurotransmission.

New biotechnology-based therapeutic interventions for brain pathologies have involved engineering of novel nanomaterials, such as graphene, the one carbon atom thick 2-dimensional (2D) material [13]. Graphene or its derivatives such as its oxide form, graphene oxide (GO), have been exploited as components of bioelectronic devices, as (nano) vectors in drug-delivery platforms and engineered as promising tissue scaffolds [14–17]. We have previously shown the ability of small graphene oxide nanosheets (s-GO), to transiently impair glutamatergic transmission in the rat hippocampus, both *in vitro* and *in vivo*, presumably with a direct interference with the presynaptic glutamate release machinery [18]. More recently, additional studies sustained s-GO synapse specificity and kinetics when injected in specific Central Nervous

Abbreviations: EPM, elevated plus maze; EPSC, glutamatergic postsynaptic currents; IPSC, inhibitory postsynaptic currents; LA, lateral amygdala; OF, open field apparatus; s-GO, small graphene oxide.

* Corresponding author.
E-mail address: laura.ballerini@sissa.it (L. Ballerini).
[1] These authors contributed equally to this work.

https://doi.org/10.1016/j.biomaterials.2021.120749
Received 30 November 2020; Received in revised form 23 February 2021; Accepted 27 February 2021
Available online 4 March 2021

System (CNS) areas and further showed in zebrafish larvae *in vivo* that s-GO injected directly to the spinal cord were able to reduce glutamatergic transmission, effectively impairing locomotor behavior [19]. In the current work, a rat model of an anxiety disorder (post-traumatic stress disorder (PTSD)) was established, and a suspension of thin s-GO nanosheets was administered in a single dose in the LA to prevent pathological long-term enhancement in excitatory neurotransmission. Behavioral studies combined with tissue histology, confocal microscopy and *ex vivo* electrophysiology, demonstrated that s-GO sheets were able to block LA glutamatergic synaptic plasticity *in vitro*, to impair long-term aversive memory and long-lasting anxiety-related responses *in vivo*.

2. Material and methods

2.1. Graphene oxide material synthesis and characterization

s-GO solution was prepared by the modified Hummers' method as previously described [20], using graphite powder (Sigma-Aldrich) as a starting material [21] and under endotoxin-free conditions [22]. The physicochemical characterization of the s-GO sheets was performed as previously described [23] and is summarized in Table S1.

Scanning electron microscopy (SEM) was performed using a FEI Magellan 400 L XHR SE microscope equipped with a newly developed electron column with a monochromator, UC (UniColore) Technology. Landing energy of 20.00 kV and beam current of 0.10 nA were used and signal was acquired with secondary electrons through-lens detector (TLD). 20 μL of s-GO solution at 100 μg/mL were deposited on an ultrathin carbon film on lacey carbon TEM grid and dried for at least 24 h. Lateral dimension distribution was performed by manual counting of the longest sheet dimension on Image J software. The oxidation of the material has been studied by several techniques such as Raman spectroscopy, surface charge (ζ-potential) measurements, TGA and XPS analysis (Table S1).

Animals, overall experimental design and surgery: All experimental procedures were carried out in accordance with the Italian law (decree 26/14) and the EU guidelines (2007/526/CE and 2010/63/UE) and were approved by the Italian Ministry of Health (n. 689/2017-PR). Male adult Wistar rats weighed 230–250 g (n = 60) were used to perform the *in vivo* experiments. Food and water were provided at libitum. The enclosure was maintained at 20 ± 2 °C on a light-dark cycle (lights on from 7 a.m. to 7 p.m.). Behavioral experiments were performed between 9 a.m. and 2 p.m. Rats undergoing surgical procedures were deeply anaesthetized. Analgesic and antibiotic medications were administrated postoperatively. All experimental procedures were planned to minimize the number of animals used and their suffering. We evaluated the aversive memory by the odor avoidance box, which consisted of a rectangular arena (40 × 26 × 36 cm) with black acrylic-plexiglass walls covered with a transparent plexiglass lid. At one side of the arena, an alligator clip fixed in the wall is positioned 4 cm above the floor. In the opposite direction, a smaller box (20 × 26 × 22 cm) covered with a black plexiglass lid is positioned, named hide box. The arena and the hide box were separated by a small 6 × 6 cm square hole allowing free access to both chambers. Rats were placed (10 min) inside the hide box with free access to the arena for 3 consecutive days to habituate to the apparatus. On the fourth day, the time spent in the following defensive behavior was recorded: head out (namely, the rat scanning the environment from a protected position, measured as poking of the head, or of head and shoulders, outside of the hide box but with the bulk of the rat body inside of it). Rats were divided in two groups (n = 6 per group), exposed to a piece (2 cm) of an unworn collar (UC), without any cat odor, and the group exposed to the collar previously worn by the cat, named worn collar (WC). Collars were worn by an encaged cat. Rats were re-exposed (10 min) to the context, arena without the cat collar to evaluate the aversive memory related to the conditioned fear. Behaviors were analyzed during the re-exposure to the context at 2 days and 6 days post-exposure. Long-term anxiety-related behavior was measured using the elevated plus maze (EPM). This apparatus consisted of four arms (50 × 10 × 40 cm), two open arms (without walls) and two closed arms (with 40 cm high walls) connected by a central square (10 × 10 cm). The maze was elevated 50 cm from the ground. Rats (n = 6 per group) were placed in the closed arm and were allowed to freely explore the apparatus for 5 min. Duration and frequency of entrance in the open and closed zone was evaluated. Entry into a zone was scored when the center-point of the rat's body was within it. We adopted an *anxiety index* which was previously validated [24] and calculated for each rat based on the EPM behavioral scores. In this scoring system, high anxiety index values represent an elevated anxiety-like behavior expression. The following formula was applied:

anxiety index = 1- [(time spent in the open arms/ total time in the maze) + (number of entries to the open arms/ total time of maze exploration)]/2.

Exploratory and locomotor activities of rats (n = 6 per group) were measured by the open field (OF) apparatus, a square arena with the 60 × 60 cm transparent plexiglass walls and the floor divided into 16 sections (15 × 15 cm). Number of crossings (considered when the rat crossed the border line of each section with four paws) were analyzed following the EPM testing. All behavioral tests were performed under 40 lx luminosity and videorecorded for off-line analysis. The XPloRat software [25] was used to score the behaviors. Animals were anaesthetized with intraperitoneal injection of ketamine (Ketamine Imalgene®, Merial Laboratories) and xylazine (Sedaxylan®, Dechra Veterinary Products) at 92 mg/kg and 10 mg/kg body weight, respectively, and fixed in a stereotaxic frame. A stainless-steel guide cannula (outer diameter, 0.6 mm, and inner diameter, 0.4 mm) was implanted in the diencephalon aimed to the LA. The upper incisor bar was set at 3.3 mm below the interaural line so that the skull was horizontal between bregma and lambda. The guide cannula was vertically introduced using bregma as the reference and the following coordinates: A.P.−3.48 mm, M.L.−5.2 mm and D.V.−7 mm, according to Ref. [26]. At the end of the surgery, the acrylic resin and two stainless steel screws were used to fix the guide cannula in the skull. In order to protect the guide cannula from obstruction a stainless-steel wire was used to seal it. Three days later, rats were gently wrapped in a cloth and held while they received a random treatment into LA of either s-GO (50 μg/mL) or ACSF solution (composition described below) delivered by a needle (0.3 mm of outer diameter) linked to a syringe (Hamilton) through a polyethylene tube. The injection needle was inserted through the guide-cannula until it reached the LA (1 mm below the guide-cannula). 48 h later animals were submitted to the behavioral testing.

2.2. Histology, microscopy and image analysis

Rats were anaesthetized as described above and submitted to the transcardial perfusion with 0.1 M PBS followed by 4% formaldehyde (prepared from fresh paraformaldehyde; PFA, Sigma, St Louis, MO, USA) in PBS. The brain was removed from the skull and prepared as described previously [27]. Briefly, brains were post fixed, cryoprotected, frozen on dry-ice and sectioned on a cryostat (Microm HM 550, Thermo Fisher Scientific). The brain slices (30 μm coronal sections) were mounted on glass slides and processed according to either cresyl violet staining or immunohistochemical methods. Brain slices were stained in 0.1% cresyl violet (Sigma) solution for 5 min, rinsed in distilled water twice for 2 min each wash and dehydrated in a graded ethyl alcohol series: 50%, 70%, 95% and 100%. Thereafter, they were cleared in xylene for 3 min and mounted with Permount (Fisher Scientific). Histological sections were analyzed and images were acquired using a Leica DM6000 upright microscope with a 2.5 × dry objective. Alternatively, brain slices were washed out with 0.1 M PBS, incubated with a blocking solution composed of 3% BSA, 3% FBS, and 0.3% Triton X-100 in PBS for 45 min at room temperature (RT). The primary antibodies anti-ionized calcium-binding adaptor molecule 1 (Iba1; Wako, specific marker for

microglia, 1:500) and mouse anti-glial fibrillary acidic protein (GFAP; Sigma-Aldrich, specific marker for glial cells, 1:400, diluted in saline and 5% fetal bovine serum), were incubated overnight. Sections were washed 3 times for 5 min each, incubated with the secondary antibodies (1:400) AlexaFluor 488 goat anti-mouse (Thermo Fisher Scientific) and AlexaFluor 594 goat anti-rabbit, (Thermo Fisher Scientific), for 3 h in the dark and washed. Nuclei were labeled with DAPI (Invitron, 1:500) in PBS for 25 min at RT. All slides were cover slipped Fluoromounting [18].

Using a Nikon A1R confocal microscope, equipped with argon/krypton, helium/neon, and UV lasers images were acquired with a 40 × (1.2 NA) objective and confocal sections were acquired every 0.5 μm up to a total Z-stack thickness of 20 μm. Gain, pixel-resolution, and exposure time remained constant for all images. From each section, we selected six regions of interest (ROI, 320 × 320 μm^2), where the cell densities of Iba1 and GFAP positive cells were calculated and normalized for those of the contralateral hemisphere. In order to investigate the presence of s-GO in the LA 48 h after injection, the same brain slices immunolabelled for DAPI, GFAP and Iba1 were visualized using the reflection mode property during the confocal acquisition [28] at 40 × (1.2 NA) with ROI of 140.77 × 140.77 μm^2.

Image analysis was performed using Volocity software (Volocity 3D image analysis software, PerkinElmer, U.S.A.).

2.3. Immunohistochemistry and golgi-staining and quantification of dendritic spines

After behavioral experiments, a group of rats (n = 8) re-exposed to the context (6 days) were anaesthetized as described above and decapitated, their brains were collected and prepared to the Golgi-Cox staining protocol [29]. Briefly, brains were incubated in the Golgi-Cox solution (1% potassium dichromate, 0.8% potassium chromate and 1% mercuric chloride) in the dark at RT for 25 days. After that, brains were incubated in sucrose solution at 30% for 24 h and sectioned in coronal sections (400 μm thickness) at the level of the amygdala using a vibratome (Leica VT100S). Brain slices were mounted onto microscope slides with Permount (Fisher Scientific). Histological sections were analyzed and images stacks of the LA neurons were acquired using a Leica DM6000 upright microscope with a 63 × oil immersion objective. The serial section images were aligned and dendritic spines of pyramidal neurons were blind analyzed [30] in RECONSTRUCT software (http://synapses.clm.utexas.edu/tools/reconstruct/reconstruct.stm; RID: SCR_002716). Dendrite originating directly from the cell body with a length of 70 μm from its origin was analyzed [31,32]. All dendrite protrusions were considered as spines, regardless to their morphological characteristics.

2.4. In vitro amygdala preparations

All experimental procedures were carried out in accordance with the Italian law (decree 26/14) and the EU guidelines (2007/526/CE and 2010/63/UE) and were approved by the Italian Ministry of Health (n. 689/2017-PR, n. 22DAB.N.1Z8 and n. 22DAB.N.1WO). For acute slices male P12–P16 juvenile Wistar rats (n = 17) were used. Briefly, after being decapitated, the brain was quickly removed from the skull and placed in ice-cold solution containing (in mM): sucrose 215, KCl 3.5, NaH_2PO_4 1.2, $NaHCO_3$ 25, $CaCl_2$ 2, $MgCl_2$ 1.3, glucose 25 and ascorbic acid 4, saturated with 95% O_2–5% CO_2 (pH 7.3–7.4). Coronal amygdalar slices (300 μm thick) were cut with a vibratome (LeicaVT1000S) and stored at room temperature in a holding bath containing 130 mM NaCl instead of sucrose that was gassed with 95% O_2–5% CO_2 (artificial cerebrospinal fluid solution, ACSF).

For cultures, postnatal P7-10 Wistar rats were used. Dissociated amygdalar cultures were prepared as previously described [33]. Briefly, brains were quickly removed and cut in coronal sections (400 μm thickness) using a vibratome (Leica VT100S). Three sections at the level of the amygdalar complex were collected using the following coordinates: Bregma −1.8 mm, −2.4 mm and 2.8 mm [34]. From these, the amygdaloid complex was visually identified under a dissection microscope and dissected using a biopsy punch. The collected tissue was enzymatically and mechanically dissociated and cells were seeded onto poly-L-ornithine-coated glass coverslips at a density of 800 cells/mm^2 and maintained in controlled conditions (at 37 °C, 5% CO2) for 8–12 days prior to voltage-clamp recordings.

2.5. s-GO treatments in vitro

Acute slices were incubated for 5 h with 50 μg/mL of s-GO, added directly to the ACSF, and as control, sister slices were kept in ACSF alone (saline-treated). At the end of incubation time, an individual slice was transferred to a submerged recording chamber and continuously perfused at 33–34 °C with ACSF. In the experiments in which s-GO were applied acutely, a gravity driven perfusion system was used and a solution of 10 μg/mL s-GO was applied at a speed of 2 mL/min for 5 min. In the experiments on dissociated cultures, s-GO were applied at a concentration of 20 μg/mL for 30 s through the perfusion system in combination with 50 μM of glutamate.

2.6. Electrophysiology

Patch clamp whole-cell recordings were obtained with glass pipettes (resistance 5–7 MΩ) filled with the following solution (in mM) 120 K gluconate, 20 KCl, 10 HEPES, 10 EGTA, 2 $MgCl_2$, 2 Na_2ATP (pH 7.3, osmolarity adjusted to 300 mOsm). The extracellular solution was ACSF for acute slices, and for dissociated cultures, the following saline solution (in mM): 150 NaCl, 4 KCl, 2 $CaCl_2$, 1 $MgCl_2$, 10 HEPES, 10 glucose, pH 7.4. Principal neurons of the lateral amygdala were visually identified thanks to their typical pyramidal shape [35] with an upright microscope (Eclipse FN1; Nikon, Japan) equipped with differential interference contrast optics and digital videocamera (Nikon, Japan). Data were collected by Multiclamp 700 A patch amplifier (Axon CNS, Molecular Devices) and digitized at 10 KHz with the pClamp 10.6 acquisition-software (Molecular Devices LLC, USA). Membrane potential values were not corrected for the liquid junction potential that was of ~15 mV (calculated with the Clampex software; Molecular Devices, Sunnyvale, CA, USA). The stability of the patch was checked by repetitively monitoring the input and series resistance during the experiments. Cells exhibiting 15% changes were excluded from the analysis. The series resistance was <20 MΩ and it was not compensated. Input resistance and cells capacitance were measured online with the membrane test feature of the pClamp software. In pyramidal neurons in the LA slices, cell capacitance, input resistance and resting membrane potential did not show any statistically significant difference between in s-GO treated and saline treated neurons ($p > 0.05$, Table S2).

In current clamp experiments, 1 s long lasting steps of positive current with increasing amplitude (10, 20, 30, 40, 50, 60, 70, 80, 90, 100 pA) were injected in pyramidal cells from a resting membrane potential of −65 mV. Both s-GO-treated and untreated neurons showed comparable firing properties (Fig. 4C), measured as threshold for action potential, amount of injected current needed to reach it and action potential amplitudes. No statistically significant differences were observed between the two groups ($p > 0.05$, Table S2).

In the experiments where slices were chronically incubated in s-GO, the glutamatergic synaptic activity was recorded at a holding potential of - 65 mV, in the presence of gabazine (10 μM; a blocker of $GABA_A$ receptor mediated postsynaptic currents). EPSCs were collected from traces and averaged (showed in Fig. 4F) and no differences were observed in their amplitude (in saline-treated neurons: 9 ± 1 pA and in s-GO-treated ones: 8 ± 2 pA), rise time (in saline-treated neurons: 1.2 ± 0.2 ms and in s-GO-treated ones: 1.1 ± 0.1 ms) and decay time constant τ (in saline-treated neurons: 5.4 ± 0.9 ms and in s-GO-treated ones: 4.7 ± 0.4 ms) when incubated with s-GO (n = 8 cells) in respect to control (n = 9 cells; $p > 0.05$). After recording spontaneous activity for 8 min as

baseline, LTP was induced in dissociated cultures by applying 50 μM of glutamate for 30 s, while the membrane potential of the recorded cell was depolarized from −58 mV to +4 mV (under voltage clamp mode). The effects of LTP induction were monitored for 30 min by measuring EPSC and IPSC frequencies and amplitudes. The values reported are averages calculated between 24 and 30 min after LTP induction and normalized for the pre-treatment baseline values. In the experiments of s-GO application through the perfusion system in acute slices and in dissociated cultures, sPSCs were recorded in the absence of any drugs and were analyzed offline using the software AxoGraph X (Axograph Scientific), which exploits a detection algorithm based on a sliding templates to separate EPSCs and IPSCs on the basis of their different decay times (see Results). For each recording, events were collected and averaged to measure the peak amplitude and kinetic properties on the resulting trace. The decay time of PSCs was calculated by fitting the decaying phase of the current with a mono-exponential function. In paired recordings, the presynaptic neuron in current clamp mode was held at −70 mV (by ≤ 0.02 nA negative current injection), and action potentials were evoked by delivering short (4 ms) positive (1 nA) square current pulses. Monosynaptic connections were identified by their short delay (<3 ms) [18], measured between the peak of the evoked action potential and the onset of the unitary evoked PSCs. Recordings of EPSCs and IPSCs at different holding potentials were used to extrapolate I/V curves (Supplementary Figure S2**).**

2.7. Data analysis and statistics

Data from independent groups of animals exposed to the cat collar were checked for normality and homogeneity and analyzed using Student's unpaired two-tailed *t*-test. All comparisons between more than 2 or 3 groups were made with one-way ANOVA and two-way ANOVAs, respectively, followed by Bonferroni post hoc test. For electrophysiological data, Shapiro-Wilk normality test was applied to evaluate the statistical distribution of the data sets. Statistically significant difference between two data sets was assessed by one-way ANOVA (if distributed as a Gaussian distribution) or by Mann–Whitney test (if not). In experiments obtained from dissociated amygdalar cells, for parametric data, the statistically significant difference among the three groups was assessed through one-way ANOVA, using Holm-Sidak's multiple comparisons test for post hoc analysis. Not parametric data were analyzed with Kruskal-Wallis test and post hoc analysis was done with Dunn's multiple comparison test. All values are expressed as mean ± SEM. P-value < 0.05 was considered statistically significant and n is the number of animals if not otherwise stated.

3. Results

The produced biology-grade s-GO dispersion [18] was characterized by AFM and SEM; in both measures s-GO flakes displayed a similar range of lateral dimensions: 0.06–1.7 μm by AFM (Fig. 1A and B) and 0.10–2.0 μm by SEM (Fig. 1D and E). Fig. 1C shows s-GO thickness, that ranged between 1 and 1.5 nm in accordance with single or few-layer sheets. The oxidation of the material was analyzed by Raman spectroscopy, surface charge (ζ-potential) measurements, TGA and XPS analysis, these measures are summarized in Table S1.

Structural and morphological characterization of s-GO sheets by

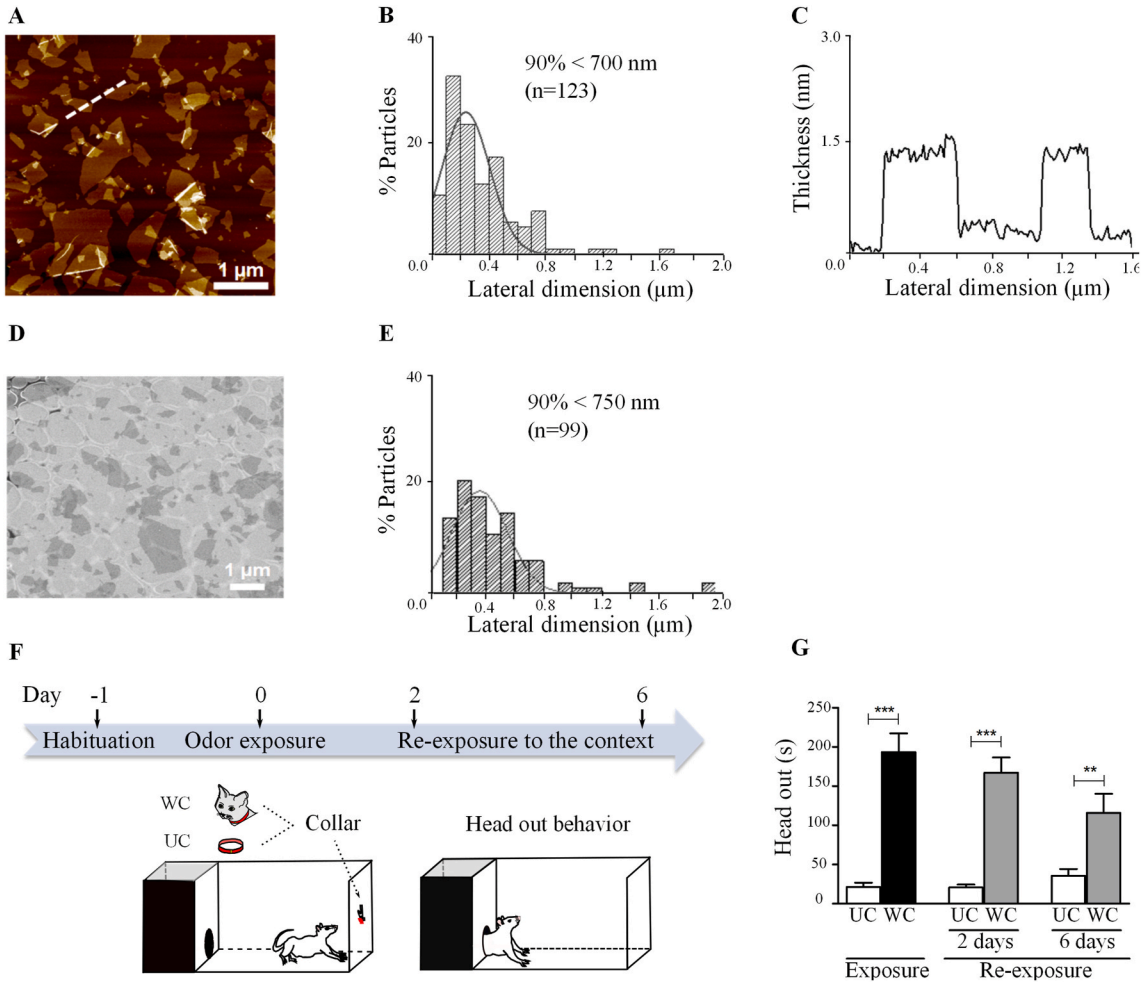

Fig. 1. s-GO AFM and SEM features and the behavioral model of short- and long-term fear memories induced by aversive olfactory stimulus.

AFM: (A) height image; (B) lateral dimension distribution (based on 123 sheets); (C) cross section analysis highlighted by the dashed line in the height image; and by SEM: (D) micrograph; (E) lateral dimension distribution (based on 99 sheets). (F) Sketched experimental settings and timeline. Upon habituation in the avoidance box, adult rats were exposed to either worn (WC) or unworn (UC) cat collar. 2 and 6 days after the exposure, rats were re-exposed to the context. (G) Bar plots summarize the increase in the time of head out defensive response in rats caused by either the cat odor exposure or the re-exposure to the context 2 or 6 days later, namely short- and long-term aversive memory, respectively. N = 6 each group. ***p < 0.001; **p < 0.01 versus UC groups.

To test thin s-GO efficacy to affect neurotransmission in the LA, preventing excitatory synapses reinforcement and anxiety disorders, we established a model of PTSD upon rat exposure to an aversive stimulus, the predator (cat) odor, known to activate the amygdaloid complex [36,37]. Such a treatment leads to hyperexcitability of LA circuits, fear responses and altered behavior [38,39]. In adult rats, immediate innate fear response was induced by single experience of an aversive (predator) olfactory stimulus and the emergence of long-lasting specific anxiety behavior was evaluated by re-exposure to the context. We adopted an odor avoidance box (sketched in Fig. 1F) to quantify the emergence of defensive behavior ("head out" [40]; see methods). We compared defensive behavior in two groups of rats, one group exposed to a cat-worn collar (WC; n = 12) and a control group exposed to an unworn collar (UC; n = 12). In Fig. 1G the bar plots show the significant (t (10) = 7.01, p < 0.001) increase in "head out" behavior when comparing WC with UC exposed animals. The avoidance fear response was also significantly increased when comparing UC with WC groups re-exposed to the context after 2 days (t (10) = 7.46, p < 0.001) and after 6 days (t (10) = 3.13, p < 0.01), suggesting the induction of short- and long-term aversive memories, related to PTSD emergence [41,42]. The emergence of PTSD has been associated to augmented dendritic spines in the amygdala nuclei [31,32]. This anatomical signature of synaptic plasticity was confirmed in the amygdala of WC groups (6 days after first exposure, n = 4) where the number of dendritic spines in LA was significantly (p < 0.05) higher when compared to UC groups (n = 4; Supplementary Figure S1).

3.1. s-GOs locally delivered in the LA impair long-term fear memories

The contextual avoidance behavior to predatory odor is ultimately

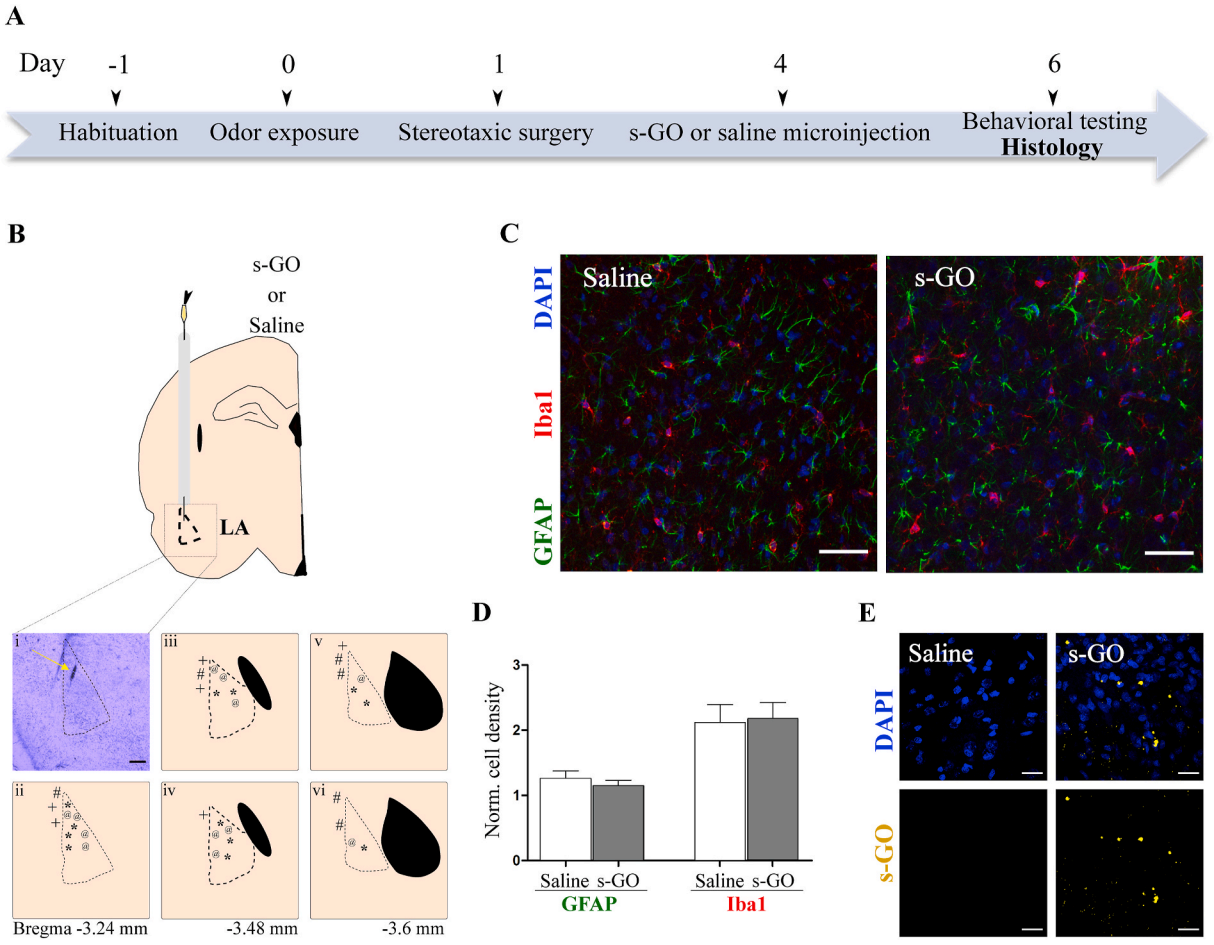

Fig. 2. Lateral amygdala (LA) treatment by s-GO local injection. (A) Schematic representation of experimental timeline showing the sequence of the experimental procedures, from habituation to stereotaxic surgery and histology. (B) Top, diagram of the rat brain showing the target area for s-GO or saline microinjections. Bottom, (i) representative photomicrograph of Nissl-staining (yellow arrow indicates the site of s-GO injection); scale bar 300 μm. In (ii, iii, iv, v, vi) schematic drawings of rat brain sections summarizing the microinjection points of either s-GO (* when in the LA, # when in the perirhinal cortex) or saline (@ when in the LA, + when in the perirhinal cortex). Each symbol represents an independent experiment made on a single rat. (C) Confocal photomicrographs showing GFAP- (green), Iba1- (red) reactivity and DAPI- (blue) stained nuclei in the LA slices of rats treated with either saline (left) or s-GO (right). (D) The bar plot summarizes the tissue responses in saline or s-GO treatments, N = 6 slices each group. *p > 0.05 according to the unpaired *t*-test. Scale bar 50 μm. (E) Representative images of LA slices (48 h after injection; same samples as in C, different fields) with DAPI (in blue) and s-GO sheets (in yellow) visualized by the reflection mode of the confocal system. Note that s-GO is visible as aggregates only in s-GO injected animals. Scale bar 20 μm. (For interpretation of the references to colour in this figure legend, the reader is referred to the Web version of this article.)

organized by the LA glutamatergic neurons [43]. We tested the hypothesis that s-GO injection into the LA, *via* transient impairment of glutamatergic synapses [18], may prevent PTSD-related behavior emergence in rodents. Such an effect would fortify the strategy of selective and transient targeting of synapses to prevent the development of brain pathologies.

Two independent groups of rats (n = 36) were exposed to WC or UC context and, after 24 h, a guided cannula was stereotaxically implanted into the rat brain, targeting the LA or, alternatively, the perirhinal cortex, to deliver locally, three days later, either s-GO (50 μg/mL) [18] or the vehicle (saline solution). Two days after s-GO or saline delivery, WC and UC groups of animals were re-exposed to the context (i.e. 6 days after the first exposure) and then euthanized (sketched in Fig. 2A). The position of the cannula was confirmed histologically in all animals both when targeting the LA and when targeting the perirhinal cortex, a neighboring brain structure (see Methods, schematic drawings and histology of Fig. 2B). Tissue reactivity was studied by immunofluorescence assessment of GFAP-positive astrocytes and Iba1-positive microglia. At 6 days post-surgery, tissue reactivity was comparable in the two animal groups, saline or s-GO treated (Fig. 2C and bar plot in D).

We tested the presence of s-GO within the LA (48 h post-injection) by operating the confocal microscopy under reflection mode, which allows the visualization of s-GO [28]. Fig. 2E shows confocal reconstructions of saline and s-GO treated LA, in the latter residual aggregates of s-GO (in yellow, reflection mode) were detected, confirming our previous observations on the duration of s-GO permanence once injected in the adult brain [18].

In all animals, aversive behavior prior to surgery was quantified and the avoidance response was significantly higher in the WC group when compared to UC one ($t(10) = 4.09$, $p < 0.05$; Fig. 3A and B). We then analyzed long-term aversive memory related behavior at day 6, namely 2 days after delivery of s-GO or saline in WC and UC groups. During the re-exposure to the stress-related context, in LA saline-treated animals, we detected the expected (see also Fig. 1G) significant increase in the "head out" response in WC ($F(1,20) = 0.04$, $p < 0.001$) when compared to UC group. Remarkably, in LA s-GO-treated animals, flakes injection reversed the long-term conditioned fear reaction in WC ($F(1,20) = 19$, $p < 0.01$) when compared to LA saline-treated WC ($p > 0.05$; Fig. 3A and B) and s-GO effect was lost when delivered outside the LA, in the closeby perirhinal cortex ($P > 0.05$; Fig. 3B). To evaluate the effective ability of s-GO to remove long-term aversive memory and thus PTSD-associated behavior in WC upon s-GO injections, we quantified rat behavior in UC, WC saline and WC s-GO, using the elevated plus maze (EPM) and open field (OF) apparatus (Fig. 3B).

We quantified PTSD-like behavior by measuring the anxiety index in the EPM. WC rats, injected with saline, exhibited a significantly higher ($F(91,20) = 0.88$, $p < 0.05$) anxiety index 6 days after the exposure to the predator odor respect to that of UC (saline treated) group. On the contrary, s-GO microinjection into LA reduced the PTSD related behavior in WC animals, decreasing the anxiety index in a statistically significant manner ($F(1,20) = 13.43$, $p < 0.01$), if compared to that of the WC saline treated rats. In addition, WC rodents treated with s-GO did not differ from UC (saline or sGO injected) animals (Fig. 3B). We ruled out mere alterations in animal locomotion due to s-GO by testing locomotor behavior *via* the OF apparatus ($p > 0.05$; Fig. 3B).

3.2. s-GO flakes decrease the activity of glutamatergic synapses in the LA

Suggested molecular mechanisms of the fear components that underlie PTSD include synaptic long-term potentiation (LTP) in LA glutamatergic synapses [44]. We hypothesize that s-GO, once injected in the LA, transiently impair local excitatory glutamatergic synapses, as

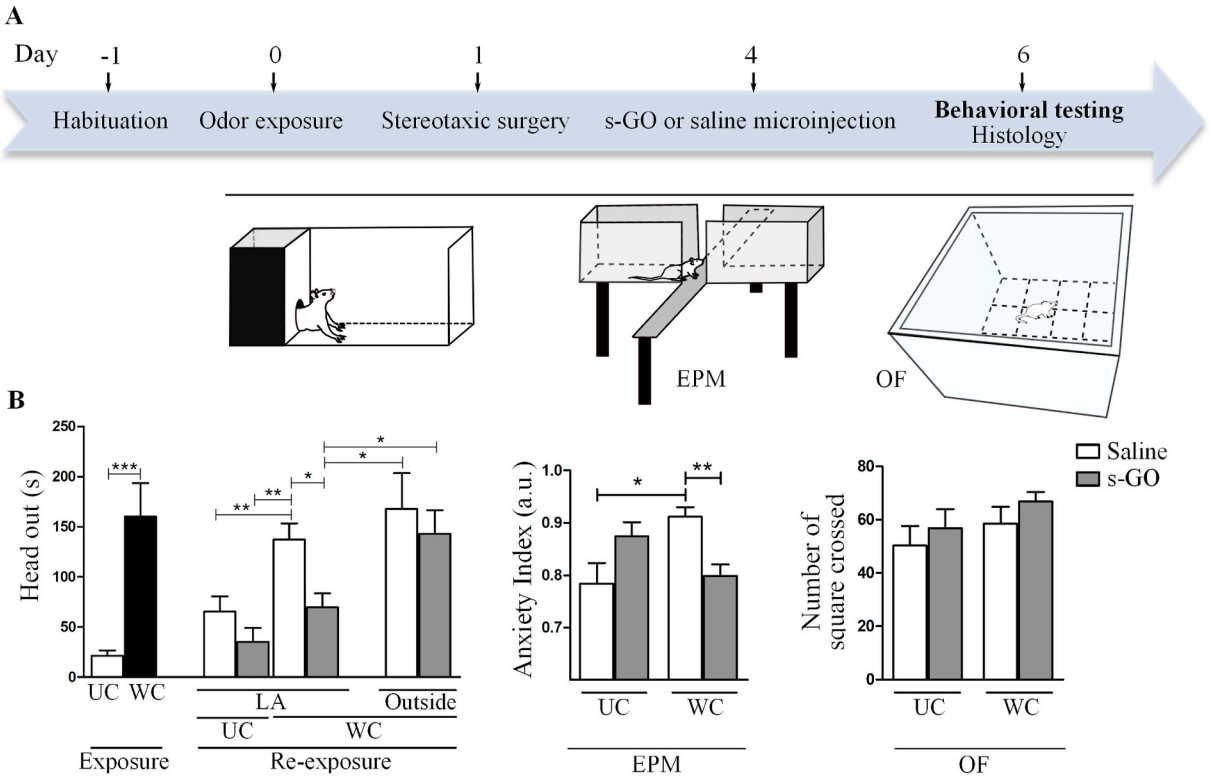

Fig. 3. s-GO delivery in LA impairs long-term fear memories. (A) Schematic representation of the experimental timeline and behavioral testing (at day 6). (B) On the left, bar plot summarizing the head out behavioral responses evoked by the exposure to UC or WC and by the re-exposure to the context after s-GO or saline microinjections into either the lateral amygdala (LA) or the perirhinal cortex. In the middle, bar plot showing the anxiety index evaluated in the EPM test in UC and WC treated with s-GO or saline. On the right, bar plot reporting OF test in UC and WC treated with s-GO or saline. N = 6 for each group. ***p < 0.001; **p < 0.01; *p < 0.05.

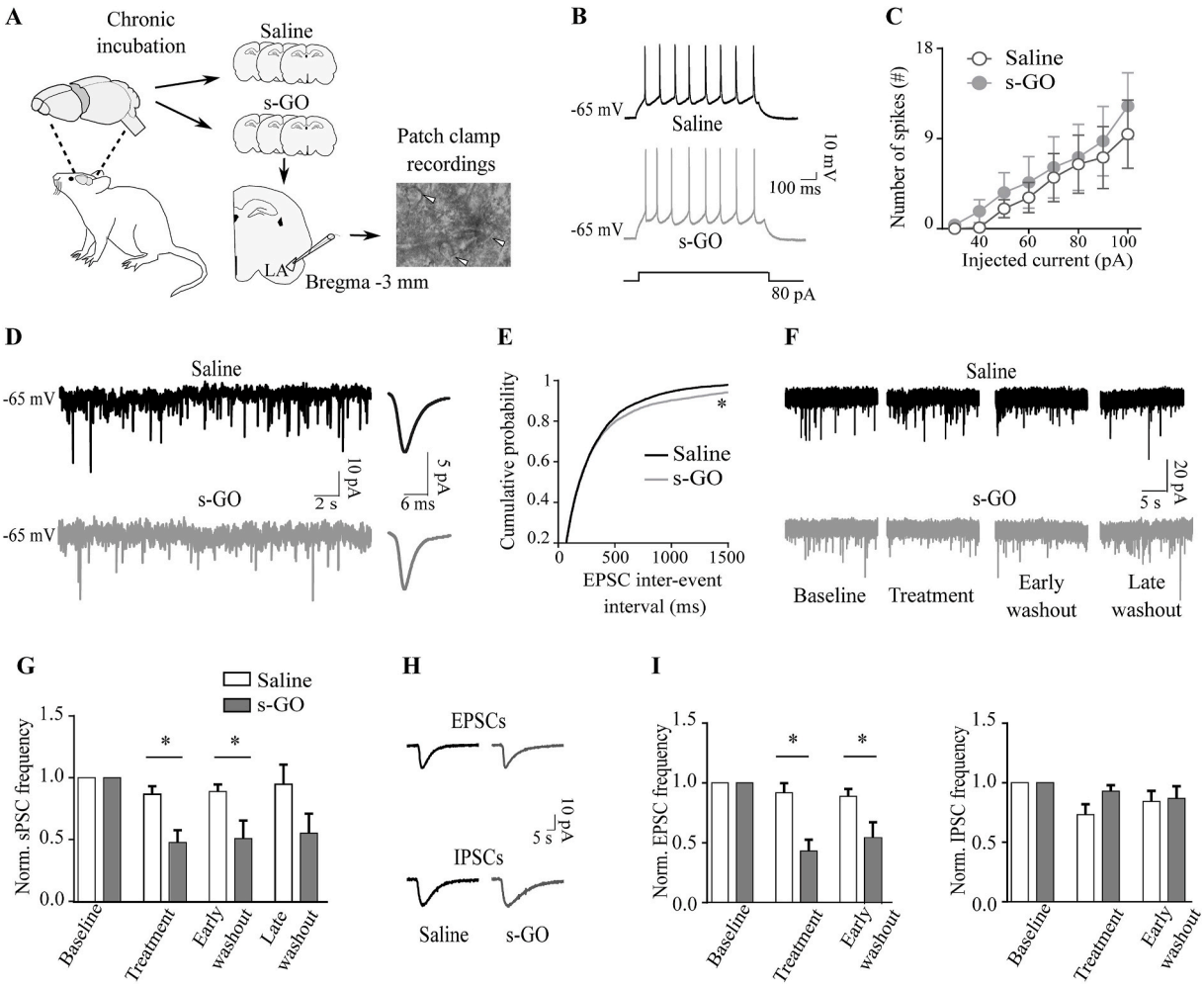

Fig. 4. s-GO downregulate the activity of glutamatergic synapses in the LA (A) Sketch of the experimental settings. (B) Current clamp traces of elicited firing activity in control neurons and in s-GO treated ones. (C) Plot reporting the number of APs fired versus the current injected, for saline-treated (n = 9) and s-GO-treated cells (n = 8). (D) On the left, voltage clamp traces of spontaneous EPSCs recorded in the presence of gabazine (10 μM) in control neurons and s-GO treated ones. On the right, averaged EPSCs waveforms (same cells as left). (E) Cumulative probability plot of the inter event interval of EPSCs for control and s-GO treated neurons: s-GO shift the curve toward larger values. (F) Voltage clamp recordings of sPSCs during acute application of s-GO (n = 9 cells) or saline as control (n = 8 cells) through the perfusion system. Note the downregulation of neuronal activity in s-GO treated cell, while no effect was observed in control. (G) Bar plot showing the statistically significant decrease in normalized sPSCs frequency in s-GO treated cells respect to controls. (H) Averaged EPSCs and IPSCs (same cells as in G) isolated offline on the basis of their different decay times. (I) Bar plots of normalized EPSCs and IPSCs frequency showing that s-GO affect specifically excitatory synapses. Normalized EPSC frequency was decreased ($p = 0.0016$) during the treatment and during the early phase of the wash out ($p = 0.036$). Diversely, the normalized IPSCs frequency was not changed by s-GO application.

observed in previous studies [18,19]. Thus, mechanistically, s-GO reduction in glutamatergic synaptic efficacy might prevent LTP expression, crucial to PTSD development. We challenged this hypothesis by single cell electrophysiology *in vitro*. We first incubated acute brain explants containing the amygdala complex with saline or s-GO (50 μg/mL, in saline, 5 h; sketched in Fig. 4A). Under current clamp mode, a homogeneous population of neurons was recorded, identified by their passive (see methods and Table S2) and active (Table S2, Fig. 4B and C) membrane properties, which were not altered by s-GO treatments.

In voltage clamp mode the inter-event interval of spontaneous excitatory glutamatergic postsynaptic currents (EPSCs), pharmacologically isolated in the presence of gabazine (10 μM; see methods and Fig. 4D) were increased after s-GO treatments (432 ± 10 ms) in respect to controls (326 ± 5 ms; see cumulative plot in Fig. 4E; P value < 0.0001). This finding suggests that LA ex-vivo slices, upon prolonged exposure to s-GO [18], displayed a downregulation of glutamatergic transmission. To gain more insights on s-GO dynamics, we administered the nanomaterial acutely (10 μg/mL, 5 min) to the amygdala brain explants while monitoring heterogeneous spontaneous post synaptic currents (sPSCs) in the absence of pharmacological blockers. Fig. 4F–G shows that s-GO significantly reduced sPSCs frequency when compared to saline (for saline: 0.87 ± 0.06 and for s-GO: 0.47 ± 0.09 Hz; $p = 0.0053$) and this reduction was maintained during the early phase of s-GO removal (for saline: 0.89 ± 0.06 Hz; and for s-GO: 0.51 ± 0.14; $p = 0.0297$), with a partial recovery after 10 min washout (for saline: 0.95 ± 0.16 and for s-GO: 0.55 ± 0.16; $p > 0.05$). Fig. 4H–I shows that in the same experimental conditions, s-GO specifically targeted EPSCs and was ineffective on inhibitory $GABA_A$ receptor mediated postsynaptic currents (IPSCs), identified by their kinetic properties (shown in Fig. 4H, EPSCs displayed typical fast ~5 ms day, while IPSCs featured a slower ~13 ms one [18]) and pharmacology (10 μM CNQX readily abolished fast event, while 10 μM gabazine removed slow ones). Such analysis confirmed that the effect of s-GO in LA tissue was specific for glutamatergic synapses [18,19].

3.3. *In vitro long-term potentiation of amygdala synapses is impaired by s-GO*

The rescue of anxiety related behaviors observed in animals injected with s-GO hinted at the nanomaterial interference with the building up of the pathological LTP induced by the odor exposure [45]. To explore this possibility, we adopted a simplified *in vitro* model of LTP induction in the amygdala, which allows direct experimental control and access to glutamatergic synapses. We induced synaptic plasticity in dissociated amygdala cultures (Fig. 5A–C) by coupling a brief (30 s) application of glutamate (50 μM) with a depolarization (+4 mV) of the neuronal membrane, favoring the activation of glutamate NMDA receptors, involved in LTP induction [46,47]. Such a treatment resulted in a 30 min long lasting and stable increase in the amplitude of EPSCs (identified by their kinetic properties, voltage dependence and pharmacology, as shown in the Supplementary Figure 2) in respect to the baseline values, while in the controls, that underwent to membrane depolarization in the absence of glutamate application, no changes were detected (normalized amplitudes were 0.81 ± 0.09 in controls, n = 14; 1.72 ± 0.21 in glutamate treated cells, n = 20; p = 0.0004, Fig. 5B–D, 30 min). s-GO (20 μg/mL, 30 s) applied simultaneously to glutamate, blocked the EPSC potentiation (p = 0.0007, Fig. 5C–D). EPCSs frequency remained unaltered in all treatments (Fig. 5E). IPSCs amplitude (Fig. 5 D) and frequency (Fig. 5E) were not modulated by these treatments.

These findings indicate that s-GO target specifically glutamatergic synapses in LA and further suggest that, when applied in conjunction with the LTP inducing stimuli, s-GO may prevent the development of glutamatergic synaptic plasticity.

4. Discussion

We describe here the efficacy of s-GO in preventing the reinforcement of aversive memory and the development of long-term anxiety behavior only when targeting synapses in the LA. We propose that this effect is due to the ability of s-GO to transiently inhibit glutamatergic activity in LA excitatory circuits in a synapse-specific and localized manner, ultimately preventing the emergence of LA dysfunctional plasticity.

We used a widely accepted [36,37] animal model of PTSD. This model is characterized by a correlation between hyperactivity in the LA glutamatergic circuitry and the emergence of anxiety disorders [39,48]. In our experiments, the aversive stimulus induced an innate fear response, measured as an increase in the head out behavior [49]. The rat maintenance of such a behavior when re-exposed to the cat odor-associated context (i.e. neutral environment) [49] supported the fear memory consolidation and, in animals tested six days after the first exposure to the stressful event, the development of long lasting anxiety, as indicated by the EPM test [42]. Long-term aversive memory and the development of long-term anxiety, evoked by a predator odor stress, represent a model of PTSD [50]. In PTSD patients an involvement of amygdala subregion dysfunctional connectivity has been reported [51], accordingly, in the experimental PTSD rat model, neuronal circuitry in the LA undergoes to a reshaping of excitatory glutamatergic synapses [52] featuring the progressive building up of LA synaptic potentiation [53]. Such a boosted excitatory neuronal activity is proposed to trigger the long-term anxiety related behavior [54].

s-GO has been reported to specifically interact with glutamatergic

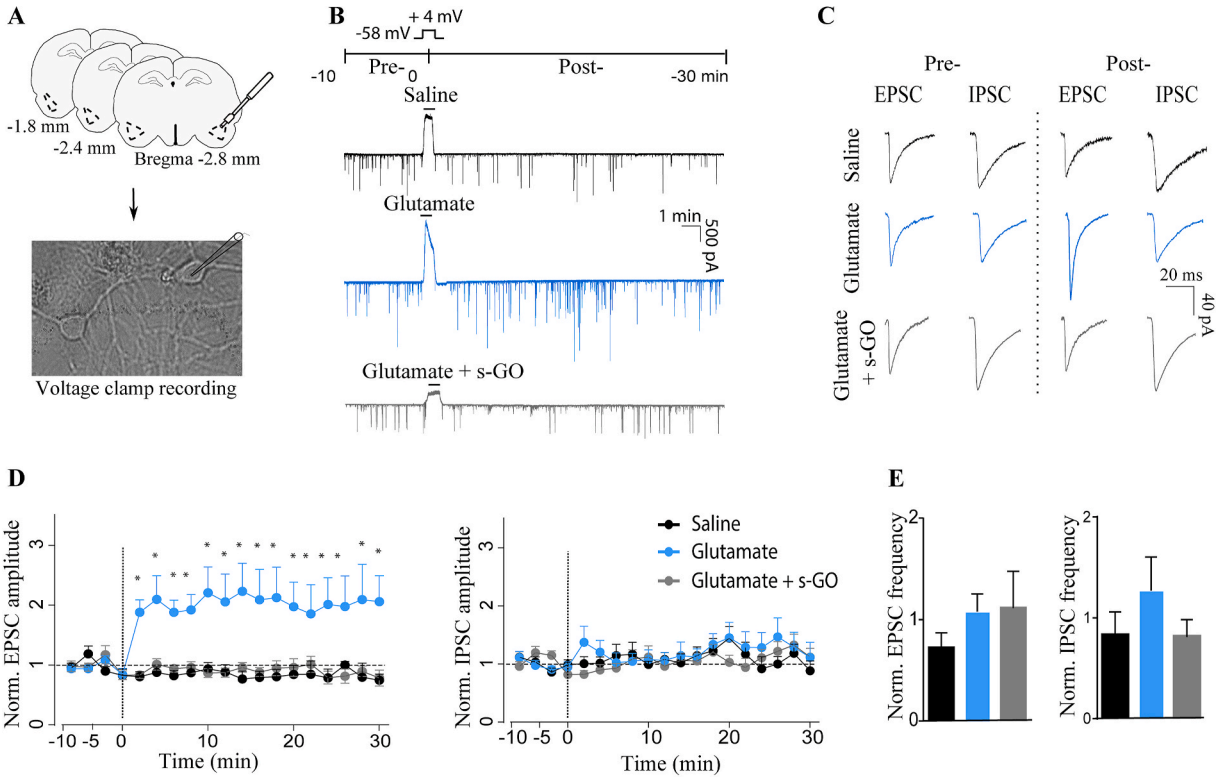

Fig. 5. s-GO impair the long-term potentiation of amygdala synapses *in vitro*. (**A**) Schematic representation of amygdala dissociated cultures and bright field image of cultured cells. (**B**) Representative traces of neuronal spontaneous synaptic activity showing LTP induction in amygdala cultures and its impairment upon s-GO treatment. Chemical LTP was obtained by coupling the depolarization of postsynaptic membrane potential with the application of glutamate at the concentration of 50 μM for 30 s (n = 20 cells). In s-GO treated cells, the nanomaterial was applied together with glutamate under the same condition (n = 17 cells), while control cells were perfused with saline (n = 14 cells). Note the lack of potentiation in s-GO treated cell. (**C**) Offline analysis of sPSCs isolated EPSCs and IPSCs, before and after the treatments. Note that only upon glutamate treatment there is a potentiation of neuronal activity detectable as an increment of the EPSCs amplitude. (**D**) Plots showing that s-GO treatment blocks the 30 min long lasting increase in EPSCs amplitude, observed in neurons undergone to the LTP induction protocol. (**E**) Bar plots showing that the frequency of EPSCs or IPSCs was not affected either by LTP induction or s-GO application. *p < 0.05.

synapses in the CNS inducing a downregulation of excitatory neurotransmission when applied chronically *in vitro* at a concentration of 10 μg/mL [55] or delivered *in vivo* in one single application at a higher dose. [18,19] *In vivo* s-GO inhibition of glutamatergic synapses in the spinal cord modulates motor behavior [19] and in the rat hippocampus local delivery of s-GO significantly and selectively sized down glutamatergic activity for 48 h, without altering neuronal viability [18]. In that study, we explored the time course of s-GO fate, which was found to match the synaptic silencing reversibility [18]. Based on these previous evidences, we injected a single dose of s-GO in the LA four days after the exposure to the cat odor to impair glutamatergic transmission for 48 h and eventually interrupt the building up of glutamatergic synaptic plasticity. Indeed, the presence of s-GO in the treated amygdala at 48 h post injection was confirmed and s-GO treatment was effective in disrupting both long term aversive memory and anxiety related behaviors. We ruled out potential s-GO nonspecific effects, in fact anxiety responses were unperturbed after 48 h of s-GO delivery outside the LA. In addition, we never detected motor alterations in s-GO treated animals, potentially affecting nonspecifically rat defensive behavior. In this framework, also a generic impact of the surgery procedure or an increased tissue reactivity brought about by s-GO injections and affecting synaptic reinforcement, were excluded.

We adopted *in vitro* amygdala models to experimentally test the mechanistic interaction between s-GO and excitatory synapses. In acute amygdala slices we confirmed that chronic (mimicking *in vivo* accumulation) or sub-acute (mimicking *in vivo* diffusion) exposures to s-GO both resulted in a specific reduction in EPSCs frequency, leaving IPSCs unchanged, in accordance to previous reports where s-GO was tested in different CNS areas [18,19,55]. s-GO has been suggested to target presynaptic glutamate release in the hippocampus [18], a feature in principle enabling the alteration of presynaptic mechanisms and glutamatergic transmission engaged in LTP. We further tested in cultured amygdala circuits [33] whether s-GO could impair glutamatergic synaptic potentiation. We successfully potentiated EPSCs by chemical LTP paradigm (cLTP) [46,56–58] and the application of s-GO during cLTP induction counteracted the synaptic potentiation. Although we cannot demonstrate that *in vivo* s-GO prevented the potentiation of amygdala circuits usually linked to PTSD development [44], it is tempting to speculate that the injection of s-GO in the LA during a temporal window crucial to the reinforcement of plastic changes related to the contextual fear memory acquisition [38], effectively reduced glutamatergic transmission potentiation and the onset of downstream long lasting anxiety-related behavior. s-GO nanoflakes might therefore be clinically exploited in the broader area of engineered nanoparticles for precision-medicine applications [59], to allow improved sub-cellular (*i.e.* synaptic) targeting in neurological disorders.

5. Conclusion

Our experiments suggest that s-GO nanoflakes, thanks to their action as synaptic and behavioral modulators, might effectively hinder pathological behaviors based on aberrant glutamatergic transmission.

Author contributions

AFB and NCC designed the PTSD paradigm; AFB performed the behavior, surgery and histology; RC performed confocal microscopy; GC designed the electrophysiology; GC and EP performed the electrophysiology; AFB, GC and EP analyzed data; NL, BB and KK design, produced and characterized materials; LB conceived the idea, designed research and wrote the MS.

Declaration of competing interest

The authors declare that they have no known competing financial interests or personal relationships that could have appeared to influence the work reported in this paper.

Acknowledgements

This work has received funding from the European Union Horizon 2020 Research and Innovation Programme under Grant Agreement numbers GrapheneCore2 (785219) and GrapheneCore3 (881603) and from the São Paulo Research Foundation (FAPESP) number 2016/18218–0. We would like to acknowledge the staff of the Electron Microscopy Unit at ICN2 for their expertise and assistance on the SEM. The ICN2 is funded by the CERCA programme, Generalitat de Catalunya, and is supported by the Severo Ochoa Centres of Excellence programme by the Spanish Research Agency (AEI, grant no. SEV-2017-0706).

Appendix A. Supplementary data

Supplementary data to this article can be found online at https://doi.org/10.1016/j.biomaterials.2021.120749.

Data and materials availability

The data that support the findings of this study are available from the corresponding authors upon reasonable request.

References

[1] E.R. Duval, J. Sheynin, A.P. King, K.L. Phan, N.M. Simon, B. Martis, K.E. Porter, S. B. Norman, I. Liberzon, S.A.M. Rauch, Depress. Anxiety 37 (2020) 670–681.
[2] A.L. Gold, R. Abend, J.C. Britton, B. Behrens, M. Farber, E. Ronkin, G. Chen, E. Leibenluft, D.S. Pine, Am. J. Psychiatr. 177 (2020) 454–463.
[3] J.E. Hassell Jr., K.T. Nguyen, C.A. Gates, C.A. Lowry, Curr Top Behav Neurosci 43 (2019) 271–321.
[4] N.C. Coimbra, T. Paschoalin-Maurin, G.S. Bassi, A. Kanashiro, A.F. Biagioni, T. T. Felippotti, D.H. Elias-Filho, J. Mendes-Gomes, J.P. Cysne-Coimbra, R.C. Almada, B. Lobão-Soares, Rev. Bras. Psiquiatr. 39 (2017) 72–83.
[5] P. Tovote, J.P. Fadok, A. Lüthi, Nat. Rev. Neurosci. 16 (2015) 317–331.
[6] D. Busti, R. Geracitano, N. Whittle, Y. Dalezios, M. Mańko, W. Kaufmann, K. Sätzler, N. Singewald, M. Capogna, F. Ferraguti, J. Neurosci. 31 (2011) 5131–5144.
[7] R.K. Butler, A.C. Sharko, E.M. Oliver, P. Brito-Vargas, K.F. Kaigler, J.R. Fadel, M. A. Wilson, Bone 23 (2011) 133–144.
[8] S. Duvarci, D. Pare, Neuron 82 (2014) 966–980.
[9] M.P. Parsons, L.A. Raymond, Neuron 82 (2014) 279–293.
[10] D.M. Bannerman, R. Sprengel, D.J. Sanderson, S.B. Mchugh, J.N.P. Rawlins, H. Monyer, P.H. Seeburg, Nat. Rev. Neurosci. 15 (2014) 181–192.
[11] L. Musazzi, G. Racagni, M. Popoli, Neurochem. Int. 59 (2011) 138–149.
[12] J.-Y. Zhang, T.-H. Liu, Y. He, H.-Q. Pan, W.-H. Zhang, X.-P. Yin, X.-L. Tian, B.-M. Li, X.-D. Wang, A. Holmes, T.-F. Yuan, B.-X. Pan, Biol. Psychiatr. 85 (2019) 189–201.
[13] A.K. Geim, K.S. Novoselov, Nat. Mater. 6 (2007) 183–191.
[14] L. Feng, L. Wu, X. Qu, Adv. Mater. 25 (2013) 168–186.
[15] G. Yang, J. Su, J. Gao, X. Hu, C. Geng, Q. Fu, J. Supercrit. Fluids 73 (2013) 1–9.
[16] K. Kostarelos, M. Vincent, C. Hebert, J.A. Garrido, Adv. Mater. 29 (2017) 1–7.
[17] M. Bramini, G. Alberini, E. Colombo, M. Chiacchiaretta, M.L. DiFrancesco, J. F. Maya-Vetencourt, L. Maragliano, F. Benfenati, F. Cesca, Front. Syst. Neurosci. 12 (2018) 1–22.
[18] R. Rauti, M. Medelin, L. Newman, S. Vranic, G. Reina, A. Bianco, M. Prato, K. Kostarelos, L. Ballerini, Nano Lett. 19 (2019) 2858–2870.
[19] G. Cellot, S. Vranic, Y. Shin, R. Worsley, A.F. Rodrigues, C. Bussy, C. Casiraghi, K. Kostarelos, J.R. McDearmid, Nanoscale Horizons 5 (2020) 1250–1263.
[20] H. Ali-Boucetta, D. Bitounis, R. Raveendran-Nair, A. Servant, J. Van den Bossche, K. Kostarelos, Adv. Healthc. Mater. 2 (2013) 433–441.
[21] D.A. Jasim, N. Lozano, K. Kostarelos, 2D Mater. 3 (2016), 014006.
[22] S.P. Mukherjee, N. Lozano, M. Kucki, A.E. Del Rio-Castillo, L. Newman, E. Vazquez, K. Kostarelos, P. Wick, B. Fadeel, PloS One 11 (2016), e0166816.
[23] A.F. Rodrigues, L. Newman, D.A. Jasim, I.A. Vacchi, C. Ménard-Moyon, L.E. Crica, A. Bianco, K. Kostarelos, C. Bussy, Arch. Toxicol. 92 (2018) 3359–3379.
[24] H. Cohen, J. Zohar, Z. Kaplan, J. Arnt, Eur. Neuropsychopharmacol 28 (2018) 63–74.
[25] J. Tejada, K.T. Chaim, S. Morato, Psicol. Teor. Pesqui. 33 (2017) e3322.
[26] G. Paxinos, C.R. Watson, The Rat Brain in Stereotaxic Coordinates, sixth ed., Elsevier Academic Press, San Diego, 2007.
[27] A.F. Biagioni, R.C. de Oliveira, R. de Oliveira, J.A. da Silva, T. dos Anjos-Garcia, C. M. Roncon, A.P. Corrado, H. Zangrossi, N.C. Coimbra, Eur. Neuropsychopharmacol 26 (2016) 532–545.
[28] M. Musto, R. Rauti, A.F. Rodrigues, E. Bonechi, C. Ballerini, K. Kostarelos, L. Ballerini, Front. Syst. Neurosci. 13 (2019) 1–15.
[29] E.L. Louth, C.D. Sutton, A.L. Mendell, N.J. Maclusky, C.D.C. Bailey, JoVE 122 (2017), e55358.

[30] W.C. Risher, T. Ustunkaya, J.S. Alvarado, C. Eroglu, PloS One 9 (2014), e107591.
[31] P. Chakraborty, S. Chattarji, Psychopharmacology 236 (2019) 73–86.
[32] R. Mitra, R. Adamec, R. Sapolsky, Behav. Pharmacol. 205 (2009) 535–543.
[33] N. Secomandi, A. Franceschi Biagioni, K. Kostarelos, G. Cellot, L. Ballerini, Nanomed. Nanotechnol. Biol. Med. 26 (2020) 102174.
[34] R. Khazipov, D. Zaynutdinova, E. Ogievetsky, G. Valeeva, O. Mitrukhina, J. B. Manent, A. Represa, Front. Neuroanat. 9 (2015) 1–5.
[35] J.P. Johansen, H. Hamanaka, M.H. Monfils, R. Behnia, K. Deisseroth, H.T. Blair, J. E. LeDoux, Proc. Natl. Acad. Sci. U. S. A 107 (2010) 12692–12697.
[36] R.A. Dielenberg, G.E. Hunt, I.S. McGregor, Neuroscience 104 (2001) 1085–1097.
[37] L.K. Takahashi, B.R. Nakashima, H. Hong, K. Watanabe, Neurosci. Biobehav. Rev. 29 (2005) 1157–1167.
[38] N.S. Canteras, E. Pavesi, A.P. Carobrez, Front. Neurosci. 9 (2015) 1–10.
[39] J.A. Rosenkranz, E.R. Venheim, M. Padival, Biol. 67 (2010) 1128–1136.
[40] L.G. Staples, I.S. McGregor, R. Apfelbach, G.E. Hunt, Neuroscience 151 (2008) 937–947.
[41] A. Berardi, V. Trezza, M. Palmery, L. Trabace, V. Cuomo, P. Campolongo, Front. Behav. Neurosci. 8 (2014) 1–12.
[42] C. Muñoz-Abellán, R. Andero, R. Nadal, A. Armario, Psychoneuroendocrinology 33 (2008) 1139–1150.
[43] R.C. Martinez, E.F. Carvalho-Netto, É.R. Ribeiro-Barbosa, M.V.C. Baldo, N. S. Canteras, Neuroscience 172 (2011) 314–328.
[44] A.L. Mahan, K.J. Ressler, Trends Neurosci. 35 (2012) 24–35.
[45] K.J. Wallace, J.B. Rosen, J. Neurosci. 21 (2001) 3619–3627.
[46] A. Malgaroli, R.W. Tsien, Nature 357 (1992) 134–139.
[47] R.J. Cormier, P.T. Kelly, J. Neurophysiol. 75 (1996) 1909–1918.
[48] H.T. Blair, G.E. Schafe, E.P. Bauer, S.M. Rodrigues, J.E. LeDoux, Learn. Mem. 8 (2001) 229–242.
[49] I.S. McGregor, L. Schrama, P. Ambermoon, R.A. Dielenberg, Behav. Brain Res. 129 (2002) 1–16.
[50] M.A. Matar, H. Cohen, Z. Kaplan, J. Zohar, Neuropsychopharmacology 31 (2006) 2610–2618.
[51] D. Rabellino, M. Densmore, P.A. Frewen, J. Théberge, M.C. McKinnon, R.A. Lanius, PloS One 11 (2016), e0163097.
[52] B.M. Sharp, Transl. Psychiatry 7 (2017) e1194.
[53] J.P. Johansen, C.K. Cain, L.E. Ostroff, J.E. LeDoux, Cell 147 (2011) 509–524.
[54] O. Babaev, C. Piletti Chatain, D. Krueger-Burg, Exp. Mol. Med. 50 (2018) 1–16.
[55] R. Rauti, N. Lozano, V. León, D. Scaini, M. Musto, I. Rago, F.P. Ulloa Severino, A. Fabbro, L. Casalis, E. Vázquez, K. Kostarelos, M. Prato, L. Ballerini, ACS Nano 10 (2016) 4459–4471.
[56] R.J. Cormier, M.D. Mauk, P.T. Kelly, Neuron 10 (1993) 907–919.
[57] A. Louveau, J. Angibaud, F. Haspot, M.C. Opazo, R. Thinard, V. Thepenier, S. J. Baudouin, L. Lescaudron, P. Hulin, C.A. Riedel, H. Boudin, J. Neurosci. 33 (2013) 18672–18685.
[58] M. Kintscher, C. Wozny, F.W. Johenning, D. Schmitz, J. Breustedt, Nat. Commun. 4 (2013) 1–8.
[59] M.J. Mitchell, M.M. Billingsley, R.M. Haley, M.E. Wechsler, N.A. Peppas, R. Langer, Nat. Rev. Drug Discov. 20 (2020) 101–124.

Graphene oxide-based intervention on anxiety related amygdala plasticity: a nanoscale strategy to target pathological presynaptic release.

Elisa Pati[1], Audrey Franceschi Biagioni[1], Raffaele Casani[1], Neus Lozano[2], Kostas Kostarelos[2,3], Giada Cellot[1], Laura Ballerini[1*]*

[1]International School for Advanced Studies (SISSA/ISAS), 34136 Trieste, Italy

[2]Catalan Institute of Nanoscience and Nanotechnology (ICN2), 08193, Barcelona, Spain

[3]Nanomedicine Lab, and Faculty of Biology, Medicine & Health, The National Graphene Institute, University of Manchester, Manchester, M13 9PL, United Kingdom

ABSTRACT

In the last decade, graphene-based nanomaterials (GBNs) have been proposed as innovative therapeutic tools in the field of precision medicine for neuroscience applications. In detail, graphene oxide (GO) nanoflakes with small lateral dimension (s-GO) were found to target specifically and transiently glutamatergic synapses *in vivo*. Recently, this ability was used to rescue the aberrantly potentiated glutamatergic transmission of the lateral amygdala and correlated anxiety behaviours, characterizing post-traumatic stress disorders (PTSD). Here, by using *in vitro* amygdala potentiated glutamatergic synapses, we explore from a mechanistic perspective how s-GO interferes at synaptic level with the pathological long-term potentiation (LTP) underlying PTSD. Thanks to simultaneous patch clamp pair recordings of unitary synaptic activity, live imaging of presynaptic vesicles release and confocal microscopy for structural analysis of synapses, we propose that s-GO prevents the long-term plasticity associated with PTSD by targeting precisely the release of glutamate from presynaptic site of excitatory synapses. In addition, we show that a single administration of s-GO in the lateral amygdala of an *in vivo* PTSD model abolishes the development of the pathological plasticity, thus inhibiting in the long-

term period anxiety-related behaviours. These findings might find application for the treatment of neuro-pathologies whose pathogenesis is characterized by exceeding glutamate signalling.

INTRODUCTION

Thanks to their reduced size and peculiar chemical-physical properties (Geim A.K. and Novoselov K.S., 2007, Garcia-Etxarri, A. et al., 2021; Drexler E.K et al., 1991; Bayda, S. et al., 2020), nanoscaled graphene-based nanomaterials (GBNs) have been recently proposed as alternative therapeutic strategies for the treatment of central nervous system (CNS) diseases (Feng L. et al., 2014; Kostarelos K. et al., 2017; Bramini M. et al., 2018; Cellot G. et al., 2022).

Among GBNs, small-graphene oxide (s-GO, < 500 nm lateral dimension) have been reported to target specifically the activity of glutamatergic synapses, by reducing in a reversible manner the excitatory transmission both *in vitro* and *in vivo* (Rauti R. et al., 2019). In addition, the targeted delivery of s-GO to a specific neuronal network has been used to modulate the animal behaviour emerging from the activity of that circuit (Cellot G. et al., 2020). This ability of the nanomaterial was recently exploited also in a pathological context. Post-traumatic stress disorder (PTSD), belonging to the group of anxiety diseases, is characterized by a dysfunctional long-term potentiation (LTP) in the lateral amygdala (LA) nucleus causing a hyperactivity of glutamatergic synapses (Shin L.M. et al., 2010; Bannerman, D. et al., 2014; Parsons M.P. et al., 2014) which correlates with anxiety-related behaviours (Somerville L.H. et al., 2004; Pacella M.L. et al., 2013). In this framework, s-GO, when stereotaxically injected into the LA during the consolidation of the pathological plasticity, prevented efficiently PTSD-related behavioural responses (Franceschi B.A. et al., 2021).

Although a direct interference of the nanomaterial with the presynaptic site of synapses was proposed (Rauti R. et al., 2019), the mechanism through which s-GO modulate synaptic activity of pathologically potentiated neuronal circuits has not been clearly investigated yet.

In the current work, we used an *in vitro* model of amygdala circuits to investigate the interaction of the nanomaterial at synaptic level with pathological LTP. By combining structural analysis of synapses, with live imaging of synaptic vesicle recycling and pair recordings to assess changes in the probability of glutamate release from presynaptic terminals, we detected that LTP-induced modifications of morphological and functional aspects of synapses were both impaired by the treatment with s-GO. We found that s-GO decreased the probability of glutamate release from the presynaptic site of excitatory synapses, thus counteracting the synaptic effect of LTP. Furthermore, through our rat behavioural model of PTSD, we showed as a single injection of the

nanomaterial in the LA during the development of plastic changes was sufficient to inhibit *in vivo* the anxiety related behaviours in a long-term manner.

RESULTS

1. s-GO reverts chemical LTP-induced changes in the amygdala synaptic structure

In the first set of experiments, we combined chemical LTP (cLTP) protocol with confocal analysis to investigate structural modifications of potentiated excitatory synapses and the potential effect of s-GO on them. To this aim, dissociated amygdala cultures underwent to cLTP procedure (30 s exposure to 50 μM of glutamate, Franceschi B.A. et al., 2021) in the presence or absence of s-GO (20 μg/mL, co-applied with glutamate), and after 30 minutes were fixed for immuno-labelling (Fig. 1A). As control, we used cultures not exposed to any treatment. As shown in the confocal z-stack reconstructions of Fig. 1B, neurons undergone to different treatments were stained with antibodies against the neuronal marker β-tubulin III (in blue, Rauti R. et al., 2019), the glutamatergic presynaptic marker VGlut1 (in green, Pampaloni N. et al., 2018) and the glutamatergic postsynaptic marker PSD95 (in red, Yoo K.S. et al., 2019; Borczyk M et al., 2019).

In β-tubulin III positive cells, the quantification of VGlut1-, PSD95- and VGlut1+ PSD95 co-localization puncta, indicative for the presence of synaptic contacts (McLeod F. et al., 2017), revealed that cLTP induced modifications in both the pre- and post-synaptic terminals, resulting in an overall increment in the number of glutamatergic synapses respect to the control condition. VGlut1 puncta were 7.2 ± 1.0 a.u. in control and 12.2 ± 1.1 a.u. in cLTP-treated samples ($p = 0.004$), PSD95 puncta were 14.2 ± 1.4 a.u. in control and 23.7 ± 3.8 a.u. in cLTP-treated samples ($p = 0.021$) and VGlut1+ PSD95 co-localization puncta were 6.9 ± 1.3 a.u. in control and 12.2 ± 1.2 a.u. in cLTP-treated cultures ($p = 0.015$; n = 20 fields, 4 cultures each; bar plots in Fig. 1C). When s-GO was applied during cLTP (i.e., together with glutamate), the structural changes observed in potentiated synapses, including pre-, postsynaptic modifications and the increased number of excitatory synapses, were reverted at the level of controls. In glut+s-GO treated samples, VGlut1 puncta were 7.0 ± 1.0 a.u. ($p = 0.003$, glut vs glut+s-GO), PSD95 puncta were 15.4 ± 1.2 a.u. ($p = 0.036$) and VGlut1+ PSD95 co-localization puncta were 7.0 ± 1.4 a.u. ($p = 0.015$, Fig. 1C). We also assessed the impact of the nanomaterial on the control cultures in the absence of potentiation, demonstrating that an application of s-GO (20 μg/mL) for 30 s in neurons not exposed to glutamate, did not affect in a statistically significant manner the number of excitatory synapses respect to untreated cultures (Supplementary Fig. 1A-B). These morphological results indicated that in our model cLTP had both pre- and post-site of expression,

resulting in an enhancement of the synaptic connectivity; however, all the cLTP-related structural modifications observed were rescued by the application of s-GO during cLTP induction.

Next, we confirmed these results through electrophysiological recordings of miniature postsynaptic currents (mPSC, Fig. 1D), obtained in the presence of the fast-inactivating voltage-gated sodium channel blocker tetrodotoxin (TTX, 1 μM). In this condition, action potential driven neuronal activity was abolished and the residual detected postsynaptic currents, due to the stochastic release of neurotransmitter-containing synaptic vesicles from presynaptic compartments, were informative for structural changes in synapses (Uteshev V.V. and Pennefather P.S., 1996).

Since mPSC were monitored in voltage clamp mode, to ensure the development of plasticity in the recorded neuron, we coupled the 30 s long lasting application of glutamate (50 μM) with a simultaneous depolarization of the membrane potential (+4 mV), thus favouring glutamate NMDA receptors activation fundamental for LTP induction (Malgaroli A. et al., 1992, Cormier R.J. et al., 1996, Fig. 1D). As in the previous experiments, s-GO was applied together with glutamate for 30 s (during the membrane depolarization), while control neurons were depolarized to + 4 mV for 30 s only. For the three conditions, we monitored changes in mPSC frequency and amplitude for 24 min after treatments. Fig. 1E depicts exemplificative traces obtained during the last minutes of recordings, showing that cLTP treatment (in light blue) induced an increase in both the frequency and amplitude of mPSC respect to the control (in black), changes reverted by the co-application of s-GO (in gray, Fig. 1E).

Values of miniature excitatory postsynaptic currents (mEPSC) frequency and amplitude, normalized for the baseline ones (pre-treatment, 8 min) are reported in plots of Fig. 1F. Most of neurons undergone to cLTP (61%) presented, respect to controls, a statistically significant increment of mEPSC amplitude, which started immediately after cLTP induction and stably lasted for all the monitored time. At 24 min post treatment, normalized mEPSC amplitude was 1.00 ± 0.02 in controls (n = 17) and 1.20 ± 0.11 in glutamate treated cells (n = 11; p = 0.01). In all cLTP treated neurons, mEPSC frequency was increased, but with a delay of 14 min after LTP induction. At 24 min post treatment, normalized mEPSC frequency was 0.88 ± 0.07 in controls (n = 17) and 1.79 ± 0.30 in glutamate treated cells (n = 18; p = 0.01; Fig.1F).

As for the confocal results, s-GO application during cLTP induction reverted all changes related to synaptic potentiation: in this case, both mEPSC frequency and amplitude were decreased to control values (at 24 min post treatment, normalized mEPSC amplitude was 0.95 ± 0.04, p = 0.014, and normalized mEPSC frequency was 0.77 ± 0.07, p = 0.011; n= 16). When we

applied 20 μg/mL of s-GO for 30 s to control cultures not exposed to glutamate no statistically significant differences were detected respect to controls (see Supplementary Figure 1C-D).

No modifications were observed in inhibitory synapses upon the different treatments. At 24 min post treatment, normalized miniature inhibitory postsynaptic current (mIPSC) amplitude was 0.98 ± 0.03 in controls (n = 17), 0.95 ± 0.03 in glutamate treated cells (n = 18), 0.96 ± 0.04 in glut+s-GO treated samples (n = 16), while normalized mIPSC frequency was 0.91 ± 0.07 in controls, 0.92 ± 0.16 in glutamate treated cells and 0.89 ± 0.08 in s-GO-treated samples (all $p>0.05$).

All together, these experiments indicated that in our cultures cLTP procedure was successful in inducing a synaptic potentiation characterized by both pre- and postsynaptic site of expression. In addition, the application of the nanomaterials during cLTP induction reverted all the observed plastic changes of excitatory synapses in potentiated cultures. Next experiments were aimed to identify the subcellular target of s-GO.

2. s-GO acts on the presynaptic terminal of amygdala neurons affecting presynaptic vesicle dynamics

Since previously published data (Rauti R. et al, 2019; Cellot G. et al., 2020) reported that s-GO modifies synaptic activity by interfering with the presynaptic terminal of synapses, we supported the hypothesis that also for potentiated synapses the nanomaterial could target this site. In addition, we excluded that the nanomaterial could affect the activity of postsynaptic glutamatergic receptors or could remove the exogenously applied glutamate (e.g., through adsorption). As illustrated in Supplementary Fig. 2, the inward current in response to glutamate application (50 μM glutamate, with 1 μM TTX to inhibit further release of endogenous glutamate), was not altered by s-GO (for glutamate 13.4 ± 5.1 pA*ms, n= 12, and for glut+s-GO 10.2 ± 6.2 pA*ms, n=10, $p>0.05$).

Therefore, we investigated the impact of s-GO on the presynaptic terminal of potentiated synapses by measuring synaptic vesicle dynamics by real-time imaging of vesicles labelled with the fluorescent styryl dye FM1–43 dye (Gaffield M. et al., 2006; Betz W. et al, 1992; Ryan T.A, 1999; Fig. 2A). Synaptic vesicles in the presynaptic terminals of our cultures were loaded with FM1–43 dye in an activity dependent manner thanks to endocytosis activated by cell depolarization (through the application of 50 mM KCl, Supplementary Fig. 3A; Ryan T.A. 1999). Next, in the presence of TTX (1 μM) to avoid synaptic vesicle release, samples were exposed to

different treatments, namely cLTP (50 μM of glutamate for 30 s) in the presence or absence of s-GO (20 μg/). Controls underwent no treatments. Presynaptic function was studied in the different conditions 30 min after treatments by evoking endocytosis through a second KCl application based-depolarizing stimulus (Fig. 2A). The resulting destaining of FM1–43 dye from the presynaptic boutons was a direct measure of presynaptic release efficacy (Zakharenko S.S. et al., 2001).

Although FM1-43 dye loading was not specific for glutamatergic vesicles, we focused on presynaptic terminal of presumed pyramidal neurons selected for their morphology (Rainnie D.G. et al., 1993). When we analysed the rate of FM1-43 destaining, we observed that samples undergone to cLTP presented a faster kinetic of dye unloading respect to that of controls (Fig. 2B). This was quantified by measuring the decay time constant (τ) that was 18.5 ± 2.3 s in control, n=200 terminals, and 9.6 ± 0.37 s in cLTP, n=200 terminals ($p < 0.0001$; Fig. 2C). Differently, the co-application of glutamate and s-GO delayed the destaining rate at the level of controls (16.4 ± 1.7 s, n=199 terminals, $p < 0.0001$ for cLTP vs cLTP+s-GO; n= 5 series of cultures for each condition, Fig. 2B-C). In reference experiments, the image series captured on FM1-43-stained cells without the high- K^+ destaining stimulus, produced a baseline reference plot (Fig. 2B, named bleaching). In addition, the application of s-GO in cultures not treated with glutamate presented a slower destaining compared to controls (Supplementary Fig. 3B-C).

Since the kinetic of the activity dependent FM 1-43 unloading reflects the mobility of synaptic vesicles (Ryan T.A. et al., 1999) and correlates with the probability of neurotransmitter release from the presynaptic terminals (Zakharenko S.S. et al., 2001), these results suggested that s-GO affected synaptic vesicles dynamics, and, in potentiated glutamatergic synapses, prevented the increased mobility of synaptic vesicles and related enhanced probability of release (p_r) observed after cLTP.

3. s-GO reduces the probability of glutamate release from the presynaptic terminal in potentiated amygdala neurons

To further probe whether the nanomaterial could affect the increased probability of glutamate release in potentiated synapses, we performed dual electrophysiological recordings from pairs of monosynaptically connected excitatory amygdala neurons. In these experiments, we adopted a pair pulse stimulation protocol to measure changes in the probability of neurotransmitter release (Gasparini S. et al., 2000; Murthy V.N. et al., 1997; Zucker R.S. 1989;

Debanne D. et al., 1996). Presynaptic neurons were stimulated in current clamp mode to fire two action potentials at 20 Hz while simultaneously the postsynaptic cells were monitored in voltage clamp mode to assess changes in the amplitude of the consecutive evoked excitatory postsynaptic currents (eEPSC), that were pharmacologically isolated in the presence of gabazine (10 μM), a synaptic blocker for $GABA_A$ receptors (Fig. 3A). Pair recordings confirmed the efficacy of s-GO in interfering with cLTP, as we observed that cLTP induced an increment in the amplitude of the first eEPSC (values normalized for the baseline were 1.7 ± 0.12) respect to the control (0.84 ± 0.07; p= 0.003), and such enhancement was prevented in cultures co-treated with s-GO (0.80 ± 0.09; p = 0.003, Fig.3B-C).

Changes in the pair pulse ratio (PPR), the ratio between the second and the first eEPSC amplitudes (Manabe T. et al., 1993; Debanne D. et al., 1996), were monitored before and after the different treatments as an indicator of the modification in the p_r. Decreases and increases in PPR are indicative for an enhanced and reduced p_r, respectively (Manabe T. et al., 1993; Debanne D. et al., 1996). As shown in Fig. 3B, in control cultures (black traces) postsynaptic cells presented from the begin to the end of the experiment stable short-term depression of consecutive eEPSC (at 24 min post treatment, PPR, normalized to baseline, was 1.00 ± 0.03 n= 6 pairs; Fig. 3BD). Differently, cells undergone to cLTP (in light blue, Fig. 3B), showed after the treatment a stronger short-term depression of consecutive eEPSC (normalized PPR was 0.68 ± 0.08, n=8 pairs; p = 0.008; Fig. 3BD). When s-GO was co-applied with glutamate (in grey, Fig. 3B), we detected no modifications of the short-term plasticity respect to controls (normalized PPR was 0.97 ± 0.07, n = 6 pairs; p = 0.039; Fig. 3BD).

Since the application of s-GO to control neurons induced post treatment decrease in the amplitude of the normalized first eEPSC (0.49 ± 0.12; p= 0.026; Supplementary Fig. 3C-D) and a change in the short term plasticity of consecutive eEPSC from depression to facilitation (at 24 min post treatment, normalized PPR was 1.5 ± 0.20, n = 6 pairs, p = 0.002 for control vs s-GO, Supplementary Fig. 3C-E), these results strongly indicate that the nanomaterial hampered LTP-induced functional synaptic changes by interfering with the probability of synaptic vesicles release.

In addition, the effect of s-GO in decreasing the p_r could be detected already immediately after its application, both in unpotentiated (at 6 min post treatment, normalized PPR was 1.02 ± 0.04 in control and 1.62 ± 0.35, in control+s-GO, n = 6 pairs, p = 0.0076) and potentiated conditions (at 6 min post treatment, normalized PPR was 1.00 ± 0.03 in cLTP and 0.98 ± 0.05 in

cLTP+s-GO, n = 6 pairs, p = 0.0118). Such immediate impact of the nanomaterial might affect the rescue of cLTP-dependent changes also in postsynaptic terminals.

4. A single s-GO injection, by preventing the stress-induced plasticity in the LA, reduces the PTSD-like behaviour

In the next set of experiments, we assessed in a long-term period the ability of s-GO in interrupting *in vivo* the plasticity of the amygdala neurons. To this aim, we used a rat behavioural model of PTSD, in which the exposure to the predator odour, induces an increase in the excitability of LA glutamatergic synapses (Rosenkranz J.A. et al., 2010), causing the long-lasting behavioural response related to traumatic disorders (Dielenberg R.A. et al, 2001).

In our experiments, after being habituated to an avoidance box, an apparatus to study contextual fear memory (Muñoz-Abellán C. et al., 2009), first animals were exposed to a collar previously worn by a cat (WC) or to an unworn collar (UC) as control (Fig. 4A). Compared to the UC exposed group, the exposure to the WC induced immediately a significant innate fear response characterized by an increase ($t(10) = 8.54$, $p = 0.0001$; Fig. 4B) in the head out behaviour, during which the animal scanned the environment from a protected position.

The day after, rats were submitted to a stereotaxic surgery to implant a cannula targeting the LA, through which, 4 days later, 0.5 μL of s-GO (50 μg/mL) or saline were microinjected. All the groups of rats were re-exposed to the context 8 days after odour exposure in the absence of the collars. At that time point, while saline treated animals previously exposed to WC presented an increase in head out behaviour respect to those exposed to UC and injected either with saline ($F (1, 5) = 11.76$, $p = 0.0036$) or s-GO ($F (1, 5) = 11.76$, $p=0.0113$), the s-GO injection in rats exposed to WC reverted head out defensive behaviour ($F (1, 5) = 24.71$, $p = 0.0187$; Fig. 4B).

These results indicated that a single injection of the nanomaterial in the LA during the formation of plastic change in synapses inhibited the contextual fear behaviour in a long-term manner.

In order to investigate whether the s-GO could revert the long-term anxiety-related response, immediate after the re-exposure test, rats were submitted to the elevated plus maze (EPM), an apparatus composed of 4 interconnected arms, two open and two closed, used to measure anxiety-like responses (Coimbra N.C. et al., 2017). WC rats, treated with saline, exhibited a statistically significant decrease ($F (1,5) = 9.219$, $p = 0.0289$) in the time spent in the

open and aversive arms of EPM compared to UC (saline treated) group, indicative for a long-term anxiety related to PTSD. Differently, s-GO microinjection into LA increased ($F(1,5) = 12.79$, $p = 0.0159$) the time spent in the open arms in WC animals, when compared to WC saline treated rats (Fig. 4C). Finally, assessment of open field (OF) locomotor activity showed no alterations in animal locomotion due to s-GO treatment ($p > 0.05$; Fig. 4D).

All together, these findings suggest that s-GO could rescue behavioural alterations related to PTSD, by targeting the glutamatergic synapses activity in the LA. The mechanism of s-GO blockage of developing plasticity appeared confirmed by the morphological analysis of LA neurons. After behavioural experiments, rodents were sacrificed, and brains were stained with Golgi-Cox method. This was done to confirm *post-mortem* the correct targeting of the cannula to LA (Fig. 4E, as injection needle tracts into the LA between bregma −2.64 mm and −3.96 mm) and to analyze dendritic spine density, whose increase was considered a hallmark of amygdala plasticity associated with the development of PTSD (Chakraborty P, Chattarji S., 2019; Mitra R. et al., 2009).

This synaptic plasticity modification was confirmed in WC group treated with saline where the number of dendritic spines per μm in LA was significantly higher (1.12 ± 0.05) when compared to UC-saline (0.92 ± 0.06, $F(1,11) = 3.925$, $p = 0.0142$) and UC-s-GO treated group (0.83 ± 0.08, $F(1,11) = 5.368$, $p = 0.0014$; Fig. 4F). As expected, dendritic spine density was reduced by the s-GO injection (0.88 ± 0.04, $F(1,11) = 3.69$, $p = 0.0214$, Fig. 4F). Such reduction arose probably by the impairment in the formation of new dendritic structures.

DISCUSSION

Our results indicate that s-GO prevented LTP in amygdala synapses, by affecting presynaptic terminal vesicle dynamics, thus reducing the probability of glutamate release at excitatory synapses. This finding was also translated to an *in vivo* model of PTSD, in which s-GO administration in the LA and its interference with glutamatergic synapses resulted in an inhibition of long-lasting anxiety-related behaviours and associated LTP-dependent morphological changes of synapses.

To dissect mechanistically how the nanomaterial prevents LTP in glutamatergic synapses, we adopted an *in vitro* model of dissociated amygdala cultures in which we previously reported that the application of s-GO during the cLTP induction counteracted the long-term synaptic potentiation (Franceschi A.B. et al., 2021). In the current work, we applied to this preparation

confocal analysis and electrophysiological recordings of mPSC, in order to identify the site of LTP expression. The former was used to evaluate changes in pre-/postsynaptic markers (namely VGlut1 and PSD95), while the latter was exploited to get knowledge of synaptic structure, as modifications of the presynaptic or postsynaptic terminals are traditionally detected as changes in the frequency or in the amplitude of mPSC, respectively (Uteshev V.V. and Pennefather P.S., 1996). Since we observed increments in both pre- and postsynaptic markers, as well as enhancement in the frequency and amplitude of mEPSC, we demonstrated that in dissociated amygdala cultures synaptic potentiation relied on modifications of both the synaptic sites. In these experiments, we observed late onset changes in mEPSC frequency, that may depend on later modifications of the presynaptic site.

Although no data in literature were available for dissociated amygdala cultures, these results were in line with studies performed on acute slices obtained from animals undergone to Pavlovian fear conditioning, showing the involvement of both pre- and post-synaptic factors in LTP expression of LA (Maren S., 2005; Rumpel S. et al., 2005).

Furthermore, in acute brain slices undergoing to LTP induction through high frequency stimulation of afferent fibres, the site of expression of amygdala LTP is strongly dependent on the innervation received by neurons, with stimulation of thalamic and cortical fibres inducing post- and presynaptic LTP, respectively (Humeau Y. et al., 2005; Huang Y.Y. and Kandel E.R., 1998; Humeau Y. et al., 2003). Since our dissociated amygdala cultures are composed by heterogeneous neurons coming from various amygdala regions, it is reasonable that both pre- and postsynaptic forms of LTP expression could co-exist.

As shown by electrophysiological pair recordings in which we monitored changes in eEPSC amplitude occurring after cLTP in the presence or absence of s-GO, we confirmed the ability of the nanomaterial in preventing the potentiation of synaptic communication between excitatory amygdala neurons.

Although, through structural analysis of synapses, we detected, after nanomaterial treatment, changes in LTP expression at both the sites of synapses, previous studies reported that in basal physiological conditions (not potentiated synaptic transmission), s-GO targeted specifically presynaptic glutamatergic terminals (Rauti R. et al, 2019; Cellot G. et al., 2020). We extended this finding to synapses that were artificially potentiated to mimic the pathological condition of PTSD (McKernan M.G., Shinnick-Gallagher P. 1997; Richter-Levin G. et al., 2018; le Feber J., 2019), demonstrating that s-GO, by reducing the p_r of presynaptic excitatory sites of

amygdala neurons counteracted the enhanced synaptic communication of the potentiated synapses.

Indeed, thanks to the similarity of inward currents generated by glutamate application in the presence or absence of the nanomaterial, we could exclude any chemical interaction between s-GO and glutamate, as well as with the postsynaptic glutamatergic receptors. In opposition, we verified s-GO impact on presynaptic terminals by monitoring synaptic vesicles dynamics through live FM 1-43 imaging. Although not selective for glutamatergic vesicles, these experiments revealed the ability of the nanomaterials in reverting to control levels the kinetics of vesicles unloading in putative pyramidal cells (Rainnie D.G. et al., 1993), found slowed down in cultures undergone to cLTP.

Only through simultaneous dual recordings from monosynaptically connected excitatory neurons, we could demonstrate that the nanomaterial interference with potentiated synaptic communication arose from a modification of the probability of glutamate release from presynaptic site. Indeed, in these experiments we observed both in control and in potentiated conditions a change from a short-term depression to a short-term facilitation after s-GO application (or to a weaker short-term depression), indicative for a modification of p_r at presynaptic level (Manabe T. et al., 1993, Debanne D. et al., 1996).

Notably, thanks to this experiment we detected already during the first five minutes after its application the effect of s-GO in targeting the presynaptic site of synapses and in reducing the probability of glutamate release. Such immediate impact of the nanomaterial might explain the rescue of cLTP-dependent changes also in postsynaptic terminals (i.e., the increment in mEPSC amplitude and PSD95 puncta density), even if without any direct interaction of the nanomaterial.

Supported by our *in vitro* results, we used an *in vivo* model of PTSD induced by the exposure to the predator odour (Franceschi B.A. et al., 2021) to evaluate the impact of s-GO in the long-term condition. We previously demonstrated as a single s-GO microinjection in the LA during a temporal window which was crucial to the reinforcement of plastic changes related to the fear memory storage (Canteras N.S. et la., 2015) was able to reduce anxiety-related behaviours (Franceschi B.A. et al., 2021). In these previous experiments animal behaviour was tested 2 days after s-GO administration, when the nanomaterial still persisted in the tissue (Rauti R. et al., 2019), not allowing to distinguish between a direct effect of nanomaterials on synaptic communication and an impairment of the building up of pathological plasticity (Franceschi B.A. et al., 2021).

To dissect this issue, in the current work we postponed animal testing to 6 days after nanomaterial administration. At this temporal point, when the nanomaterial should be already cleared from the LA, our results showed that rats previously exposed to predator odour and treated with s-GO not only presented a decreased in head out behaviour, indicative for a reduction of contextual fear memory, but they also exhibited an increased time spent in the open arm of the EPM, that was representative for the decrement in generalized long term anxiety. As shown by our post-sacrifice staining of LA neurons, such an effect was due to the nanomaterial interaction at synaptic level that prevented the formation of dendritic spines in the LA, a hallmark of LTP (Bosch M. et al., 2014).

These results strongly indicated that s-GO-induced reduction of anxiety-related behaviours arose from the impairment of the building up of pathological plasticity in the amygdala, occurring, as suggested by *in vitro* experiments, through an interference of the nanomaterial with presynaptic site of glutamatergic synapses.

This work illustrated the mechanisms of s-GO interaction with potentiated synapses. By targeting presynaptically the glutamatergic transmission also when aberrantly potentiated, s-GO nanoflakes could be used as highly selective sub-cellular modulators to hinder synaptic and behavioural alterations of neurodisorders, whose pathogenesis is characterized by altered glutamatergic signalling. Although further investigations regarding the biosafety of this nanomaterial are required, s-GO can be proposed as an alternative nanotool for future applications in the field of precision medicine.

MATERIALS AND METODS

Graphene oxide synthesis and characterization

The s-GO material used in these studies has been synthesized according to the protocols that have already been reported and characterized extensively in our previous published work (Rauti R. et al, 2019, Secomandi N. et al., 2020, Franceschi A.B. et al., 2021). The specific batch of GO nanosheets used here, were thin (1-3 carbon layers) and of a few hundred nanometers in lateral dimension (100-400nm), with reproducibly demonstrated biocompatibility and purity.

In vitro dissociated amygdala cultures

All experimental procedures were performed in agreement with the Italian law (decree 26/14) and the European Union (EU) guidelines (2007/526/CE and 2010/63/UE) and were authorized by the Italian Ministry of Health (n. 689/2017-PR, n. 22DAB.N.1Z8 and n. 22DAB.N.1WO). The animal handling was approved by the local veterinary authorities and by the institutional (SISSA) ethical committee.

Primary cultures of amygdala cells were obtained from postnatal (P 7-10) juvenile Wistar rats and prepared as previously described (Secomandi N. et al., 2020) with slight modifications. In brief, rat brains were quickly removed from the skull and placed in fresh ice-cold artificial cerebrospinal fluid (ACSF) containing (in mM): 124 NaCl, 24 $NaHCO_3$, 13 glucose, 5 HEPES, 2.5 KCl, 2 $CaCl_2$, 2 $MgSO_4$ and 1,2 $NaPO_4H_2$ with a pH of 7.3-7.4 when saturated with 95% O_2 and 5% CO_2 (Wu Y.E. et al., 2017). Coronal brain sections were cut using a vibratome (LeicaVT1000S) and under a dissecting microscope (Olympus SZ40), the regions containing the amygdaloid complex was visually identified following defined anatomical coordinates: Bregma -1.8 mm, - 2.4 mm and 2.8 mm (Khazipov R. et al., 2015). Using a biopsy punch with a diameter of 1 mm (Kai Medical, Japan) the amygdala tissue was collected to be enzymatically and mechanically dissociated following standard protocol (Cellot G. et al., 2011). Cells were seeded onto poly-L-ornithine-coated glass coverslips at a density of 1000 cells/mm^2 and maintained in controlled conditions (at 37 ◦C, 5% CO^2) for 8–12 days *in vitro* (DIV) prior to experiments in Neurobasal A Medium (Invitrogen) containing B27 supplement (Thermofisher).

Immunohistochemistry and confocal microscopy

Cultured amygdala neurons (5 cultures; 8-12 DIV) were fixed by 4% formaldehyde (prepared from fresh paraformaldehyde, PFA; Sigma) in PBS at room temperature (RT). After 15 min in glycine 0.3M in PBS, cells were blocked and permeabilized in 10% fetal bovine serum (FBS), 3% bovin serum albumin (BSA), 0.3% Triton-X 100 in PBS (blocking solution) for 30 min at RT. As primary antibodies, we used rabbit polyclonal anti-β-tubulin III (Sigma-Aldrich, 1:500 dilution), mouse monoclonal anti-PSD95 (Invitrogen, 1:400 dilution), and guinea pig anti-vesicular glutamate transporter 1 (VGlut1; Sigma-Aldrich, 1:1000), diluted in the blocking solution for 60 min at RT. As secondary antibodies, we used Alexa 405 goat anti-rabbit (Invitrogen, dilution 1:500), Alexa 594 goat anti-mouse (Invitrogen, dilution 1:500), and Alexa 488 goat anti-guinea pig (Invitrogen, 1:500) diluted in normal goat serum (NGS) 5% in PBS for 45 min at RT. Finally, cells were mounted on 1 mm thick glass coverslips using the Fluoromount mounting medium (Sigma-Aldrich). To quantify VGlut1 and PSD95 puncta, $n = 50 \pm 10$ *z*-stacks

(acquired every 0.15 μm) were taken from $n = 5$ randomly selected fields (70.64 μm × 70.64 μm) per coverslip using a Nikon C2 Confocal, equipped with Ar/Kr, He/Ne, and UV lasers. Images were acquired with a 60× (1.4 NA) oil-objective (using oil mounting medium, 1.515 refractive index). We selected only VGlut1-positive and PSD95-positive puncta (≥0.1-0.8≥ μm^3) co-localized with β-tubulin III-positive signal in 6 different ROIs (32.9 μm × 8.9 μm) per image containing one or more distal neurites. For each image, VGlut1 puncta were normalized to the β-tubulin III positive volume. Images were analysed using the Volocity software (Perkin Elmer).

Electrophysiology

Patch clamp whole-cell recordings were obtained from dissociated amygdala neurons using glass micropipettes with a resistance of 4–7 MΩ once filled with the following intracellular saline solution (in mM): 120 K gluconate, 20 KCl, 10 HEPES, 10 EGTA, 2 $MgCl_2$, 2 Na_2ATP (pH 7.3, osmolarity adjusted to 300 mOsm). All experiments were performed at RT with the standard extracellular solution containing (in mM) 150 NaCl, 4 KCl, 2 $CaCl_2$, 1 $MgCl_2$, 10 HEPES, 10 glucose (pH 7.4) and continuously perfused at 2 ml/min. All data were collected by means of a Multiclamp 700A patch amplifier (Axon CNS, Molecular Devices) and digitized at 10 KHz with the pClamp 10.6 acquisition-software (Molecular Devices LLC, USA). Input resistance and cells capacitance were measured online with the membrane test feature of the pClamp software. Spontaneous activity was recorded in voltage clamp mode at a holding potential of −58 mV, not corrected for the liquid junction potential which was −12 mV (calculated with the Clampex software; Molecular Devices, Sunnyvale, CA, USA). The stability of the patch was repetitively monitored during the experiments by checking the input and series resistance. Cells exhibiting 15% changes were excluded from the analysis. The series resistance was <20 MΩ and it was not compensated. Input resistance and cells capacitance were measured online with the membrane test feature of the pClamp software.

To induce LTP in dissociated cultures under voltage clamp mode, our previously described protocol was applied (Franceschi B.A. et al., 2021). Briefly, after recording spontaneous activity for 8 min as baseline, 50 μM of glutamate for 30 s was applied, while the membrane potential of the recorded cell was depolarized from -58 mV to +4 mV. In the experiments where dissociated cells were treated with s-GO, it was applied at a concentration of 20 μg/mL for 30 s through the perfusion system, alone or in combination with 50 μM of glutamate.

The effects of LTP induction and s-GO interference were monitored for 24 min after the baseline collection. mPSC were recorded in the presence of TTX (1 μM) to block fast voltage-dependent sodium channels. They were analyzed offline using the software AxoGraph X (Axograph Scientific), which exploits a detection algorithm based on a sliding template. Templates characterized by diverse decay times were used to separate offline glutamate AMPA-receptor mediated postsynaptic currents (~3 ms) and those mediated by $GABA_A$ -receptors (~20 ms). For each recording, all the collected events were averaged, and the peak amplitude and kinetic properties of the mean current were measured. The averaged values of sPSC and mPSC were calculated between 18 and 24 min after LTP induction and normalized for the pre-treatment baseline values.

In paired recordings, monosynaptically connected glutamatergic neurons, recorded in the presence of gabazine (10 μM) were recognized by the short latency (<3 ms; Rauti R. et al., 2016; Pavlidis P. et al., 2000) between the peak of the presynaptic neuron and the onset of eEPSC. The presynaptic neuron in current clamp mode was held at -70 mV (by ≤ 0.02 nA negative current injection), and action potentials were evoked by delivering short (4 ms) positive (1 nA) square current pulses. To characterize the short-term dynamics of synaptic contacts as well as changes in the p_r from the presynaptic neurons, we delivered to presynaptic neurons repeated paired pulse stimulation at 20 Hz (every 20 s; 6 times that were pooled together and averaged). We estimated the p_r of glutamatergic amygdala synapses by quantifying the PPR (calculating the ratio between the mean peak amplitude of the second and the first eEPSC, Manabe, T et al., 1993; Debanne, D et al., 1996) and we indirectly assessed changes in its efficacy monitoring the PPR up to 24 min after different treatments. The averaged values of PPR were calculated between 18 and 24 min after treatment and normalized for the pre-treatment baseline values.

Glutamate-induced inward currents were assessed by a 30 s-long application of glutamate (50 μM) in the presence of TTX 1 μM and the area under the current was measured through the pClamp software.

FM1-43 Imaging

Depolarization-dependent staining of synaptic terminals with the styryl dye N-(3-triethylammoniumpropyl)- 4-(4-(dibutylamino)styryl)pyridinium dibromide (FM1-43, Molecular Probes, Life Technology) was obtained by incubating amygdala cultures (after 10 min saline buffer wash at RT) for 2 min with 2 mL of extracellular recording solution containing 50 mM

KCl and 15 μM FM1–43 dye. Next, this buffer was replaced with 2 mL of extracellular recording solution containing FM1-43, and cells were left to recover for 10 min to ensure complete recycling of the vesicles (Rauti R. et al., 2016). Cells were then incubated for 10 min with TTX (1 μM) to prevent network activity altering the rate of FM release. After loading with FM1-43 dye, cultures were treated with 50 μM of Glutamate, in the presence or absence of 20 μg/mL of s-GO or with saline for 30 s at RT. As further control we treated cultures with s-GO only. For live imaging, cultures were transferred to the stage of a Nikon Eclipse Ti−U inverted microscope where they were continuously perfused (5 mL/minute) at RT with the extracellular recording solution containing TTX (1 μM). FM1-43-loaded cells were recorded with a 40x objective (PlanFluor, 0.60 NA) and excited at 488 nm with a mercury short lamp (Osram, Munich, Germany). Excitation light was separated from the light emitted from the specimens using a 395 nm dichroic mirror and DN filter (1/32). Images were constantly acquired at 7 fps every 150 ms using an ORCA-Flash4.0 V2 sCMOS camera (Hamamatsu Photonics, Japan) with a spatial resolution of 512 × 512 pixels. The set-up was controlled by HCImage Live software. After a basal recording (2 min), application of 50 mM KCl (2 min), followed by a 2 min of washout, was used to stimulate vesicle exocytosis from the dye-containing terminals, measured as a fluorescence loss. Offline analysis was performed on the image sequence with the image processing package Fiji (Rauti R. et al., 2016). After background subtraction, time-dependent fluorescence changes on FM1–43 labelled terminals were obtained by drawing regions of interest (ROIs) around fluorescent spots (typically 6 × 6 pixels in diameter drawn on neural processes), including as little background possible. Corresponding tracings were transferred to Clampfit software (pClamp suite, 10.6 version; Molecular Device LLC, US) and the decay time constant (τ) was measured from averaged traces by fitting it with a mono-exponential function ($f(t)=\sum_{i=1}^{n} A_i e^{-t/\tau_i} + C$). To avoid imaging nonselective FM staining, only puncta that showed stimulus-dependent destaining were included in the analyse (Rauti R. et al., 2016).

Experimental design for in vivo procedure

Experimental procedures were carried out in accordance with the Italian law (decree 26/14) and the EU guidelines (2007/526/CE and 2010/63/UE) and were approved by the Italian Ministry of Health (n. 22DAB.11). Male adult Wistar rats weighed 230-280 g (n = 24) were used to perform the *in vivo* experiments. Food and water were provided at libitum. The enclosure was maintained at 21 ± 2 °C on a light-dark cycle (lights on from 7 p.m. to 7 a.m.). Behavioural experiments were performed as described previously (Franceschi B.A. et al., 2021). Briefly,

aversive memory behavioural responses were evaluated in the avoidance box, which consisted of a rectangular arena (40 x 26 x 36 cm) with black acrylic-plexiglass walls covered with a transparent plexiglass lid. At one side of the arena, an alligator clip fixed in the wall is positioned 4 cm above the floor. A smaller box (20 x 26 x 22 cm) covered with a black plexiglass lid, named hide box, is positioned in the opposite direction of the rectangular arena. Arena and hide box were separated by a small 6 x 6 cm square hole allowing free access to both chambers. Rats were placed inside the hide box with free access to the arena for 3 consecutive days to habituate to the apparatus during 10 minutes. On the fourth day, the time spent in the following defensive behaviour was recorded: head out (namely, the rat scanning the environment from a protected position, measured as poking of the head, or of head and shoulders, outside of the hide box but with the bulk of the rat body inside of it). Next, rats were divided in two groups (n=6 per group), exposed to either a piece (2 cm) of an unworn collar (UC), without any cat odour or a piece of the collar previously worn by the cat, named worn collar (WC). Collars were worn by an encaged cat. Rats were re-exposed (10 minutes) to the context, arena without the cat collar to evaluate the aversive memory related to the conditioned fear. Head out behavioural response was analyzed during the re-exposure to the context at 8 days post-exposure. Shortly thereafter, long-term anxiety-related behaviour was evaluated using the EPM. Which consisted of four arms (50 x 10 x 40 cm), two open arms (without walls) and two closed arms (with 40 cm high walls) connected by a central square (10 x 10 cm). The maze was elevated 50 cm from the ground. Rats (n=6 per group) were placed in the closed arm and were allowed to freely explore the apparatus for 5 minutes. Percentage of time spent in the open zone was evaluated.

Exploratory and locomotor activities of rats (n = 6 per group) were measured in the OF apparatus, a square arena with the 60 x 60 x 40 cm black plexiglass walls and floor. Total distance moved (cm) in the OF were analyzed following the EPM testing. All behavioural tests were performed between 8 a.m. and 12 p.m. under 40 lx luminosity and videorecorded for off-line analysis. The XPloRat software (Tejada et al., 2018) was used to score the behaviours. Next day, animals were submitted to stereotaxic surgery as described previously (Biagioni A.F. et al., 2016). Briefly, animals were anesthetized with intraperitoneal injection of ketamine (Ketamine Imalgene®, Merial Laboratories) and xylazine (Sedaxylan®, Dechra Veterinary Products) at 92 mg/kg and 10 mg/kg body weight, respectively, and fixed in a stereotaxic frame. A stainless-steel guide cannula (outer diameter, 0.6 mm, and inner diameter, 0.4 mm) was implanted in the diencephalon aimed to the LA. The upper incisor bar was set at 3.3 mm below the interaural line so that the skull was horizontal between bregma and lambda. The guide cannula was vertically introduced using bregma as the reference and the following coordinates: A.P.−3.48 mm, M.L.−5.2

mm and D.V.−7 mm, according to Paxinos and Watson, 2007. At the end of the surgery, the acrylic resin and two stainless steel screws were used to fix the guide cannula in the skull. In order to protect the guide cannula from obstruction a stainless-steel wire was used to seal it. Analgesic and antibiotic medications were administrated postoperatively. Three days later, rats were gently wrapped in a cloth and held while they received a random treatment into LA of either s-GO (50 μg/mL) or ACSF solution (composition described below) delivered by a needle (0.3 mm of outer diameter) linked to a syringe (Hamilton) through a polyethylene tube. The injection needle was inserted through the guide-cannula until it reached the LA (2 mm below the guide-cannula). Only rats that needle tip reached the LA were included in the study. Four days later, animals were submitted to the behavioural testing. All experimental procedures were planned to minimize the number of animals used and their suffering.

Golgi-cox staining and dendritic spine analysis

After behavioural experiments, rats (n = 20) were anaesthetized as described above and decapitated, their brains were collected and prepared to the Golgi-Cox staining protocol (Louth et al., 2017). Briefly, brains were incubated in the Golgi-Cox solution (1% potassium dichromate, 0.8% potassium chromate and 1% mercuric chloride) in the dark at RT for 25 days. After that, brains were incubated in sucrose solution at 30% for 48 hours and sliced in coronal sections (200 μm thickness) at the level of the amygdala using a vibratome (Leica VT100S). Brain slices were mounted onto microscope slides with Eukitt Quick-hardening mounting medium (Sigma-Aldrich). Histological sections were analyzed and images stacks of the LA neurons were acquired using a Leica DM6000 upright microscope with a 63x oil immersion objective. The serial section images were aligned, and dendritic spines of pyramidal neurons were blind analyzed (Risher et al., 2014) in RECONSTRUCT software (http://synapses.clm.utexas.edu/tools/reconstruct/reconstruct.stm; RID:SCR_002716). Primary and secondary dendrite, defined as any branch emerging from the soma and branch emerging from a primary dendrite, respectively, with a length of 40 μm from its origin was analyzed (Chakraborty P., Chattarji S., 2019; Mitra R. et al., 2009). All dendrite protrusions were considered as spines, regardless to their morphological characteristics.

Data analysis and statistics

All values from samples subjected to the same experimental protocols were pooled together and expressed as mean ± s.e.m with n = number of cells, unless otherwise indicated. For electrophysiological data, Shapiro-Wilk normality test was applied to evaluate the statistical distribution of the data sets. Statistically significant difference between two data sets was assessed by Student's t-test for parametric data and by Mann–Whitney for non-parametric ones. All comparisons between more than 2 groups were made with one-way ANOVA for parametric data, followed by using Holm-Sidak's multiple comparisons test for post hoc analysis. Not parametric data were analyzed with Kruskal-Wallis test and post hoc analysis was done with Dunn's multiple comparison test. For *in vivo* experiments, data from independent groups of animals exposed to the cat collar were checked for normality and homogeneity and analyzed using Student's unpaired two-tailed t-test. All comparisons between two independent variables were made with two-way ANOVAs, followed by Bonferroni or Tukey' multiple comparison test when appropriated. Statistical significance was determined at $P < 0.05$, unless otherwise indicated.

References

1. Apergis-Schoute AM, Debiec J, Doyère V, LeDoux JE, Schafe GE. Auditory fear conditioning and long-term potentiation in the lateral amygdala require ERK/MAP kinase signaling in the auditory thalamus: a role for presynaptic plasticity in the fear system. J Neurosci. 2005 Jun 15;25(24):5730-9.

2. Bannerman DM, Sprengel R, Sanderson DJ, McHugh SB, Rawlins JN, Monyer H, Seeburg PH. Hippocampal synaptic plasticity, spatial memory and anxiety. Nat Rev Neurosci. 2014 Mar;15(3):181-92.

3. Bayda, S.; Adeel, M.; Tuccinardi, T.; Cordani, M.; Rizzolio, F. The History of Nanoscience and Nanotechnology: From Chemical–Physical Applications to Nanomedicine. Molecules 2020, 25, 112.

4. Betz, W. J.; Bewick, G. S. Optical Analysis of Synaptic Vesicle Recycling at the Frog Neuromuscular Junction. Science 1992, 255, 200−203.

5. Biagioni AF, de Oliveira RC, de Oliveira R, da Silva JA, dos Anjos-Garcia T, Roncon CM, Corrado AP, Zangrossi H Jr, Coimbra NC. 5-Hydroxytryptamine 1A receptors in the dorsomedial hypothalamus connected to dorsal raphe nucleus inputs modulate defensive

behaviours and mediate innate fear-induced antinociception. Eur Neuropsychopharmacol. 2016 Mar;26(3):532-45.

6. Borczyk, M., Śliwińska, M.A., Caly, A. et al. Neuronal plasticity affects correlation between the size of dendritic spine and its postsynaptic density. Sci Rep 9, 2019, 1693.

7. Bosch M, Castro J, Saneyoshi T, Matsuno H, Sur M, Hayashi Y. Structural and molecular remodeling of dendritic spine substructures during long-term potentiation. Neuron. 2014 Apr 16; 82(2):444-59.

8. Bramini M, Alberini G, Colombo E, Chiacchiaretta M, DiFrancesco ML, Maya-Vetencourt JF, Maragliano L, Benfenati F, Cesca F. Interfacing Graphene-Based Materials With Neural Cells. Front Syst Neurosci. 2018 Apr 11;12:12.

9. Canteras NS, Pavesi E, Carobrez AP. Olfactory instruction for fear: neural system analysis. Front Neurosci. 2015 Aug 6;9:276.

10. Cellot G, Franceschi Biagioni A, Ballerini L. Nanomedicine and graphene-based materials: advanced technologies for potential treatments of diseases in the developing nervous system. Pediatr Res. 2022 Jul;92(1):71-79.

11. Cellot G, Toma FM, Varley ZK, Laishram J, Villari A, Quintana M, Cipollone S, Prato M, Ballerini L. Carbon nanotube scaffolds tune synaptic strength in cultured neural circuits: novel frontiers in nanomaterial-tissue interactions. J Neurosci. 2011 Sep 7;31(36):12945-53.

12. Cellot G, Vranic S, Shin Y, Worsley R, Rodrigues AF, Bussy C, Casiraghi C, Kostarelos K, McDearmid JR. Graphene oxide nanosheets modulate spinal glutamatergic transmission and modify locomotor behaviour in an *in vivo* zebrafish model. Nanoscale Horiz. 2020 Aug 1;5(8):1250-1263.

13. Chakraborty P, Chattarji S. Timing is everything: differential effects of chronic stress on fear extinction. Psychopharmacology (Berl). 2019 Jan;236(1):73-86.

14. Cormier RJ, Mauk MD, Kelly PT. Glutamate iontophoresis induces long-term potentiation in the absence of evoked presynaptic activity. Neuron. 1993 May;10(5):907-19.

15. Debanne D, Guérineau NC, Gähwiler BH, Thompson SM. Paired-pulse facilitation and depression at unitary synapses in rat hippocampus: quantal fluctuation affects subsequent release. J Physiol. 1996 Feb 15;491 (Pt 1)(Pt 1):163-76.

16. Dielenberg RA, Hunt GE, McGregor IS. "When a rat smells a cat": the distribution of Fos immunoreactivity in rat brain following exposure to a predatory odor. Neuroscience. 2001;104(4):1085-97.

17. Drexler, E.K.; Peterson, C.; Pergamit, G. Unbounding the Future: The Nanotechnology Revolution; William Morrow and Company, Inc.: New York, NY, USA, 1991.

18. Feng L, Wu L, Qu X. New horizons for diagnostics and therapeutic applications of graphene and graphene oxide. Adv Mater. 2013 Jan 11;25(2):168-86.

19. Franceschi Biagioni A, Cellot G, Pati E, Lozano N, Ballesteros B, Casani R, Coimbra NC, Kostarelos K, Ballerini L. Graphene oxide prevents lateral amygdala dysfunctional synaptic plasticity and reverts long lasting anxiety behavior in rats. Biomaterials. 2021 Apr;271:120749.

20. Gaffield MA, Betz WJ. Imaging synaptic vesicle exocytosis and endocytosis with FM dyes. Nat Protoc. 2006;1(6):2916-21.

21. Garcia-Etxarri A, Yuste R. Time for NanoNeuro. Nat Methods. 2021 Nov;18(11):1287-1293.

22. Gasparini S, Saviane C, Voronin LL, Cherubini E. Silent synapses in the developing hippocampus: lack of functional AMPA receptors or low probability of glutamate release? Proc Natl Acad Sci U S A. 2000 Aug 15;97(17):9741-6.

23. Geim AK, Novoselov KS. The rise of graphene. Nat Mater. 2007 Mar;6(3):183-91.

24. Guanghui Yang, Juanjuan Su, Jian Gao, Xin Hu, Chengzhen Geng, Qiang Fu, Fabrication of well-controlled porous foams of graphene oxide modified poly(propylene-carbonate) using supercritical carbon dioxide and its potential tissue engineering applications, The Journal of Supercritical Fluids, 2013, Volume 73

25. Huang YY, Kandel ER. Postsynaptic induction and PKA-dependent expression of LTP in the lateral amygdala. Neuron. 1998 Jul;21(1):169-78.

26. Humeau Y, Herry C, Kemp N, Shaban H, Fourcaudot E, Bissière S, Lüthi A. Dendritic spine heterogeneity determines afferent-specific Hebbian plasticity in the amygdala. Neuron. 2005 Jan 6;45(1):119-31.

27. Humeau Y, Shaban H, Bissière S, Lüthi A. Presynaptic induction of heterosynaptic associative plasticity in the mammalian brain. Nature. 2003 Dec 18;426(6968):841-5.

28. Khazipov R, Zaynutdinova D, Ogievetsky E, Valeeva G, Mitrukhina O, Manent JB, Represa A. Atlas of the Postnatal Rat Brain in Stereotaxic Coordinates. Front Neuroanat. 2015 Dec 23;9:161.

29. Khazipov R, Zaynutdinova D, Ogievetsky E, Valeeva G, Mitrukhina O, Manent JB, Represa A. Atlas of the Postnatal Rat Brain in Stereotaxic Coordinates. Front Neuroanat. 2015 Dec 23;9:161.

30. Kostarelos K, Vincent M, Hebert C, Garrido JA. Graphene in the Design and Engineering of Next-Generation Neural Interfaces. Adv Mater. 2017 Nov;29(42).

31. le Feber J. *In Vitro* Models of Brain Disorders. Adv Neurobiol. 2019; 22:19-49.

32. Louth EL, Sutton CD, Mendell AL, MacLusky NJ, Bailey CDC. Imaging Neurons within Thick Brain Sections Using the Golgi-Cox Method. J Vis Exp. 2017 Apr 18;(122):55358.

33. Malgaroli A, Tsien RW. Glutamate-induced long-term potentiation of the frequency of miniature synaptic currents in cultured hippocampal neurons. Nature. 1992 May 14;357(6374):134-9.

34. Manabe, T.; Wyllie, D. J.; Perkel, D. J.; Nicoll, R. A. Modulation of synaptic transmission and long-term potentiation: effects on paired pulse facilitation and EPSC variance in the CA1 region of the hippocampus. J. Neurophysiol. 1993, 70, 1451−9.

35. Maren S. Synaptic mechanisms of associative memory in the amygdala. Neuron. 2005 Sep 15;47(6):783-6.

36. McKernan MG, Shinnick-Gallagher P. Fear conditioning induces a lasting potentiation of synaptic currents *in vitro*. Nature. 1997 Dec 11; 390(6660):607-11.

37. McLeod F, Marzo A, Podpolny M, Galli S, Salinas P. Evaluation of Synapse Density in Hippocampal Rodent Brain Slices. J Vis Exp. 2017 Oct 6;(128):56153.

38. Mitra R, Adamec R, Sapolsky R. Resilience against predator stress and dendritic morphology of amygdala neurons. Behav Brain Res. 2009 Dec 28;205(2):535-43.

39. Muñoz-Abellán C, Daviu N, Rabasa C, Nadal R, Armario A. Cat odor causes long-lasting contextual fear conditioning and increased pituitary-adrenal activation, without modifying anxiety. Horm Behav. 2009 Oct;56(4):465-71.

40. Murthy, V. N.; Sejnowski, T. J.; Stevens, C. F. Heterogeneous release properties of visualized individual hippocampal synapses. Neuron 1997, 18, 599−612.

41. N.C. Coimbra, T. Paschoalin-Maurin, G.S. Bassi, A. Kanashiro, A.F. Biagioni, T. T. Felippotti, D.H. Elias-Filho, J. Mendes-Gomes, J.P. Cysne-Coimbra, R.C. Almada, B. Lob˜ao-Soares, Rev. Bras. Psiquiatr. 39. 2017, 72–83.

42. Pacella ML, Hruska B, Delahanty DL. The physical health consequences of PTSD and PTSD symptoms: a meta-analytic review. J Anxiety Disord. 2013 Jan;27(1):33-46.

43. Pampaloni NP, Lottner M, Giugliano M, Matruglio A, D'Amico F, Prato M, Garrido JA, Ballerini L, Scaini D. Single-layer graphene modulates neuronal communication and augments membrane ion currents. Nat Nanotechnol. 2018 Aug;13(8):755-764.

44. Parsons MP, Raymond LA. Extrasynaptic NMDA receptor involvement in central nervous system disorders. Neuron. 2014 Apr 16;82(2):279-93.

45. Pavlidis P, Montgomery J, Madison DV. Presynaptic protein kinase activity supports long-term potentiation at synapses between individual hippocampal neurons. J Neurosci. 2000 Jun 15;20(12):4497-505.

46. Rainnie DG, Asprodini EK, Shinnick-Gallagher P. Intracellular recordings from morphologically identified neurons of the basolateral amygdala. J Neurophysiol. 1993 Apr;69(4):1350-62.

47. Rauti R, Lozano N, León V, Scaini D, Musto M, Rago I, Ulloa Severino FP, Fabbro A, Casalis L, Vázquez E, Kostarelos K, Prato M, Ballerini L. Graphene Oxide Nanosheets Reshape Synaptic Function in Cultured Brain Networks. ACS Nano. 2016 Apr 26;10(4):4459-71.

48. Rauti R, Medelin M, Newman L, Vranic S, Reina G, Bianco A, Prato M, Kostarelos K, Ballerini L. Graphene Oxide Flakes Tune Excitatory Neurotransmission *in Vivo* by Targeting Hippocampal Synapses. Nano Lett. 2019 May 8;19(5):2858-2870.

49. Richter-Levin G, Stork O, Schmidt MV. Animal models of PTSD: a challenge to be met. Mol Psychiatry. 2019 Aug; 24(8):1135-1156.

50. Risher WC, Ustunkaya T, Singh Alvarado J, Eroglu C. Rapid Golgi analysis method for efficient and unbiased classification of dendritic spines. PLoS One. 2014 Sep 10;9(9):e107591.

51. Rosenkranz JA, Venheim ER, Padival M. Chronic stress causes amygdala hyperexcitability in rodents. Biol Psychiatry. 2010 Jun 15;67(12):1128-36.

52. Rumpel S, LeDoux J, Zador A, Malinow R. Postsynaptic receptor trafficking underlying a form of associative learning. Science. 2005 Apr 1;308(5718):83-8.

53. Ryan, T. A.; Reuter, H.; Wendland, B.; Schweizer, F. E.; Tsien, R. W.; Smith, S. J. The Kinetics of Synaptic Vesicle Recycling Measured at Single Presynaptic Boutons. Neuron 1993, 11, 713−724.

54. Secomandi N, Franceschi Biagioni A, Kostarelos K, Cellot G, Ballerini L. Thin graphene oxide nanoflakes modulate glutamatergic synapses in the amygdala cultured circuits: Exploiting synaptic approaches to anxiety disorders. Nanomedicine. 2020 Jun;26:102174.

55. Shin LM, Liberzon I. The neurocircuitry of fear, stress, and anxiety disorders. Neuropsychopharmacology. 2010 Jan;35(1):169-91.

56. Somerville LH, Kim H, Johnstone T, Alexander AL, Whalen PJ. Human amygdala responses during presentation of happy and neutral faces: correlations with state anxiety. Biol Psychiatry. 2004 May 1;55(9):897-903.

57. Tejada J., Chaim K. T., Morato S. X-PloRat: a software for scoring animal behavior in enclosed spaces. Psicol. Teor. Pesqui. 2018, 33:e3322.

58. Tsvetkov E, Carlezon WA, Benes FM, Kandel ER, Bolshakov VY. Fear conditioning occludes LTP-induced presynaptic enhancement of synaptic transmission in the cortical pathway to the lateral amygdala. Neuron. 2002 Apr 11;34(2):289-300

59. Uteshev VV, Pennefather PS. A mathematical description of miniature postsynaptic current generation at central nervous system synapses. Biophys J. 1996 Sep;71(3):1256-66.

60. Wu YE, Pan L, Zuo Y, Li X, Hong W. Detecting Activated Cell Populations Using Single-Cell RNA-Seq. Neuron. 2017 Oct 11;96(2):313-329.e6.

61. Yoo KS, Lee K, Oh JY, Lee H, Park H, Park YS, Kim HK. Postsynaptic density protein 95 (PSD-95) is transported by KIF5 to dendritic regions. Mol Brain. 2019 Nov 21;12(1):97.

62. Zakharenko SS, Zablow L, Siegelbaum SA. Visualization of changes in presynaptic function during long-term synaptic plasticity. Nat Neurosci. 2001 Jul;4(7):711-7.

63. Zucker, R. S. Short-term synaptic plasticity. Annu. Rev. Neurosci. 1989, 12, 13−31.

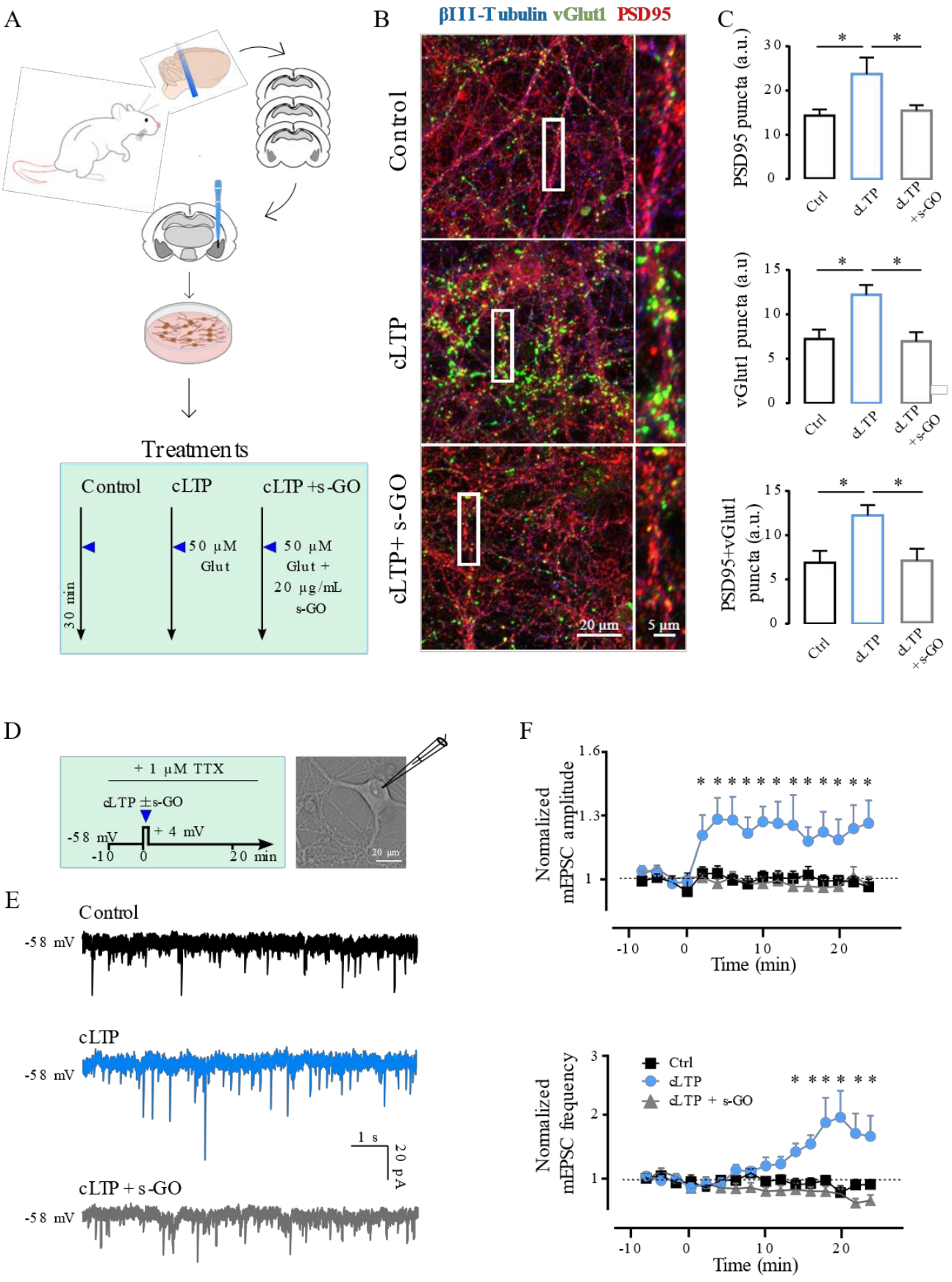

Figure 1. *s-GO rescues cLTP-related structural modifications in the amygdala culture.* (A) Schematic representation of the experimental setting. Dissociated amygdalar cultures were

obtained from juvenile rats: from brain slices the amygdala nuclei are precisely isolated with a biopsy punch and then enzymatically dissociated to obtain neuronal cultures. These were exposed to treatments with saline (control), glutamate (cLTP) or glutamate + s-GO (cLTP + s-GO). (B) Confocal images of neuronal cultures in control, cLTP and cLTP + s-GO labelled for VGlut1 (in green) and PSD95 (in red) and β -tubulin III (blue). Higher magnifications of the region in the white rectangles are reported on the right. (C) Histograms summarizing PSD95, VGlut1 and PSD95 + VGlut1 puncta densities in the three conditions. (D) Experimental protocol (left) for single-cell voltage clamp recordings (right, bright field image). (E) Exemplificative traces of mPSC detected 20 min after the 30 s long-lasting application of saline (saline, in black), glutamate (cLTP, in blue) or glutamate + s-GO (cLTP + s-GO, in grey). (F) Plots showing that s-GO treatment blocked the 24 min long lasting increase in mEPSC amplitude (top), and frequency (bottom) observed in neurons undergone to the LTP induction. *$P < 0.05$

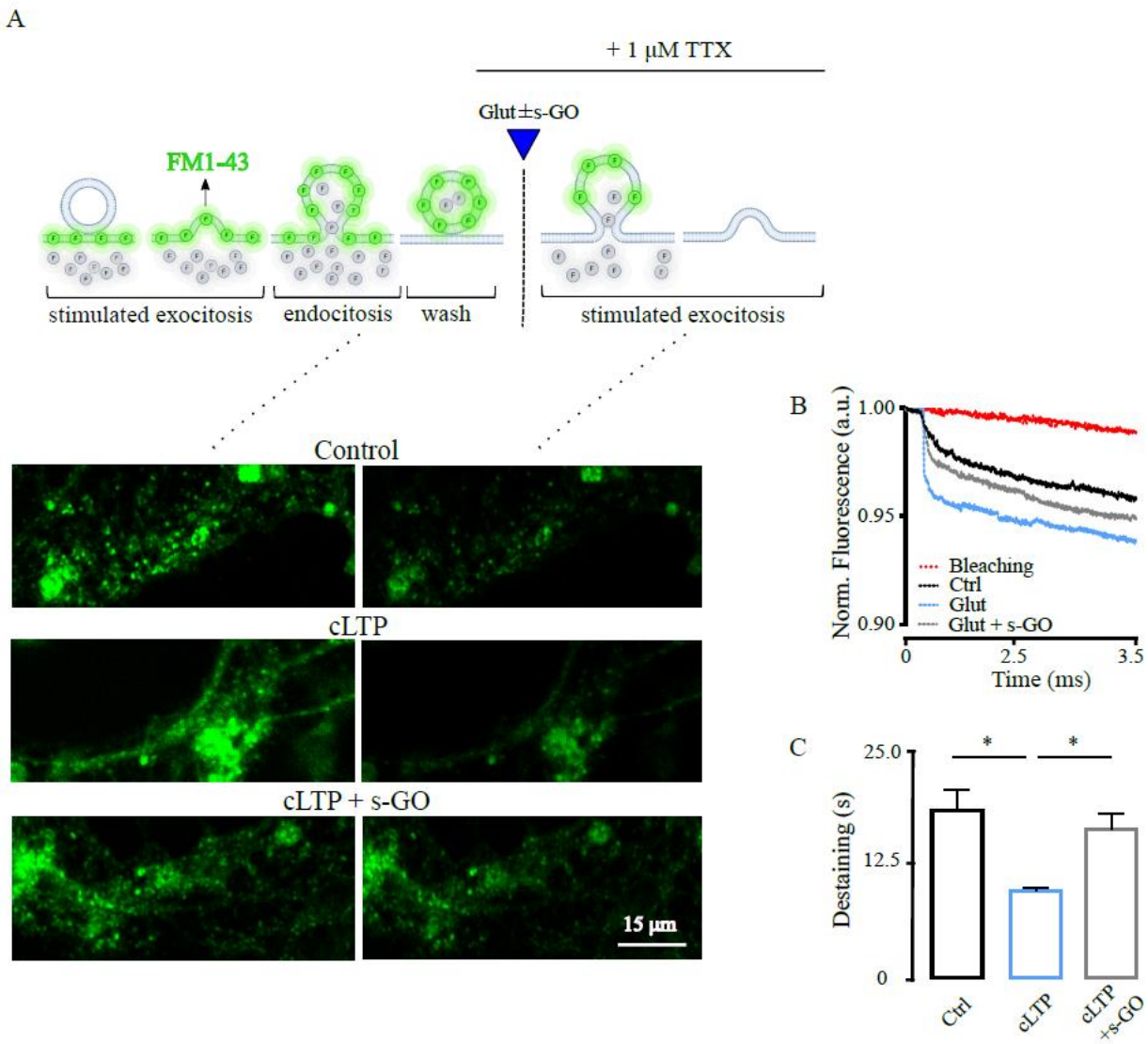

Figure 2. *s-GO affects the presynaptic vesicle release from amygdala neurons.* (A) Sketch of the experimental setting (top) of sequential FM1–43 staining and destaining (bottom): fluorescence images show the extensive neurite staining with FM1–43 (right) followed by 50 KCl-induced destaining (left) in control, cLTP and cLTP + s-GO amygdala samples. (B) Representative traces of fluorescence decrease following KCl stimulation in control (black line), cLTP (blue line) and cLTP + s-GO (grey line). In red the fluorescence bleaching after KCl stimulation. Note that each trace has been normalized to the maximum fluorescence detected. (C) The histogram summarizes the decay time constant (τ) of FM1-43 destaining in the three conditions. *P < 0.05

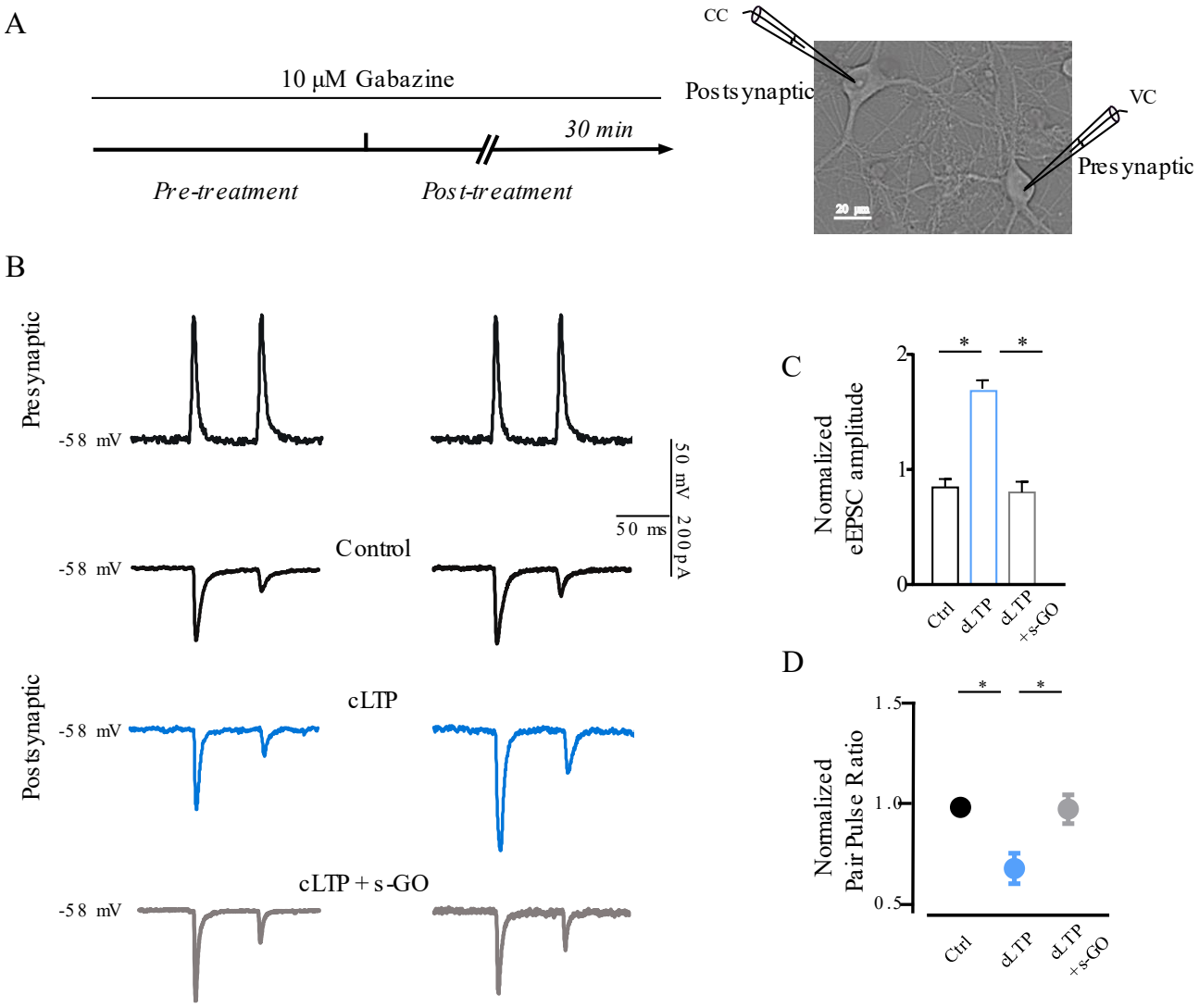

Figure 3. *s-GO reduces the probability of glutamate release in potentiated amygdala excitatory neurons.* (A) Schematic representation of the experimental procedure (right) of simultaneous recordings from two monosynaptically connected amygdala neurons (left, bright field image). (B) Recordings from neurons undergone to different treatments. Top traces represent presynaptic action potentials while bottom ones represent the corresponding eEPSC prior (left) and 24 min after (right) treatment with saline (control, black traces), glutamate (cLTP, blue traces) or glutamate + s-GO (cLTP + s-GO, grey traces). Note that s-GO rescued the increased short-term depression of consecutive eEPSC observed in neurons undergone to cLTP induction protocol. (C-D) Plots summarize the normalized amplitude of first eEPSC (C) and the normalized paired-pulse ratio (D) measured 24 min after treatment with saline (control), glutamate (cLTP) or glutamate + s-GO (cLTP + s-GO). *P < 0.05

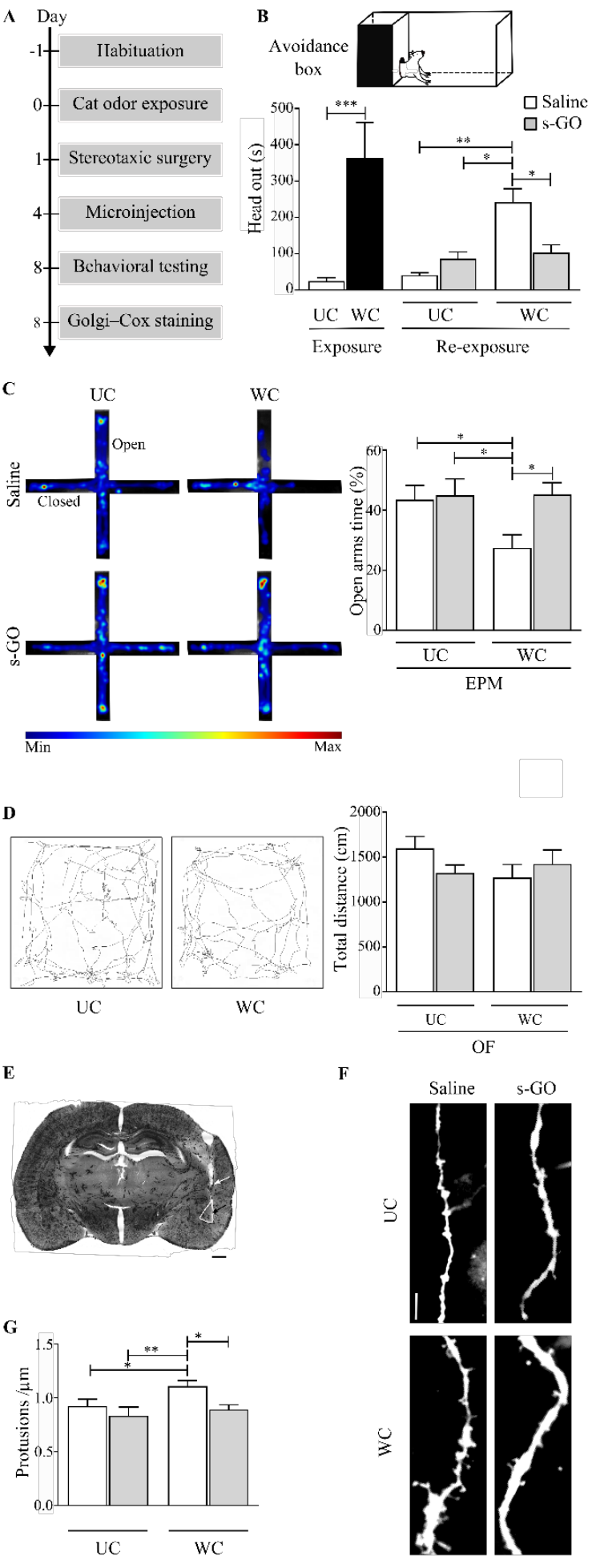

Figure 4. *Memory consolidation impairment caused by s-GO injected into LA.* (A) Schematic representation of the experimental timeline and behavioural testing. (B) On the top, representative image of avoidance box showing the head out behaviour; Bar plot (bottom) summarizing the head out behavioural responses evoked by the exposure to UC or WC and by the re-exposure to the context after s-GO or saline microinjections into the LA. (C) On the left, cumulative heat maps of the time spent in the arms of the EPM by UC and WC group treated with s-GO or saline; on the right, bar plot showing the time spent in the open arms of EPM apparatus in UC and WC group treated with s-GO or saline. (D) On the left, illustration of two representative sample tracks from a UC (left) and WC (right) group recorded during the OF test; on the right, bar plot reporting the total distance travelled in the OF apparatus in UC and WC treated with s-GO or saline. N = 6 for each group. (E) On the top left,

photomicrographs of a Golgi-Cox-impregnated coronal section with a representative cannula placement directed to LA. The white head arrow indicates the end of the guide cannula, and the black head arrow indicates the tip of the microinjection needle. (F) Representative dendritic segments of LA neurons in UC and WC rats treated with s-GO or saline. Scale bar 1 mm and 5 µm. (G) Bar plot shows the mean number of spines detected within 40 µm segment of LA dendrites in UC and WC rats. N=4 per group, N=12 neurons per group. ***p < 0.001; **p < 0.01; *p < 0.05.

SUPPLEMENTARY FIGURES

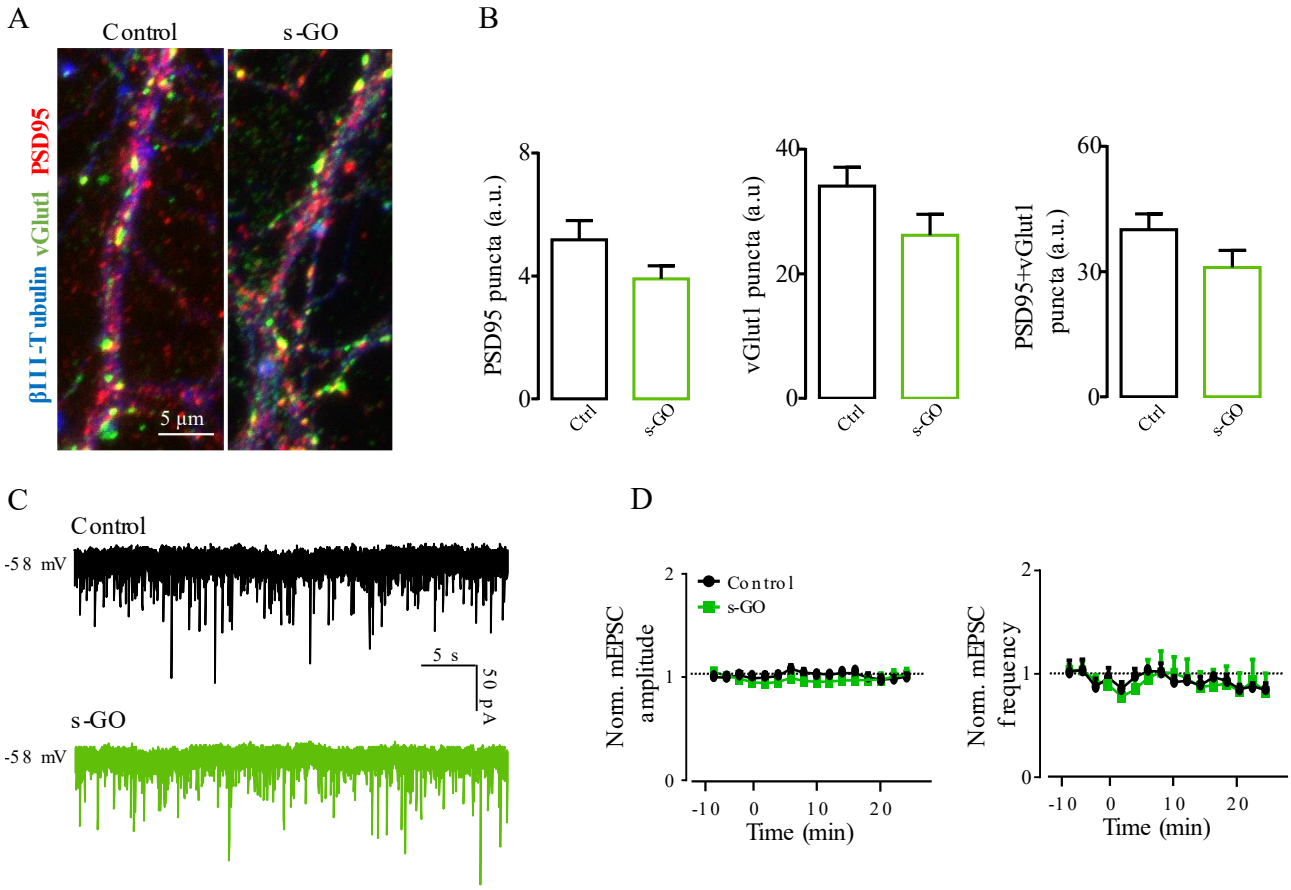

Supplementary Figure 1. *s-GO does not alter the structure of the amygdala synapses in control conditions.* (A) Confocal images of β-tubulin III positive (in blue) amygdala neurites co-labelled with the presynaptic (Vglut1, in green) and the postsynaptic (PSD95, in red) neuronal markers, in the absence (right) or presence of s-GO (left). (B) Bar plot summarizing the lack of difference in the density of PSD95 puncta (5.2 ± 0.6 a.u. in control and 3.9 ± 0.4 a.u. in s-GO-treated samples,

n= 15 fields, 3 cultures each; p = 0.102), VGlut1 puncta (34.1 ± 3.0 a.u. in control and 26.2 ± 3.3 a.u. in s-GO-treated samples, n= 15 fields, 3 cultures each; p = 0.09), and PSD95 + VGlut1 co-localization puncta (40.1 ± 3.8 a.u. in control and 31.0 ± 4.1 a.u. in s-GO-treated samples, n= 15 fields, 3 cultures each; p = 0.114) with or without nanomaterial. (C) Representative traces of mPSC recorded from amygdala cells 24 min after the treatment with saline (black trace) or 20 µg/mL s-GO (green trace). (D) Plots of the normalized mEPSC amplitude (right, 0.98 ± 0.03 in controls, n = 7, and 0.99 ± 0.06 in s-GO-treated cells, n = 8; p =0.920, 24 min) and frequency (left, 0.88 ± 0.04 in controls, n =7, and 0.87 ± 0.18 in s-GO-treated cells, n = 8; p = 0.903, 24 min) showing no effect upon 30 s long lasting s-GO treatment.

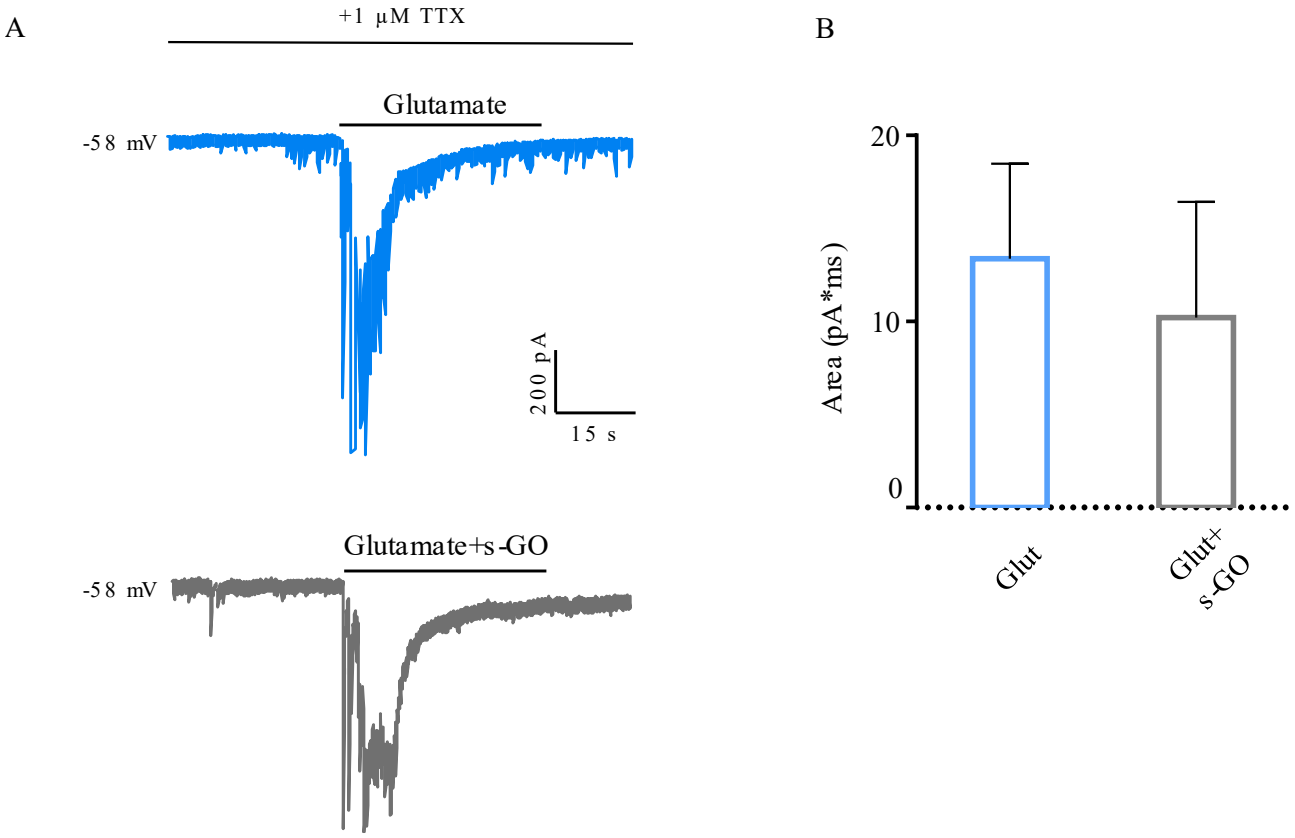

Supplementary Figure 2. *s-GO does not affect either the activity of postsynaptic glutamatergic receptors or the exogenously applied glutamate.* (A) The application of 50 µM glutamate activated glutamatergic receptor-mediated inward currents, independently from the presence of s-GO. (C) Bar plot illustrating a similar area of the glutamate-induced inward current with or without s-GO (13.36 ± 5.10 pA*ms in glutamate-treated samples, n =12, and 10.20 ± 6.21 in glutamate + s-GO-treated cells, n = 10; p > 0.05).

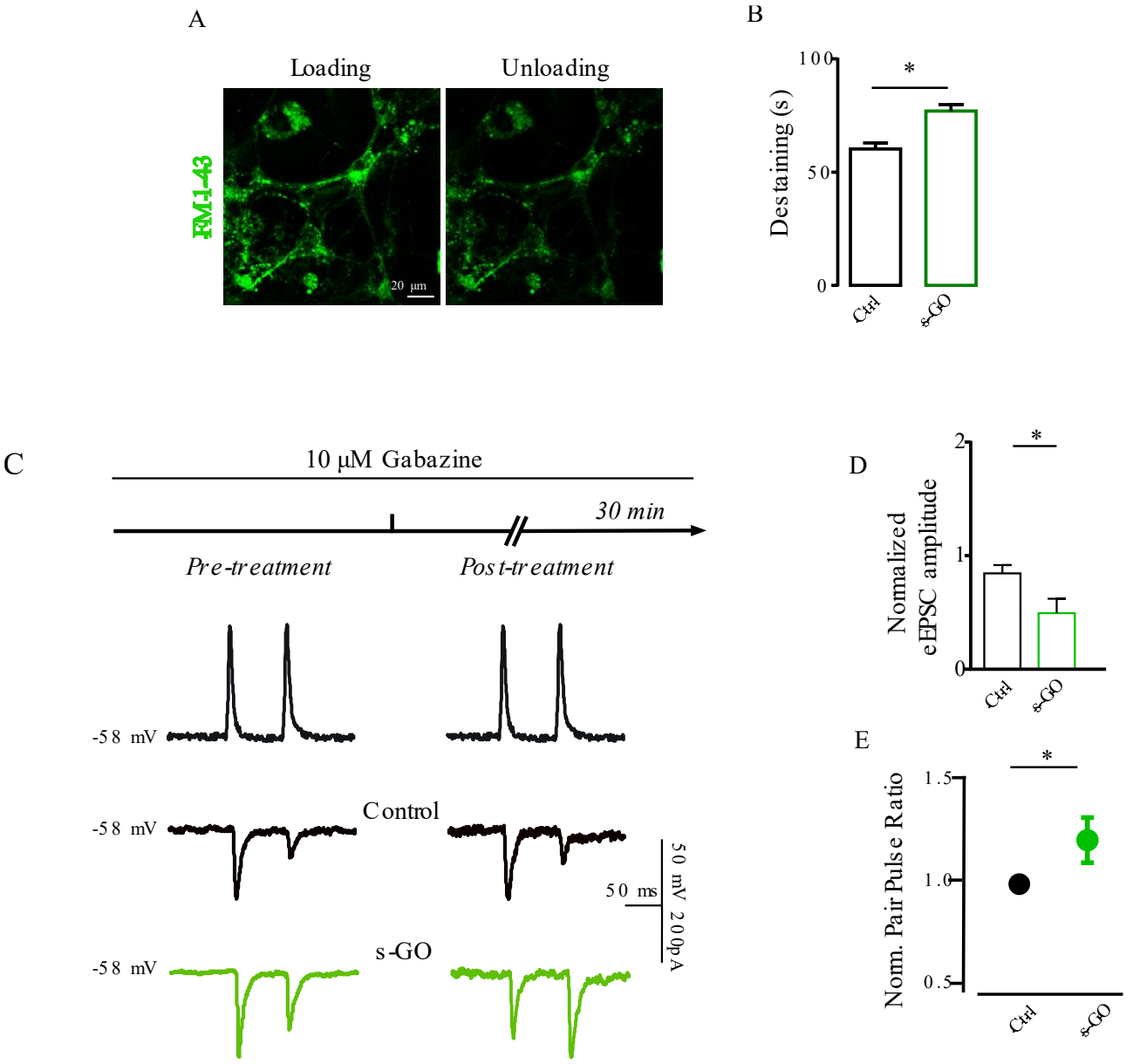

Supplementary Figure 3. *By interfering presynaptically, the application of s-GO to control culture affects the dynamics of vesicle release from amygdala excitatory neurons.* (A) Fluorescence images of the amygdala cells during FM1-43 loading (right) and unloading (left) of presynaptic vesicles. (B) The histogram summarizes the decay time constant (τ) of FM1-43 destaining in the presence of absence of the nanomaterial. To note the increment in the rate of synaptic release from synaptic terminals following KCl stimulation upon s-GO application (expressed as τ, that was 60.27 ± 2.66 s in control, n=80 terminals, and 76.95 ± 2.87 s in s-GO, n=80 terminals, $p < 0.0001$). (C) Sketch of the experimental procedure (top) and representative traces of simultaneous pair recordings (bottom). In the first row, presynaptic action potentials and below the corresponding monosynaptic eEPSC, prior (left) and 24 min after (right) treatment with

saline (control, black traces) or 20 ug/mL s-GO (s-GO, green traces). (D-E) Plots showing as the application of s-GO to control neurons induced a decrement in the post-treatment eEPSC amplitude (normalized eEPSC amplitude was 0.49 ± 0.12 for s-GO, n=6 pairs; 0.84 ± 0.07 for control, n=6 pairs; p= 0.0263;D), as well as a change in the short-term plasticity behaviour of consecutive eEPSC from depression to facilitation (at 24 min post treatment, normalized PPR was 0.99 ± 0.02 for control and 1.5 ± 0.2 for s-GO, n = 6 pairs, n = 6 pairs p = 0.002; E). *P < 0.05

Nano-formulated neuropeptide Y adsorbed on small-graphene oxide nanoflakes prevents abnormal amygdala plasticity and associated anxiety-related behaviour.

Elisa Pati[1], Audrey Franceschi Biagioni[1], Raffaele Casani[1], Neus Lozano[2], Giada Cellot[1], Kostas Kostarelos[2,3], Laura Ballerini[1*]*

[1]International School for Advanced Studies (SISSA/ISAS), 34136 Trieste, Italy

[2]Catalan Institute of Nanoscience and Nanotechnology (ICN2), 08193, Barcelona, Spain

[3]Nanomedicine Lab, and Faculty of Biology, Medicine & Health, The National Graphene Institute, University of Manchester, Manchester, M13 9PL, United Kingdom

ABSTRACT

Graphene-based nanomaterials (GBNs) are a heterogeneous family of materials differing for lateral dimension, surface area and composition. Among these, thanks to its chemistry and its good biocompatibility, graphene oxide with small lateral dimension (s-GO) has been proposed as an ideal core structure to carry bioactive molecules, to develop novel nano-based drug delivery systems. Recently, neuropeptide Y (NPY), an endogenous modulator of neuronal transmission, has shown potential as therapeutic for the treatment of anxiety diseases, although its short-lived peptidic nature rose questions on its translation into therapy. Here, we developed and tested the impact of a nano-formulation in which NPY was adsorbed onto s-GO (s-GO:NPY) on *in vitro* and *in vivo* models of anxiety disorders. By performing electrophysiological recordings during acute or sub-acute applications of s-GO:NPY, we found that both the nanomaterial and the peptide retained their bioactivity on synapses once complexed together. In addition, the NPY complexed to s-GO could prevent long term potentiation (LTP) of amygdala synapses similarly to the free NPY. According to this, when injected in the lateral amygdala (LA) of a rat model of post-

traumatic stress disorder (PTSD), s-GO:NPY and NPY exerted comparable effects impairing the contextual fear memory in a long-term manner. This work supports a future use of s-GO as a smart platform for nanomaterial-based drug delivery for the treatment of central nervous system (CNS) pathologies.

INTRODUCTION

The nanoscale dimension of GBNs which is equivalent to that of the subcellular elements of neuronal tissue (i.e., dendritic spines or synaptic vesicles; Zhang B. et al., 1998; Smith K.R. et al., 2014; Pchitskaya E. et al., 2020), makes them excellent tools for the development of neuroscience applications in biomedicine (Xia X., 2008; Silva G.A., 2006; Kitko E.Z. et al., 2019). In this regard, their unique chemo-physical properties (Geim A.K. 2009; Kostarelos K, Novoselov KS, 2020; Sanchez V.C. et al., 2012) have been exploited in the field of drug delivery for higher selective targeting. Among these GBNs, s-GO represents an ideal candidate for targeted drug delivery in the CNS, because of its chemistry, favouring the adsorption of bioactive molecules on its surface (Pinto A.V. et al., 2022), together with its good biocompatibility (Mousavi S.M. et al., 2019). In addition, this nanomaterial has been reported to target specifically glutamatergic synapses, by tuning neuronal activity (Rauti R. et al., 2016; Rauti R. et al., 2019; Cellot G. et al., 2020; Franceschi B.A. et al, 2021), ability that might be exploited to design a drug delivery system in which the carrier shows active properties on neuronal function *per se*.

In order to validate s-GO as a drug nanocarrier for the treatment of brain neuropathologies, it is essential to characterize the activity of the drug delivery system when applied to neurons. By using a nanoformulation in which NPY, an endogenous modulator of neuronal transmission (Colmers W.F. et al., 1988; Klapstein G.J. et al., 1993; Bacci A. et al., 2002) recently proposed as therapeutic for anxiety disorders (Kautz et al., 2017), was adsorbed onto s-GO, we tried to address the following issues:

(i) if NPY and the nanomaterial were still bioactive once complexed together,

(ii) if the pharmacokinetic properties of NPY (transient effect due to short half-life) were modified by the complexation with s-GO,

(iii) if the complex could inhibit long term synaptic potentiation of amygdala cultures, which models *in vitro* synaptic alterations observed in anxiety disorders, and

(iv) if the complex, once injected *in vivo* in the lateral amygdala of a rat model of PTSD could ameliorate anxiety-related behaviours.

By combining electrophysiological recordings from *in vitro* neuronal networks with behavioural experiments in PTSD rat model, we found that both s-GO and NPY were still bioactive when complexed together in the nanoformulation. In addition, we proved that NPY effect on excitatory synapses was prolonged by the complexation with s-GO. When the nanoformulation was used in dissociated amygdala cultures artificially potentiated through a procedure of chemical LTP (cLTP), s-GO:NPY prevented functional changes related to synaptic potentiation similarly to uncomplexed NPY. These results were recapitulated in *in vivo* experiments, where NPY and s-GO:NPY affected contextual fear memory in a comparable manner in the PTSD model.

RESULTS

1. Both NPY and s-GO retain their pharmacological activity when complexed together

Before evaluating s-GO:NPY complex as an alternative nanocarrier to deliver drugs in PTSD models, we characterized the pharmacological responses of the nanoformulation on dissociated hippocampal cultures, to understand if s-GO and NPY were still bioactive when complexed together. We used this *in vitro* preparation since it represents our validated standard model for testing the impact of nanomaterials on neuronal function (Rauti R. et al., 2016; Rauti R. et al., 2019; Di Mauro G. et al., 2021).

We firstly verified whether NPY was still able to exert its pharmacological activity modulating synaptic currents once adsorbed to s-GO nanoplatform. To this aim, we systematically compared the biological activity s-GO (10 μg/mL), NPY (1 μM) and s-GO:NPY (10 μg/mL and 1 μM, respectively) through their sub-acute applications (5 min) during the recording of spontaneous postsynaptic currents (sPSC) of neurons (Fig. 1A). We chose the 5-min application as such exposure time was compatible with the activation of NPY receptors (Colmers W.F. et al., 1988a; Acuna-Goycolea C. et al., 2005; Qian J. et al., 1997). Representative traces in figure 1B show that both NPY (in green) and s-GO:NPY (in orange) applications caused respect to controls (in black) and s-GO (in grey) a progressive and significant decrement in the frequency of sPSC during the late phase of application (3.5-7 min), with a complete upon prolonged washout (7-12 min). In details, during the initial application phase (0-3.5 min), sPSC frequencies normalized for baselines values were similar between the different treatments (0.96 ± 0.06 in control, n= 18, 0.85

± 0.10 in s-GO, n=11, 0.93 ± 0.13 in s-GO-NPY, n=14 and 0.93 ± 0.08 in NPY, n=9). Normalized sPSC frequencies started to decrease ≥ 5 min NPY (free or complexed) application and remained low for the next ~3 min of washout (0.98 ± 0.07 in control, 0.81 ± 0.08 in s-GO, 0.67 ± 0.07 in s-GO-NPY and 0.5 ± 0.09 in NPY). Finally, they recovered completely 7 minutes after the beginning of application (0.90 ± 0.07 in control, 1.1 ± 0.11 in s-GO, 0.90 ± 0.11 in s-GO-NPY and 0.86 ± 0.08 in NPY, fig. 1C).

In the late phase of application (3.5-7 min), the differences were statistically significant for the control vs s-GO-NPY (p=0.045) and for the control vs NPY (p=0.007), while p was >0.05 for s-GO-NPY vs NPY and saline vs s-GO (Fig. 1B-C). No changes were observed in normalized sPSC amplitudes (during the 0-3.5 min post-application: 0.92 ± 0.07 in control, 0.86 ± 0.08 in s-GO, 0.91 ± 0.11 in s-GO:NPY and 0.94 ± 0.09 in NPY; during 3.5-7 min post application 0.83 ± 0.07 in control, 0.83 ± 0.12 in s-GO, 0.95 ± 0.07 in s-GO:NPY and 0.76 ± 0.08 in NPY; P values >0.05).

These data suggested that NPY maintained its pharmacological activity once complexed to s-GO, thus reducing neuronal activity as free NPY. It was not surprising that uncomplexed s-GO did not produce changes in neuronal activity through this type of administration, as nanomaterial induced synaptic depression in hippocampal neurons requires longer incubation time (Rauti R. et al., 2019).

Next, we evaluated whether s-GO complexed to the bioactive NPY retained the biological activity on synapses observed for the nanomaterial alone (Rauti R. et al., 2019; Secomandi N. et al., 2020). We exposed voltage-clamped hippocampal neurons to acute (500 ms) pressure ejections (puffs) of s-GO, s-GO:NPY or saline solution, used as control, positioning a second pipette close to the recorded neuron (sketched in Fig. 1D; see the Materials and Methods; Rauti R. et al., 2019; Secomandi N. et al., 2020). In this type of acute application, the nanomaterial has been reported to exert a transient increment of the sPSC frequency, as consequence of s-GO/synapse interference (Rauti R. et al., 2019). In addition, puff duration was too brief to allow NPY modulation of neuronal activity (Colmers W.F. et al., 1988a; Acuna-Goycolea C. et al., 2005; Qian J. et al., 1997), allowing to dissect in the complex the contribution of the nanomaterial in modulating synaptic activity. We applied puffs of saline solution, uncomplexed s-GO (100 μg/mL) or s-GO:NPY complex (100 μg/mL of nanomaterial with 10 μM of peptide). This higher concentration was selected considering a 10% dilution in the volume of recording solution (Rauti R. et al., 2019).

The traces reported in figure 1E demonstrate as s-GO, even in the complex formulation (in orange) was still able to tune the neuronal activity after the puff ejection, similarly to the uncomplexed condition (in grey), while samples exposed to saline (in black) did not present any changes. Although the number of experiments has to be increased to make statistical analysis, we observed as the s-GO, alone or complexed to NPY, induced an increment in the post-puff frequencies of sPSC normalized for the baseline pre-puff values (0.90 ± 0.25 for control, n=4, 1.45 ± 0.12 for s-GO n=4, 1.43 ± 0.37 for s-GO:NPY, n=4; fig. 1F). No variations were observed in normalized post-puff sPSC amplitude upon all different treatments (0.78 ± 0.16 for control, 0.86 ± 0.17 for s-GO, 0.75 ± 0.15 for s-GO:NPY, P>0.05). These experiments strongly suggested that s-GO complexed to NPY did not lose its ability to regulate synaptic function.

In addition, we performed electrophysiological recordings to assess if the observed modulation of neuronal activity induced by s-GO:NPY was effectively due to the activation of NPY receptors and not to an unspecific effect of the complex. As illustrated in Supplementary Figure 1A, during the recording of the spontaneous synaptic activity we sub-acutely applied NPY both in the complex formulation (orange traces, left) or alone (green traces, right), in the absence (top traces) or presence (bottom traces) of Y1 and Y2 receptor antagonists (BIBO3304 and BIIE0246, respectively, 30 nM each; Vollmer L.L. et al., 2016; Colmers W.F. et al., 2003). As for NPY, no synaptic depression was observed upon application of s-GO:NPY in the presence of the antagonists, confirming that in this type of application the complex exerted its bioactivity through the activation of NPY receptors.

Considered that our goal was to evaluate the potential use of the complex in anxiety diseases that rely on pathologically increased glutamatergic signaling (Masneuf S. et al., 2014), we focused on the effects of NPY and s-GO:NPY on excitatory synapses. To this aim, after pharmacological isolation of excitatory postsynaptic currents (EPSC) with gabazine (10 μM, $GABA_A$ receptor-blocker), we characterized them before and after the sub-acute applications of s-GO:NPY and NPY (Supplementary Figure 1B-C). Since we did not observe any effect of s-GO on synaptic function during sub-acute application (Fig. 1B-C), we did not test s-GO in this set of experiments.

We found that normalized EPSC frequencies were similarly affected by NPY and s-GO:NPY, showing a statistically significant decrement compared to control (saline) during the late phase of application (3.5-7 min, 0.89 ± 0.05 in control, 0.44 ± 0.10 in s-GO:NPY and 0.4 ± 0.06 in NPY, p=0.015 control vs s-GO:NPY and p=0.008 control vs NPY; Supplementary Fig.

1B-C). Notably, upon s-GO:NPY application, the normalized EPSC frequency continued to be depressed even during the recovery period (7-12 min) compared to saline (0.94 ± 0.06 in control, 0.55 ± 0.07 in s-GO:NPY and 0.7 ± 0.09 in NPY, p=0.025 control vs s-GO:NPY; Supplementary Fig. 1B-C). No changes were observed in normalized EPSC amplitudes: during the 0-3.5 min post-application, these were 1.21 ± 0.10 in control, 1.07 ± 0.07 in s-GO:NPY and 1.02 ± 0.1 in NPY; during 3.5-7 min post application, 1.12 ± 0.11 in control, 0.81 ± 0.1 in s-GO:NPY and 0.98 ± 0.12 in NPY; during 7-12 min post application, 1.0 ± 0.14 in control, 0.8 ± 0.11 in s-GO:NPY and 0.97 ± 0.16 in NPY, P values >0.05). These results suggested that the adsorption of NPY onto the nanomaterial could enhance the duration of NPY pharmacological activity.

All together, these experiments indicated that both s-GO and NPY were still bioactive in the complex and that the complexed NPY modulated neuronal activity via activation of its receptors, with a specific and prolonged effect on excitatory synapses.

2. s-GO:NPY complex is able to prevent the synaptic potentiation of amygdala neurons

Since this drug delivery system was thought to be applied in pathological conditions, our next experiments were focused on investigating the potential of the complex in hampering an altered synaptic plasticity, characteristic of anxiety disorders. To this aim, our next set of experiments were performed on an *in vitro* model of artificially potentiated amygdala cultures, mimicking the hyperactivity observed in the amygdala of subjects affected by PTSD. Our previous study showed that the cLTP induction of these cultures by a brief exposure (30 s) to glutamate (50 μM) induced a long-lasting increase in spontaneous EPSC amplitude, while the co-application of s-GO (20 μg/mL) during cLTP interrupted such synaptic potentiation (Franceschi B.A. et al., 2021)

Once ensured by immunofluorescence micrographs that our model expressed both Y1 and Y2 receptors (Fig. 2A, amygdala neurons co-labelled with antibodies against the specific neuronal marker β-tubulin III and against NPY receptor Y1 and Y2), we assessed the effect of s-GO:NPY (10 μg/mL and 1 μM, respectively) or NPY (1 μM) on synaptic potentiation. In details, these were applied for 5 min before and during the 30 s long-lasting cLTP induction (Fig. 2B). As illustrated by the traces in figure 2C, while cLTP treated neurons (in light blue) presented a post treatment increment in the amplitude of EPSC respect to that of controls (saline, in black), both s-GO:NPY (in orange) and NPY (in green) prevented the synaptic potentiation of amygdala network upon cLTP, as post-treatment EPSC amplitudes were similar to control ones.

As expected, potentiated cells showed a statistically significant increment in the amplitude of EPSC (values measured at 18-24 min post cLTP and normalized for the baseline were 0.78 ± 0.07 in control, n=5 and 1.75 ± 0.13 in cLTP, n=8, p=0.001 fig. 2D). Although the number of samples was too small to make statistical analysis, we observed values of normalized EPSC amplitudes similar to those of control in cultures undergone to cLTP but in the presence of s-GO:NPY (0.88 ± 0.14, n=4) or NPY (1.02 ± 0.02, n= 3, fig. 2D). No changes in the frequency of EPSC among different treatments were evaluated (values measured at 18-24 min post cLTP and normalized for the baseline were 1.22 ± 0.28 in control, 1.36 ± 0.28 in cLTP, 1.32 ± 0.39 for s-GO:NPY and 0.89 ± 0.19 in NPY, P>0.05; fig. 2E).

These preliminary experiments suggested that NPY alone or complexed to s-GO could prevent the development of functional plastic changes in synaptic transmission of artificially potentiated amygdala cultures.

We cannot exclude that the lack of cLTP in s-GO:NPY be due to a summation of s-GO and NPY effects, since uncomplexed s-GO was shown to prevent synaptic potentiation in a previous study.

3. The injection of s-GO:NPY in the LA impairs the aversive memory behaviour

In the next set of experiments, we tested the ability of s-GO:NPY and free NPY or s-GO in interrupting *in vivo* the plasticity of the amygdala neurons in a long-term period. To this aim, we used a rat behavioural model of PTSD, in which the exposure to a predator odour, induced an increase in the excitability of LA glutamatergic synapses (Rosenkranz J.A. et al., 2010), causing the long-lasting behavioural responses related to traumatic disorders (Dielenberg R.A. et al., 2001). In our experiments, after being habituated to an avoidance box, an apparatus to study contextual fear memory (Muñoz-Abellán C. et al., 2009), firstly animals were exposed to a collar previously worn by a cat (WC) or to an unworn collar (UC) as control (Fig. 3A). Two independent groups of rats were exposed to WC or UC context and, after 24 h, a guided cannula was stereotaxically implanted into the rat brain, targeting the LA to deliver locally, three days later, either s-GO, s-GO:NPY, NPY or the vehicle (saline solution). Four days after WC and UC groups of animals were re-exposed to the context (i.e., 8 days after the odour exposure) and then euthanized (sketched in Fig. 3A).

Cat odour exposure induced a significant innate fear response characterised by an increase in the head out behavioural response ($t(10) = 9$, $p < 0.0001$) compared to the UC exposed group.

Furthermore, the exposure to the predator odour also raised the head out response in the saline-treated group during the re-exposure to the context, evaluated 8 days later, compared to saline-($t(5.5) = 10$, $p < 0.001$) treated group previously exposed to UC. According to previous results performed in our laboratory, the LA treatment with s-GO reversed rats head out conditioned fear reaction ($F(3, 19) = 6.39$, $p < 0.01$), in a long-term period, when s-GO was not present anymore in the LA. Remarkably, the treatment with NPY and s-GO:NPY also decreased the expression of the head out behaviour ($F(3, 19) = 6.39$, $p < 0.05$; fig. 3B). These data suggest that the s-GO:NPY complex was active *in vivo* and impaired the aversive memory behaviour when injected into the LA.

In order to test the impact of the s-GO:NPY complex in the long-term anxiety-related response, rats were submitted to EPM apparatus, immediately after the re-exposure testing. Results showed that WC rats, treated with saline, exhibited a statistically significant decrease ($F(2,55) = 1.48$, $p < 0.05$) in the time spent in the open and aversive arms of EPM compared to UC (saline treated) group (Fig. 3C). No effect was observed with the others treatment ($p > 0.05$). Finally, assessment of open field (OF) locomotor activity showed no alteration in animals locomotion after s-GO, s-GO:NPY or NPY treatments ($p > 0.05$; Fig. 3D). All these findings suggested that s-GO:NPY, similarly to uncomplexed NPY, could impair aversive memory related behaviours, but not long-term anxiety responses.

DISCUSSION

The main findings of this work can be summarized as follow. As demonstrated when acutely and sub-acutely applied to dissociated hippocampal cultures, both compounds forming the nanoformulation (the nanoplatform and NPY) retained their properties of neuromodulators, observed in the free, uncomplexed, condition. Moreover, we showed that s-GO:NPY complex, similarly to free NPY, was able to prevent an abnormal neuroplasticity at the base of anxiety disorders, once applied to an *in vitro* model of amygdala synapses artificially potentiated through cLTP. Finally, behavioural testing of our *in vivo* model of PTSD (Franceschi B.A. et al., 2021) showed as s-GO:NPY microinjected into the LA selectively impaired in a long-term manner stress-related contextual fear memory, but not long-term generalized anxiety responses. Since this effect was comparable to that of free NPY, this finding suggested a specific targeting of the drug delivery system to neuronal circuits expressing NPY receptors.

In our *in vitro* experiments, we used acute and sub-acute applications of s-GO:NPY to dissect if the biological effects observed on neuronal cultures were due to s-GO or NPY. When acutely applied through 500 ms long-lasting pressure puff, s-GO:NPY exerted exactly the same increment in the frequency of sPSC previously found for s-GO (Rauti R. et al., 2019; Secomandi N. et al, 2020) and suggestive for a direct interaction of the nanomaterial with synapses. Considered that this type of application was too short to activate NPY receptors (Colmers W.F. et al., 1988a; Acuna-Goycolea C. et al., 2005; Qian J. et al., 1997), this experiment strongly indicated that the nanomaterial retained its pharmacological activity on synapses also when complexed to NPY. On the other hand, 5 min long-lasting sub-acute treatments were used to validate the effect of NPY in the complex. This application time was not sufficient to induce s-GO mediated synaptic depression (Rauti R. et al, 2019), but was compatible with NPY receptors activation (Colmers W.F. et al., 1988a; Acuna-Goycolea C. et al., 2005; Qian J. et al., 1997). Thanks to these recordings, in which we observed comparable synaptic modulation of s-GO:NPY and NPY, we demonstrated the preservation of peptide bioactivity in the complex.

Additional experiments performed on dissociated hippocampal cultures demonstrated that the main target of s-GO:NPY was the excitatory synapses, with a percentage of synaptic depression similar to that observed without inhibition of GABAergic synapses. The pharmacological isolation of glutamatergic synapses through the application of gabazine, a specific blocker of $GABA_A$ receptors (Wermuth C.G. et al., 1987), also revealed a prolongation of NPY effect on glutamatergic synapses, suggesting a potentially advantageous modification of the peptide pharmacokinetic, usually characterized by a short half-life (Wagner L. et al., 2015). We used these recordings also to assess that the biological activity of s-GO:NPY observed during sub-acute application was due to NPY receptors activation and not to a mere unspecific effect of the complex on neurons. The lack of synaptic depression observed for s-GO:NPY in the presence of Y1 and Y2 receptors antagonists confirmed our hypothesis.

In light of these results, we compared NPY with the complex in targeting anxiety diseases that rely on pathologically increased glutamatergic signaling (Masneuf S. et al., 2014). Through our *in vitro* model of artificially potentiated amygdala circuitry (Franceschi B.A. et al., 2021), we showed that s-GO:NPY, similarly to free NPY, prevented the potentiation of the amygdala cultures. Since in our previous work (Franceschi B.A. et al., 2021), we reported the ability of s-GO *per se* in hampering cLTP, further experiments will be necessary to dissect if also the nanomaterial in the complex contributed to abolish the effect of LTP induction.

Finally, through our rat behavioural model of PTSD (Franceschi B. A. et al., 2021) we tested the ability of s-GO:NPY in reverting *in vivo* anxiety-related behaviours, that are due to the pathological plasticity of the LA neurons. In detail, our results showed that s-GO, NPY and s-GO:NPY treatment into LA caused similar effects by decreasing the development of aversive memory-dependent behavioural response. This is in line with the literature reporting that NPY receptor activation induces stress resilience when injected into the amygdala (Sajdyk T.J. et al., 2008). On the other hand, only s-GO injection was able to decrease the long-term generalized anxiety response, measured in the EPM. Although other studies have indicated that NPY treatment may cause anxiolytic effects in the EPM (Broqua P. et al., 1995; Heilig M., 1995; Kask A. et al., 1998), this discrepancy may be due to different administration routes respect to our work. In addition, the different impact of s-GO and s-GO:NPY may depend on the fact that the delivery of s-GO is driven by NPY to specific neuronal circuits expressing NPY receptors.

Once completed by further studies to evaluate the biosafety of the complex, our preliminary findings will contribute to the translation in medicine of s-GO:NPY complex as an alternative drug delivery strategy for the treatment of anxiety disorders, where the nanomaterial not only prolongs NPY effect but behaves as an active ingredient.

MATERIALS AND METODS

Graphene oxide and complex synthesis and characterization

The non-covalent s-GO:NPY complex was prepared by mixing neutralized aqueous solutions of s-GO with reconstituted NPY in water for injection, at the starting concentrations of 1 mg/mL and 100 uM, respectively. The pH was monitored at every step. The complex formation was then promoted by placing the mixture in an orbital shaker for 30 minutes (1 x g, RT). The complex was then left to rest for 1 hour. Unbound NPY was removed by several cycles of centrifugation employing ultrafiltration columns having pores suitable to retain s-GO flakes while washing away small peptides. The quantification of unbound NPY peptide was assessed by HPLC and UV-Vis spectrophotometer, and further verification by direct quantification of NPY peptide was performed by solubilizing the adsorbed complex s-GO:NPY with SDS and quantified by HPLC. No evidence of unbound peptide was detected and 93-99% was directly quantified onto the s-GO surface. The purified s-GO:NPY complex was then characterized by absorption spectroscopy, AFM, SEM, Raman, XPS and XRD. The colloidal stability was evaluated over 2

months by DLS and zeta-potential, and the peptide detachment from the s-GO was studied over 2 months by HPLC, being the complex stable over this period.

In vitro dissociated hippocampal cultures

Dissociated hippocampal cultures were prepared from 2 to 3 days postnatal (P2−P3) rats (Cellot G. et al., 2011). All procedures were done in agreement with the Italian law (decree 26/14) and the EU guidelines (2007/526/CE and 2010/63/UE). The animal use was authorized by the Italian Ministry of Health (authorization number: 22DAB.NYQA) and approved by the local veterinary authorities. After hippocampus isolation, cells were enzymatically and mechanically dissociated, then seeded on poly-L-ornithine-coated glass coverslips (24 × 12 mm2, Kindler, EU) at a density of 250,000 cells/mL. Neuronal cultures were maintained in stable conditions (37 °C, 5 % CO2) in medium consisting of MEM (Gibco), 35 mM glucose, 1 mM Apo-transferrin, 15 mM HEPES, 1 mM insulin, 4 μM biotin, 3 μM vitamin B12, 500 nM gentamicin and 10 % fetal bovine serum (FBS; Invitrogen). After two days, the culture medium was replaced with one containing 1B-arabinofuranosilcitosina (Ara-C, 5 μM), to prevent glial over-proliferation, and then changed every three days.

In vitro dissociated amygdala cultures

All experimental procedures were performed in agreement with the Italian law (decree 26/14) and the European Union (EU) guidelines (2007/526/CE and 2010/63/UE) and were authorized by the Italian Ministry of Health (n. 689/2017-PR, n. 22DAB.N.1Z8 and n. 22DAB.N.1WO). The animal handling was approved by the local veterinary authorities and by the institutional (SISSA) ethical committee.

Primary cultures of amygdala cells were obtained from postnatal (P 7-10) juvenile Wistar rats and prepared as previously described (Secomandi N. et al., 2018) with slight modifications. In brief, rat brains were quickly removed from the skull and placed in fresh ice-cold artificial cerebrospinal fluid (ACSF) containing (in mM): 124 NaCl, 24 NaHCO3, 13 glucose, 5 HEPES, 2.5 KCl, 2 CaCl2, 2 MgSO4 and 1,2 NaPO4H2 with a pH of 7.3-7.4 when saturated with 95% O2 and 5% CO2 (Wu Y.E. et al., 2017). Coronal brain sections (800 μm of thickness) were cut using a vibratome (LeicaVT1000S) and under a dissecting microscope (Olympus SZ40), the regions containing the amygdaloid complex was visually identified following defined anatomical coordinates: Bregma - 1.8 mm, - 2.4 mm and 2.8 mm (Khazipov R. et al., 2015). Using a biopsy

punch with a diameter of 1 mm (Kai Medical, Japan) the amygdala tissue was collected to be enzymatically and mechanically dissociated following standard protocol (Cellot G. et al., 2011). Cells were seeded onto poly-L-ornithine-coated glass coverslips at a density of 1000 cells/mm2 and maintained in controlled conditions (at 37 ◦C, 5% CO2) for 8–12 days *in vitro* (DIV) prior to experiments in Neurobasal A Medium (Invitrogen) containing B27 supplement (Thermofisher).

Immunohistochemistry and confocal microscopy

Cultured amygdala neurons were fixed in PBS containing 4 % paraformaldehyde (PFA) for 20 min at room temperature (RT). Cells were permeabilized with 1 % Triton X-100 for 30 min, blocked with 5 % FBS in PBS for 30 min at RT and incubated with primary antibodies for 60 min. The primary antibodies used were mouse polyclonal anti-β-tubulin III (Sigma, 1:250 dilution), guinea-pig polyclonal anti GFAP (Alomone,1:500 dilution), rabbit polyclonal anti-NPY1 receptor (Abcam Plc, 1:500 dilution), and rabbit polyclonal anti-NPY2 receptor (Thermofisher, dilution 1:2000). After the primary incubation and PBS washes, neurons were incubated for 60 min with the secondary antibodies AlexaFluor 488 goat anti-rabbit (Invitrogen, dilution 1:500), AlexaFluor 594 goat anti-mouse (Invitrogen, dilution 1:500), AlexaFluor 647 goat anti-guinea pig (Invitrogen, dilution 1:500). Finally, cells were finally mounted on 1 mm thick glass coverslips using the Fluoromount mounting medium (Sigma-Aldrich). Image acquisition was taken from randomly selected fields (70.64 μm × 70.64 μm) per coverslip using a Nikon C2 Confocal, equipped with Ar/Kr, He/Ne, and UV lasers. Images were acquired with a 60× (1.4 NA) oil-objective (using oil mounting medium, 1.515 refractive index).

Electrophysiology

Single cell patch clamp recordings of neuronal activity were obtained from both dissociated hippocampal and amygdala cultures after 10-15 days of differentiation *in vitro*. Voltage clamp whole-cell recordings were performed at RT using glass micropipettes with a resistance of 4–7 MΩ once filled with the following intracellular saline solution (in mM): 120 K gluconate, 20 KCl, 10 HEPES, 10 EGTA, 2 MgCl2, 2 Na2ATP (pH 7.3, osmolarity adjusted to 300 mOsm). All experiments were performed at RT with the standard extracellular solution containing (in mM): 150 NaCl, 4 KCl, 2 CaCl2, 1 MgCl2, 10 HEPES, 10 glucose (pH 7.4) and continuously perfused at 2 ml/min. Cultures were mounted on a chamber and visualized with an inverted microscope (Eclipse TE-200, Nikon, Japan). All data were collected by means of a

Multiclamp 700A patch amplifier (Axon CNS, Molecular Devices) with a sampling rate of 10 kHz with the pClamp 10.6 acquisition-software (Molecular Devices LLC, USA). Input resistance and cells capacitance were measured online with the membrane test feature of the pClamp software. Spontaneous activity was recorded in voltage clamp mode at a holding potential of −58 mV, not corrected for the liquid junction potential which was −12 mV (calculated with the Clampex software; Molecular Devices, Sunnyvale, CA, USA). The stability of the recording was checked by repetitively monitoring the series resistance (<20 MΩ and not compensated) during the experiments and cells showing 15 % changes were excluded. The recorded traces were analyzed offline with the AxoGraph 1.4.4 event detection software (Axon CNS, Molecular Devices) to analyze sPSC frequency and amplitude.

Sub-acute and acute applications of complex

The complex and the related controls were applied through sub-acute and acute treatments. Regarding sub-acute treatments, after monitoring baseline neuronal activity for 5 min, complex (10 μg/mL and 1 μM, for s-GO and NPY, respectively) or s-GO (10 μg/mL) were applied through the perfusion system for 5 minutes and then washed out for additional 7 min.

In acute applications, by using a Picospritzer (PDES-02DX; NPI electronic GmbH, Germany), an injection of pressurized air (500 ms, 0.5 PSI) was used to deliver a puff of solution containing the nanomaterial or the complex to hippocampal neurons. The puff pipette, located at a distance of 200 μm from the recorded cell, was filled with extracellular solution (control), s-GO (100 μg/mL) or s-GO-NPY (100 μg/mL and 10 μM, respectively), all diluted in extracellular saline solution. Considering the volume (1 mL) of the extracellular solutions in the recording chamber, the final concentration of complex, s-GO (or control solution) reaching the patch-clamped neurons was 10 % of that present in the puff pipette (Secomandi N. et al., 2020). sPSC were recorded before and after (10 min each) the local ejection.

Chemical LTP induction to amygdala neurons and sub-acute application of compelx

To induce LTP in dissociated amygdala cultures under voltage clamp mode, our previously described protocol was applied (Franceschi B.A. et al., 2021). Briefly, after recording spontaneous activity for 8 min as baseline, 50 μM of glutamate for 30 s was applied to the entire chamber, while the membrane potential of the recorded cell was depolarized from -58 mV to +4 mV. In the experiments where dissociated cells were treated with s-GO:NPY or NPY, they were

applied through the perfusion system at a concentration of 10 μg/mL and 1 μM, respectively, for 5 min before the 30 s-long lasting application of 50 μM of glutamate.

The effects of LTP induction and s-GO interference were monitored 24 min after the baseline collection through the measure of EPSC frequencies and amplitudes, in the absence of any drugs.

Experimental design for in vivo procedure

Experimental procedures were carried out in accordance with the Italian law (decree 26/14) and the EU guidelines (2007/526/CE and 2010/63/UE) and were approved by the Italian Ministry of Health (n. 22DAB.11). Male adult Wistar rats weighed 230-280 g (n=29) were used to perform the *in vivo* experiments. Food and water were provided at libitum. The enclosure was maintained at 21 ± 2 °C on a light-dark cycle (lights on from 7 p.m. to 7 a.m.).

Behavioural experiments were performed as described previously (Franceschi B.A. et al., 2021). Briefly, aversive memory behavioural responses were evaluated in the avoidance box, which consisted of a rectangular arena (40 x 26 x 36 cm) with black acrylic-plexiglass walls covered with a transparent plexiglass lid. At one side of the arena, an alligator clip fixed in the wall is positioned 4 cm above the floor. A smaller box (20 x 26 x 22 cm) covered with a black plexiglass lid, named hide box, is positioned in the opposite direction of the rectangular arena. Arena and hide box were separated by a small 6 x 6 cm square hole allowing free access to both chambers. Rats were placed inside the hide box with free access to the arena for 3 consecutive days to habituate to the apparatus for 10 minutes.

On the fourth day, the time spent in the following defensive behaviour was recorded: head out (namely, the rat scanning the environment from a protected position, measured as poking of the head, or of head and shoulders, outside of the hide box but with the bulk of the rat body inside of it). After, rats were divided in two groups (n=6 per group), exposed to either a piece (2 cm) of an unworn collar (UC), without any cat odour or a piece of the collar previously worn by the cat, named worn collar (WC). Collars were worn by an encaged cat. Rats were re-exposed (10 minutes) to the context, arena without the cat collar to evaluate the aversive memory related to the conditioned fear.

Head out behavioural response was analyzed during the re-exposure to the context at 8 days post-exposure. Shortly thereafter, long-term anxiety-related behaviour was evaluated using the elevated plus maze (EPM). Which consisted of four arms (50 x 10 x 40 cm), two open arms

(without walls) and two closed arms (with 40 cm high walls) connected by a central square (10 x 10 cm). The maze was elevated 50 cm from the ground. Rats (n=6 per group) were placed in the closed arm and were allowed to freely explore the apparatus for 5 minutes. Percentage of time spent in the open zone was evaluated.

Exploratory and locomotor activities of rats (n = 6 per group) were measured in the OF apparatus, a square arena with the 60 x 60 x 40 cm black plexiglass walls and floor. Total distance moved (cm) in the open field were analyzed following the EPM testing.

All behavioural tests were performed between 8 a.m. and 12 p.m. under 12 lx luminosity and videorecorded for off-line analysis. The XPloRat software (Tejada et al., 2017) was used to score the behaviours. Next day, animals were submitted to stereotaxic surgery as described previously (Biagioni A.F. et al., 2016). Briefly, animals were anesthetized with intraperitoneal injection of ketamine (Ketamine Imalgene®, Merial Laboratories) and xylazine (Sedaxylan®, Dechra Veterinary Products) at 92 mg/kg and 10 mg/kg body weight, respectively, and fixed in a stereotaxic frame.

A stainless-steel guide cannula (outer diameter, 0.6 mm, and inner diameter, 0.4 mm) was implanted in the diencephalon aimed to the LA. The upper incisor bar was set at 3.3 mm below the interaural line so that the skull was horizontal between bregma and lambda. The guide cannula was vertically introduced using bregma as the reference and the following coordinates: A.P.−3.48 mm, M.L.−5.2 mm and D.V.−7 mm, according to Paxinos G. and Watson C.R., 2007. At the end of the surgery, the acrylic resin and two stainless steel screws were used to fix the guide cannula in the skull. In order to protect the guide cannula from obstruction a stainless-steel wire was used to seal it.

Analgesic and antibiotic medications were administrated postoperatively. Three days later, rats were gently wrapped in a cloth and held while they received a random treatment into LA of either s-GO (50 μg/mL), NPY (μ5M) s-GO/NPY or ACSF solution (composition described below) delivered by a needle (0.3 mm of outer diameter) linked to a syringe (Hamilton) through a polyethylene tube. The injection needle was inserted through the guide-cannula until it reached the LA (2 mm below the guide-cannula). Only rats that needle tip reached the LA were included in the study. Four days later, animals were submitted to the behavioural testing.

All experimental procedures were planned to minimize the number of animals used and their suffering.

Data analysis and statistics

All values from samples subjected to the same experimental protocols were pooled together and expressed as mean ± s.e.m with n = number of cells, unless otherwise indicated. For electrophysiological data, Shapiro-Wilk normality test was applied to evaluate the statistical distribution of the data sets. Statistically significant difference between two data sets was assessed by Student's t-test for parametric data and by Mann–Whitney for non-parametric ones. All comparisons between more than 2 groups were made with one-way ANOVA for parametric data, followed by using Holm-Sidak's multiple comparisons test for post hoc analysis. Not parametric data were analyzed with Kruskal-Wallis test and post hoc analysis was done with Dunn's multiple comparison test. Data from independent groups of animals exposed to the cat collar were checked for normality and homogeneity and analyzed using Student's unpaired two-tailed t-test. All comparisons between two independent variables were made with one-way ANOVAs, followed by Tukey' multiple comparison test when appropriated.

References

1. A.F. Biagioni, R.C. de Oliveira, R. de Oliveira, J.A. da Silva, T. dos Anjos-Garcia, C. M. Roncon, A.P. Corrado, H. Zangrossi, N.C. Coimbra, Eur. Neuropsychopharmacol 26 (2016) 532–545.

2. Acuna-Goycolea C, Tamamaki N, Yanagawa Y, Obata K, van den Pol AN. Mechanisms of Neuropeptide Y, Peptide YY, and Pancreatic Polypeptide Inhibition of Identified Green Fluorescent Protein-Expressing GABA Neurons in the Hypothalamic Neuroendocrine Arcuate Nucleus. J. Neurosci. 2005;25:7406–7419.

3. Bacci A, Huguenard JR, Prince DA. Differential modulation of synaptic transmission by neuropeptide Y in rat neocortical neurons. PNAS 2002;99:17125–17130.

4. Bramini M, Sacchetti S, Armirotti A, Rocchi A, Vázquez E, León Castellanos V, Bandiera T, Cesca F, Benfenati F. Graphene oxide nanosheets disrupt lipid composition, Ca2+ homeostasis, and synaptic transmission in primary cortical neurons. ACS Nano 2016;10:7154–7171.

5. Broqua P, Wettstein JG, Rocher MN, Gauthier-Martin B, Junien JL. Behavioural effects of neuropeptide Y receptor agonists in the elevated plus-maze and fear-potentiated startle procedures. Behav Pharmacol. 1995 Apr;6(3):215-222.

6. Cellot G, Toma, FM, Varley ZK, Laishram J, Villari A, Quintana M, Cipollone S, Prato M, Ballerini, L. Carbon Nanotube Scaffolds Tune Synaptic Strength in Cultured Neural Circuits: Novel Frontiers in Nanomaterial–Tissue Interactions. J. Neurosci. 2011;31:12945–12953.

7. Cellot G, Vranic S, Shin Y, Worsley R, Rodrigues AF, Bussy C, Casiraghi C, Kostarelos K, McDearmid JR. Graphene oxide nanosheets modulate spinal glutamatergic transmission and modify locomotor behaviour in an *in vivo* zebrafish model. Nanoscale Horiz. 2020;5:1250–1263.

8. Chen Y,Star A, Vidal S. Sweet carbon nanostructures: Carbohydrate conjugates with carbon nanotubes and graphene and their applications. Chem. Soc. Rev. 2013;42:4532–42.

9. Colmers WF, El Bahh B. Neuropeptide Y and Epilepsy. Epilepsy Curr. 2003;3:53–58.

10. Colmers WF, Lukowiak K, Pittma QJ. Neuropeptide Y Action in the Rat Hippocampal slices: Site and Mechanism of Presynaptic Inhibition. J. Neurosci. 1988;8:3827–3837

11. Colmers WF, Lukowiak K, Pittman QJ. Presynaptic action of neuropeptide Y in area CA1 of the rat hippocampal slice. J. Physiol. 1988a;383:285–299.

12. Di Mauro G, Rauti R, Casani R, Chimowa G, Galibert AM, Flahaut E, Cellot G, Ballerini L. Tuning the Reduction of Graphene Oxide Nanoflakes Differently Affects Neuronal Networks in the Zebrafish. Nanomaterials. (2021).

13. Dielenberg RA, Hunt GE, McGregor IS. "When a rat smells a cat": the distribution of Fos immunoreactivity in rat brain following exposure to a predatory odour. Neuroscience. 2001;104(4):1085-97.

14. Franceschi Biagioni A, Cellot G, Pati E, Lozano N, Ballesteros B, Casani R, Coimbra N, Kostarelos K, Ballerini L. Graphene oxide prevents lateral amygdala dysfunctional synaptic plasticity and reverts long lasting anxiety behaviour in rats. Biomaterials 2021;271:120749.

15. G. Paxinos, C.R. Watson, The Rat Brain in Stereotaxic Coordinates, sixth ed., Elsevier Academic Press, San Diego, 2007.

16. Geim AK Graphene: Status and Prospects. Science 2009;324:1530–4.

17. Heilig M. Antisense inhibition of neuropeptide Y (NPY)-Y1 receptor expression blocks the anxiolytic-like action of NPY in amygdala and paradoxically increases feeding. Regul Pept. 1995 Oct 20;59(2):201-5.

18. J. Tejada, K.T. Chaim, S. Morato, Psicol. Teor. Pesqui. 33 (2017) e3322**.**

19. John AA, Subramanian AP, Vellayappan M V, Balaji A, Mohandas H, Jaganathan SK. Carbon nanotubes and graphene as emerging candidates in neuroregeneration and neurodrug delivery. Int. J. Nanomedicine 2015;10:4267–77.

20. Kask A, Rägo L, Harro J. Anxiolytic-like effect of neuropeptide Y (NPY) and NPY13-36 microinjected into vicinity of locus coeruleus in rats. Brain Res. 1998 Mar 30;788(1-2):345-8.

21. Kautz M, Charney DS, Murrough JW. Neuropeptide Y, resilience, and PTSD therapeutics. Neurosci Lett. 2017 May 10;649:164-169.

22. Khazipov R, Zaynutdinova D, Ogievetsky E, Valeeva G, Mitrukhina O, Manent JB, Represa A. Atlas of the Postnatal Rat Brain in Stereotaxic Coordinates. Front Neuroanat. 2015 Dec 23;9:161.

23. Kitko KE, Zhang Q. Graphene-based nanomaterials: from production to integration with modern tools in neuroscience. Front. Syst. Neurosci. 2019;13:26.

24. Klapstein GJ, Colmers WF. On the Sites of Presynaptic Inhibition by Neuropeptide Y in Rat Hippocampus *in vitro*. Hippocampus 1993;3:103–112.

25. Kostarelos K, Novoselov KS. Exploring the Interface of Graphene and Biology. Mater. Sci. 2020;21:261–3.

26. Masneuf S, Lowery-Gionta E, Colacicco G, Pleil KE, Li C, Crowley N, Flynn S, Holmes A, Kash T. Glutamatergic mechanisms associated with stress-induced amygdala excitability and anxiety-related behaviour. Neuropharmacology. 2014 Oct;85:190-7.

27. Mousavi SM, Hashemi SA, Ghasemi Y, Amani AM, Babapoor A, Arjmand O. Applications of graphene oxide in case of nanomedicines and nanocarriers for biomolecules: review study. Drug Metab Rev. 2019 Feb;51(1):12-41. 69.

28. Muñoz-Abellán C, Daviu N, Rabasa C, Nadal R, Armario A. Cat odour causes long-lasting contextual fear conditioning and increased pituitary-adrenal activation, without modifying anxiety. Horm Behav. 2009 Oct;56(4):465-71.

29. Pchitskaya E, Bezprozvanny I. Dendritic spines shape analysis—classification or clusterization? Perspective. Front. Synaptic Neurosci. 2020;12:31.

30. Pinto AV, Ferreira P, Fernandes PA, Magalhães AL, Ramos MJ. Development of Nanoscale Graphene Oxide Models for the Adsorption of Biological Molecules. J Phys Chem B. 2022 Oct 25.

31. Qian J, Colmers WF, Saggau P. Inhibition of Synaptic Transmission by Neuropeptide Y in Rat Hippocampal Area CA1: Modulation of Presynaptic Ca2+Entry. J. Neurosci. 1997;17:8169–8177.

32. Rauti R, Lozano N, León V, Scaini D, Musto M, Rago I Ulloa Severino FP, Fabbro A, Casalis L, Vázquez E, Kostarelos K, Prato M, Ballerini L. Graphene oxide nanosheets reshape synaptic function in cultured brain networks. ACS Nano 2016;10:4459–4471.

33. Rauti R, Medelin, M, Newman, L, Vranic, S, Reina G, Bianco A, Prato M, Kostarelos K, Ballerini L. Graphene oxide flakes tune excitatory neurotransmission *in vivo* by targeting hippocampal synapses. Nano Lett. 2019;19:2858–2870.

34. Rosenkranz JA, Venheim ER, Padival M. Chronic stress causes amygdala hyperexcitability in rodents. Biol Psychiatry. 2010 Jun 15;67(12):1128-36.

35. Sajdyk TJ, Johnson PL, Leitermann RJ, Fitz SD, Dietrich A, Morin M, Gehlert DR, Urban JH, Shekhar A. Neuropeptide Y in the amygdala induces long-term resilience to stress-induced reductions in social responses but not hypothalamic-adrenal-pituitary axis activity or hyperthermia. J Neurosci. 2008 Jan 23;28(4):893-903.

36. Sanchez VC, Jachak A, Hurt RH, Kane AB. Biological interactions of graphene-family nanomaterials: An interdisciplinary review. Chem. Res. Toxicol. 2012;25:15–34.

37. Secomandi N, Franceschi Biagioni A, Kostarelos K, Cellot G, Ballerini L. Thin graphene oxide nanoflakes modulate glutamatergic synapses in the amygdala cultured circuits: Exploiting synaptic approaches to anxiety disorders. Nanomedicine: NBM 2020;26:102174.

38. Silva GA. Neuroscience nanotechnology: progress, opportunities and challenges. Nat. Rev. Neurosci. 2006;7:65–74.

39. Smith KR, Kopeikina KJ, Fawcett-Patel JM, Leaderbrand K, Gao R, Schurmann B, Myczek K, Radulovic J, Swanson GT, Penzes P. Psychiatric risk factor ANK3/Ankyrin-G nanodomains regulate the structure and function of glutamatergic synapses. Neuron 2014;84:399–415.

40. Vollmer LL, Schmeltzer S, Schurdak J, Ahlbrand R, Rush J, Dolgas CM, Baccei ML, Sah R. Neuropeptide Y Impairs Retrieval of Extinguished Fear and Modulates Excitability of Neurons in the Infralimbic Prefrontal Cortex. J Neurosci. 2016 Jan 27;36(4):1306-15.

41. Wagner L, Wolf R, Zeitschel U, Rossner S, Petersén A, Leavitt BR, Kästner F, Rothermundt M, Gärtner U, Gündel D, Schlenzig D, Frerker N, Schade J Manhart S, Rahfeld J, Demuth H, Hörsten S. Proteolytic degradation of neuropeptide Y (NPY) from head to toe: Identification of novel NPY-cleaving peptidases and potential drug interactions in CNS and Periphery. J. Neurochem. 2015;135:1019–37.

42. Wermuth CG, Bourguignon JJ, Schlewer G, Gies JP, Schoenfelder A, Melikian A, Bouchet MJ, Chantreux D, Molimard JC, Heaulme M, et al. Synthesis and structure-activity relationships of a series of aminopyridazine derivatives of gamma-aminobutyric acid acting as selective GABA-A antagonists. J Med Chem. 1987 Feb;30(2):239-49.

43. Wu YE, Pan L, Zuo Y, Li X, Hong W. Detecting Activated Cell Populations Using Single-Cell RNA-Seq. Neuron. 2017 Oct 11;96(2):313-329.e6.

44. Xia Y. Nanomaterials at work in biomedical research. Nat. Mater. 2008;7:758–60.

45. Zhang B, Koh Y H, Beckstead R B, Budnik V, Ganetzky B, Bellen H J. Synaptic vesicle size and number are regulated by a clathrin adaptor protein required for endocytosis. Neuron 1998;21: 1465–1475.

46. Zhang Y, Liu C, Chen W, Shi Y, Wang C, Lin S, He, H. Regulation of neuropeptide Y in body microenvironments and its potential application in therapies: a review. Cell & Bioscience 2021;11:151.

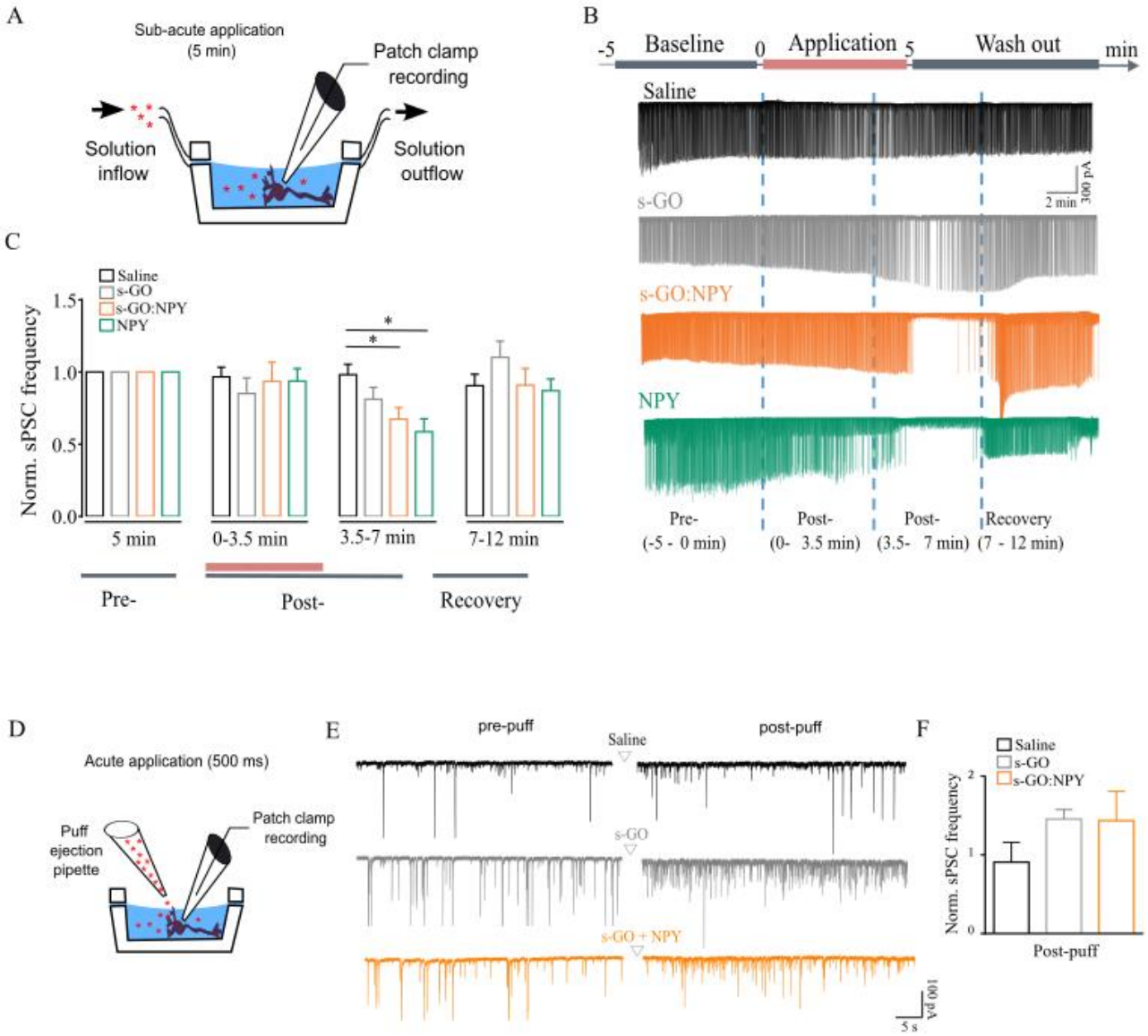

Figure 1. *Both s-GO and NPY retain their modulatory activity on synapses once complexed in the drug delivery system.* (A) Sketch of the experimental setting: patch clamp recording of a single neuron during sub-acute (5 min) application of saline, s-GO, s-GO:NPY or NPY. (B) Exemplificative traces of patch clamp recordings performed during different treatments (saline in black, s-GO in grey, s-GO:NPY in orange and NPY in green), showing as free NPY or in complex with s-GO induced a transient decrease in neuronal activity after peptide application. (C) Bar plots of normalized sPSC frequency for the different treatments at various time points after treatments. Note that both s-GO:NPY and NPY induced a similar decrease in sPSC frequency between 3.5 and 7 min after the beginning of the application. (D) Sketch of acute pressure puff application during patch clamp recordings of hippocampal neurons in voltage clamp mode. (E) Exemplificative traces of recorded neurons before and after the puff applications of different treatments (saline in black, s-GO in grey and s-GO:NPY in orange), illustrating as both

uncomplexed and complexed s-GO induced an increment of the frequency of sPSC. (F) Graph showing normalized sPSC frequency after the different treatments. Note the tendency of a post-application increase in sPSC frequencies of both uncomplexed and complexed s-GO. *P<0.05.

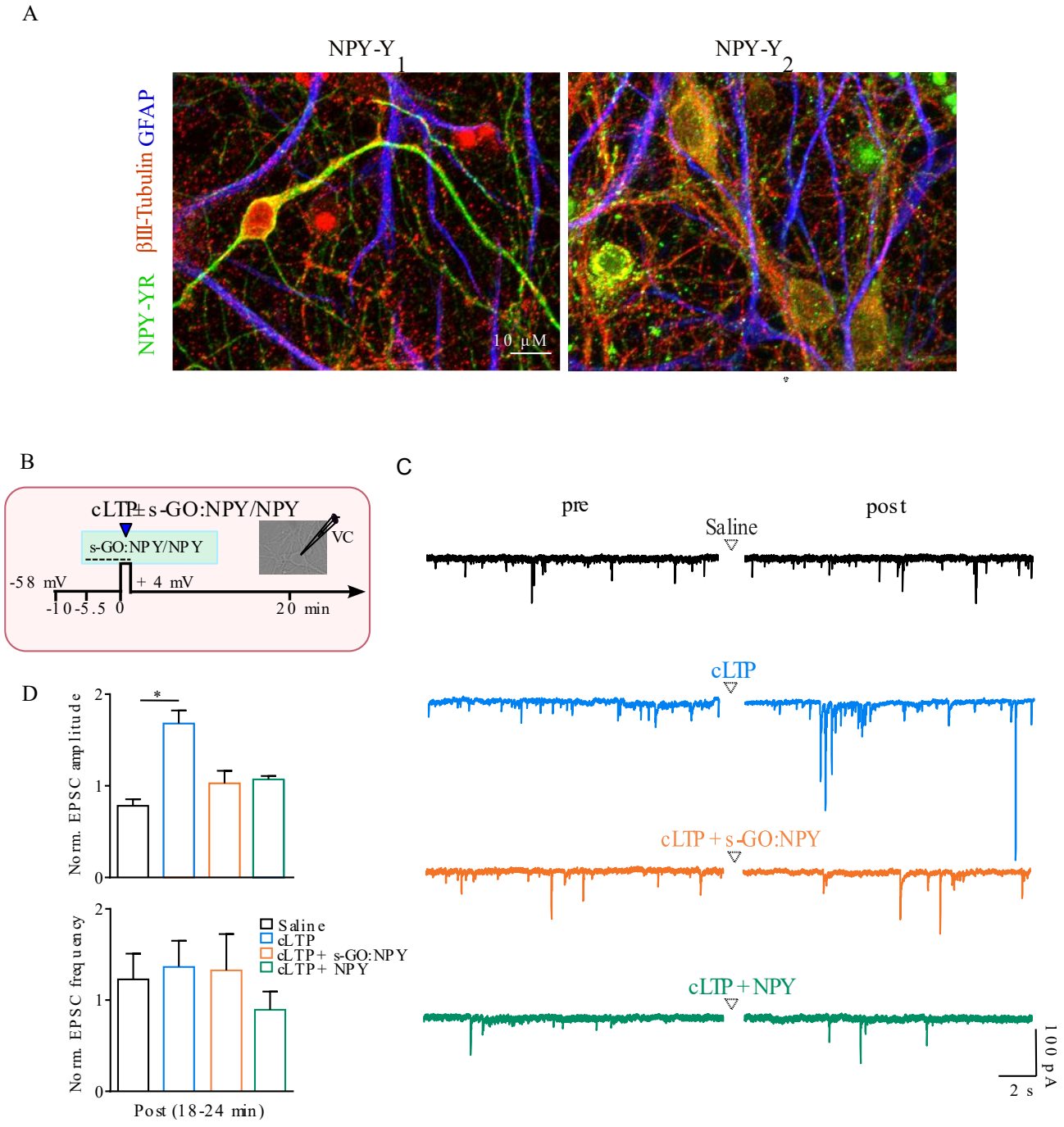

Figure 2. *Uncomplexed or s-GO complexed NPY are able to prevent the cLTP of amygdala dissociated cultures.* (A) Representative fluorescence microscopy images of amygdala cultured cells showing the labelling for β-tubulin-positive neurons (in red) and for neuropeptide Y

receptors (in green) type 1 (NPY1; left) and type 2 (NPY2; right), respectively. In blue, GFAP-positive astrocytes. (B) Sketch of the experimental setting: single neuron recorded in voltage clamp is treated with NPY or s-GO:NPY 5 minutes before and during the 30 s-long lasting application of glutamate (50 uM) and the depolarization to positive values of membrane potential to induce cLTP. (C) Representative traces of recordings performed before and after different treatments, showing as the increment of sPSC amplitude after cLTP induction (in blue) was prevented by the application of s-GO:NPY (in orange) or NPY (in green). (D) Plots of normalized EPSC frequencies and amplitudes 18 min after cLTP (valued in 6 min time). Note the tendency after application of NPY or s-GO:NPY to rescue the increased EPSC amplitude observed in cLTP-treated cells, while the EPSC frequency was not affected. *P<0.05.

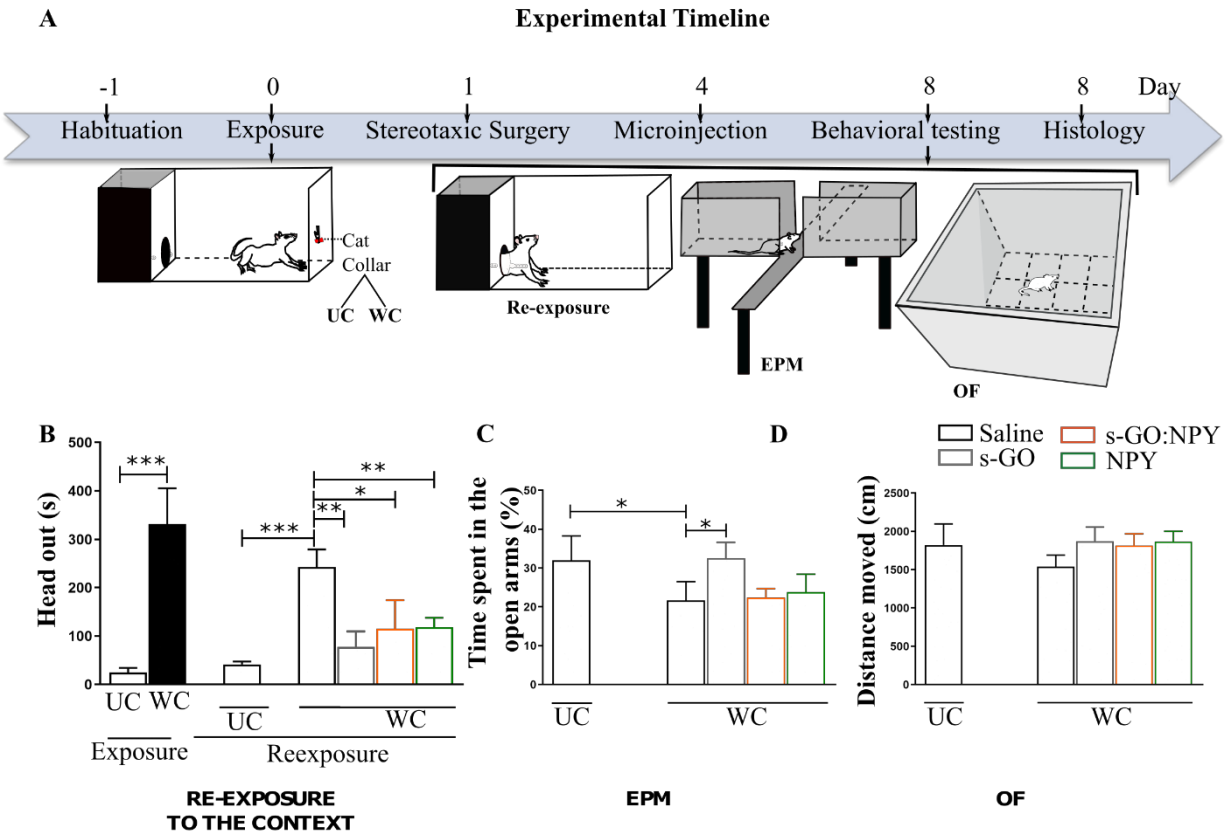

Figure 3. *Aversive memory impairment exerted by NPY or s-GO:NPY complex injected into LA*. (A) Schematic representation of the experimental timeline and behavioural testing. (B) On the left, bar plot summarizing the head out behavioural responses evoked by the exposure to UC or WC and by the re-exposure to the context after s-GO, s-GO:NPY, NPY or saline microinjections into the LA. In the middle, bar plot showing the time spent in the open arms of EPM apparatus in

UC and WC treated with s-GO, s-GO:NPY, NPY or saline. On the right, bar plot reporting the total distance travelled in the OF apparatus in UC and WC treated with s-GO, s-GO:NPY, NPY or saline. N = 5-7 for each group. *p < 0.05.

SUPPLEMENTARY FIGURE

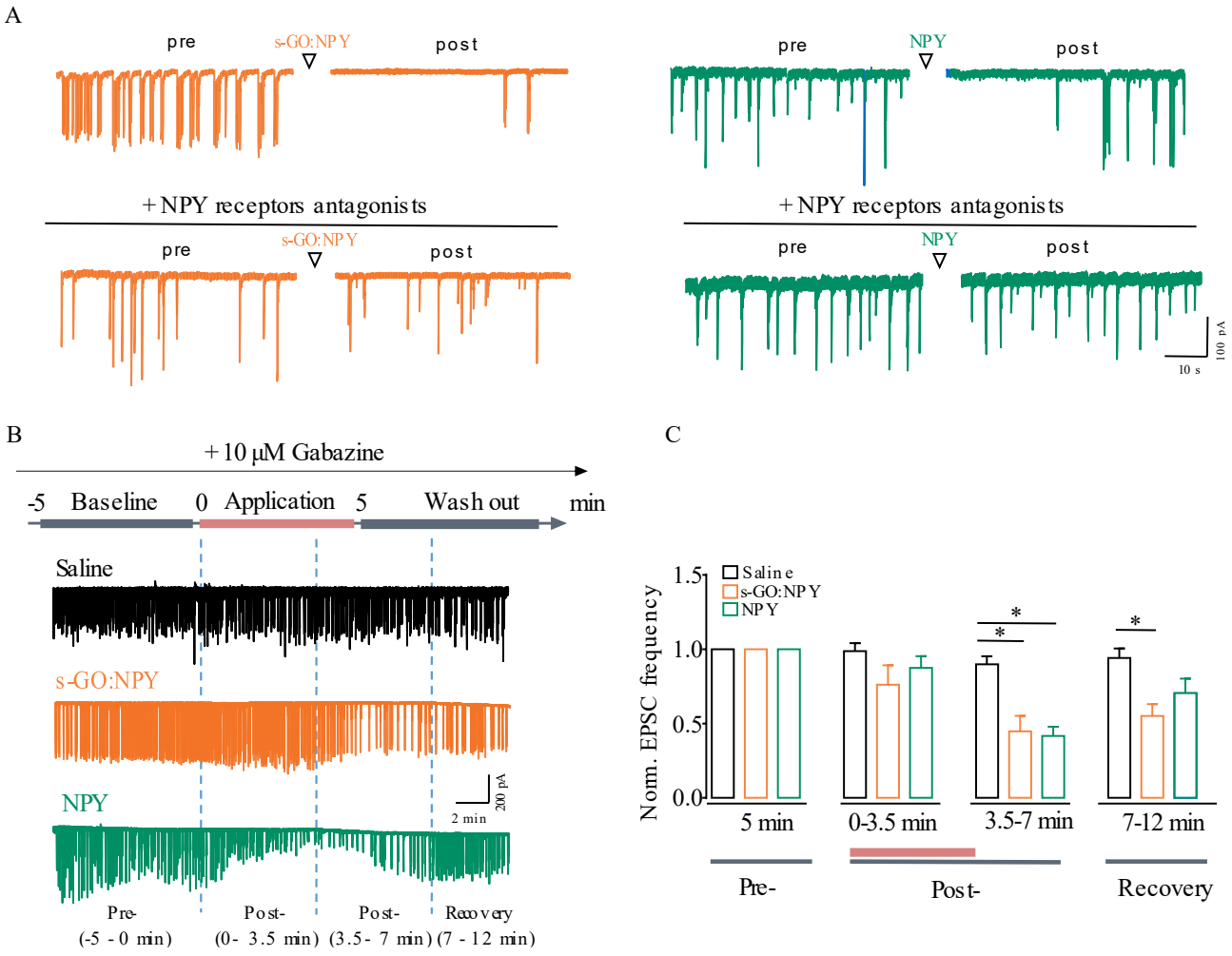

Supplementary Figure 1. *s-GO:NPY complex exerts its biological activity of neuromodulation binding NPY receptors and selectively targeting glutamatergic synapses.* (A) Representative traces of recordings performed during the sub-acute application of NPY, both in the complex formulation (orange traces, right) or alone (green traces, left), and in the absence (top traces) or presence (bottom traces) of Y1 and Y2 receptor antagonists. No modification of synaptic activity

was observed under the presence of the antagonists. (B) Exemplificative traces of voltage clamp recordings of EPSC, pharmacologically isolated with gabazine (10 μM), acquired during different treatments (saline in black, s-GO-NPY in orange and NPY in green), showing as pure NPY or in complex with s-GO induced a decrease in neuronal activity from 3.5 to 7 min after the beginning of the treatment. (C) Bar plots of normalized EPSC frequency and for the different treatments during the 3.5, 7 and 12 minutes after the beginning of application. Note that both s-GO-NPY and NPY induced a similar decrease in sPSC frequency from 3.5 to 7 min after the beginning of the application, but only the effect of the complex persists during the recovery phase. *$P<0.05$.

APPENDIX

In this section, additional series of experiments that were performed in relation to the thesis main subject are illustrated. These data support future directions of this line of research but they are described separately as we did not obtain the expected outcomes. However, they open new perspectives to be tested in the next future. The topic addressed here was to test and compare the biological effects of different ligands selected for Y2 receptor selectivity of NPY.

NPY: SUBTYPE SELECTIVITY STUDIES

The NPY family is a multireceptor/multiligand system consisting of four G-protein coupled receptors in humans (hY1, hY2, hY4, hY5) and three agonists (NPY, PYY, PP) which bind and activate them with different potency and affinity (Pedragosa-Badia X. et al., 2013). NPY receptors plays different roles in regulating several biological processes making this NPY system particularly intricate in both physiology and pathology. The heterogeneity of NPY receptors was first observed in studies of sympathetic neuroeffector junctions, where diverse NPY signalling pharmacology was evaluated (Wahlestedt C. et al., 1986). In the brain, these receptors are differentially distributed and exert different roles. For instance, human Y1 receptor seems to have anti-stress and anxiolytic effects in both the hippocampus (Olesen M.V. et al., 2012) and amygdala (Heilig M. et al., 2004; Kautz et al., 2017) even if, in the hippocampus it seems to have pro-epileptic and pro-convulsant outcome (Colmers W.F. et al., 2003). Conversely, potentiation of Y2 signalling seems to be anxiogenic (Heilig M. et al., 2004, Sajdyk T.J. et al., 2002; 2002a) but also anti-epileptic by reducing the probability of release of the glutamate neurotransmitter (Vezzani A. et al., 2004). In the therapeutic field, the importance of the NPY affinity for specific receptors leads to the design of selective analogues. To obtain subtype selective ligands, the peptide has to be modified in key positions permitting the modulation of the ligand preference for a receptor. The selectivity to a particular receptor subtype can be obtained by the truncation of one or more fragments and one of the most investigated approaches are N- or C- terminal truncations.

Y2 receptor in mood disorders

The role of NPY in anxiety, depression and epilepsy has been extensively studied but only a few efforts have focused on developing a NPY receptor modulator for psychiatric purposes (Brothers S.P. et al, 2010).

The Y2 receptor is predominantly expressed presynaptically in hippocampal neurons, in the thalamus, hypothalamus, and in the peripheral nervous system (Widdowson P.S., 1993; Cabrele C. and Beck-Sickinger A.G., 2000). It acts through a negative-feedback pathway of NPY release (King P.J. et al, 1999). This led to speculate that, since NPY is an anxiolytic-like substance, a synthetic compound that blocks the Y2 receptor or Y2 receptor antagonists would increase NPY levels in the CNS and may treat certain psychiatric diseases. Hence, since Y2 receptor controls the release of neurotransmitter by the presynaptic terminal, a reduction of glutamate in the amygdala through Y2 blockage may inhibit the pathological LTP associated to PTSD (Parsons M.P. et al., 2014). However, to date there are not enough data on efficacy and side effect outcomes of NPY-related compounds. In this regard, there is a pressing need to develop useful NPY related small molecule ligands to

finally understand the role of NPY in pathologies and to assess the clinical therapeutic potential of NPY signalling pathways.

For such reasons, during the last year of my PhD, we decided to test some Y2 receptor selective NPY sequences.

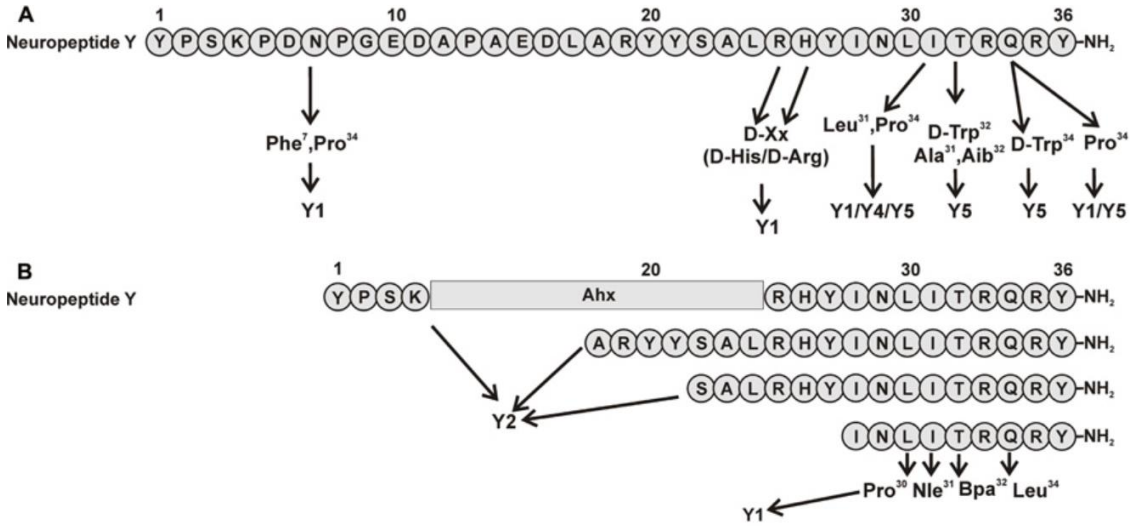

Figure 1. *Relevant amino acid positions* (A) and truncated peptides (B) to introduce selectivity to NPY receptors (from Pedragosa-Badia X. et al., 2013).

RESULTS

Since most used Y2 receptor selective NPY-analogues are the N-terminally truncated forms of NPY (Fig.1, Pedragosa-Badia X. et al., 2013), we collaborated with Prof. Alberto Bianco's group (Strasbourg University, France) where two C-terminal NPY short peptides were synthetised: NPY 13-36 and 26-36. The two different sequences, corresponding to the truncated sequences of the NPY peptide containing the C-terminal α-helix, are X-PAEDMARYYSALRHYINLITRQRY-NH2 and X-HYINLITRQRY-NH2, X corresponding to the 5-hexynoic acid modification as the previous NPY peptide. The first sequence corresponds to the complete sequence of the α-helix present in the human NPY, devoid of the N-terminal part of the peptide. This sequence is the first agonist reported to act preferentially at NPY Y2 receptors (Brothers S.P. et al, 2010). NPY 26-36 is instead a fragment of the C-terminal part of the peptide but still localized in the helical part, which also possesses a specificity toward human Y2 receptors (Wieland H.A. et al, Peptides, Volume 16, Issue 8, 1995).

Once tested through pharmacological experiments that the NPY effects in our model of cultured hippocampal neurons are mediated mainly by the Y2 receptor (Cellot G. et al., 2022, ACS Applied Nano Materials, *under revision*), we firstly verified if these short sequences exerted biological activity. As depicted in the figure 2, we applied these compounds sub-acutely (5 minutes; 1 μM) in our hippocampal cultures during patch clamp recordings of the spontaneous synaptic activity of neurons. Our data reported that, differently from NPY entire sequence used as control, both NPY 13-36 and 26-36 peptides did not exert any effect on neuronal synaptic activity (Fig.2). According to NPY 26-36, we confirmed previous works reporting this short peptide as inactive (Barraco R.A. et al., 1991). Conversely, for NPY 13-36 we concluded that this short sequence has no modulatory activity on synaptic function in our *in vitro* hippocampal model. Since the inactivity

of the free form of these short peptides, we did not proceed in testing the effect of conjugates with s-GO.

In our opinion, the detection of small compounds which can bind with high level of selectivity NPY receptor subtypes is a focus for the scientific community over the next years. In fact, although the promising background, no clinically approved CNS therapeutics based on NPY receptor ligands are currently available. It is therefore our future objective to test additional specific ligands of NPY receptors to be conjugated with GO on different *in vitro* brain networks.

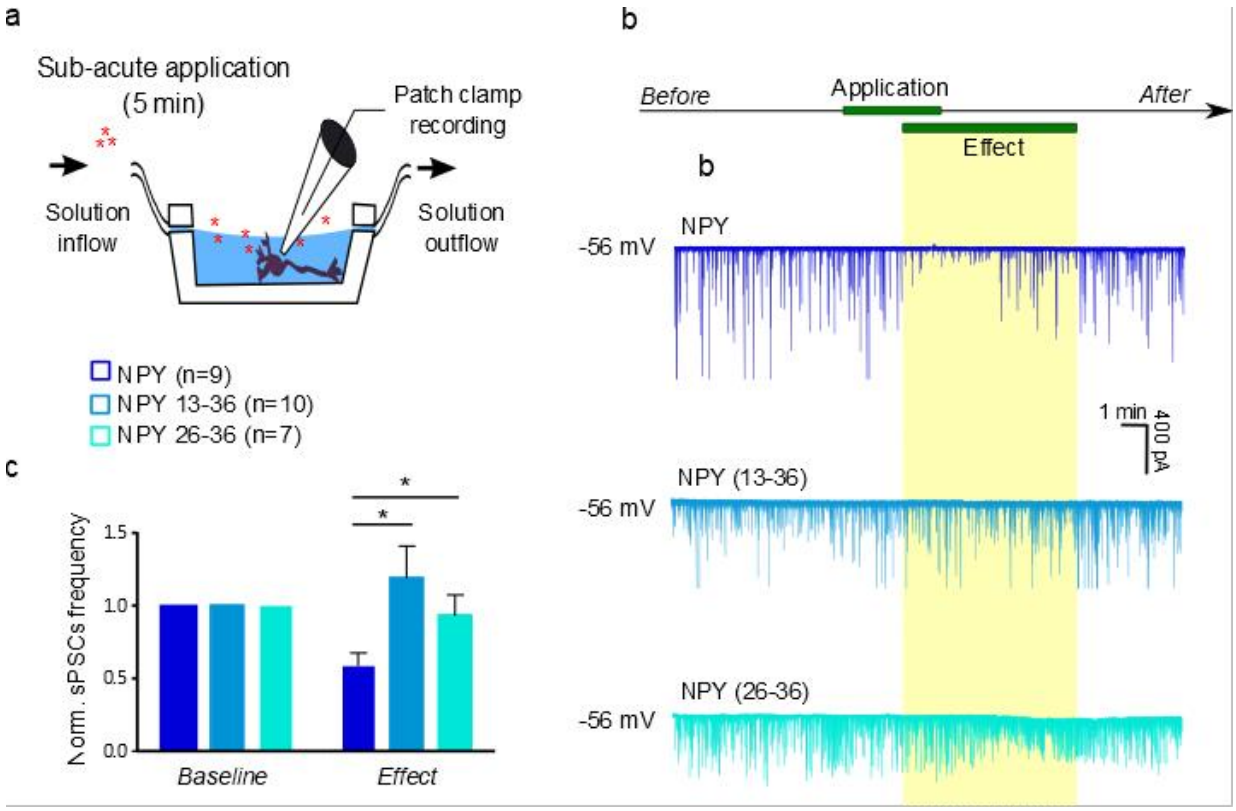

Figure 2. *Short NPY sequences do not modulate neuronal activity*. (a) Experimental setting. (b) Exemplificative traces of recordings performed during different treatments (NPY entire sequence in blue, NPY 13-36 in light blue and NPY 26-36 in cyan) showing that the two short sequences were not able to induce effect of synaptic activity reduction, as instead shown for NPY. (c) Plots showing normalized sPSC frequency for the different treatments during the effect phase (corresponding to the last two minutes of application together with the initial phase of wash out). This was 0.59 ± 0.09 for NPY, 1.19 ± 0.22 for NPY 13-36 and 0.93 ± 0.14 for NPY 26-36. Note that only NPY long sequence induced a statistically significant decrease in sPSC frequency among NPY fragments, *P<0.05.

CONCLUSIVE REMARKS

Nanomaterials might offer exciting alternatives to cope with the growing demand for more effective and safer treatments in biomedicine. Among them, in the last few years GBNs have been acquiring increasing attention in neuroscience. Thanks to their peculiar physical-chemical properties, GBNs can be exploited as components of promising nano-tools for personalized medical approaches, such as bioelectronic devices, tissue scaffolds, as well as nanovectors in drug-delivery systems (Wang K. et al., 2021; Gui W. et al., 2018; Reina G. et al., 2017; Feng L. et al., 2013; Kostarelos K. et al., 2017; Bramini M. et al., 2018). It is therefore extremely urgent a detailed study of the interactions between the nanomaterial and the neuronal function, under both pathological and physiological conditions.

Our previous results showed that s-GO interfered with the glutamatergic synaptic activity of rat hippocampal neurons both *in vitro* and *in vivo* (Rauti R. et al., 2016; Rauti R. et al., 2019). This result was confirmed by our recent investigations where s-GO emerged not only as synaptic modulator, but also as nano-tool to modulate behaviours that correlates with the activity of neuronal network exposed to the nanomaterial (Cellot G. et al., 2020; Franceschi B.A. et al., 2021).

In this thesis, my main goal was to investigate from a mechanistic perspective how s-GO acted on amygdala glutamatergic neurons at the synaptic level in a pathological condition characterized by exceeding excitatory transmission (PTSD) and if this interference could prevent correlated anxiety-related behaviours.

In details, I focused on an *in vitro* model of artificially potentiated amygdala synapses, which recapitulates the abnormal hyperexcitability occurring in anxiety-related diseases (Hadley D. et al., 2014; Klein R.C., et al., 2014; Duval E.R. et al., 2020). Through a combination of electrophysiological investigations and imaging analysis, first I demonstrated that the application of s-GO during cLTP prevented synaptic potentiation and, second, that such an effect was mediated by targeting of presynaptic excitatory terminals, where the nanomaterial interfered with the machinery of vesicle dynamics, reducing the probability of glutamate release.

Under the supervision of Dr. A. Franceschi Biagioni, other members of Prof. Ballerini's group, confirmed and extended my results to an *in vivo* animal model of PTSD (Franceschi B.A. et al., 2021) to address s-GO interfering with the long-lasting behavioural responses related to anxiety disorders. Thanks to this paradigm, we found that a single injection of the nanomaterial, delivered in the LA in the time window critical for the formation of the pathological plasticity, reverted plastic changes in dendritic spines related to the LTP and decrease anxiety-related behaviours. All together *in vitro* and *in vivo* findings suggest that s-GO, by reducing the probability of glutamate release from presynaptic terminals, could hamper the expression of LTP in the LA, thus inhibiting the appearance of correlated anxiety behaviours.

s-GO biocompatibility, its dispersibility in water solutions and the precise targeting of excitatory synapses make this nanomaterial ideal as platform for selective drug delivery systems. Hence, the final part of my thesis focused on the characterization of a nano-complex formulation where NPY, a modulator of neuronal transmission (Colmers W.F. et al., 1988; Klapstein G.J. et al., 1993; Bacci A. et al., 2002) was absorbed onto s-GO. The peptidic nature of NPY makes it quickly degradable and limits its use in therapeutic approaches for the treatment of neurodisorders (Wagner L. et al., 2015), thus the complexation to the nanomaterial might be a successful strategy to improve the pharmacokinetic properties of NPY.

In the framework of potential therapeutic applications for anxiety disorders, I performed preliminary experiments to test the effect of NPY in nano-complex formulation with s-GO. Through acute and subacute applications of s-GO:NPY to hippocampal cultures (our standard for testing novel nanomaterials, Rauti R. et al., 2016; Rauti R. et al., 2019; Secomandi N. et al., 2020; Di Mauro G. et al., 2021), we observed that both the nanomaterial and the carried bioactive molecule retained their biological activity of modulators of synaptic activity. When we used this nano-formulation in our *in vitro* model of potentiated amygdala cultures, we observed that both s-GO:NPY and free NPY prevented in a similar manner the onset of LTP when applied during cLTP induction, suggesting the lack of a summation between nanomaterial and peptide effects (or a saturation of the pathway involved).

Preliminary experiments carried out by my colleagues on the PTSD rat model confirmed that NPY complexed to the nanomaterials retained *in vivo* its biological activity on neurons. However, differently from not complexed s-GO effect, the rescue of the contextual fear memory (but not of the anxiety-related responses) observed in animals treated with s-GO:NPY or NPY suggested that the drug delivery system could be driven to specific neuronal circuit by NPY. In this light, this nano-formulation may be exploited as a highly selective targeting towards specific neurons expressing NPY receptors.

As indicated by some preliminary experiments reported in the appendix, future perspective for this project will be to identify NPY short sequences to be complexed to s-GO, in order to increase selectivity for Y2 receptor. In the context of a therapy, this could reduce potential side effects related to the existence to multiple NPY receptors involved in several physiological functions (Olesen M.V. et al., 2012, Kautz et al., 2017, Colmers W.F. et al., 2003).

In conclusion, the work of my thesis characterized in pathological condition the efficacy of s-GO, free or in complexation with bioactive compounds, as modulator of synaptic activity and correlated behaviours.

Thanks to the mechanistic insight of this research, I contributed to identify a novel nano-tool that might be used for the treatment of anxiety-related disorders and, more in general, for other neuropathologies characterized by exceeding glutamatergic transmission.

BIBLIOGRAPHY

1. Acaròn Ledesma H, Li X, Carvalho-de-Souza JL, Wei W, Bezanilla F, Tian B. An atlas of nano-enabled neural interfaces. Nat Nanotechnol. 2019 Jul;14(7):645-657.
2. Adolphs R, Tranel D, Damasio H, Damasio A. Impaired recognition of emotion in facial expressions following bilateral damage to the human amygdala. Nature. 1994 Dec 15;372(6507):669-72.
3. Akhavan O, Ghaderi E, Rahighi R. Toward single-DNA electrochemical biosensing by graphene nanowalls. ACS Nano. 2012 Apr 24;6(4):2904-16.
4. Akhavan O, Ghaderi E. Toxicity of graphene and graphene oxide nanowalls against bacteria. ACS Nano. 2010 Oct 26;4(10):5731-6.
5. Akhavan, O., Ghaderi, E., Aghayee, S.M., Fereydooni, Y., & Talebi, A. The use of a glucose-reduced graphene oxide suspension for photothermal cancer therapy. Journal of Materials Chemistry 2012b; 22:13773-13781.
6. Albensi BC, Oliver DR, Toupin J, Odero G. Electrical stimulation protocols for hippocampal synaptic plasticity and neuronal hyper-excitability: are they effective or relevant? Exp Neurol. 2007 Mar;204(1):1-13.
7. Amaral DG and Insausti R. Retrograde transport of D-[3H]-aspartate injected into the monkey amygdaloid complex. Exp Brain Res 1992;88:375–388.
8. American Psychiatric Association. Diagnostic and statistical manual of mental disorders (5th ed.). Arlington, VA: American Psychiatric Publishing, 2013.
9. Aniksztejn L, Ben-Ari Y. Expression of LTP by AMPA and/or NMDA receptors is determined by the extent of NMDA receptors activation during the tetanus. J Neurophysiol. 1995 Dec;74(6):2349-57.
10. Appleby VJ, Corrêa SA, Duckworth JK, Nash JE, Noël J, Fitzjohn SM, Collingridge GL, Molnár E. LTP in hippocampal neurons is associated with a CaMKII-mediated increase in GluA1 surface expression. J Neurochem. 2011 Feb;116(4):530-43.
11. Bacci A, Huguenard JR, Prince DA. Differential modulation of synaptic transmission by neuropeptide Y in rat neocortical neurons. PNAS 2002;99:17125–17130.
12. Bagri A, Mattevi C, Acik M, Chabal YJ, Chhowalla M, Shenoy VB. Structural evolution during the reduction of chemically derived graphene oxide. Nat Chem. 2010 Jul;2(7):581-7.
13. Bandelow B, Michaelis S, Wedekind D. Treatment of anxiety disorders. Dialogues Clin Neurosci. 2017 Jun;19(2):93-107.
14. Bandelow B, Michaelis S. Epidemiology of anxiety disorders in the 21st century. Dialogues Clin Neurosci. 2015 Sep;17(3):327-35.
15. Bandelow B, Sher L, Bunevicius R, Hollander E, Kasper S, Zohar J, Möller HJ; WFSBP Task Force on Mental Disorders in Primary Care; WFSBP Task Force on Anxiety Disorders, OCD and PTSD. Guidelines for the pharmacological treatment of anxiety disorders, obsessive-compulsive disorder and posttraumatic stress disorder in primary care. Int J Psychiatry Clin Pract. 2012 Jun;16(2):77-84.

16. Banker, G.A., Cowan, W.M. Rat hippocampal neurons in dispersed cell culture. Brain Res, 1997;126, 397-42.

17. Bar-Elli O, Steinitz D, Yang G, Tenne R, Ludwig A, Kuo Y, Triller A, Weiss S, Oron D. Rapid Voltage Sensing with Single Nanorods via the Quantum Confined Stark Effect. ACS Photonics. 2018 Jul 18;5(7):2860-2867.

18. Barker-Haliski M, White HS. Glutamatergic Mechanisms Associated with Seizures and Epilepsy. Cold Spring Harb Perspect Med. 2015 Jun 22;5(8):a022863.

19. Barraco RA, Ergene E, Dunbar JC, Ganduri YL, Anderson GF. Y2 receptors for neuropeptide Y in the nucleus of the solitary tract mediate depressor responses. Peptides. 1991 Jul-Aug;12(4):691-8.

20. Barria A, Muller D, Derkach V, Griffith LC, Soderling TR. Regulatory phosphorylation of AMPA-type glutamate receptors by CaM-KII during long-term potentiation. Science. 1997 Jun 27;276(5321):2042-5.

21. Barry JF, Turner MJ, Schloss JM, Glenn DR, Song Y, Lukin MD, Park H, Walsworth RL. Optical magnetic detection of single-neuron action potentials using quantum defects in diamond. Proc Natl Acad Sci U S A. 2016 Dec 6;113(49):14133-14138.

22. Basso AM, Spina M, Rivier J, Vale W, Koob GF. Corticotropin-releasing factor antagonist attenuates the "anxiogenic-like" effect in the defensive burying paradigm but not in the elevated plus-maze following chronic cocaine in rats. Psychopharmacology (Berl). 1999 Jul;145(1):21-30.

23. Bayda S, Adeel M, Tuccinardi T, Cordani M, Rizzolio F. The History of Nanoscience and Nanotechnology: From Chemical-Physical Applications to Nanomedicine. Molecules. 2019 Dec 27;25(1):112.

24. Bear MF, Huber KM, Warren ST. The mGluR theory of fragile X mental retardation. Trends Neurosci. 2004 Jul;27(7):370-7.

25. Bellgowan PS, Helmstetter FJ. Neural systems for the expression of hypoalgesia during nonassociative fear. Behav Neurosci. 1996 Aug;110(4):727-36.

26. Belzung C, Lemoine M. Criteria of validity for animal models of psychiatric disorders: focus on anxiety disorders and depression. Biol Mood Anxiety Disord. 2011 Nov 7;1(1):9.

27. Benabid AL, Pollak P, Louveau A, Henry S, de Rougemont J. Combined (thalamotomy and stimulation) stereotactic surgery of the VIM thalamic nucleus for bilateral Parkinson disease. Appl Neurophysiol. 1987;50(1-6):344-6.

28. Ben-Ari Y. Excitatory actions of gaba during development: the nature of the nurture. Nat Rev Neurosci. 2002 Sep;3(9):728-39.

29. Benarroch EE. The amygdala: functional organization and involvement in neurologic disorders. Neurology. 2015 Jan 20;84(3):313-24.

30. Bendali A, Hess LH, Seifert M, Forster V, Stephan AF, Garrido JA, Picaud S. Purified neurons can survive on peptide-free graphene layers. Adv Healthc Mater. 2013 Jul;2(7):929-33.

31. Betz, W. J.; Bewick, G. S. Optical Analysis of Synaptic Vesicle Recycling at the Frog Neuromuscular Junction. Science 1992, 255, 200−203.

32. Bhakar AL, Dölen G, Bear MF. The pathophysiology of fragile X (and what it teaches us about synapses). Annu Rev Neurosci. 2012;35:417-43.

33. Bi GQ, Poo MM. Synaptic modifications in cultured hippocampal neurons: dependence on spike timing, synaptic strength, and postsynaptic cell type. J Neurosci. 1998 Dec 15;18(24):10464-72.

34. Bianchi R, Chuang SC, Zhao W, Young SR, Wong RK. Cellular plasticity for group I mGluR-mediated epileptogenesis. J Neurosci. 2009 Mar 18;29(11):3497-507.

35. Binnig G, Quate CF, Gerber C. Atomic force microscope. Phys Rev Lett. 1986 Mar 3;56(9):930-933.

36. Bissière S, Humeau Y, Lüthi A. Dopamine gates LTP induction in lateral amygdala by suppressing feedforward inhibition. Nat Neurosci. 2003 Jun;6(6):587-92.

37. Blanchard DC, Blanchard RJ. Innate and conditioned reactions to threat in rats with amygdaloid lesions. J Comp Physiol Psychol. 1972 Nov;81(2):281-90.

38. Bledsoe AC, Oliver KM, Scholl JL, Forster GL. Anxiety states induced by post-weaning social isolation are mediated by CRF receptors in the dorsal raphe nucleus. Brain Res Bull. 2011 May 30;85(3-4):117-22.

39. Bliss Tim V.P., Collingridge Graham L., Morris Richard G.M. and Reymann, Klaus G.. “Long-term potentiation in the hippocampus: discovery, mechanisms and function” Neuroforum, vol. 24, no. 3, 2018, pp. A103-A120.

40. Bliss TV, Collingridge GL. A synaptic model of memory: long-term potentiation in the hippocampus. Nature. 1993 Jan 7;361(6407):31-9.

41. Bliss TV, Lomo T. Long-lasting potentiation of synaptic transmission in the dentate area of the anaesthetized rabbit following stimulation of the perforant path. J Physiol. 1973 Jul;232(2):331-56.

42. Bodart C, Rossetti N, Hagler J, Chevreau P, Chhin D, Soavi F, Schougaard SB, Amzica F, Cicoira F. Electropolymerized Poly(3,4-ethylenedioxythiophene) (PEDOT) Coatings for Implantable Deep-Brain-Stimulating Microelectrodes. ACS Appl Mater Interfaces. 2019 May 15;11(19):17226-17233.

43. Bolshakov VY, Golan H, Kandel ER, Siegelbaum SA. Recruitment of new sites of synaptic transmission during the cAMP-dependent late phase of LTP at CA3-CA1 synapses in the hippocampus. Neuron. 1997 Sep;19(3):635-51.

44. Bonne O, Brandes D, Gilboa A, Gomori JM, Shenton ME, Pitman RK, Shalev AY. Longitudinal MRI study of hippocampal volume in trauma survivors with PTSD. Am J Psychiatry. 2001 Aug;158(8):1248-51.

45. Bramini M, Alberini G, Colombo E, Chiacchiaretta M, DiFrancesco ML, Maya-Vetencourt JF, Maragliano L, Benfenati F, Cesca F. Interfacing Graphene-Based Materials With Neural Cells. Front Syst Neurosci. 2018 Apr 11;12:12.

46. Bramini M, Sacchetti S, Armirotti A, Rocchi A, Vázquez E, León Castellanos V, Bandiera T, Cesca F, Benfenati F. Graphene Oxide Nanosheets Disrupt Lipid Composition, Ca(2+) Homeostasis, and Synaptic Transmission in Primary Cortical Neurons. ACS Nano. 2016 Jul 26;10(7):7154-71.

47. Brandon EP, Zhuo M, Huang YY, Qi M, Gerhold KA, Burton KA, Kandel ER, McKnight GS, Idzerda RL. Hippocampal long-term depression and depotentiation are defective in mice carrying a targeted disruption of the gene encoding the RI beta subunit of cAMP-dependent protein kinase. Proc Natl Acad Sci U S A. 1995 Sep 12;92(19):8851-5.

48. Brocke KS, Staufner C, Luksch H, Geiger KD, Stepulak A, Marzahn J, Schackert G, Temme A, Ikonomidou C. Glutamate receptors in pediatric tumors of the central nervous system. Cancer Biol Ther. 2010 Mar 15;9(6):455-68.

49. Broqua P, Wettstein JG, Rocher MN, Gauthier-Martin B, Junien JL. Behavioral effects of neuropeptide Y receptor agonists in the elevated plus-maze and fear-potentiated startle procedures. Behav Pharmacol. 1995,6:215-222.

50. Brothers SP, Wahlestedt C. Therapeutic potential of neuropeptide Y (NPY) receptor ligands. EMBO Mol Med. 2010;2:429-39.

51. Brzosko Z, Mierau SB, Paulsen O. Neuromodulation of Spike-Timing-Dependent Plasticity: Past, Present, and Future. Neuron. 2019 Aug 21;103(4):563-581.

52. Budde T, Mager R, Pape HC. Different Types of Potassium Outward Current in Relay Neurons Acutely Isolated from the Rat Lateral Geniculate Nucleus. Eur J Neurosci. 1992;4(8):708-722.

53. Buffalari DM, Grace AA. Noradrenergic modulation of basolateral amygdala neuronal activity: opposing influences of alpha-2 and beta receptor activation. J Neurosci. 2007 Nov 7;27(45):12358-66.

54. Burra N, Hervais-Adelman A, Kerzel D, Tamietto M, de Gelder B, Pegna AJ. Amygdala activation for eye contact despite complete cortical blindness. J Neurosci. 2013 Jun 19;33(25):10483-9.

55. Buskila Y, Breen PP, Tapson J, van Schaik A, Barton M, Morley JW. Extending the viability of acute brain slices. Sci Rep. 2014 Jun 16;4:5309.

56. Butler PD, Weiss JM, Stout JC, Nemeroff CB. Corticotropin-releasing factor produces fear-enhancing and behavioral activating effects following infusion into the locus coeruleus. J Neurosci. 1990 Jan;10(1):176-83.

57. Caberlotto L, Fuxe K, Hurd YL. Characterization of NPY mRNA-expressing cells in the human brain: co-localization with Y2 but not Y1 mRNA in the cerebral cortex, hippocampus, amygdala, and striatum. J Chem Neuroanat. 2000;20:327-37.

58. Cabrele C, Beck-Sickinger AG. Molecular characterization of the ligand-receptor interaction of the neuropeptide Y family. J Pept Sci. 2000 Mar;6(3):97-122.

59. Cao W, He L, Cao W, Huang X, Jia K, Dai J. Recent progress of graphene oxide as a potential vaccine carrier and adjuvant. Acta Biomater. 2020 Aug;112:14-28.

60. Capogrosso M, Milekovic T, Borton D, Wagner F, Moraud EM, Mignardot JB, Buse N, Gandar J, Barraud Q, Xing D, Rey E, Duis S, Jianzhong Y, Ko WK, Li Q, Detemple P, Denison T, Micera S, Bezard E, Bloch J, Courtine G. A brain-spine interface alleviating gait deficits after spinal cord injury in primates. Nature. 2016 Nov 10;539(7628):284-288.

61. Castro EV, Novoselov KS, Morozov SV, Peres NM, Lopes dos Santos JM, Nilsson J, Guinea F, Geim AK, Castro Neto AH. Electronic properties of a biased graphene bilayer. J Phys Condens Matter. 2010 May 5;22(17):175503.

62. Cellot G, Franceschi Biagioni A, Ballerini L. Nanomedicine and graphene-based materials: advanced technologies for potential treatments of diseases in the developing nervous system. Pediatr Res. 2022 Jul;92(1):71-79.

63. Cellot G, Vranic S, Shin Y, Worsley R, Rodrigues AF, Bussy C, Casiraghi C, Kostarelos K, McDearmid JR. Graphene oxide nanosheets modulate spinal glutamatergic transmission and modify locomotor behaviour in an in vivo zebrafish model. Nanoscale Horiz. 2020 Aug 1;5(8):1250-1263.

64. Chai D, Hao B, Hu R, Zhang F, Yan J, Sun Y, Huang X, Zhang Q, Jiang H. Delivery of Oridonin and Methotrexate via PEGylated Graphene Oxide. ACS Appl Mater Interfaces. 2019 Jul 3;11(26):22915-22924.

65. Chapman PF, Kairiss EW, Keenan CL, Brown TH. Long-term synaptic potentiation in the amygdala. Synapse. 1990;6(3):271-8.

66. Chen Y, Liu L. Modern methods for delivery of drugs across the blood-brain barrier. Adv Drug Deliv Rev. 2012 May 15;64(7):640-65.

67. Chhatwal JP, Stanek-Rattiner L, Davis M, Ressler KJ. Amygdala BDNF signaling is required for consolidation but not encoding of extinction. Nat Neurosci. 2006 Jul;9(7):870-2.

68. Chiacchiaretta M, Bramini M, Rocchi A, Armirotti A, Giordano E, Vázquez E, Bandiera T, Ferroni S, Cesca F, Benfenati F. Graphene Oxide Upregulates the Homeostatic Functions of Primary Astrocytes and Modulates Astrocyte-to-Neuron Communication. Nano Lett. 2018 Sep 12;18(9):5827-5838.

69. Cipriani A, Furukawa TA, Salanti G, Geddes JR, Higgins JP, Churchill R, Watanabe N, Nakagawa A, Omori IM, McGuire H, Tansella M, Barbui C. Comparative efficacy and acceptability of 12 new-generation antidepressants: a multiple-treatments meta-analysis. Lancet. 2009 Feb 28;373(9665):746-58.

70. Coan AC, Morita ME, Campos BM, Bergo FP, Kubota BY, Cendes F. Amygdala enlargement occurs in patients with mesial temporal lobe epilepsy and hippocampal sclerosis with early epilepsy onset. Epilepsy Behav. 2013 Nov;29(2):390-4.

71. Cohen H, Kaplan Z, Matar MA, Loewenthal U, Zohar J, Richter-Levin G. Long-lasting behavioral effects of juvenile trauma in an animal model of PTSD associated with a failure of the autonomic nervous system to recover. Eur Neuropsychopharmacol. 2007 May-Jun;17(6-7):464-77.

72. Cohen H, Liu T, Kozlovsky N, Kaplan Z, Zohar J, Mathé AA. The neuropeptide Y (NPY)-ergic system is associated with behavioral resilience to stress exposure in an animal model of post-traumatic stress disorder. Neuropsychopharmacology. 2012;37:350-63.

73. Cohen MR, Moiseenkova-Bell VY. Structure of thermally activated TRP channels. Curr Top Membr. 2014;74:181-211.

74. Collingridge GL, Peineau S, Howland JG, Wang YT. Long-term depression in the CNS. Nat Rev Neurosci. 2010 Jul;11(7):459-73.

75. Colmers WF, El Bahh B. Neuropeptide Y and Epilepsy. Epilepsy Curr. 2003 Mar;3(2):53-58.

76. Colmers WF, Lukowiak K, Pittma QJ. Neuropeptide Y Action in the Rat Hippocampal slices: Site and Mechanism of Presynaptic Inhibition. J. Neurosci. 1988;8:3827–3837

77. Conlon P, Kertesz A, Mount J. Kluver Bucy syndrome with severe amnesia secondary to herpes encephalitis. Can J Psychiatry. 1988 Nov;33(8):754-6.

78. Contractor A, Klyachko VA, Portera-Cailliau C. Altered Neuronal and Circuit Excitability in Fragile X Syndrome. Neuron. 2015 Aug 19;87(4):699-715.

79. Cormier RJ, Mauk MD, Kelly PT. Glutamate iontophoresis induces long-term potentiation in the absence of evoked presynaptic activity. Neuron. 1993 May;10(5):907-19.

80. Cortese BM, Phan KL. The role of glutamate in anxiety and related disorders. CNS Spectr. 2005 Oct;10(10):820-30.

81. Cote LJ, Kim F, Huang J. Langmuir-Blodgett assembly of graphite oxide single layers. J Am Chem Soc. 2009 Jan 28;131(3):1043-9.

82. Coyle JT. The glutamatergic dysfunction hypothesis for schizophrenia. Harv Rev Psychiatry. 1996 Jan-Feb;3(5):241-53.

83. Craske MG, Kircanski K, Zelikowsky M, Mystkowski J, Chowdhury N, Baker A. Optimizing inhibitory learning during exposure therapy. Behav Res Ther. 2008 Jan;46(1):5-27.

84. Dan Y, Poo MM. Spike timing-dependent plasticity: from synapse to perception. Physiol Rev. 2006 Jul;86(3):1033-48.

85. Darwin C. The Expression of the Emotions in Man and Animals. Chicago, IL: Univ. of Chicago Press 1872.

86. Davies SN, Lester RA, Reymann KG, Collingridge GL. Temporally distinct pre- and post-synaptic mechanisms maintain long-term potentiation. Nature. 1989 Apr;338(6215):500-503.

87. Davis M, Rainnie D, Cassell M. Neurotransmission in the rat amygdala related to fear and anxiety. Trends Neurosci. 1994 May;17(5):208-14.

88. Debanne D, Guérineau NC, Gähwiler BH, Thompson SM. Paired-pulse facilitation and depression at unitary synapses in rat hippocampus: quantal fluctuation affects subsequent release. J Physiol. 1996 Feb 15;491 (Pt 1)(Pt 1):163-76.

89. Debanne D, Guérineau NC, Gähwiler BH, Thompson SM. Paired-pulse facilitation and depression at unitary synapses in rat hippocampus: quantal fluctuation affects subsequent release. J Physiol. 1996 Feb 15;491 (Pt 1)(Pt 1):163-76.

90. Delahanty DL, Nugent NR. Predicting PTSD prospectively based on prior trauma history and immediate biological responses. Ann N Y Acad Sci. 2006 Jul;1071:27-40.

91. Di Mauro G, Rauti R, Casani R, Chimowa G, Galibert AM, Flahaut E, Cellot G, Ballerini L. Tuning the Reduction of Graphene Oxide Nanoflakes Differently Affects Neuronal Networks in the Zebrafish. Nanomaterials (Basel). 2021 Aug 24;11(9):2161.

92. Dideikin AT and Vul' AY. Graphene Oxide and Derivatives: The Place in Graphene Family. Front. Phys. 2019;6:149.

93. Diehl LA, Alvares LO, Noschang C, Engelke D, Andreazza AC, Gonçalves CA, Quillfeldt JA, Dalmaz C. Long-lasting effects of maternal separation on an animal model of post-traumatic stress disorder: effects on memory and hippocampal oxidative stress. Neurochem Res. 2012 Apr;37(4):700-7.

94. Dielenberg RA, Hunt GE, McGregor IS. "When a rat smells a cat": the distribution of Fos immunoreactivity in rat brain following exposure to a predatory odor. Neuroscience. 2001;104(4):1085-97.

95. Dong X, Shi Y, Huang W, Chen P, Li LJ. Electrical detection of DNA hybridization with single-base specificity using transistors based on CVD-grown graphene sheets. Adv Mater. 2010 Apr 12;22(14):1649-53.

96. Drexler, E.K. Engines of Creation: The Coming Era of Nanotechnology; Anchor Press: Garden City, NY, USA, 1986.

97. Drexler, E.K.; Peterson, C.; Pergamit, G. Unbounding the Future: The Nanotechnology Revolution; William Morrow and Company, Inc.: New York, NY, USA, 1991.

98. Duval ER, Sheynin J, King AP, Phan KL, Simon NM, Martis B, Porter KE, Norman SB, Liberzon I, Rauch SAM. Neural function during emotion processing and modulation associated with treatment response in a randomized clinical trial for posttraumatic stress disorder. Depress Anxiety. 2020 Jul;37(7):670-681.

99. Duvarci S, Paré D. Glucocorticoids enhance the excitability of principal basolateral amygdala neurons. J Neurosci. 2007 Apr 18;27(16):4482-91.

100. Eduardo E. Benarroch, Clinical Implications Of Neuroscience Research, Neurology (2016).

101. Egan MF, Kojima M, Callicott JH, Goldberg TE, Kolachana BS, Bertolino A, Zaitsev E, Gold B, Goldman D, Dean M, Lu B, Weinberger DR. The BDNF val66met polymorphism affects activity-dependent secretion of BDNF and human memory and hippocampal function. Cell. 2003 Jan 24;112(2):257-69.

102. Ehlers CL, Somes C, Lopez A, Kirby D, Rivier JE. Electrophysiological actions of neuropeptide Y and its analogs: new measures for anxiolytic therapy? Neuropsychopharmacology. 1997;17:34-43.

103. Ehrlich I, Humeau Y, Grenier F, Ciocchi S, Herry C, Lüthi A. Amygdala inhibitory circuits and the control of fear memory. Neuron. 2009 Jun 25;62(6):757-71.

104. El Bahh B, Cao JQ, Beck-Sickinger AG, Colmers WF. Blockade of neuropeptide Y(2) receptors and suppression of NPY's anti-epileptic actions in the rat hippocampal slice by BIIE0246. Br J Pharmacol. 2002 Jun;136(4):502-9.

105. Elias DC, Nair RR, Mohiuddin TM, Morozov SV, Blake P, Halsall MP, Ferrari AC, Boukhvalov DW, Katsnelson MI, Geim AK, Novoselov KS. Control of graphene's properties by reversible hydrogenation: evidence for graphane. Science. 2009 Jan 30;323(5914):610-3.

106. English JD and Sweatt JD. A requirement for the mitogen activated protein kinase cascade in hippocampal long term potentiation. Biol Chem 1997;272:19103–19116.

107. Esteves da Silva, J.C.G.; Gonçalves, H.M.R. Analytical and bioanalytical applications of carbon dots. TrAC Trends Anal. Chem. 2011, 30, 1327–1336.

108. Etherton MR, Tabuchi K, Sharma M, Ko J, Südhof TC. An autism-associated point mutation in the neuroligin cytoplasmic tail selectively impairs AMPA receptor-mediated synaptic transmission in hippocampus. EMBO J. 2011 Jun 3;30(14):2908-19.

109. Faber ES, Delaney AJ, Power JM, Sedlak PL, Crane JW, Sah P. Modulation of SK channel trafficking by beta adrenoceptors enhances excitatory synaptic transmission and plasticity in the amygdala. J Neurosci. 2008 Oct 22;28(43):10803-13.

110. Fadeel B, Bussy C, Merino S, Vázquez E, Flahaut E, Mouchet F, Evariste L, Gauthier L, Koivisto AJ, Vogel U, Martín C, Delogu LG, Buerki-Thurnherr T, Wick P, Beloin-Saint-Pierre D, Hischier R, Pelin M, Candotto Carniel F, Tretiach M, Cesca F, Benfenati F, Scaini D, Ballerini L, Kostarelos K, Prato M, Bianco A. Safety Assessment of Graphene-Based Materials: Focus on Human Health and the Environment. ACS Nano. 2018 Nov 27;12(11):10582-10620.

111. Fang Y, Jiang Y, Acaron Ledesma H, Yi J, Gao X, Weiss DE, Shi F, Tian B. Texturing Silicon Nanowires for Highly Localized Optical Modulation of Cellular Dynamics. Nano Lett. 2018 Jul 11;18(7):4487-4492.

112. Feldman De, Nicoll RA, and Malenka RC. Synaptic plasticity at thalamocortical synapses in developing rat somatosensory cortex: LTP, LTD, and silent synapses. J Neurobiol 1999;41:92–101.

113. Feldman DE. The spike-timing dependence of plasticity. Neuron. 2012 Aug 23;75(4):556-71.

114. Fendt M, Bürki H, Imobersteg S, Lingenhöhl K, McAllister KH, Orain D, Uzunov DP, Chaperon F. Fear-reducing effects of intra-amygdala neuropeptide Y infusion in animal models of conditioned fear: an NPY Y1 receptor independent effect. Psychopharmacology (Berl), 2009; 206:291-301.

115. Fendt M. Injections of the NMDA receptor antagonist aminophosphonopentanoic acid into the lateral nucleus of the amygdala block the expression of fear-potentiated startle and freezing. J Neurosci. 2001 Jun 1;21(11):4111-5.

116. Feng, L., Wu, L., and Qu, X. New Horizons for Diagnostics and Therapeutic Applications of Graphene and Graphene Oxide. Adv. Mater. 2013; 25, 168–186.

117. Feynman R.P. There's plenty of room at the bottom. Eng. Sci. 1960;23: 22–36.

118. File SE. The use of social interaction as a method for detecting anxiolytic activity of chlordiazepoxide-like drugs. J Neurosci Methods. 1980;2:219-38.

119. Fitzjohn SM, Pickard L, Duckworth JK, Molnar E, Henley JM, Collingridge GL, Noël J. An electrophysiological characterisation of long-term potentiation in cultured dissociated hippocampal neurones. Neuropharmacology. 2001 Nov;41(6):693-9.

120. Fonnum F. Glutamate: a neurotransmitter in mammalian brain. J Neurochem. 1984 Jan;42(1):1-11.

121. Foo CY, Fu RZ. Unravelling the potential of graphene in glioblastoma therapy. Mater Sci Eng C Mater Biol Appl. 2021 Sep;128:112330.

122. Forster, G. L. , Novick, A. M. , Scholl, J. L. , Watt, M. J. . The Role of the Amygdala in Anxiety Disorders. In: Ferry, B. , editor. The Amygdala – A Discrete Multitasking Manager [Internet]. London: IntechOpen; 2012.

123. Franceschi Biagioni A, Cellot G, Pati E, Lozano N, Ballesteros B, Casani R, Coimbra NC, Kostarelos K, Ballerini L. Graphene oxide prevents lateral amygdala dysfunctional synaptic plasticity and reverts long lasting anxiety behavior in rats. Biomaterials. 2021 Apr;271:120749.

124. Gallagher M, Holland PC. The amygdala complex: multiple roles in associative learning and attention. Proc Natl Acad Sci U S A. 1994 Dec 6;91(25):11771-6. Doi: 10.1073/pnas.91.25.11771. PMID: 7991534; PMCID: PMC45317.

125. Galvin C, Lee FS, Ninan I. Alteration of the Centromedial Amygdala Glutamatergic Synapses by the BDNF Val66Met Polymorphism. Neuropsychopharmacology. 2015 Aug;40(9):2269-77.

126. Garcia-Etxarri A, Yuste R. Time for NanoNeuro. Nat Methods. 2021 Nov;18(11):1287-1293.

127. Gasparini S, Saviane C, Voronin LL, Cherubini E. Silent synapses in the developing hippocampus: lack of functional AMPA receptors or low probability of glutamate release? Proc Natl Acad Sci U S A. 2000 Aug 15;97(17):9741-6.

128. Gautam V, Naureen S, Shahid N, Gao Q, Wang Y, Nisbet D, Jagadish C, Daria VR. Engineering Highly Interconnected Neuronal Networks on Nanowire Scaffolds. Nano Lett. 2017 Jun 14;17(6):3369-3375.

129. Geim AK, Novoselov KS. The rise of graphene. Nat Mater. 2007 Mar;6(3):183-91.

130. Geim AK. Graphene: status and prospects. Science. 2009 Jun 19;324(5934):1530-4.

131. Georgakilas V, Tiwari JN, Kemp KC, Perman JA, Bourlinos AB, Kim KS, Zboril R. Noncovalent Functionalization of Graphene and Graphene Oxide for Energy Materials, Biosensing, Catalytic, and Biomedical Applications. Chem Rev. 2016 May 11;116(9):5464-519.

132. Gloor P, Vera CL, Sperti L. Electrophysiological studies of hippocampal neurons. 3. Responses of hippocampal neurons to repetitive perforant path volleys. Electroencephalogr Clin Neurophysiol. 1964 Oct;17:353-70.

133. Gloor P. Experiential phenomena of temporal lobe epilepsy. Facts and hypotheses. Brain. 1990 Dec;113 (Pt 6):1673-94.

134. Goldin M, Segal M, Avignone E. Functional plasticity triggers formation and pruning of dendritic spines in cultured hippocampal networks. J Neurosci. 2001 Jan 1;21(1):186-93.

135. Gonçalves G, Vila M, Bdikin I, de Andrés A, Emami N, Ferreira RA, Carlos LD, Grácio J, Marques PA. Breakdown into nanoscale of graphene oxide: confined hot spot atomic reduction and fragmentation. Sci Rep. 2014 Oct 23;4:6735.

136. Gorman JM, Kent JM, Sullivan GM, Coplan JD. Neuroanatomical hypothesis of panic disorder, revised. Am J Psychiatry. 2000 Apr;157(4):493-505.

137. Grastyan E, LissaK K, Madarasz I, Donhoffer H. Hippocampal electrical activity during the development of conditioned reflexes. Electroencephalogr Clin Neurophysiol. 1959 Aug;11(3):409-30.

138. Gray EG, Paula-Barbosa M, Roher A. Alzheimer's disease: paired helical filaments and cytomembranes. Neuropathol Appl Neurobiol. 1987 Mar-Apr;13(2):91-110.

139. Greengard P, Valtorta F, Czernik A, and Benfenati F. Synaptic vesicle phosphoproteins and regulation of synaptic function. Science 1993;259: 780–785.

140. Grosshans DR, Clayton DA, Coultrap SJ, Browning MD. LTP leads to rapid surface expression of NMDA but not AMPA receptors in adult rat CA1. Nat Neurosci. 2002 Jan;5(1):27-33.

141. Gui W, Zhang J, Chen X, Yu D, Ma Q. N-Doped graphene quantum dot@mesoporous silica nanoparticles modified with hyaluronic acid for fluorescent imaging of tumor cells and drug delivery. Mikrochim Acta. 2017 Dec 18;185(1):66.

142. Guimerà-Brunet A, Masvidal-Codina E, Cisneros-Fernández J, Serra-Graells F, Garrido JA. Novel transducers for high-channel-count neuroelectronic recording interfaces. Curr Opin Biotechnol. 2021 Dec;72:39-47.

143. Gutman AR, Yang Y, Ressler KJ, Davis M. The role of neuropeptide Y in the expression and extinction of fear-potentiated startle. J Neurosci. 2008;28:12682-90.

144. Hadley D, Wu ZL, Kao C, Kini A, Mohamed-Hadley A, Thomas K, Vazquez L, Qiu H, Mentch F, Pellegrino R, Kim C, Connolly J; AGP Consortium, Glessner J, Hakonarson H. The impact of the metabotropic glutamate receptor and other gene family interaction networks on autism. Nat Commun. 2014 Jun 13;5:4074.

145. Han S, Sun J, He S, Tang M, Chai R. The application of graphene-based biomaterials in biomedicine. Am J Transl Res. 2019 Jun 15;11(6):3246-3260.

146. Han X, Li S, Peng Z, Al-Yuobi AO, Omar Bashammakh AS, El-Shahawi MS, Leblanc RM. Interactions between Carbon Nanomaterials and Biomolecules. J Oleo Sci. 2016;65(1):1-7.

147. Hare TA, Tottenham N, Galvan A, Voss HU, Glover GH, Casey BJ. Biological substrates of emotional reactivity and regulation in adolescence during an emotional go-nogo task. Biol Psychiatry. 2008 May 15;63(10):927-34.

148. Harris AR , Allitt BJ , Paolini AG . Predicting neural recording performance of implantable electrodes. Analyst. 2019 Apr 23;144(9):2973-2983.

149. Hasan SA, Rigueur JL, Harl RR, Krejci AJ, Gonzalo-Juan I, Rogers BR, Dickerson JH. Transferable graphene oxide films with tunable microstructures. ACS Nano. 2010 Dec 28;4(12):7367-72.

150. Haziza S, Mohan N, Loe-Mie Y, Lepagnol-Bestel AM, Massou S, Adam MP, Le XL, Viard J, Plancon C, Daudin R, Koebel P, Dorard E, Rose C, Hsieh FJ, Wu CC, Potier B, Herault Y, Sala C, Corvin A, Allinquant B, Chang HC, Treussart F, Simonneau M. Fluorescent nanodiamond tracking reveals intraneuronal transport abnormalities induced by brain-disease-related genetic risk factors. Nat Nanotechnol. 2017 May;12(4):322-328.

151. Heilig M, Söderpalm B, Engel JA, Widerlöv E. Centrally administered neuropeptide Y (NPY) produces anxiolytic-like effects in animal anxiety models. Psychopharmacology (Berl) 1989;98:524-9.

152. Heilig M, Zachrisson O, Thorsell A, Ehnvall A, Mottagui-Tabar S, Sjögren M, Asberg M, Ekman R, Wahlestedt C, Agren H. Decreased cerebrospinal fluid neuropeptide Y (NPY) in patients with treatment refractory unipolar major depression: preliminary evidence for association with preproNPY gene polymorphism. J Psychiatr Res. 2004;38:113-21.

153. Heilig M. Antisense inhibition of neuropeptide Y (NPY)-Y1 receptor expression blocks the anxiolytic-like action of NPY in amygdala and paradoxically increases feeding. Regul Pept. 1995;59:201-5.

154. Heilig M. The NPY system in stress, anxiety and depression. Neuropeptides. 2004;38:213-24.

155. Hirai K, Yoshioka H, Kihara M, Hasegawa K, Sakamoto T, Sawada T, Fushiki S. Inhibiting neuronal migration by blocking NMDA receptors in the embryonic rat cerebral cortex: a tissue culture study. Brain Res Dev Brain Res. 1999 Apr 12;114(1):63-7.

156. Hopf FW, Seif T, Mohamedi ML, Chen BT, Bonci A. The small-conductance calcium-activated potassium channel is a key modulator of firing and long-term depression in the dorsal striatum. Eur J Neurosci. 2010 Jun;31(11):1946-59.

157. Hosokawa T, Rusakov DA, Bliss TV, Fine A. Repeated confocal imaging of individual dendritic spines in the living hippocampal slice: evidence for changes in length and orientation associated with chemically induced LTP. J Neurosci. 1995 Aug;15(8):5560-73.

158. Hostetler ED, Sanabria-Bohórquez S, Fan H, Zeng Z, Gantert L, Williams M, Miller P, O'Malley S, Kameda M, Ando M, Sato N, Ozaki S, Tokita S, Ohta H, Williams D, Sur C, Cook JJ, Burns HD, Hargreaves R. Synthesis, characterization, and monkey positron emission tomography (PET) studies of [18F]Y1-973, a PET tracer for the neuropeptide Y Y1 receptor. Neuroimage. 2011;54:2635-42.

159. Huang YY and Kandel ER. Postsynaptic induction and PKA-dependent expression of LTP in the lateral amygdala. Neuron 1998;21:169–178.

160. Huerta PT, Lisman JE. Bidirectional synaptic plasticity induced by a single burst during cholinergic theta oscillation in CA1 *in vitro*. Neuron. 1995 Nov;15(5):1053-63.

161. Huguet G, Ey E, Bourgeron T. The genetic landscapes of autism spectrum disorders. Annu Rev Genomics Hum Genet. 2013;14:191-213.

162. Hunn BH, Cragg SJ, Bolam JP, Spillantini MG, Wade-Martins R. Impaired intracellular trafficking defines early Parkinson's disease. Trends Neurosci. 2015 Mar;38(3):178-88.

163. Hutter-Schmid B, Kniewallner KM, Humpel C. Organotypic brain slice cultures as a model to study angiogenesis of brain vessels. Front Cell Dev Biol. 2015 Sep 2;3:52.

164. Iijima, S. Helical microtubules of graphitic carbon. Nature 1991;354:56–58.

165. Inglebert Y, Debanne D. Calcium and Spike Timing-Dependent Plasticity. Front Cell Neurosci. 2021 Sep 20;15:727336.

166. Isaac JT, Nicoll RA, Malenka RC. Evidence for silent synapses: implications for the expression of LTP. Neuron. 1995 Aug;15(2):427-34.

167. Ivenshitz M, Segal M. Simultaneous NMDA-dependent long-term potentiation of EPSCs and long-term depression of IPSCs in cultured rat hippocampal neurons. J Neurosci. 2006 Jan 25;26(4):1199-210.

168. Jagiello J, Chlanda A, Baran M, Gwiazda M, Lipińska L. Synthesis and Characterization of Graphene Oxide and Reduced Graphene Oxide Composites with Inorganic Nanoparticles for Biomedical Applications. Nanomaterials (Basel). 2020 Sep 15;10(9):1846.

169. James W. Principles of Psychology. New York: Holt 1890.

170. Jamjoom AAB, Rhodes J, Andrews PJD, Grant SGN. The synapse in traumatic brain injury. Brain. 2021 Feb 12;144(1):18-31.

171. Jampilek J, Kralova K. Advances in Drug Delivery Nanosystems Using Graphene-Based Materials and Carbon Nanotubes. Materials (Basel). 2021 Feb 24;14(5):1059.

172. Janak PH, Tye KM. From circuits to behaviour in the amygdala. Nature. 2015 Jan 15;517(7534):284-92.

173. Jarvis ED, et al. Avian brains and a new understanding of vertebrate brain evolution. Nature Rev. Neurosci. (2005).

174. Javitt DC, Zukin SR. Recent advances in the phencyclidine model of schizophrenia. Am J Psychiatry. 1991 Oct;148(10):1301-8.

175. Jayant K, Hirtz JJ, Plante IJ, Tsai DM, De Boer WD, Semonche A, Peterka DS, Owen JS, Sahin O, Shepard KL, Yuste R. Targeted intracellular voltage recordings from dendritic spines using quantum-dot-coated nanopipettes. Nat Nanotechnol. 2017 May;12(4):335-342.

176. Jayant K, Wenzel M, Bando Y, Hamm JP, Mandriota N, Rabinowitz JH, Plante IJ, Owen JS, Sahin O, Shepard KL, Yuste R. Flexible Nanopipettes for Minimally Invasive Intracellular Electrophysiology *In Vivo*. Cell Rep. 2019 Jan 2;26(1):266-278.e5.

177. Jeong YC, Lee HE, Shin A, Kim DG, Lee KJ, Kim D. Progress in Brain-Compatible Interfaces with Soft Nanomaterials. Adv Mater. 2020 Sep;32(35):e1907522.

178. Jiang H, Li FR, Li W, Lu X, Ling K. Multiplexed determination of intracellular messenger RNA by using a graphene oxide nanoprobe modified with target-recognizing fluorescent oligonucleotides. Mikrochim Acta. 2018 Nov 15;185(12):552.

179. Jiang, Biqiang, Kaiming Zhou, Changle Wang, Qizhen Sun, Guolu Yin, Zhijun Tai, Karen Wilson, Jianlin Zhao and Lin Zhang. Label-free glucose biosensor based on enzymatic graphene oxide-functionalized tilted fiber grating. Sensors and Actuators B-chemical 2018; 254: 1033-1039.

180. Johansen JP, Hamanaka H, Monfils MH, Behnia R, Deisseroth K, Blair HT, LeDoux JE. Optical activation of lateral amygdala pyramidal cells instructs associative fear learning. Proc Natl Acad Sci U S A. 2010 Jul 13;107(28):12692-7.

181. Johnston JB. Further contributions to the study of the evolution of the forebrain. J. Comp. Neurol. (1923).

182. Jolkkonen E, Pitkänen A. Intrinsic connections of the rat amygdaloid complex: projections originating in the central nucleus. J Comp Neurol. 1998 May 25;395(1):53-72.

183. KAADA BR. Somato-motor, autonomic and electrocorticographic responses to electrical stimulation of rhinencephalic and other structures in primates, cat, and dog; a study of responses from the limbic, subcallosal, orbito-insular, piriform and temporal cortex, hippocampus-fornix and amygdala. Acta Physiol Scand Suppl. 1951;24(83):1-262.

184. Kaneda M, Akaike N. The low-threshold Ca current in isolated amygdaloid neurons in the rat. Brain Res. 1989 Sep 11;497(1):187-90. Doi: 10.1016/0006-8993(89)90987-6. PMID: 2790453.

185. Kang P., Wang M.C. and Nam S., Bioelectronics with two-dimensional materials. Microelectron. Eng. 2016; 161:18-35

186. Kang Y, Liu J, Yin S, Jiang Y, Feng X, Wu J, Zhang Y, Chen A, Zhang Y, Shao L. Oxidation of Reduced Graphene Oxide via Cellular Redox Signaling Modulates Actin-Mediated Neurotransmission. ACS Nano. 2020 Mar 24;14(3):3059-3074.

187. Kargar S, Khoei S, Khoee S, Shirvalilou S, Mahdavi SR. Evaluation of the combined effect of NIR laser and ionizing radiation on cellular damages induced by IUdR-loaded PLGA-coated Nano-graphene oxide. Photodiagnosis Photodyn Ther. 2018 Mar;21:91-97.

188. Karlsson RM, Choe JS, Cameron HA, Thorsell A, Crawley JN, Holmes A, Heilig M. The neuropeptide Y Y1 receptor subtype is necessary for the anxiolytic-like effects of neuropeptide Y, but not the antidepressant-like effects of fluoxetine, in mice. Psychopharmacology (Berl). 2008;195:547-57.

189. Kask A, Harro J, von Hörsten S, Redrobe JP, Dumont Y, Quirion R. The neurocircuitry and receptor subtypes mediating anxiolytic-like effects of neuropeptide Y. Neurosci Biobehav Rev. 2002;26:259-83.

190. Kask A, Vasar E, Heidmets LT, Allikmets L, Wikberg JE. Neuropeptide Y Y(5) receptor antagonist CGP71683A: the effects on food intake and anxiety-related behavior in the rat. Eur J Pharmacol. 2001;414:215-24.

191. Kautz M, Charney DS, Murrough JW. Neuropeptide Y, resilience, and PTSD therapeutics. Neurosci Lett. 2017 May 10;649:164-169.

192. Kessler RC, McGonagle KA, Zhao S, Nelson CB, Hughes M, Eshleman S, Wittchen HU, Kendler KS. Lifetime and 12-month prevalence of DSM-III-R psychiatric disorders in the

United States. Results from the National Comorbidity Survey. Arch Gen Psychiatry. 1994 Jan;51(1):8-19.

193. Kessler RC, Petukhova M, Sampson NA, Zaslavsky AM, Wittchen H -U. Twelve-month and lifetime prevalence and lifetime morbid risk of anxiety and mood disorders in the United States. Int J Methods Psychiatr Res. 2012 Sep;21(3):169-84.

194. Khetani S, Ozhukil Kollath V, Kundra V, Nguyen MD, Debert C, Sen A, Karan K, Sanati-Nezhad A. Polyethylenimine Modified Graphene-Oxide Electrochemical Immunosensor for the Detection of Glial Fibrillary Acidic Protein in Central Nervous System Injury. ACS Sens. 2018 Apr 27;3(4):844-851.

195. Kikusui T, Takeuchi Y, Mori Y. Involvement of corticotropin-releasing factor in the retrieval process of fear-conditioned ultrasonic vocalization in rats. Physiol Behav. 2000 Nov 1-15;71(3-4):323-8.

196. Kile SJ, Ellis WG, Olichney JM, Farias S, DeCarli C. Alzheimer abnormalities of the amygdala with Klüver-Bucy syndrome symptoms: an amygdaloid variant of Alzheimer disease. Arch Neurol. 2009 Jan;66(1):125-9.

197. Killcross S, Robbins TW, Everitt BJ. Different types of fear-conditioned behaviour mediated by separate nuclei within amygdala. Nature. 1997 Jul 24;388(6640):377-80. Doi: 10.1038/41097. PMID: 9237754.

198. King PJ, Widdowson PS, Doods HN, Williams G. Regulation of neuropeptide Y release by neuropeptide Y receptor ligands and calcium channel antagonists in hypothalamic slices. J Neurochem. 1999 Aug;73(2):641-6.

199. Kirkpatrick HA, Heller GM. Post-traumatic stress disorder: theory and treatment update. Int J Psychiatry Med. 2014;47(4):337-46.

200. Klapstein GJ, Colmers WF. On the Sites of Presynaptic Inhibition by Neuropeptide Y in Rat Hippocampus in vitro. Hippocampus 1993;3:103–112.

201. Klein RC, Acheson SK, Mace BE, Sullivan PM, Moore SD. Altered neurotransmission in the lateral amygdala in aged human apoE4 targeted replacement mice. Neurobiol Aging. 2014 Sep;35(9):2046-52.

202. Klüver, H., & Bucy, P. C. “Psychic blindness” and other symptoms following bilateral temporal lobectomy in Rhesus monkeys. American Journal of Physiology, 1973.

203. Kopec CD, Real E, Kessels HW, Malinow R. GluR1 links structural and functional plasticity at excitatory synapses. J Neurosci. 2007 Dec 12;27(50):13706-18.

204. Kostarelos K, Novoselov KS. Materials science. Exploring the interface of graphene and biology. Science. 2014 Apr 18;344(6181):261-3.

205. Kostarelos K, Vincent M, Hebert C, Garrido JA. Graphene in the Design and Engineering of Next-Generation Neural Interfaces. Adv Mater. 2017 Nov;29(42).

206. Kotov, N.A., Winter, J.O., Clements, I.P., Jan, E., Timko, B.P., Campidelli, S., Pathak, S., Mazzatenta, A., Lieber, C.M., Prato, M., Bellamkonda, R.V., Silva, G.A., Kam, N.W.S., Patolsky, F. and Ballerini, L. Nanomaterials for Neural Interfaces. Adv. Mater., 2009; 21(4): 3970-4004.

207. Krishna KV, Ménard-Moyon C, Verma S, Bianco A. Graphene-based nanomaterials for nanobiotechnology and biomedical applications. Nanomedicine (Lond). 2013 Oct;8(10):1669-88.

208. Kurapati, R.; Bonachera, F.; Russier, J.; Sureshbabu, A. R.; Ménard-Moyon, C.; Kostarelos, K.; Bianco, A. Covalent Chemical Functionalization Enhances the Biodegradation of Graphene Oxide. 2D Mater. 2018.

209. Kwon JT, Choi JS. Cornering the fear engram: long-term synaptic changes in the lateral nucleus of the amygdala after fear conditioning. J Neurosci. 2009 Aug 5;29(31):9700-3.

210. Lanuza E, Belekhova M, Martínez-Marcos A, Font C, Martínez-García F. Identification of the reptilian basolateral amygdala: an anatomical investigation of the afferents to the posterior dorsal ventricular ridge of the lizard Podarcis hispanica. Eur. J. Neurosci. (1998).

211. Larson J, Lynch G. Induction of synaptic potentiation in hippocampus by patterned stimulation involves two events. Science. 1986 May 23;232(4753):985-8.

212. Larson J, Munkácsy E. Theta-burst LTP. Brain Res. 2015 Sep 24;1621:38-50.

213. le Feber J. *In Vitro* Models of Brain Disorders. Adv Neurobiol. 2019;22:19-49.

214. LeDoux J. Fear and the brain: where have we been, and where are we going? Biol Psychiatry. 1998 Dec 15;44(12):1229-38.

215. LeDoux J. The emotional brain, fear, and the amygdala. Cell Mol Neurobiol. (2003).

216. LeDoux JE, Cicchetti P, Xagoraris A, Romanski LM. The lateral amygdaloid nucleus: sensory interface of the amygdala in fear conditioning. J Neurosci. 1990 Apr;10(4):1062-9.

217. LeDoux JE, Farb C, Ruggiero DA. Topographic organization of neurons in the acoustic thalamus that project to the amygdala. J Neurosci. 1990 Apr;10(4):1043-54.

218. LeDoux JE. Brain mechanisms of emotion and emotional learning. Curr Opin Neurobiol. 1992 Apr;2(2):191-7.

219. LeDoux JE. Emotion circuits in the brain. Annu Rev Neurosci. 2000;23:155-84.

220. Lee C, Wei X, Kysar JW, Hone J. Measurement of the elastic properties and intrinsic strength of monolayer graphene. Science. 2008 Jul 18;321(5887):385-8.

221. Lee HJ, Choi JS, Brown TH, Kim JJ. Amygdalar nmda receptors are critical for the expression of multiple conditioned fear responses. J Neurosci. 2001 Jun 1;21(11):4116-24.

222. Lengyel I, Voss K, Cammarota M, Bradshaw K, Brent V, Murphy KP, Giese KP, Rostas JA, Bliss TV. Autonomous activity of CaMKII is only transiently increased following the induction of long-term potentiation in the rat hippocampus. Eur J Neurosci. 2004 Dec;20(11):3063-72.

223. Lepeta K, Lourenco MV, Schweitzer BC, Martino Adami PV, Banerjee P, Catuara-Solarz S, de La Fuente Revenga M, Guillem AM, Haidar M, Ijomone OM, Nadorp B, Qi L, Perera ND, Refsgaard LK, Reid KM, Sabbar M, Sahoo A, Schaefer N, Sheean RK, Suska A, Verma R, Vicidomini C, Wright D, Zhang XD, Seidenbecher C. Synaptopathies: synaptic dysfunction in neurological disorders - A review from students to students. J Neurochem. 2016 Sep;138(6):785-805.

224. Letzkus JJ, Kampa BM, Stuart GJ. Does spike timing-dependent synaptic plasticity underlie memory formation? Clin Exp Pharmacol Physiol. 2007 Oct;34(10):1070-6.

225. Li N, Zhang Q, Gao S, Song Q, Huang R, Wang L, Liu L, Dai J, Tang M, Cheng G. Three-dimensional graphene foam as a biocompatible and conductive scaffold for neural stem cells. Sci Rep. 2013;3:1604.

226. Li N, Zhang X, Song Q, Su R, Zhang Q, Kong T, Liu L, Jin G, Tang M, Cheng G. The promotion of neurite sprouting and outgrowth of mouse hippocampal cells in culture by graphene substrates. Biomaterials. 2011 Dec;32(35):9374-82.

227. Liang S, Wang B, Li X, et al. *In vivo* pharmacokinetics, transfer and clearance study of graphene oxide by La/Ce dual elemental labelling method. NanoImpact 2020 Feb; 17:100213

228. Liao D, Hessler NA, and Malinow R. Activation of postsynaptically silent synapses during pairing-induced LTP in CA1 region of hippocampal slice. Nature 1995;375:400–404.

229. Liao D, Scannevin RH, Huganir R. Activation of silent synapses by rapid activity-dependent synaptic recruitment of AMPA receptors. J Neurosci. 2001 Aug 15;21(16):6008-17.

230. Liao D, Zhang X, O'Brien R, Ehlers MD, Huganir RL. Regulation of morphological postsynaptic silent synapses in developing hippocampal neurons. Nat Neurosci. 1999 Jan;2(1):37-43.

231. Lin CH, Huang YC, Tsai JJ, Gean PW. Modulation of voltage-dependent calcium currents by serotonin in acutely isolated rat amygdala neurons. Synapse. 2001 Sep 15;41(4):351-9.

232. Littlejohn, S.D. Electrical Properties of Graphite Nanoparticles in Silicone. Cham: Springer International Publishing 2014.

233. Liu C, Luo X. Potential molecular and graphene oxide chelators to dissolve amyloid-β plaques in Alzheimer's disease: a density functional theory study. J Mater Chem B. 2021 Mar 21;9(11):2736-2746.

234. Liu S, Chevali VS, Xu Z, Hui D, Wang H, A review of extending performance of epoxy resins using carbon nanomaterials, Composites Part B. 2017;136:197:214.

235. Liu X, Kumar V, Tsai NP, Auerbach BD. Hyperexcitability and Homeostasis in Fragile X Syndrome. Front Mol Neurosci. 2022 Jan 6;14:805929.

236. Liu Y, Xu LP, Dai W, Dong H, Wen Y, Zhang X. Graphene quantum dots for the inhibition of β amyloid aggregation. Nanoscale. 2015 Dec 7;7(45):19060-5.

237. Liu Z, Robinson JT, Sun X, Dai H. PEGylated nanographene oxide for delivery of water-insoluble cancer drugs. J Am Chem Soc. 2008 Aug 20;130(33):10876-7.

238. Llenas M, Sandoval S, Costa PM, Oró-Solé J, Lope-Piedrafita S, Ballesteros B, Al-Jamal KT, Tobias G. Microwave-Assisted Synthesis of SPION-Reduced Graphene Oxide Hybrids for Magnetic Resonance Imaging (MRI). Nanomaterials (Basel). 2019 Sep 24;9(10):1364.

239. Loddenkemper T, Pan A, Neme S, Baker KB, Rezai AR, Dinner DS, Montgomery EB Jr, Lüders HO. Deep brain stimulation in epilepsy. J Clin Neurophysiol. 2001 Nov;18(6):514-32.

240. Lømo T. Discovering long-term potentiation (LTP) – recollections and reflections on what came after. Acta Physiol (Oxf). 2018 Feb;222(2).

241. Lømo, T. Frequency potentiation of excitatory synaptic activity in the dentate area of the hippocampal formation. Acta Physiol Scand 1996;68 (suppl. 277): 128.

242. Lu W, Man H, Ju W, Trimble WS, MacDonald JF, Wang YT. Activation of synaptic NMDA receptors induces membrane insertion of new AMPA receptors and LTP in cultured hippocampal neurons. Neuron. 2001 Jan;29(1):243-54.

243. Lynch GS, Dunwiddie T, Gribkoff V. Heterosynaptic depression: a postsynaptic correlate of long-term potentiation. Nature. 1977 Apr 21;266(5604):737-9.

244. Lynch MA. Age-related impairment in long-term potentiation in hippocampus: a role for the cytokine, interleukin-1 beta? Prog Neurobiol. 1998 Dec;56(5):571-89.

245. Lynch MA. Long-term potentiation and memory. Physiol Rev. 2004 Jan;84(1):87-136.

246. MacDonald JF, Ju W, Wang YT. LTP in a culture dish. ScientificWorldJournal. 2001 May 11;1:213-5.

247. MacMaster FP. Translational neuroimaging research in pediatric obsessive-compulsive disorder. Dialogues Clin Neurosci. 2010;12(2):165-74.

248. Madison DV, Malenka RC, Nicoll RA. Mechanisms underlying long-term potentiation of synaptic transmission. Annu Rev Neurosci. 1991;14:379-97.

249. Magee JC, Johnston D. A synaptically controlled, associative signal for Hebbian plasticity in hippocampal neurons. Science. 1997 Jan 10;275(5297):209-13.

250. Mahanty NK, Sah P. Calcium-permeable AMPA receptors mediate long-term potentiation in interneurons in the amygdala. Nature. 1998 Aug 13;394(6694):683-7.

251. Makino H, Malinow R. AMPA receptor incorporation into synapses during LTP: the role of lateral movement and exocytosis. Neuron. 2009 Nov 12;64(3):381-90.

252. Malenka RC, Bear MF. LTP and LTD: an embarrassment of riches. Neuron. 2004 Sep 30;44(1):5-21.

253. Malenka RC, Kauer JA, Perkel DJ, Mauk MD, Kelly PT, Nicoll RA, Waxham MN. An essential role for postsynaptic calmodulin and protein kinase activity in long-term potentiation. Nature. 1989 Aug 17;340(6234):554-7.

254. Maletic-Savatic M, Koothan T, Malinow R. Calcium-evoked dendritic exocytosis in cultured hippocampal neurons. Part II: mediation by calcium/calmodulin-dependent protein kinase II. J Neurosci. 1998 Sep 1;18(17):6814-21.

255. Malgaroli A, Tsien RW. Glutamate-induced long-term potentiation of the frequency of miniature synaptic currents in cultured hippocampal neurons. Nature. 1992 May 14;357(6374):134-9.

256. Malinow R, Schulman H, Tsien RW. Inhibition of postsynaptic PKC or CaMKII blocks induction but not expression of LTP. Science. 1989 Aug 25;245(4920):862-6.

257. Manabe T, Wyllie DJ, Perkel DJ, Nicoll RA. Modulation of synaptic transmission and long-term potentiation: effects on paired pulse facilitation and EPSC variance in the CA1 region of the hippocampus. J Neurophysiol. 1993 Oct;70(4):1451-9.

258. Maren, S., Aharonov, G., and Fanselow, M. S. Neurotoxic lesions of the dorsal hippocampus and Pavlovian fear conditioning in rats. Behav. Brain Res. (1997).

259. Markovic ZM, Harhaji-Trajkovic LM, Todorovic-Markovic BM, Kepić DP, Arsikin KM, Jovanović SP, Pantovic AC, Dramićanin MD, Trajkovic VS. *In vitro* comparison of the photothermal anticancer activity of graphene nanoparticles and carbon nanotubes. Biomaterials. 2011 Feb;32(4):1121-9.

260. Markram H, Lübke J, Frotscher M, Sakmann B. Regulation of synaptic efficacy by coincidence of postsynaptic Aps and EPSPs. Science. 1997 Jan 10;275(5297):213-5.

261. Marowsky A, Yanagawa Y, Obata K, Vogt KE. A specialized subclass of interneurons mediates dopaminergic facilitation of amygdala function. Neuron. 2005 Dec 22;48(6):1025-37.

262. Martin BS, Corbin JG, Huntsman MM. Deficient tonic GABAergic conductance and synaptic balance in the fragile X syndrome amygdala. J Neurophysiol. 2014 Aug 15;112(4):890-902.

263. Masneuf S, Lowery-Gionta E, Colacicco G, Pleil KE, Li C, Crowley N, Flynn S, Holmes A, Kash T. Glutamatergic mechanisms associated with stress-induced amygdala excitability and anxiety-related behavior. Neuropharmacology. 2014 Oct;85:190-7.

264. McCool BA, Farroni JS. A1 adenosine receptors inhibit multiple voltage-gated Ca2+ channel subtypes in acutely isolated rat basolateral amygdala neurons. Br J Pharmacol. 2001 Feb;132(4):879-88. Doi: 10.1038/sj.bjp.0703884. PMID: 11181429; PMCID: PMC1572624.

265. McCool BA, Frye GD, Pulido MD, Botting SK. Effects of chronic ethanol consumption on rat GABA(A) and strychnine-sensitive glycine receptors expressed by lateral/basolateral amygdala neurons. Brain Res. 2003 Feb 14;963(1-2):165-77.

266. McDonald AJ. Cortical pathways to the mammalian amygdala. Prog. Neurobiol. (1998)

267. McDonald AJ. Cytoarchitecture of the central amygdaloid nucleus of the rat. J Comp Neurol 1982;208:401–418, 1982.

268. McKernan MG, Shinnick-Gallagher P. Fear conditioning induces a lasting potentiation of synaptic currents *in vitro*. Nature. 1997 Dec 11;390(6660):607-11.

269. McQuiston AR, Colmers WF. Neuropeptide Y2 receptors inhibit the frequency of spontaneous but not miniature EPSCs in CA3 pyramidal cells of rat hippocampus. J Neurophysiol. 1996;76:3159-68.

270. Meis S, Biella G, Pape HC. Interaction between low voltage-activated currents in reticular thalamic neurons in a rat model of absence epilepsy. Eur J Neurosci. 1996 Oct;8(10):2090-7.

271. Meis, S., and Pape, H.C. Properties of a Ca 2+ -Activated K + Conductance in Acutely Isolated Pyramidal-Like Neurons From the Rat Basolateral Amygdaloid Complex. J. Neurophysiol. 1997;78, 1256–1262.

272. Menaa F, Abdelghani A, Menaa B. Graphene nanomaterials as biocompatible and conductive scaffolds for stem cells: impact for tissue engineering and regenerative medicine. J Tissue Eng Regen Med. 2015 Dec;9(12):1321-38.

273. Michel MC, Beck-Sickinger A, Cox H, Doods HN, Herzog H, Larhammar D, Quirion R, Schwartz T, Westfall T. XVI. International Union of Pharmacology recommendations for the nomenclature of neuropeptide Y, peptide YY, and pancreatic polypeptide receptors. Pharmacol Rev. 1998;50:143-50.

274. Migues PV, Lehmann IT, Fluechter L, Cammarota M, Gurd JW, Sim AT, Dickson PW, Rostas JA. Phosphorylation of CaMKII at Thr253 occurs *in vivo* and enhances binding to isolated postsynaptic densities. J Neurochem. 2006 Jul;98(1):289-99.

275. Miserendino MJ, Sananes CB, Melia KR, Davis M. Blocking of acquisition but not expression of conditioned fear-potentiated startle by NMDA antagonists in the amygdala. Nature. 1990 Jun 21;345(6277):716-8.

276. Mo B, Feng N, Renner K, Forster G. Restraint stress increases serotonin release in the central nucleus of the amygdala via activation of corticotropin-releasing factor receptors. Brain Res Bull. 2008 Jul 30;76(5):493-8.

277. Molnár E. Long-term potentiation in cultured hippocampal neurons. Semin Cell Dev Biol. 2011 Jul;22(5):506-13.

278. Molosh AI, Sajdyk TJ, Truitt WA, Zhu W, Oxford GS, Shekhar A. NPY Y1 receptors differentially modulate GABAA and NMDA receptors via divergent signal-transduction pathways to reduce excitability of amygdala neurons. Neuropsychopharmacology. 2013;38:1352-64.

279. Mukherjee SP, Lozano N, Kucki M, Del Rio-Castillo AE, Newman L, Vázquez E, Kostarelos K, Wick P, Fadeel B. Detection of Endotoxin Contamination of Graphene Based Materials Using the TNF-α Expression Test and Guidelines for Endotoxin-Free Graphene Oxide Production. PLoS One. 2016 Nov 23;11(11):e0166816.

280. Muñoz-Abellán C, Daviu N, Rabasa C, Nadal R, Armario A. Cat odor causes long-lasting contextual fear conditioning and increased pituitary-adrenal activation, without modifying anxiety. Horm Behav. 2009 Oct;56(4):465-71.

281. Murthy, V. N.; Sejnowski, T. J.; Stevens, C. F. Heterogeneous release properties of visualized individual hippocampal synapses. Neuron 1997, 18, 599−612.

282. Musto M, Rauti R, Rodrigues AF, Bonechi E, Ballerini C, Kostarelos K, Ballerini L. 3D Organotypic Spinal Cultures: Exploring Neuron and Neuroglia Responses Upon Prolonged Exposure to Graphene Oxide. Front Syst Neurosci. 2019 Jan 24;13:1.

283. N.C. Coimbra, T. Paschoalin-Maurin, G.S. Bassi, A. Kanashiro, A.F. Biagioni, T. T. Felippotti, D.H. Elias-Filho, J. Mendes-Gomes, J.P. Cysne-Coimbra, R.C. Almada, B. Lob˜ao-Soares, Rev. Bras. Psiquiatr. 39, 2017; 72–83.

284. Naaijen J, Forde NJ, Lythgoe DJ, Akkermans SE, Openneer TJ, Dietrich A, Zwiers MP, Hoekstra PJ, Buitelaar JK. Fronto-striatal glutamate in children with Tourette's disorder and attention-deficit/hyperactivity disorder. Neuroimage Clin. 2016 Nov 16;13:16-23.

285. Nabavi S, Fox R, Proulx CD, Lin JY, Tsien RY, Malinow R. Engineering a memory with LTD and LTP. Nature. 2014 Jul 17;511(7509):348-52.

286. Nader K, Schafe GE, Le Doux JE. Fear memories require protein synthesis in the amygdala for reconsolidation after retrieval. Nature. 2000 Aug 17;406(6797):722-6.

287. Nag OK, Stewart MH, Deschamps JR, Susumu K, Oh E, Tsytsarev V, Tang Q, Efros AL, Vaxenburg R, Black BJ, Chen Y,''Shaughnessy TJ, North SH, Field LD, Dawson PE, Pancrazio JJ, Medintz IL, Chen Y, Erzurumlu RS, Huston AL, Delehanty JB. Quantum Dot-Peptide-Fullerene Bioconjugates for Visualization of *in Vitro* and *in Vivo* Cellular Membrane Potential. ACS Nano. 2017 Jun 27;11(6):5598-5613.

288. Nahvi RJ, Tanelian A, Nwokafor C, Hollander CM, Peacock L, Sabban EL. Intranasal Neuropeptide Y as a Potential Therapeutic for Depressive Behavior in the Rodent Single Prolonged Stress Model in Females. Front. Behav. Neurosci. 2021;5:705579. |

289. Nair RR, Blake P, Grigorenko AN, Novoselov KS, Booth TJ, Stauber T, Peres NM, Geim AK. Fine structure constant defines visual transparency of graphene. Science. 2008 Jun 6;320(5881):1308.

290. Nakada T, Lee H, Kwee IL, Lerner AM. Epileptic Kluver-Bucy syndrome: case report. J Clin Psychiatry. 1984 Feb;45(2):87-8.

291. Nash JE, Appleby VJ, Corrêa SA, Wu H, Fitzjohn SM, Garner CC, Collingridge GL, Molnár E. Disruption of the interaction between myosin VI and SAP97 is associated with a reduction in the number of AMPARs at hippocampal synapses. J Neurochem. 2010 Feb;112(3):677-90.

292. Nel AE, Mädler L, Velegol D, Xia T, Hoek EM, Somasundaran P, Klaessig F, Castranova V, Thompson M. Understanding biophysicochemical interactions at the nano-bio interface. Nat Mater. 2009 Jul;8(7):543-57.

293. Nelson T, Zhang B, Prezhdo OV. Detection of nucleic acids with graphene nanopores: ab initio characterization of a novel sequencing device. Nano Lett. 2010 Sep 8;10(9):3237-42.

294. Neugebauer V, Zinebi F, Russell R, Gallagher JP, Shinnick-Gallagher P. Cocaine and kindling alter the sensitivity of group II and III metabotropic glutamate receptors in the central amygdala. J Neurophysiol. 2000 Aug;84(2):759-70.

295. Neumann ID, Wegener G, Homberg JR, Cohen H, Slattery DA, Zohar J, Olivier JD, Mathé AA. Animal models of depression and anxiety: What do they tell us about human condition? Prog Neuropsychopharmacol Biol Psychiatry. 2011 Aug 1;35(6):1357-75.

296. Newman, L, Rodrigues, AF, Jasim, D, Anna Vacchi, I, Ménard-Moyon, C, Bianco, A, 162ode, C & Kostarelos, K, 'Nose-to-Brain Translocation and Cerebral Biodegradation of Thin Graphene Oxide Nanosheets', Cell Reports Physical Science 2020.

297. Nguyen PV, Abel T, Kandel ER. Requirement of a critical period of transcription for induction of a late phase of LTP. Science. 1994 Aug 19;265(5175):1104-7.

298. Nicoll RA, Malenka RC. Contrasting properties of two forms of long-term potentiation in the hippocampus. Nature. 1995 Sep 14;377(6545):115-8.

299. Nilsson P, Laursen H, Hillered L, Hansen AJ. Calcium movements in traumatic brain injury: the role of glutamate receptor-operated ion channels. J Cereb Blood Flow Metab. 1996 Mar;16(2):262-70.

300. Novoselov KS, Geim AK, Morozov SV, Jiang D, Katsnelson MI, Grigorieva IV, Dubonos SV, Firsov AA. Two-dimensional gas of massless Dirac fermions in graphene. Nature. 2005 Nov 10;438(7065):197-200.

301. Novoselov KS, Geim AK, Morozov SV, Jiang D, Zhang Y, Dubonos SV, Grigorieva IV, Firsov AA. Electric field effect in atomically thin carbon films. Science. 2004 Oct 22;306(5696):666-9.

302. Nuttin B, Gybels J, Cosyns P, Gabriels L, Meyerson B, Andreewitch S, Rasmussen SA, Greenberg B, Friehs G, Rezai AR, Montgomery E, Malone D, Fins JJ. Deep brain stimulation for psychiatric disorders. Neurosurg Clin N Am. 2003 Apr;14(2):xv-xvi.

303. Oh MC, Derkach VA, Guire ES, Soderling TR. Extrasynaptic membrane trafficking regulated by GluR1 serine 845 phosphorylation primes AMPA receptors for long-term potentiation. J Biol Chem. 2006 Jan 13;281(2):752-8.

304. Ohno Y, Maehashi K, Matsumoto K. Label-free biosensors based on aptamer-modified graphene field-effect transistors. J Am Chem Soc. 2010 Dec 29;132(51):18012-3.

305. Olesen MV, Christiansen SH, Gøtzsche CR, Nikitidou L, Kokaia M, Woldbye DP. Neuropeptide Y Y1 receptor hippocampal overexpression via viral vectors is associated with modest anxiolytic-like and proconvulsant effects in mice. J Neurosci Res. 2012;90:498-507.

306. Ormond J, Woodin MA. Disinhibition mediates a form of hippocampal long-term potentiation in area CA1. PloS One. 2009 Sep 29;4(9):e7224.

307. Otmakhov N, Khibnik L, Otmakhova N, Carpenter S, Riahi S, Asrican B, Lisman J. Forskolin-induced LTP in the CA1 hippocampal region is NMDA receptor dependent. J Neurophysiol. 2004 May;91(5):1955-62.

308. Ottersen OP, Fischer BO, Rinvik E, Storm-Mathisen J. Putative amino acid transmitters in the amygdala. Adv Exp Med Biol. 1986;203:53-66.

309. Otto T, Eichenbaum H, Wiener SI, Wible CG. Learning-related patterns of CA1 spike trains parallel stimulation parameters optimal for inducing hippocampal long-term potentiation. Hippocampus. 1991 Apr;1(2):181-92.

310. Ou L, Song B, Liang H, Liu J, Feng X, Deng B, Sun T, Shao L. Toxicity of graphene-family nanoparticles: a general review of the origins and mechanisms. Part Fibre Toxicol. 2016 Oct 31;13(1):57.

311. Palazzo E, Marabese I, de Novellis V, Rossi F, Maione S. Supraspinal metabotropic glutamate receptors: a target for pain relief and beyond. Eur J Neurosci. 2014 Feb;39(3):444-54.

312. Pape HC, Pare D. Plastic synaptic networks of the amygdala for the acquisition, expression, and extinction of conditioned fear. Physiol Rev. 2010 Apr;90(2):419-63.

313. Paré D, Smith Y, Paré JF. Intra-amygdaloid projections of the basolateral and basomedial nuclei in the cat: Phaseolus vulgaris-leucoagglutinin anterograde tracing at the light and electron microscopic level. Neuroscience. 1995 Nov;69(2):567-83.

314. Park S, An J, Jung I, Piner RD, An SJ, Li X, Velamakanni A, Ruoff RS. Colloidal suspensions of highly reduced graphene oxide in a wide variety of organic solvents. Nano Lett. 2009 Apr;9(4):1593-7.

315. Park S, Ruoff RS. Chemical methods for the production of graphenes. Nat Nanotechnol. 2009 Apr;4(4):217-24. doi: 10.1038/nnano.2009.58. Epub 2009 Mar 29. Erratum in: Nat Nanotechnol. 2010 Apr;5(4):309.

316. Park SG, Jeong YC, Kim DG, Lee MH, Shin A, Park G, Ryoo J, Hong J, Bae S, Kim CH, Lee PS, Kim D. Medial preoptic circuit induces hunting-like actions to target objects and prey. Nat Neurosci. 2018 Mar;21(3):364-372.

317. Parsons MP, Raymond LA. Extrasynaptic NMDA receptor involvement in central nervous system disorders. Neuron. 2014 Apr 16;82(2):279-93.

318. Pastalkova E, Serrano P, Pinkhasova D, Wallace E, Fenton AA, Sacktor TC. Storage of spatial information by the maintenance mechanism of LTP. Science. 2006 Aug 25;313(5790):1141-4.

319. Pavlides C, Greenstein YJ, Grudman M, Winson J. Long-term potentiation in the dentate gyrus is induced preferentially on the positive phase of theta-rhythm. Brain Res. 1988 Jan 26;439(1-2):383-7.

320. Paxinos, G. and Watson, C. The Rat Brain in Stereotaxic Coordinates. San Diego, CA: Academic, 1986

321. Pedragosa-Badia X, Stichel J, Beck-Sickinger AG. Neuropeptide Y receptors: how to get subtype selectivity. Front Endocrinol (Lausanne). 2013 Feb 4;4:5.

322. Pellow S, Chopin P, File SE, Briley M. Validation of open:closed arm entries in an elevated plus-maze as a measure of anxiety in the rat. J Neurosci Methods. 1985;14:149-67.

323. Perini G, Palmieri V, Ciasca G, D'Ascenzo M, Primiano A, Gervasoni J, De Maio F, De Spirito M, Papi M. Enhanced Chemotherapy for Glioblastoma Multiforme Mediated by Functionalized Graphene Quantum Dots. Materials (Basel). 2020 Sep 17;13(18):4139.

324. Phillips RG, LeDoux JE. Differential contribution of amygdala and hippocampus to cued and contextual fear conditioning. Behav Neurosci. 1992 Apr;106(2):274-85.

325. Pich EM, Agnati LF, Zini I, Marrama P, Carani C. Neuropeptide Y produces anxiolytic effects in spontaneously hypertensive rats. Peptides. 1993;14:909-12.

326. Pickrell AM, Youle RJ. The roles of PINK1, parkin, and mitochondrial fidelity in Parkinson's disease. Neuron. 2015 Jan 21;85(2):257-73.

327. Pitkänen A, Amaral DG. The distribution of GABAergic cells, fibers, and terminals in the monkey amygdaloid complex: an immunohistochemical and in situ hybridization study. J Neurosci. 1994 Apr;14(4):2200-24.

328. Pitkänen A, savander V, and LeDoux JE. Organization of intra-amygdaloid circuitries in the rat: an emerging framework for understanding functions of the amygdala. Trends Neurosci 1997;20: 517–523.

329. Pitkänen A. Connectivity of the rat amygdaloid complex. In: The Amygdala: A Functional Analysis, edited by Aggleton JP. Oxford, UK: Oxford Univ. Press, 2000.

330. Portioli C, Bussy C, Mazza M, Lozano N, Jasim DA, Prato M, Bianco A, Bentivoglio M, Kostarelos K. Intracerebral Injection of Graphene Oxide Nanosheets Mitigates Microglial Activation Without Inducing Acute Neurotoxicity: A Pilot Comparison to Other Nanomaterials. Small. 2020 Nov 10:e2004029.

331. Poulin SP, Dautoff R, Morris JC, Barrett LF, Dickerson BC; Alzheimer's Disease Neuroimaging Initiative. Amygdala atrophy is prominent in early Alzheimer's disease and relates to symptom severity. Psychiatry Res. 2011 Oct 31;194(1):7-13.

332. Prager EM, Bergstrom HC, Wynn GH, Braga MF. The basolateral amygdala γ-aminobutyric acidergic system in health and disease. J Neurosci Res. 2016 Jun;94(6):548-67.

333. Price JL, Russchen FT, and Amaral DG. The Limbic Region. II: The Amygdaloid Complex. New York: Elsevier Science, 1987.

334. Qing H, Jin G, Zhao G, Huang G, Ma Y, Zhang X, Sha B, Luo Z, Lu TJ, Xu F. Heterostructured Silk-Nanofiber-Reduced Graphene Oxide Composite Scaffold for SH-SY5Y Cell Alignment and Differentiation. ACS Appl Mater Interfaces. 2018 Nov 14;10(45):39228-39237.

335. Raastad M, Storm JF, Andersen P. Putative Single Quantum and Single Fibre Excitatory Postsynaptic Currents Show Similar Amplitude Range and Variability in Rat Hippocampal Slices. Eur J Neurosci. 1992 Oct;4(1):113-117.

336. Raposinho PD, Pierroz DD, Broqua P, White RB, Pedrazzini T, Aubert ML. Chronic administration of neuropeptide Y into the lateral ventricle of C57BL/6J male mice produces an obesity syndrome including hyperphagia, hyperleptinemia, insulin resistance, and hypogonadism. Mol Cell Endocrinol. 2001;185:195-204.

337. Rauti R, Lozano N, León V, Scaini D, Musto M, Rago I, Ulloa Severino FP, Fabbro A, Casalis L, Vázquez E, Kostarelos K, Prato M, Ballerini L. Graphene Oxide Nanosheets Reshape Synaptic Function in Cultured Brain Networks. ACS Nano. 2016 Apr 26;10(4):4459-71.

338. Rauti R, Medelin M, Newman L, Vranic S, Reina G, Bianco A, Prato M, Kostarelos K, Ballerini L. Graphene Oxide Flakes Tune Excitatory Neurotransmission in Vivo by Targeting Hippocampal Synapses. Nano Lett. 2019 May 8;19(5):2858-2870.

339. Raymond CR, Thompson VL, Tate WP, Abraham WC. Metabotropic glutamate receptors trigger homosynaptic protein synthesis to prolong long-term potentiation. J Neurosci. 2000 Feb 1;20(3):969-76.

340. Reichmann F, Holzer P. Neuropeptide Y: A stressful review. Neuropeptides 2016;55:99–109.

341. Reina G, González-Domínguez JM, Criado A, Vázquez E, Bianco A, Prato M. Promises, facts and challenges for graphene in biomedical applications. Chem Soc Rev. 2017 Jul 31;46(15):4400-4416.

342. Roberson ED, English JD, Sweatt JD. A biochemist's view of long-term potentiation. Learn Mem. 1996 Jul-Aug;3(1):1-24.

343. Robinson JT, Jorgolli M, Shalek AK, Yoon MH, Gertner RS, Park H. Vertical nanowire electrode arrays as a scalable platform for intracellular interfacing to neuronal circuits. Nat Nanotechnol. 2012 Jan 10;7(3):180-4.

344. Rock K, McArdle O, Forde P, Dunne M, Fitzpatrick D, O'Neill B, Faul C. A clinical review of treatment outcomes in glioblastoma multiforme--the validation in a non-trial population of the results of a randomised Phase III clinical trial: has a more radical approach improved survival? Br J Radiol. 2012 Sep;85(1017):e729-33.

345. Rockenstein E, Nuber S, Overk CR, Ubhi K, Mante M, Patrick C, Adame A, Trejo-Morales M, Gerez J, Picotti P, Jensen PH, Campioni S, Riek R, Winkler J, Gage FH, Winner B, Masliah E. Accumulation of oligomer-prone α-synuclein exacerbates synaptic and neuronal degeneration *in vivo*. Brain. 2014 May;137(Pt 5):1496-513.

346. Rogan MT, LeDoux JE. Emotion: systems, cells, synaptic plasticity. Cell. 1996 May 17;85(4):469-75. Doi: 10.1016/s0092-8674(00)81247-7. PMID: 8653782.

347. Rogan MT, Stäubli UV, LeDoux JE. Fear conditioning induces associative long-term potentiation in the amygdala. Nature. 1997 Dec 11;390(6660):604-7.

348. Roozendaal B, McEwen BS, Chattarji S. Stress, memory and the amygdala. Nat Rev Neurosci. 2009 Jun;10(6):423-33.

349. Rose GM, Dunwiddie TV. Induction of hippocampal long-term potentiation using physiologically patterned stimulation. Neurosci Lett. 1986 Sep 12;69(3):244-8.

350. Rosenfeld JV, Wong YT. Neurobionics and the brain-computer interface: current applications and future horizons. Med J Aust. 2017 May 1;206(8):363-368.

351. Rosenkranz JA, Grace AA. Dopamine-mediated modulation of odour-evoked amygdala potentials during pavlovian conditioning. Nature. 2002 May 16;417(6886):282-7.

352. Rosenkranz JA, Venheim ER, Padival M. Chronic stress causes amygdala hyperexcitability in rodents. Biol Psychiatry. 2010 Jun 15;67(12):1128-36.

353. Rothemund PW. Folding DNA to create nanoscale shapes and patterns. Nature. 2006 Mar 16;440(7082):297-302.

354. Rubinstein JT. How cochlear implants encode speech. Curr Opin Otolaryngol Head Neck Surg. 2004 Oct;12(5):444-8.

355. Rumpel S, LeDoux J, Zador A, Malinow R. Postsynaptic receptor trafficking underlying a form of associative learning. Science. 2005 Apr 1;308(5718):83-8.

356. Russier J, Treossi E, Scarsi A, Perrozzi F, Dumortier H, Ottaviano L, Meneghetti M, Palermo V, Bianco A. Evidencing the mask effect of graphene oxide: a comparative study on primary human and murine phagocytic cells. Nanoscale. 2013 Nov 21;5(22):11234-47.

357. Ryan, T. A.; Reuter, H.; Wendland, B.; Schweizer, F. E.; Tsien, R. W.; Smith, S. J. The Kinetics of Synaptic Vesicle Recycling Measured at Single Presynaptic Boutons. Neuron 1993, 11, 713−724.

358. Sabban EL, Alaluf LG, Serova LI. Potential of neuropeptide Y for preventing or treating post-traumatic stress disorder. Neuropeptides. 2016 Apr;56:19-24.

359. Sah P, Faber ES, Lopez De Armentia M, Power J. The amygdaloid complex: anatomy and physiology. Physiol Rev. 2003 Jul;83(3):803-34.

360. Sahni D, Jea A, Mata JA, Marcano DC, Sivaganesan A, Berlin JM, Tatsui CE, Sun Z, Luerssen TG, Meng S, Kent TA, Tour JM. Biocompatibility of pristine graphene for neuronal interface. J Neurosurg Pediatr. 2013 May;11(5):575-83.

361. Sajdyk TJ, Schober DA, Gehlert DR. Neuropeptide Y receptor subtypes in the basolateral nucleus of the amygdala modulate anxiogenic responses in rats. Neuropharmacology. 2002;43:1165-72.

362. Sajdyk TJ, Schober DA, Smiley DL, Gehlert DR. Neuropeptide Y-Y2 receptors mediate anxiety in the amygdala. Pharmacol Biochem Behav. 2002a Mar;71(3):419-23.

363. Salter MW. LTP gets culture. Trends Neurosci. 2001 Oct;24(10):560-1.

364. Sanchez VC, Jachak A, Hurt RH, Kane AB. Biological interactions of graphene-family nanomaterials: an interdisciplinary review. Chem Res Toxicol. 2012 Jan 13;25(1):15-34.

365. Sartori SB, Singewald N. Novel pharmacological targets in drug development for the treatment of anxiety and anxiety-related disorders. Pharmacol Ther. 2019 Dec;204:107402.

366. Scaini D, Ballerini L. Nanomaterials at the neural interface. Curr Opin Neurobiol. 2018 Jun;50:50-55.

367. Schouenborg J. Biocompatible multichannel electrodes for long-term neurophysiological studies and clinical therapy–novel concepts and design. Prog Brain Res. 2011;194:61-70.

368. Schweizer E, Rickels K, Case WG, Greenblatt DJ. Long-term therapeutic use of benzodiazepines. II. Effects of gradual taper. Arch Gen Psychiatry. 1990 Oct;47(10):908-15.

369. SCOVILLE WB, MILNER B. Loss of recent memory after bilateral hippocampal lesions. J Neurol Neurosurg Psychiatry. 1957 Feb;20(1):11-21.

370. Secomandi N, Franceschi Biagioni A, Kostarelos K, Cellot G, Ballerini L. Thin graphene oxide nanoflakes modulate glutamatergic synapses in the amygdala cultured circuits: Exploiting synaptic approaches to anxiety disorders. Nanomedicine. 2020 Jun;26:102174.

371. Segev, E. et al. In Conference on Lasers and Electro-Optics (OSA, 2016).

372. Sekirnjak C, Hottowy P, Sher A, Dabrowski W, Litke AM, Chichilnisky EJ. High-resolution electrical stimulation of primate retina for epiretinal implant design. J Neurosci. 2008 Apr 23;28(17):4446-56.

373. Seo G, Lee G, Kim MJ, Baek SH, Choi M, Ku KB, Lee CS, Jun S, Park D, Kim HG, Kim SJ, Lee JO, Kim BT, Park EC, Kim SI. Rapid Detection of COVID-19 Causative Virus (SARS-CoV-2) in Human Nasopharyngeal Swab Specimens Using Field-Effect Transistor-Based Biosensor. ACS Nano. 2020 Apr 28;14(4):5135-5142.

374. Shah S, Yin PT, Uehara TM, Chueng ST, Yang L, Lee KB. Guiding stem cell differentiation into oligodendrocytes using graphene-nanofiber hybrid scaffolds. Adv Mater. 2014 Jun 11;26(22):3673-80.

375. Shahi K, Baudry M. Glycine-induced changes in synaptic efficacy in hippocampal slices involve changes in AMPA receptors. Brain Res. 1993 Nov 12;627(2):261-6.

376. Sharma S, Tiwari S. A review on biomacromolecular hydrogel classification and its applications. Int J Biol Macromol. 2020 Nov 1;162:737-747.

377. Shew WL, Yang H, Yu S, Roy R, Plenz D. Information capacity and transmission are maximized in balanced cortical networks with neuronal avalanches. J Neurosci. 2011 Jan 5;31(1):55-63.

378. Shin LM, Liberzon I. The neurocircuitry of fear, stress, and anxiety disorders. Neuropsychopharmacology. 2010 Jan;35(1):169-91.

379. Si Y, Samulski ET. Synthesis of water soluble graphene. Nano Lett. 2008 Jun;8(6):1679-82.

380. Siegmund A, Wotjak CT. Toward an animal model of posttraumatic stress disorder. Ann N Y Acad Sci. 2006 Jul;1071:324-34.

381. Somerville LH, Kim H, Johnstone T, Alexander AL, Whalen PJ. Human amygdala responses during presentation of happy and neutral faces: correlations with state anxiety. Biol Psychiatry. 2004 May 1;55(9):897-903.

382. Song MM, Xu HL, Liang JX, Xiang HH, Liu R, Shen YX. Lactoferrin modified graphene oxide iron oxide nanocomposite for glioma-targeted drug delivery. Mater Sci Eng C Mater Biol Appl. 2017 Aug 1;77:904-911.

383. Song W, Anselmo AC, Huang L. Nanotechnology intervention of the microbiome for cancer therapy. Nat Nanotechnol. 2019 Dec;14(12):1093-1103.

384. Sørensen G, Lindberg C, Wörtwein G, Bolwig TG, Woldbye DP. Differential roles for neuropeptide Y Y1 and Y5 receptors in anxiety and sedation. J Neurosci Res. 2004;77:723-9.

385. Stahl SM. Don't ask, don't tell, but benzodiazepines are still the leading treatments for anxiety disorder. J Clin Psychiatry. 2002 Sep;63(9):756-7.

386. Stankovich, S., Dikin, D. A., Piner, R. D., Kohlhaas, K. A., Kleinhammes, A., Jia, Y., Wu, Y., Nguyen, S. B. T., & Ruoff, R. S. Synthesis of graphene-based nanosheets via chemical reduction of exfoliated graphite oxide. Carbon, 2007;45(7):558-1565.

387. Stoller MD, Park S, Zhu Y, An J, Ruoff RS. Graphene-based ultracapacitors. Nano Lett. 2008 Oct;8(10):3498-502.

388. Strack S, Colbran RJ. Autophosphorylation-dependent targeting of calcium/ calmodulin-dependent protein kinase II by the NR2B subunit of the N-methyl- D-aspartate receptor. J Biol Chem. 1998 Aug 14;273(33):20689-92.

389. Stutzmann GE, McEwen BS, LeDoux JE. Serotonin modulation of sensory inputs to the lateral amygdala: dependency on corticosterone. J Neurosci. 1998 Nov 15;18(22):9529-38.

390. Su S, Wang J, Qiu J, Martinez-Zaguilan R, Sennoune SR, Wang S. In vitro study of transportation of porphyrin immobilized graphene oxide through blood brain barrier. Mater Sci Eng C Mater Biol Appl. 2020 Feb;107:110313.

391. Sun X, Wang H, Jian Y, Lan F, Zhang L, Liu H, Ge S, Yu J. Ultrasensitive microfluidic paper-based electrochemical/visual biosensor based on spherical-like cerium dioxide catalyst for miR-21 detection. Biosens Bioelectron. 2018 May 15;105:218-225.

392. Sutherland RJ, McDonald RJ. Hippocampus, amygdala, and memory deficits in rats. Behav Brain Res. 1990 Feb 12;37(1):57-79.

393. Swanson LW, Petrovich GD. What is the amygdala? Trends Neurosci. 1998 Aug;21(8):323-31.

394. Sweatt JD. The neuronal MAP kinase cascade: a biochemical signal integration system subserving synaptic plasticity and memory.J Neurochem 2001;76: 1–10.

395. Sweatt JD. Toward a molecular explanation for long-term potentiation. Learn Mem. 1999 Sep-Oct;6(5):399-416.

396. Sweeney MD, Zhao Z, Montagne A, Nelson AR, Zlokovic BV. Blood-Brain Barrier: From Physiology to Disease and Back. Physiol Rev. 2019 Jan 1;99(1):21-78.

397. Tabrizi MA, Ferré-Borrull J, Kapruwan P, Marsal LF. A photoelectrochemical sandwich immunoassay for protein S100β, a biomarker for Alzheimer's disease, using an ITO electrode modified with a reduced graphene oxide-gold conjugate and CdS-labeled secondary antibody. Mikrochim Acta. 2019 Jan 16;186(2):117.

398. Tak K, Sharma R, Dave V, Jain S, Sharma S. Clitoria ternatea Mediated Synthesis of Graphene Quantum Dots for the Treatment of Alzheimer's Disease. ACS Chem Neurosci. 2020 Nov 18;11(22):3741-3748.

399. Takkala P, Woodin MA. Muscarinic acetylcholine receptor activation prevents disinhibition-mediated LTP in the hippocampus. Front Cell Neurosci. 2013 Feb 28;7:16.

400. Taniguchi, N.; Arakawa, C.; Kobayashi, T. On the basic concept of nano-technology. In Proceedings of the International Conference on Production Engineering, Tokyo, Japan, 26–29 August 1974.

401. Tessitore A, Hariri AR, Fera F, Smith WG, Chase TN, Hyde TM, Weinberger DR, Mattay VS. Dopamine modulates the response of the human amygdala: a study in Parkinson's disease. J Neurosci. 2002 Oct 15;22(20):9099-103.

402. Tian B, Liu J, Dvir T, Jin L, Tsui JH, Qing Q, Suo Z, Langer R, Kohane DS, Lieber CM. Macroporous nanowire nanoelectronic scaffolds for synthetic tissues. Nat Mater. 2012 Nov;11(11):986-94.

403. Trivedi MH, Rush AJ, Wisniewski SR, Nierenberg AA, Warden D, Ritz L, Norquist G, Howland RH, Lebowitz B, McGrath PJ, Shores-Wilson K, Biggs MM, Balasubramani GK, Fava M; STAR*D Study Team. Evaluation of outcomes with citalopram for depression using measurement-based care in STAR*D: implications for clinical practice. Am J Psychiatry. 2006;163:28-40.

404. Truitt WA, Sajdyk TJ, Dietrich AD, Oberlin B, McDougle CJ, Shekhar A. From anxiety to autism: spectrum of abnormal social behaviors modeled by progressive disruption of inhibitory neuronal function in the basolateral amygdala in Wistar rats. Psychopharmacology (Berl). 2007 Mar;191(1):107-18.

405. Tsvetkov, E., Carlezon, W.A., Benes, F.M., Kandel, E.R., Bolshakov, V.Y. Fear conditioning occludes LTP-induced presynaptic enhancement of synaptic transmission in the cortical pathway to the lateral amygdala. Neuron 2002;34:289–300.

406. Tu Z, Qiao H, Yan Y, Guday G, Chen W, Adeli M, Haag R. Directed Graphene-Based Nanoplatforms for Hyperthermia: Overcoming Multiple Drug Resistance. Angew Chem Int Ed Engl. 2018 Aug 27;57(35):11198-11202.

407. Tully K, Li Y, Tsvetkov E, Bolshakov VY. Norepinephrine enables the induction of associative long-term potentiation at thalamo-amygdala synapses. Proc Natl Acad Sci U S A. 2007 Aug 28;104(35):14146-50.

408. Turner RW, Baimbridge KG, Miller JJ. Calcium-induced long-term potentiation in the hippocampus. Neuroscience. 1982 Jun;7(6):1411-6.

409. Turrigiano GG, Nelson SB. Hebb and homeostasis in neuronal plasticity. Curr Opin Neurobiol. 2000 Jun;10(3):358-64.

410. Turrigiano GG. The self-tuning neuron: synaptic scaling of excitatory synapses. Cell. 2008 Oct 31;135(3):422-35.

411. Tyler WJ, Pozzo-Miller LD. BDNF enhances quantal neurotransmitter release and increases the number of docked vesicles at the active zones of hippocampal excitatory synapses. J Neurosci. 2001 Jun 15;21(12):4249-58.

412. Uno Y, Coyle JT. Glutamate hypothesis in schizophrenia. Psychiatry Clin Neurosci. 2019 May;73(5):204-215.

413. Van der Worp HB, Howells DW, Sena ES, Porritt MJ, Rewell S, O'Collins V, Macleod MR. Can animal models of disease reliably inform human studies? PloS Med. 2010 Mar 30;7(3):e1000245.

414. Verbitsky A, Dopfel D, Zhang N. Rodent models of post-traumatic stress disorder: behavioral assessment. Transl Psychiatry. 2020 May 6;10(1):132.

415. Vertes RP. Hippocampal theta rhythm: a tag for short-term memory. Hippocampus. 2005;15(7):923-35.

416. Vezzani A, Sperk G. Overexpression of NPY and Y2 receptors in epileptic brain tissue: an endogenous neuroprotective mechanism in temporal lobe epilepsy? Neuropeptides. 2004 Aug;38(4):245-52.

417. Viana F, Hille B. Modulation of high voltage-activated calcium channels by somatostatin in acutely isolated rat amygdaloid neurons. J Neurosci. 1996 Oct 1;16(19):6000-11.

418. Wagner L, Wolf R, Zeitschel U, Rossner S, Petersén A, Leavitt BR, Kästner F, Rothermundt M, Gärtner U, Gündel D, Schlenzig D, Frerker N, Schade J Manhart S, Rahfeld J, Demuth H, Hörsten S. Proteolytic degradation of neuropeptide Y (NPY) from head to toe:

Identification of novel NPY-cleaving peptidases and potential drug interactions in CNS and Periphery. J. Neurochem. 2015;135:1019–37.

419. Wahlestedt C, Pich EM, Koob GF, Yee F, Heilig M. Modulation of anxiety and neuropeptide Y-Y1 receptors by antisense oligodeoxynucleotides. Science. 1993;259:528-31.

420. Wang K, Wang L, Chen L, Peng C, Luo B, Mo J, Chen W. Intranasal administration of dauricine loaded on graphene oxide: multi-target therapy for Alzheimer's disease. Drug Deliv. 2021 Dec;28(1):580-593.

421. Wang S, Tudusciuc O, Mamelak AN, Ross IB, Adolphs R, Rutishauser U. Neurons in the human amygdala selective for perceived emotion. Proc Natl Acad Sci U S A. 2014 Jul 29;111(30):E3110-9.

422. Wang SJ, Huang CC, Hsu KS, Tsai JJ, Gean PW. Inhibition of N-type calcium currents by lamotrigine in rat amygdalar neurones. Neuroreport. 1996 Nov 25;7(18):3037-40.

423. WEISKRANTZ L. Behavioral changes associated with ablation of the amygdaloid complex in monkeys. J Comp Physiol Psychol. 1956 Aug;49(4):381-91.

424. Weisskopf MG, Bauer EP, LeDoux JE. L-type voltage-gated calcium channels mediate NMDA-independent associative long-term potentiation at thalamic input synapses to the amygdala. J Neurosci. 1999 Dec 1;19(23):10512-9.

425. Whitener, K.E., and Sheehan, P.E. Graphene synthesis. Diam. Relat. Mater. 2014;46:25–34.

426. Whitlock JR, Heynen AJ, Shuler MG, Bear MF. Learning induces long-term potentiation in the hippocampus. Science. 2006 Aug 25;313(5790):1093-7.

427. Widdowson PS. Quantitative receptor autoradiography demonstrates a differential distribution of neuropeptide-Y Y1 and Y2 receptor subtypes in human and rat brain. Brain Res. 1993 Dec 17;631(1):27-38.

428. Wieland HA, Willim K, Doods HN. Receptor binding profiles of NPY analogues and fragments in different tissues and cell lines. Peptides. 1995;16(8):1389-94.

429. Willner P. Validation criteria for animal models of human mental disorders: learned helplessness as a paradigm case. Prog Neuropsychopharmacol Biol Psychiatry. 1986;10(6):677-90.

430. Won H, Lee HR, Gee HY, Mah W, Kim JI, Lee J, Ha S, Chung C, Jung ES, Cho YS, Park SG, Lee JS, Lee K, Kim D, Bae YC, Kaang BK, Lee MG, Kim E. Autistic-like social behaviour in Shank2-mutant mice improved by restoring NMDA receptor function. Nature. 2012 Jun 13;486(7402):261-5.

431. Wu G, Feder A, Wegener G, Bailey C, Saxena S, Charney D, Mathé AA. Central functions of neuropeptide Y in mood and anxiety disorders. Expert Opin Ther Targets. 2011;15:1317-31.

432. Wu GY, Deisseroth K, Tsien RW. Activity-dependent CREB phosphorylation: convergence of a fast, sensitive calmodulin kinase pathway and a slow, less sensitive mitogen-activated protein kinase pathway. Proc Natl Acad Sci U S A. 2001 Feb 27;98(5):2808-13.

433. Wyllie DJ, Manabe T, Nicoll RA. A rise in postsynaptic Ca2+ potentiates miniature excitatory postsynaptic currents and AMPA responses in hippocampal neurons. Neuron. 1994 Jan;12(1):127-38.

434. Xu X, Ray R, Gu Y, Ploehn HJ, Gearheart L, Raker K, Scrivens WA. Electrophoretic analysis and purification of fluorescent single-walled carbon nanotube fragments. J Am Chem Soc. 2004 Oct 13;126(40):12736-7.

435. Yaghoubi F, Motlagh NSH, Naghib SM, Haghiralsadat F, Jaliani HZ, Moradi A. A functionalized graphene oxide with improved cytocompatibility for stimuli-responsive co-delivery of curcumin and doxorubicin in cancer treatment. Sci Rep. 2022 Feb 4;12(1):1959.

436. Yan QL, Gozin M, Zhao FQ, Cohen A, Pang SP. Highly energetic compositions based on functionalized carbon nanomaterials. Nanoscale. 2016 Mar 7;8(9):4799-851.

437. Yao J, Wang H, Chen M, Yang M. Recent advances in graphene-based nanomaterials: properties, toxicity and applications in chemistry, biology and medicine. Mikrochim Acta. 2019 Jun 1;186(6):395.

438. Yao Y, Zhou Y, Liu L, Xu Y, Chen Q, Wang Y, Wu S, Deng Y, Zhang J, Shao A. Nanoparticle-Based Drug Delivery in Cancer Therapy and Its Role in Overcoming Drug Resistance. Front Mol Biosci. 2020 Aug 20;7:193.

439. Yehuda R, Antelman SM. Criteria for rationally evaluating animal models of posttraumatic stress disorder. Biol Psychiatry. 1993 Apr 1;33(7):479-86.

440. Yizhar O, Fenno LE, Prigge M, Schneider F, Davidson TJ, O'Shea DJ, Sohal VS, Goshen I, Finkelstein J, Paz JT, Stehfest K, Fudim R, Ramakrishnan C, Huguenard JR, Hegemann P, Deisseroth K. Neocortical excitation/inhibition balance in information processing and social dysfunction. Nature. 2011 Jul 27;477(7363):171-8.

441. Yokoyama M, Suzuki E, Sato T, Maruta S, Watanabe S, Miyaoka H. Amygdalic levels of dopamine and serotonin rise upon exposure to conditioned fear stress without elevation of glutamate. Neurosci Lett. 2005 Apr 29;379(1):37-41.

442. Yoshimura N, Kawamura M, Masaoka Y, Homma I. The amygdala of patients with Parkinson's disease is silent in response to fearful facial expressions. Neuroscience. 2005;131(2):523-34.

443. Young LD, Suomi SS, Harlow HF, McKinney WT Jr. Early stress and later response to separation in rhesus monkeys. Am J Psychiatry. 1973 Apr;130(4):400-5.

444. Yue H, Wei W, Yue Z, Wang B, Luo N, Gao Y, Ma D, Ma G, Su Z. The role of the lateral dimension of graphene oxide in the regulation of cellular responses. Biomaterials. 2012 Jun;33(16):4013-21.

445. Yulyaningsih E, Zhang L, Herzog H, Sainsbury A. NPY receptors as potential targets for anti-obesity drug development. Br J Pharmacol. 2011;63:1170-202.

446. Zakharenko SS, Zablow L, Siegelbaum SA. Visualization of changes in presynaptic function during long-term synaptic plasticity. Nat Neurosci. 2001 Jul;4(7):711-7.

447. Zanoveli JM, Carvalho MC, Cunha JM, Brandão ML. Extracellular serotonin level in the basolateral nucleus of the amygdala and dorsal periaqueductal gray under unconditioned and conditioned fear states: an in vivo microdialysis study. Brain Res. 2009 Oct 19;1294:106-15.

448. Zhang LL, Xiong Z, Zhao XS. Pillaring chemically exfoliated graphene oxide with carbon nanotubes for photocatalytic degradation of dyes under visible light irradiation. ACS Nano. 2010 Nov 23;4(11):7030-6.

449. Zhang Y, Liu C, Chen W, Shi Y, Wang C, Lin S, He, H. Regulation of neuropeptide Y in body microenvironments and its potential application in therapies: a review. Cell & Bioscience 2021;11:151.

450. Zhang, C.; Chen, S.; Alvarez, P. J. J.; Chen, W. Reduced Graphene Oxide Enhances Horseradish Peroxidase Stability by Serving as Radical Scavenger and Redox Mediator. Carbon 2015; 94:531-538

451. Zhao X, Wei Z, Zhao Z, Miao Y, Qiu Y, Yang W, Jia X, Liu Z, Hou H. Design and Development of Graphene Oxide Nanoparticle/Chitosan Hybrids Showing pH-Sensitive Surface Charge-Reversible Ability for Efficient Intracellular Doxorubicin Delivery. ACS Appl Mater Interfaces. 2018 Feb 21;10(7):6608-6617.

452. Zhou L, Wang W, Tang J, Zhou JH, Jiang HJ, Shen J. Graphene oxide noncovalent photosensitizer and its anticancer activity *in vitro*. Chemistry. 2011 Oct 17;17(43):12084-91.

453. Zhou Q, Lin Y, Zhang K, Li M, Tang D. Reduced graphene oxide/BiFeO3 nanohybrids-based signal-on photoelectrochemical sensing system for prostate-specific antigen detection coupling with magnetic microfluidic device. Biosens Bioelectron. 2018 Mar 15;101:146-152.

454. Zhou T, Hong G, Fu TM, Yang X, Schuhmann TG, Viveros RD, Lieber CM. Syringe-injectable mesh electronics integrate seamlessly with minimal chronic immune response in the brain. Proc Natl Acad Sci U S A. 2017 Jun 6;114(23):5894-5899.

455. Zola-Morgan S, Squire LR, Alvarez-Royo P, Clower RP. Independence of memory functions and emotional behavior: separate contributions of the hippocampal formation and the amygdala. Hippocampus. 1991 Apr;1(2):207-20.

456. Zucker RS. Short-term synaptic plasticity. Annu Rev Neurosci. 1989;12:13-31.